



UNIVERSITÀ  
DEGLI STUDI  
DI TRIESTE

# UNIVERSITÀ DEGLI STUDI DI TRIESTE

## XXXVI CICLO DEL DOTTORATO DI RICERCA IN

SCIENZE DELLA TERRA, FLUIDODINAMICA E MATEMATICA. INTERAZIONI E  
METODICHE

### Quartz in sedimentary rocks: OH-defects and trace elements for provenance studies

Settore scientifico-disciplinare: Geo/06 Mineralogia

Ph.D. STUDENT  
**FRANCESCO BERNARDI**

Ph.D. PROGRAM COORDINATOR  
**PROF. STEFANO MASET**

THESIS SUPERVISOR  
**PROF. DAVIDE LENAZ**

THESIS CO-SUPERVISOR  
**PROF. HENRIK SKOGBY**

ACADEMIC YEAR 2022/2023



UNIVERSITÀ DEGLI STUDI DI TRIESTE

Department of Mathematics, Informatics and  
Geosciences

Ph.D. Course in Earth Science, Fluid-Dynamics, and  
Mathematics. Interactions and methods

## Quartz in sedimentary rocks: OH-defects and trace elements for provenance studies

Ph.D. Student  
**Francesco Bernardi**

Supervisor:  
**Prof. Davide Lenaz**  
  
Co-Supervisor:  
**Prof. Henrik Skogby**

Academic Year 2022/2023

*Πάντες ἀνθρωποι τοῦ εἰδέναι ὀρέγονται φύσει*

## ABSTRACT

In the past ten years, some studies found that in quartz (a nominally anhydrous mineral or NAM) there is a certain amount of water (in OH form) due to crystal lattice defects. In contrast of other abundant minerals, quartz does not form solid solutions and it is considered a pure mineral. However, trace of chemical impurities may be incorporated as defects in crystal lattice. One of the most common is the Si<sup>4+</sup> substitution with a trivalent ion (like Al<sup>3+</sup> or B<sup>3+</sup>) and a H<sup>+</sup> or by 4H<sup>+</sup> and LiOH (Stalder and Neuser, 2013). These substitutions can be revealed by IR absorption where specific bands can be distinguished. As the formation of the different defects is dependent on pressure, temperature and chemical system, IR spectra could serve as a formation condition, and provenance tool, i.e. the total amount of defects can be used to discriminate between an igneous (>5 ppm) and a non-igneous source (<5 ppm) (Stalder et al., 2014; Stalder et al., 2017; Jaeger et al., 2019).

In provenance studies, different researchers used to verify changes in source areas by the heavy mineral assemblage. However, this method is time consuming because heavy minerals need to be concentrated as their amount is very limited in the rock samples (about 1%) and successively a counting method, or chemical analyses or other spectroscopies are needed to determine the different phases. In the SE Alps and Outer Dinarides flysch basins, several studies have been done in order to determine the sources of sediments. Works on heavy minerals like garnet and chromite suggested

different sources of the sediments for the basins (Lenaz et al., 2000; 2018). On the contrary, quartz is the second most abundant mineral of the crust so that it can be very abundant in sandstones and consequently it is very easy to select different grains for further studies. The main goal of the project is to try to verify changes in the provenance areas of the sediments filling the Julian, Brkini, and Kvarner Islands Basins by using quartz crystals.

During the Mesozoic era ( $251.0 \pm 0.4$  Ma ago –  $65.5 \pm 0.3$  Ma ago) almost all the Europe was covered by a shallow tropical sea with lagoons and coralline islands (rudists reef). In this environment, mainly carbonate platform sediments deposited, these carbonates are nowadays the main rock constituent of the Southern Alps, Dolomites, Classical Karst and Dinarides. Jurassic extensional activity due to the Western Tethys opening and the beginning of the North-Atlantic Rift, modified the seafloor creating a horst and graben morphology and the Piedmont-Ligurian Ocean with formation of oceanic crust. This extensional activity was not long-lasting, in fact during Late Mesozoic and Cenozoic, the breaking of Pangea caused the collision between African and Eurasian plates triggering Alpine orogeny. The subduction and the orogeny formation caused the creation of several foreland basins around the Alps arc. These basins collected the sediments eroded from the newborn reliefs.

Samples from the basins have been collected at different positions in the sedimentary log representing different moments in the sedimentation process. All of them are lithic wackes according to sandstones

classifications. The main constituents are quartz and calcite; minor constituents are plagioclase, clay minerals and dolomite; K-feldspar and micas are even rare.

For the detection of the above mentioned OH-defects FTIR (Fourier-Transform InfraRed spectroscopy) with cross polarized measurements of spectra has been used. However, the largest portion of OH is incorporated in water as liquid inclusion, that appears a very broad absorption spectrum that interfere with OH related bands. To avoid this problem, Stalder and Konzett (2012) found that almost all the OH-defects are orientated parallel to ordinary refractive index. The water in fluid inclusions is isotropic and can be estimated with the absorption parallel to the extraordinary index and can be eliminated by subtraction. The so found difference shows only the OH related to the substitution and can also be quantified. In order to measure spectra parallel to both refractive indices, crystals have been aligned to the c-axis in a thermoplastic resin and polished on both sides. Optical orientation has been checked by polarizing microscope with orthoscopic and conoscopic illumination (which allows to obtain the so called “flash figure”). Absorption spectra have been recorded using a spectrometer coupled to a polarizing microscope. On each specimen, two measurements on the same spot have been performed, with a 90° rotation of the polarizer. Raw data has been imported and tabulated, the difference has been calculated and all the spectra have been plotted for interpretation and quantification.

FTIR measurements have been run during a one-year exchange period at Natural History Museum of Stockholm (Sweden), with the tutorship of co-supervisor Prof. Henrik Skogby which is a world leader in water content in NAM and IR spectroscopy.

For each of the nine samples, 20 quartz crystals have been analysed. Typical absorption spectra related to OH-defects with a neat predominance of the Al-related substitution peak have been recognized in almost all of the 180 crystals. Different occurrence of other peaks (B-, Li-, and 4H-related), and difference in the peaks' areas suggest different sources for the sediments. Julian Basin's quartz shows differences in the supply source within the succession: the oldest ones (JB5 and JB1) show an almost 1:1 ratio between igneous and non-igneous origin; samples JB10 and JB17 show a change with a predominantly igneous source. Samples JB5, JB10 and JB17 are the only samples where it is possible to find OH-defects higher than 50 ppm. The youngest samples (JB23 and JB26) have a neat predominance of a non-igneous source (about 75%; Bernardi et al., 2022). Brkini samples show again a difference in the source with the older BK41 having an igneous source more abundant than in the younger BKNV (60% and 40%, respectively). Samples from the Kvarner Islands Basin indicate a predominantly non-igneous source (DOB) while in RAB1 the non-igneous source seems to be clearly prevalent, even if only few clear spectra were obtained.

Cathodoluminescence is caused by the interaction of an electron beam with a solid, which also generates backscattered and secondary electrons and characteristic X-rays. Because luminescence of solids is dominated by defect luminescence, cathodoluminescence enables visualization of the real (defect) structure of minerals and materials. The defects causing cathodoluminescence can be related to either lattice defects (vacancies, broken bonds, etc.) or to the structural incorporation of certain trace elements (e.g.,  $Mn^{2+}$ ,  $REE^{2+/3+}$ ,  $Cr^{3+}$ ). Quartz may contain a couple of defects due to vacancies of oxygen or silicon, oxygen excess, or the incorporation of several trace elements such as Al, Ti, Ge, Fe, P, H, Li, Na (Götze, 2012). Those defects cause a range of luminescence emission bands in the ultraviolet, visible, and infrared region that can be related to specific conditions of formation. Cathodoluminescence analyses have been performed at the University of Padua. Unfortunately, the results were not solid and clear enough to prove and give some sort of information about the origin of the sediments. All the analysed quartz grains show almost the same CL effects.

On the same grains, trace elements such as Al, Li, B, Ge, Ti, and others have been analysed and quantified by LA-ICP-MS at ETH in Zurich. It is interesting to notice that there are some similar trends for Ge, Al, Li, Na and K increasing from JB5 to JB17, while all the other samples show a similar behaviour with contents similar to those of JB5. Boron differentiates

all the Julian Basin samples ( $B > 2$  ppm) from those of Brkini and Kvarner Islands samples ( $B < 2$  ppm).

Regarding the Al trace content, it is important to notice that it follows the Al-related OH-defects' trend, demonstrating the possible existence of a correlation between the two analytical methods. The Ti concentration has been used to calculate the crystallization temperature ( $T_c$ ) of the quartz crystals via TitaniQ equations. The non-igneous origin of quartz in Kvarner Islands samples seems to be confirmed by these temperatures, in fact, more than 50% of the grains show  $T_c$  lower than 500 °C (about 90% lower than 650 °C). Interestingly, in JB5 crystals where there is a certain amount of crystals with more than 50 ppm OH-defects, there is the presence of 5% of crystals with a  $T_c$  higher than 800 °C.

An integrated approach linking OH-defects and trace element contents seems to be very effective in determining different source areas for the detrital quartz crystals present in a sedimentary sequence. The present study demonstrates it has been possible to discriminate igneous vs. non-igneous sources and it is possible to recognize different supplies within the sedimentary pile giving new knowledge to the story of these areas.

# CONTENTS

CHAPTER 1. INTRODUCTION .....	2
CHAPTER 2. AREA OF STUDY.....	6
2.1 Geographical framework .....	6
2.2 Geological setting.....	6
2.3 Regional geology .....	8
2.4 Julian Basin .....	12
2.5 Brkini Basin.....	15
2.6 Kvarner Islands Basin .....	18
2.7. Previous provenance studies .....	20
CHAPTER 3. MATERIALS AND METHODS.....	30
3.1 Samples .....	30
3.2 Fourier Transform Infrared Spectroscopy.....	33
3.2.1. Previous studies .....	36
3.3 Cathodoluminescence .....	39
3.3.1. Previous studies .....	40
3.4 Laser Ablation-Inductively Coupled Plasma-Mass Spectrometry .....	43
3.4.1. Previous studies .....	45
3.5 Methodology .....	46
CHAPTER 4. RESULTS .....	52
4.1 OH-defects.....	52
4.2 Cathodoluminescence .....	57
4.3 Trace elements.....	58
CHAPTER 5. DISCUSSIONS.....	61
5.1. OH-defects.....	61
5.2. Cathodoluminescence .....	66
5.3. Trace elements .....	68
CHAPTER 6. CONCLUSIONS .....	86
APPENDICES .....	89
REFERENCES .....	162

## CHAPTER 1. INTRODUCTION

In the past ten years, some studies found that in quartz (a nominally anhydrous mineral or NAM) there is a certain amount of water (in the form of OH) due to crystal lattice defects. In contrast to other abundant minerals, quartz does not form solid solutions and it is considered a pure mineral. However, trace of chemical impurities may be incorporated as defects in crystal lattice. One of the most common is the Si<sup>4+</sup> substitution with a H<sup>+</sup> and a trivalent ion (like Al<sup>3+</sup> or B<sup>3+</sup>) or by 4H<sup>+</sup> and LiOH (Stalder and Neuser, 2013). These substitutions can be revealed by IR absorption spectroscopy where specific bands can be distinguished. As the formation of the different defects is dependent on pressure, temperature and chemical system, IR spectra may serve as a formation condition, and provenance tool, i.e. the amount of Al-related defects can be used to discriminate between an igneous (>5 ppm) and a non-igneous source (<5 ppm) (Stalder et al., 2014; Stalder et al., 2017; Jaeger et al., 2019). For the detection of the above mentioned OH-defects FTIR (Fourier-Transform InfraRed spectroscopy) has been used with cross polarized measurements of spectra. The largest portion of OH is incorporated in water as liquid inclusion, that appears a very broad absorption spectrum that interfere with OH related bands. To avoid this problem, Stalder and Konzett (2012) found that almost all the OH-defects are orientated parallel to the direction of the ordinary refractive index. The water in fluid inclusions is isotropic and can be estimated with the absorption parallel to the extraordinary index and can be eliminated by

subtraction. The so obtained difference spectrum shows only the OH related to the substitutions, which can also be quantified. In order to measure spectra parallel to the directions of both refractive indices, crystals have been aligned to the c-axis in a thermoplastic resin and polished on both sides. The orientation has been checked by polarizing microscope with orthoscopic and conoscopic illumination (which allows to obtain the so called “flash figure”). Absorption spectra have been recorded using a spectrometer coupled to a polarizing microscope. On each specimen, two measurements on the same spot have been performed, with a 90° rotation of the polarizer. Raw data has been imported and tabulated, the difference has been calculated and all the spectra have been plotted for interpretation and quantification. FTIR measurements have been run during a one-year exchange period at Natural History Museum of Stockholm (Sweden), with the tutorship of co-supervisor Prof. Henrik Skogby which is a world leader in water content in NAM and IR spectroscopy.

Cathodoluminescence is caused by the interaction of an electron beam with a solid, which also generates backscattered and secondary electrons and characteristic X-rays. Because luminescence of solids is dominated by defect luminescence, cathodoluminescence enables visualization of the real (defect) structure of minerals and materials. The defects causing cathodoluminescence can be related to either lattice defects (vacancies, broken bonds, etc.) or to the structural incorporation of certain trace elements (e.g.,  $Mn^{2+}$ ,  $REE^{2+/3+}$ ,  $Cr^{3+}$ ). Quartz may contain a couple of defects due to vacancies of oxygen or silicon, oxygen excess, or the incorporation of

several trace elements such as Al, Ti, Ge, Fe, P, H, Li, Na (Götze, 2012). Those defects cause a range of luminescence emission bands in the ultraviolet, visible, and infrared region that can be related to specific conditions of formation. Cathodoluminescence analyses have been performed at the University of Padua.

Trace elements such as Al, Li, B, Ge, Ti, and others have been analysed and quantified by Laser Ablation Inductively Coupled Plasma Mass Spectrometry (LA-ICP-MS) at ETH in Zurich. There is a limited number of ions which can substitute for Si<sup>4+</sup> in the crystal lattice because of its small size and its high valence. The structural incorporation in a regular Si<sup>4+</sup> lattice position was proved by Weil (1984; 1993) for Al<sup>3+</sup>, Ga<sup>3+</sup>, Fe<sup>3+</sup>, Ge<sup>4+</sup>, Ti<sup>4+</sup> and P<sup>5+</sup>. Among them, Al is the most frequent trace element in quartz (up to 1000 ppm), which is due to its common occurrence in the Earth's crust and the similar ionic radii of Si<sup>4+</sup> and Al<sup>3+</sup>.

Titanium and aluminum are the most important trace elements since their content can be used to differentiate between different quartz types. Hydrothermal and pegmatitic quartz is characterized by lower crystallization temperatures and Ti concentrations. Rhyolitic quartz is characterized by the lowest Al abundance, the highest crystallization temperatures, and lower Al/Ti ratios. Aluminum, lithium, and hydrogen are most frequent in hydrothermal and metamorphic quartz, while magmatic quartz is generally enriched with Ti (Shah et al., 2022). In addition to these, Ti content can be used as a geothermometer for crystallization temperature (TitaniQ) (Wark & Watson, 2006).

Trace elements in quartz can be used also to discriminate within different granites. The contents of Al, Ge and Rb generally increase in the course of magmatic fractionation, while the contents of Ti decrease. The Ge/Ti value can be taken as a valuable indicator of fractionation of granitic melt from which quartz crystallized (Breiter et al., 2020).

During the Late Mesozoic and Cenozoic, the breaking of Pangea caused the collision between the African and Eurasian plates triggering Alpine orogeny. The subduction and the orogeny formation caused the creation of several foreland basins around the Alps arc. These basins collected the sediments eroded by water from the newborn reliefs. Among these, there are the Julian, Brkini and Kvarner Island Basins for which several papers regarding the heavy mineral content have been published (Lenaz, 2008; Lenaz & Princivalle, 2002; Lenaz et al., 2000; 2001; 2003; 2018; Velicogna, 2020; Garlatti, 2022-23). However, this method is time consuming because heavy minerals need to be concentrated as their amount is very limited in the rock samples (about 1%) and successively a counting method, or chemical analyses or other spectroscopies are needed to determine the different phases. On the contrary, quartz is the second most abundant mineral of the crust so that it can be very abundant in sandstones and consequently it is very easy to select for further studies. The main goal of this PhD thesis project is to reconstruct the provenance area of the most abundant mineral in the sandstones of Julian, Brkini and Kvarner Islands Basins by adopting several techniques that could be useful in determine the sources of detrital quartz crystals.

## CHAPTER 2. AREA OF STUDY

### 2.1 Geographical framework

The area of study is located between the north-eastern Italian region of *Friuli-Venezia Giulia*, the western part of Slovenia including the *Goriška statistična regija (Statistical Region of Gorizia)*, and the north-western part of Croatia including *Istarska županija (Istria County)*, and *Primorsko-goranska županija (Primorje-Gorski Kotar County)*.

The zone embraces the south-eastern portion of the Alpine arc (Carnic and Gaital Alps, Julian Alps and Prealps, and Slovenian Prealps), the Istrian peninsula, and the isles of Krk and Rab within the Kvarner Gulf.

### 2.2 Geological setting

During the Mesozoic Era, and especially from the Middle to the Upper Triassic ( $245.9 \pm 2.0$  Ma ago –  $199.6 \pm 0.6$  Ma ago) almost all the area of study was covered by a shallow tropical sea with lagoons and coralline islands. In this environment, mainly carbonate platform sediment were deposited, and these carbonates are nowadays the main rock constituent of the Southern Alps, Dolomites, Classical Karst, and Dinarides (Doglioni & Flores, 1997).

Jurassic extensional activity due to the Western Tethys opening and the beginning of the North Atlantic Rift, modified the seafloor creating a horst and graben morphology (Robertson & Karamata, 1994; Channell & Kozur, 1997) and the Piedmont-Ligurian Ocean with formation of oceanic crust.

In the higher parts continued the carbonate platform deposition, while in the depressed zone pelagic sediments like micritic limestones and turbidites were deposited. Some examples of the pelagic deposits are the micritic limestones of the Rosso Ammonitico (Middle Jurassic), Maiolica (Upper Jurassic – Lower Cretaceous), and Scaglia Rossa formations (Lower Cretaceous) in Lombard and Belluno Basins. The Trentino platform partially drowned and the deposition of Rosso Ammonitico and Maiolica (locally named ‘Biancone’) begun, these micritic limestones are typical of basins with a depth around 300-200 meters (Lukeneder, 2011). The Friulan platform did not drown so the deposition of coralline carbonate platform and rudists reef in the Classical Karst zone continued until Eocene.

This extensional activity was not long-lasting, in fact during Upper Mesozoic and Cenozoic, the breaking of Pangea caused the collision between African and Eurasian plates triggering Alpine orogeny, which still continues nowadays. Extending from Atlas Mountains in North Morocco, through European Pyrenees, Alps stricto sensu, Dinarides, Hellenides, Carpathians, Taurus in Turkey up to Zagros chain in Iran, the Alpine orogeny lifted up many portions of the Mesozoic seafloor. Mesozoic carbonates uplifted by the Alpine orogeny are now the main rock constituent of Southern Alps, Dolomites, Julian, and Carnic Alps, and Outer Dinarides.

Actually, in the first phases of the collision, the remains of the Piedmont-Ligurian oceanic crust were subducted beneath the Adria plate, a peninsular piece of continental crust of the African plate (Channell &

Horvath, 1976). Some fragments of the oceanic crust had obducted over the Eurasian continental crust and can be still recognized by the ophiolitic sequences in the Penninic nappes (NW Italy and SW Switzerland). The subduction also caused an arc-type volcanic activity and some of these volcanic rocks can be found among the ophiolites of the Penninic nappes. When all the oceanic crust was subducted, the first continental collision between Adria and Eurasia occurred; this phase, called Eo-Alpine, is sometimes considered as the first phase of Alps' formation (Lawrence et al., 1995; Channel & Kozur, 1997). The softer marine sediments and the deformed part of Adria plate uplifted by the collision form now the Austroalpine nappes and Southern Alps. Separation between Adria and Eurasian plate is recognizable in the Periadriatic Lineament, a W-E complex system of sub-vertical dipping reverse faults running for about 1000 km from NW Italy to Hungary. Within the Eastern Alps, the Periadriatic Lineament marks the border between the Southern Limestone Alps, made of deformed and slightly metamorphosed sedimentary rocks, and the Central Eastern Alps, constituted by high-grade metamorphic rocks and granite batholiths.

### **2.3 Regional geology**

The subduction and the orogeny formation caused the creation of several foreland basins around the Alps arc. These basins collected the sediments eroded from the new-born reliefs. In the early stage it is said that the basin is *underfilled*, during this phase mixed deep sea and terrigenous sediments

are deposited. The clastic fraction of sediments usually accumulates on the continental shelf; due to over accumulation, currents or earthquake events, the mass of sediments can fall quickly downwards to the abyssal plain creating undersea avalanches or turbidity currents. The deposition of the turbidity currents alternate with open sea pelagic deposits is commonly known as ‘flysch’. As the collision continue, the basin is filled with more clastic sediments entering the *overfilled* phase, it starts the deposition of ‘molasse’ sedimentary rock. It could happen that the foreland basins are uplifted themselves before the overfilled phase, emerging from the sea and showing the flysch rocks only. During the continental collision, tectonic activity could modify and deform the structure and the sedimentary succession creating folds and thrusts.

Northern part of the area shows paleokarstic structures suggesting emersion events in the Lower Jurassic (Venturini et al., 1992). In the southern parts these emersion forms are rare suggesting a tilting process of the platform block. The Middle Jurassic is characterized by depositions of oolitic calcarenite and pelagic limestones as result of a subsidence (Tunis & Venturini, 1984). In the Upper Jurassic, due to a retreat of the carbonate platform, the subsidence of the area has increased. The main deposits were composed by carbonate breccia, showing a continental slope sedimentation environment. In some part of the area, however several hiatus have been observed, probably due to tilting movements of slope blocks. Again, in the Lower Cretaceous, rates of sedimentation are increased due to strong

subsidence. Successively, major hiatus between Cretaceous and Palaeogene carbonate existing in the area were filled by bauxite deposits (Gregorić et al., 1998; Peh & Kovačević Galović, 2014). According to Mindszenty et al. (1995) their occurrence is related to the predominance of tectonic activity over eustasy.

During the Eo-Alpine phase, the area of study was characterized by many foreland basins. We can recognize the following main basins from NW to SE (Figure 2.1):

- Julian: Maastrichtian (Upper Cretaceous) – Middle Eocene (Ogorelec et al., 1976; Tunis & Pirini Radrizzani, 1987)
- Brkini: Lower – Middle Eocene (Pavlovec et al., 1991; Tunis & Venturini, 1996)
- Istrian and Kvarner Islands: Middle – Upper Eocene (Magdalenić, 1972).

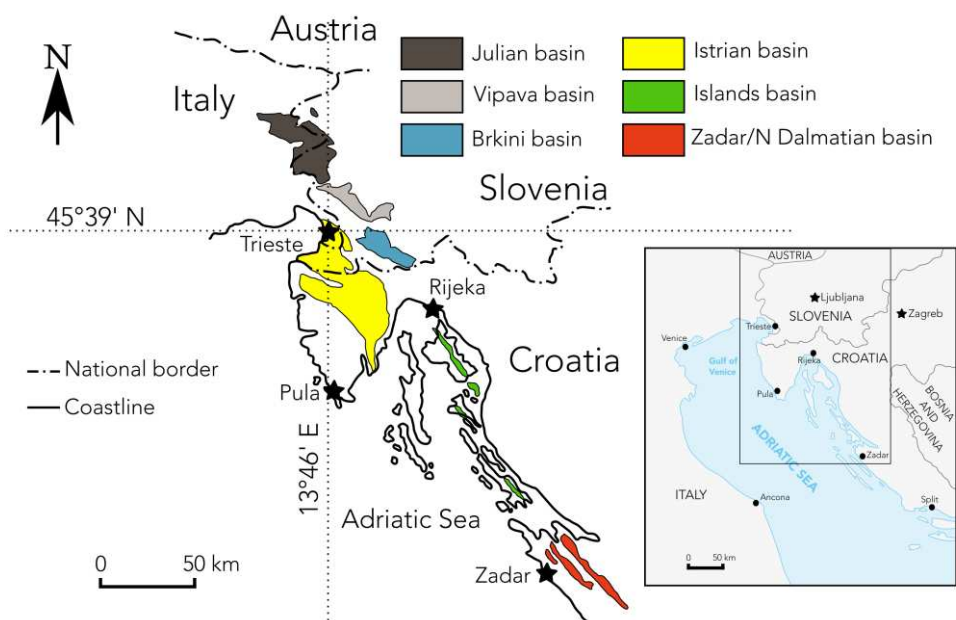


**Figure 2.1.** Flysch deposits of the SE Alps and Outer Dinarides (redrawn from Velicogna, 2020 and according to Lenaz et al., 2003).

As can be seen from the dating, the basins are not contemporary. Progressive northward movement of the Adria plate caused a southward shifting of basins (Csontos & Vörös, 2004) with the gradual emersion of the northernmost basins. As proof of this uplifting we can find bauxite deposits in the Istrian zone testifying the subaerial bauxitic weathering of the carbonates (Gregorić et al., 1998; Lenaz & Princivalle, 2002).

Several studies have been done in order to determine the source of the sediments of the basins. At the state of the art for the Julian Basin most sediments seem to come from the North (Venturini & Tunis, 1992) but there are some evidence of a Dinaric provision basing on Cr-spinels (Lenaz et al., 2000). Brkini Basin source is the most controversial because, according to sedimentary structure, some authors suggest a NW flux of sediment (Tunis & Venturini, 1996) while others suggest a SE flux (Orehek, 1972, 1991). More recent studies based on heavy minerals propose a double source from both the domains and the possibility of a recycling of sediments from other near basins (Lenaz et al., 2001, 2018). The Istrian Basin can be divided in three sub-basins: the Trieste/Koper, the Pazin, and the Kvarner Islands ones. For the Trieste/Koper, a NW source is supposed (Marinčić et al., 1996) with some supply from the Dinarides (Lenaz & Princivalle, 1996; Lenaz et al., 2003); the Pazin Basin and the Kvarner Islands Basin are supposed to belong almost entirely to the Dinaric domain but with some Alpine contamination (Magdalenić, 1972; Lenaz et al., 2003).

## 2.4 Julian Basin

The Julian Basin (JB) is a sedimentary basin that has been active from the Maastrichtian (Upper Cretaceous) to the Middle Eocene. It extends between Italy and Slovenia and goes from the Julian Prealps in Bovec area at North to the Vipavska Dolina at South, its oriental limit is drawn by the Tolmin Mountains in Slovenia while southwestern border is represented by the Friulan Carbonate Platform. The basin shows a stretched form with a NW-SE direction of elongation (Figure 2.2).

A new tectonic phase in Maastrichtian caused southward movements of platform margin and slope. These events started the main turbiditic deposition that occurred until Middle Eocene and reached a maximum thickness of 4000 m. Initially made by material coming from collapsing of the Carbonate platform forming a breccia, at the end the deposition of hemipelagic siliciclastic strata started. Siliciclastic turbidites are occasionally alternated with carbonate strata from Dinaric Carbonate Platform in regression (Miklavić & Rožić, 2008). The provenance of siliciclastic sediments of Julian flysch is supposed to be located in the nearby North and Northeast areas of the basin, in the South Alpine (Venturini & Tunis, 1992). Rare igneous clasts have been found in the Maastrichtian flysch of the Bovec area (De Min et al., 2007) showing a tholeiitic affinity with arc-type signature. The source area of these clasts has been located in the Internal Dinarides belonging to the Vardar-arc system (De Min et al., 2007).

The stratigraphy of JB has been studied by several researchers (Tunis & Venturini, 1984, 1996; Venturini & Tunis, 1991) and is commonly divided in eight units:

1. Drenchia Unit (Lower Maastrichtian), near Drenchia village, consisting of erosion breccia followed by siltites and calcarenites.
2. Clodig Flysch (Lower Maastrichtian), Iudrio Valley and Obranche. 250 m thick, made of calcarenites, calcilutites with carbonate and marls interbedded; rare sandstone in lowest part.
3. Iudrio Flysch (Lower – Upper Maastrichtian). Sandstones, marls, calcarenites and calcilutites.
4. Brieka Flysch (Middle – Upper Maastrichtian), around 40 m thick near Mt. Brieka. Mainly constituted by sandstones and marls, embedded with calcarenites and calcilutites.
5. Calla Flysch (Lower – Middle Palaeocene), Reddish and greenish marls, rare calcarenites and calcilutites. Thickness between 120 m (near Mt. Ioanaz) and 170 m (in the Rodda area, East of Natisone Valley)
6. Flysch “di Masarolis” (Middle – Upper Palaeocene), central-eastern sector of Natisone Valley. Medium thick siliciclastic turbidites of quartz-litharenite and grey marls.
7. Flysch “del Grivò” (Upper Palaeocene – Lower Eocene), from Faeit area, across Natisone Valley and Goriška Brda. Distal siliciclastic and carbonate turbidites, hybrid sandstones. There are several carbonate megabeds (debris flow) such as those of Mt. Ioanaz (MT3), Mt. Staipa

(MT4), Topli Uorch (MT6), Vernasso (MT11), and Porzus (MT15) (Tunis & Venturini, 1987; Ogata et al., 2014; 2019).

8. Cormons Flysch (Lower – Middle Eocene). The succession shows the entire evolution from epibathial turbidites to delta plane facies.

Five samples have been collected (JB1 in Bovec, JB5 in Obranche, JB10 in Podgora, JB17 in Monteaperta, and JB26 in Monte Candia), with JB5 and JB26 representing the bottom and the top of the stratigraphic column respectively (Figure 2.2).

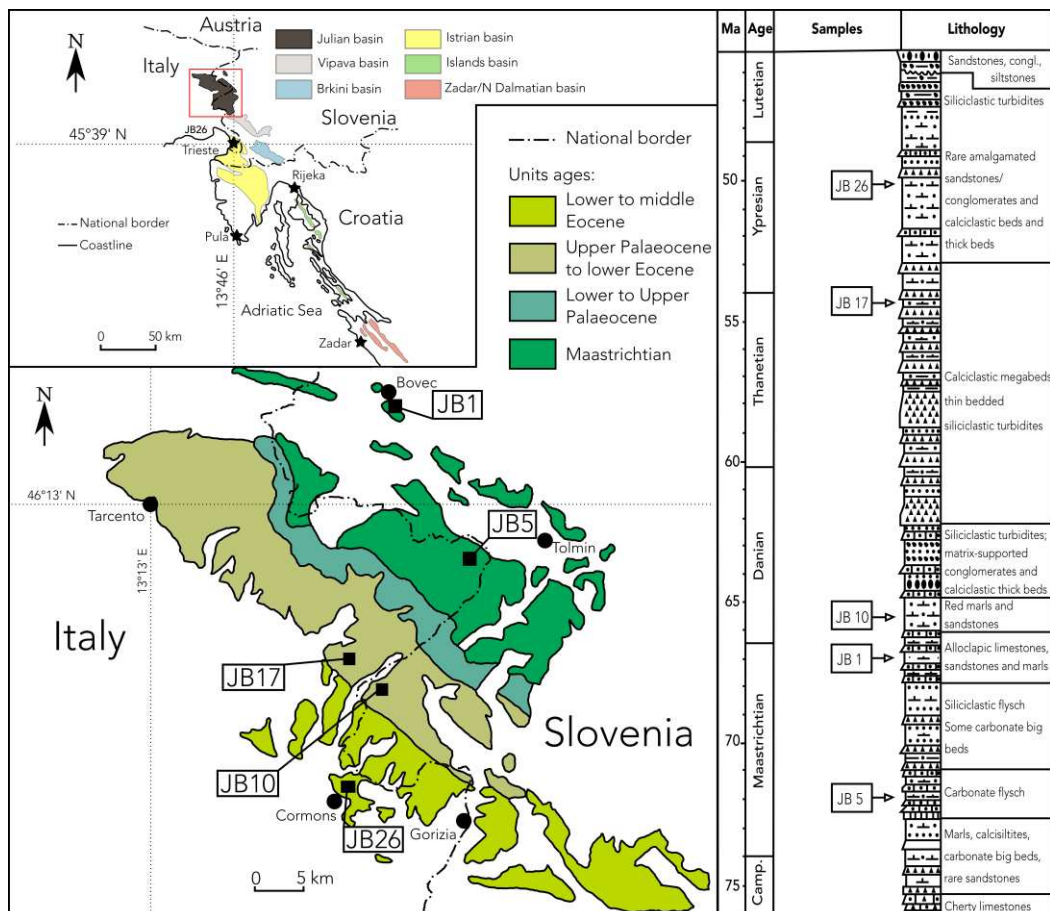


**Figure 2.2.** Geological map of the Julian Basin, position of samples, and stratigraphic column, after Tunis & Uchman, 1996 (redrawn from Velicogna, 2020).

## 2.5 Brkini Basin

The Brkini Basin (BK) occupies a synclinal located in SW Slovenia, with an elongated NW-SE shape (Figure 2.3). Sedimentation was active from the Late Paleocene and in particular flyschoid and molassic material filled the basin during the Eocene to a thickness of about 1000 m (Tunis & Venturini, 1996).

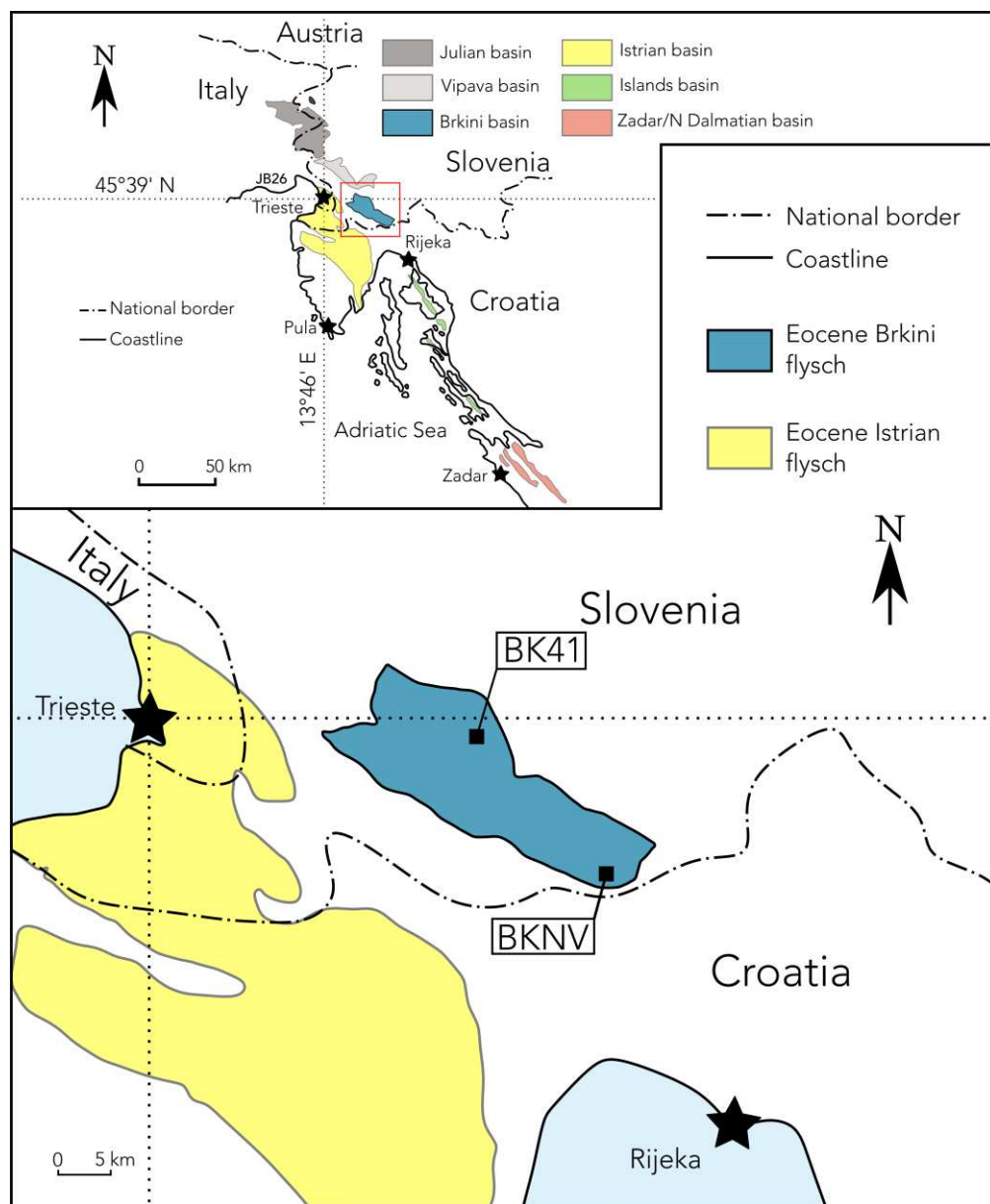


**Figure 2.3.** Simplified geological map of the Brkini Basin area, and position of samples after Cigna (1996-97) (redrawn from Velicogna, 2020).

The basin's structure is quite complex due to the presence of many sub-vertical faults and folds which interrupt the sequence (Velic et al., 1995; Jurkovesk et al., 1996). For these reasons, the stratigraphy of BK has been divided in eight segments without a proper stratigraphic column (Tunis & Venturini, 1996):

1. The basement is composed by an underwater landslide which could be related to a large calciruditic-calcarenite block that crops out South of Ruttars, representing the only re-sedimentation episode of the coeval Cormons flysch (JB).
2. Terrigenous turbiditic deposits (with the presence of large calcareous blocks) embedded with calcarenite strata that show a fining upwards granulometry, becoming marls with strata thickness of over 10 m.
3. Segment composed by an alternation of fine sandstones and marls.
4. Marl-arenaceous flysch rich in bioturbation with frequent hybrid turbiditic strata and bio-calcarenites.
5. Conglomerates related mainly to distal terrigenous turbidites and hybrid turbiditic strata.
6. A series of distal terrigenous turbidites rarely interrupted by thin calcarenite strata.
7. Thickening of the arenaceous fraction with the presence of the first thick conglomeratic sandstone strata.

8. The basin ends with grey-yellowish siltitic strata and silts-marls, which are overlain by thin poorly cemented sandstones with a thickness of ~100 m.

The studies of Orehek (1972; 1991) indicates signals of paleocurrents with main North-West and partially West flow directions, suggesting the basement rocks buried in the Adriatic and Gorski Kotar (Croatia) areas as possible sediment sources. On the contrary, Tunis & Venturini (1996) observed several flute casts suggesting opposite directions, similar to those measured in the Cormons area, Dornberk (Slovenia) and Ajdovščina (Slovenia). The two authors agree with possible paleogeographic link among the Brkini Basin and those located in the nearby western area. This is partially confirmed by Lenaz et al. (2018), observing similarities between garnets coming from deep portions of Brkini and the ones from Julian Basin. In the higher strata meanwhile, they observed garnets without relationships with the JB's ones.

Two samples have been collected (BK41 in Janezevo Brdo, and BKNV in Nova Vas). They represent two different moments of the activity of the basin, with the first from the main stage of flysch sedimentation's activity, and the latter representing the basin's closure (molasse).

## 2.6 Kvarner Islands Basin

The Kvarner Island Basins (KVI) is formally a member of the Istrian Basin which is composed by two other different members, the Trieste-Koper, and the Pazin Basins. The Kvarner Island Basin is represented by Krk, Rab and Pag islands. The Trieste-Koper is mainly composed by the Trieste Province area, in particular the zone just below the High Karst Plateau, together with the San Dorligo della Valle, Muggia, and Koper areas, while the Pazin Basin extends all over the N-NE Istrian Peninsula.

Istrian Basin shows a body with elongated form that suggests that it filled a narrow deep foreland basin. This has been filled from Middle to Late Eocene as testified by the studies of macrofossils, nummulites, and the planktonic foraminiferal biostratigraphy (Babić et al., 2007; Živkovic & Glumac, 2007). The Istrian Flysch basin is composed by the alternation of gravity flow deposits with hemipelagic marls. The low ratio between sandstone and marls thickness suggests that the flysch has been deposited in a distal foredeep.

In the Krk Island, the Eocene flysch mainly fill the central depression of the island, and outcrops along the NE and SW coast as small, stretched bodies in the Dobrinj area in the North, and in the Baška area to the South (Figure 2.4a). The sedimentation of the clastics (marls and sandstones) occurred during the Eocene, filling deep basins (NW–SE elongated) formed during the tectonic movements that resulted in the Dinarides uplift.

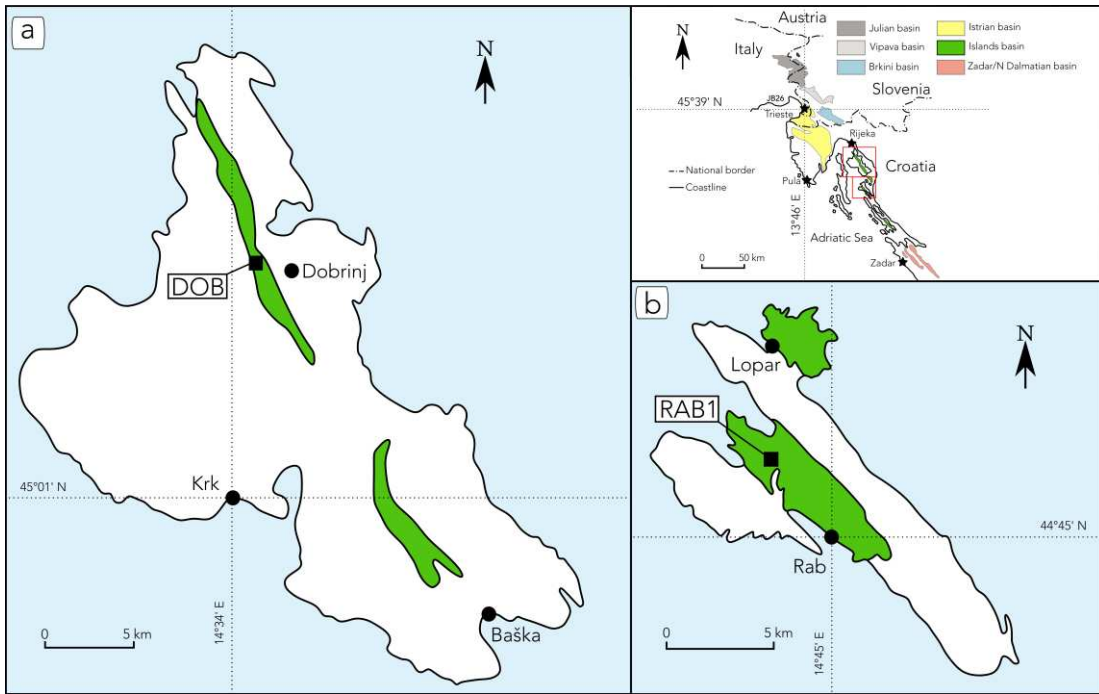


**Figure 2.4.** Geological map of the Kvarner Islands Basins and position of samples in a) Krk (according to Benac et al., 2013), and b) Rab (according to Marjanac & Marjanac, 1991) (redrawn from Velicogna, 2020).

The flysch of the Rab Island has been dated as Middle-Late Eocene (Magaš, 2000), it outcrops along the central body of the island, and in the Lopar peninsula in the NE part of the island (Figure 2.4b).

The rocks can be divided in two units, the upper Lopar Sandstones, and the lower San Marino Marl. They have been interpreted as flysch deposits and shallow tidal-marine sediments. The siliciclastic mineral composition of the sandstones indicates a provenance from the outside of the Dinaric area, probably in the Alps Region (Marjanac & Marjanac, 2007).

Two samples have been collected, one coming from Krk Island (DOB, Dobrinj), and one coming from Rab Island (RAB1).

## 2.7. Previous provenance studies

In addition to the ones before mentioned, many other different studies deal with the mineralogy, including works on heavy minerals, and bulk rock geochemistry have been done.

Kamenetsky et al. (2001), in order to distinguish between spinels from peridotitic and mantle-derived volcanic rocks, suggested to use their  $\text{TiO}_2$  content coupled with the  $\text{Fe}^{2+}/\text{Fe}^{3+}$  ratio. Peridotitic spinels show  $\text{TiO}_2 < 0.2$  wt.% and  $\text{Fe}^{2+}/\text{Fe}^{3+} > 3$ , while volcanic ones show  $\text{TiO}_2 > 0.2$  wt.% and  $\text{Fe}^{2+}/\text{Fe}^{3+} < 4$ . According to this distinction, Lenaz et al. (2000) studied the detrital spinels of the Julian Basin and found that peridotitic spinels are predominant in all the studied samples with the exception of JB17 that has more than 60% of volcanic spinels. Their results, combined with the data on regional ophiolitic occurrence, favour the Internal Dinarides (former Yugoslavia) as the possible source.

The detrital Cr-spinels found in the sandstones in BK and IB show a predominant peridotitic population (Lenaz et al., 2001; 2003). In addition to the sources already suggested for analogous spinels of the JB, in these basins Lenaz et al. (2001; 2003) found Cr-spinels with low Cr# [ $\text{Cr}/(\text{Cr}+\text{Al})$ ], suggesting a lherzolitic affinity to be placed in the External Dinarides. Minerals from BK show similarities with minerals from both JB and IB suggesting supplies from NW and SE, in line with paleocurrent data obtained by both Tunis & Venturini (1996) and Orehek (1972; 1991).

Detrital amphiboles (actinolite, Mg-hornblende, barroisite, and glaucophane) associated with omphacitic pyroxenes have been found in Lower Eocene (about 52 Ma) turbidites of Julian Basin (Lenaz & Princivalle, 2002). Actinolite and Mg-hornblende are derived from low to medium grade metamorphic rocks (metavolcanics in greenschist facies). Barroisite is the ultra-high-pressure type of hornblende and is considered as a marker of retrogressive metamorphism. Glaucophane crystals are representative of high-pressure metamorphic rocks in blueschist facies. Omphacites are related to subsolidus recrystallisation of basic igneous rocks at high-pressure and temperature in eclogite facies. All that mentioned above suggests an oceanic crust material supply. Evidence of mixing between eclogite-derived dacitic magmas and mantle peridotites suggests a suprasubduction zone as a source of the sediments. These minerals are supposed to be supplied from Internal Dinarides, where several ophiolitic bodies outcrop. According to the low amount and distribution of these minerals, Lenaz and Princivalle (2002) suggested that they belong to limited metamorphic bodies exhumed at about 56 Ma during an uplift phase of the Dinarides (Lawrence et al., 1995).

Detrital pyroxenes (i.e., augites and pigeonites) have been found in Trieste-Koper and Krk Island flysch (Lenaz, 2008). These pyroxenes are related to subalkaline parent rocks (within-plate tholeiites; calc-alkaline basalts) crystallised at a pressure between 0 and 5 kbar. According to the chemistry, it seems possible that their source could be the basaltic andesites

of Ljubač in northern Dalmatia. An alternative hypothesis is that these pyroxenes are related to within-plate tholeiites similar to those, actually altered, outcropping in Požeška Gora Mt. In this case, the pyroxenes are the only unaltered representative of this volcanism. The presence of similar pyroxenes in Trieste-Koper and Krk Island flysch, and their absence in BK, suggest that the Krk basin was more linked with Trieste-Koper basin than with Brkini one.

The occurrence of Cr-spinels, pyroxenes and amphibole suggest that the main supply area of the siliciclastic fraction of the Maastrichtian-Eocene turbidites should reside in the Internal Dinarides. The authors identified the suprasubduction zone of the ancient Vardar Ocean as the main source rocks for the detrital Cr-spinel. This supplied detritus acted since the beginning of the sedimentation in the Julian and Brkini Basins. During the Early Eocene, a second input of similar material filled JB, BK, and IB, while only by the Middle Eocene the lherzolite-like spinels have been transported from the External Dinarides into the Brkini and Istrian Basin. Furthermore, the presence of the clinopyroxene only in the IB suggests that the basins probably have different supply areas depending on the time of deposition and the location of the trough (Velicogna, 2020).

More recently, a work on trace and RE (Rare Earth) elements in garnets has been done (Lenaz et al., 2018). The authors analysed about 250 garnets from different basins in SE Alps, including Julian, Brkini, and Kvarner Islands ones. According to Mange & Morton (2007), garnets can be subdivided in

different groups characterized by different (almandine + spessartine), pyrope and grossular content. In the studied basins, garnets were preferentially clustered in two different groups (Figure 2.5).

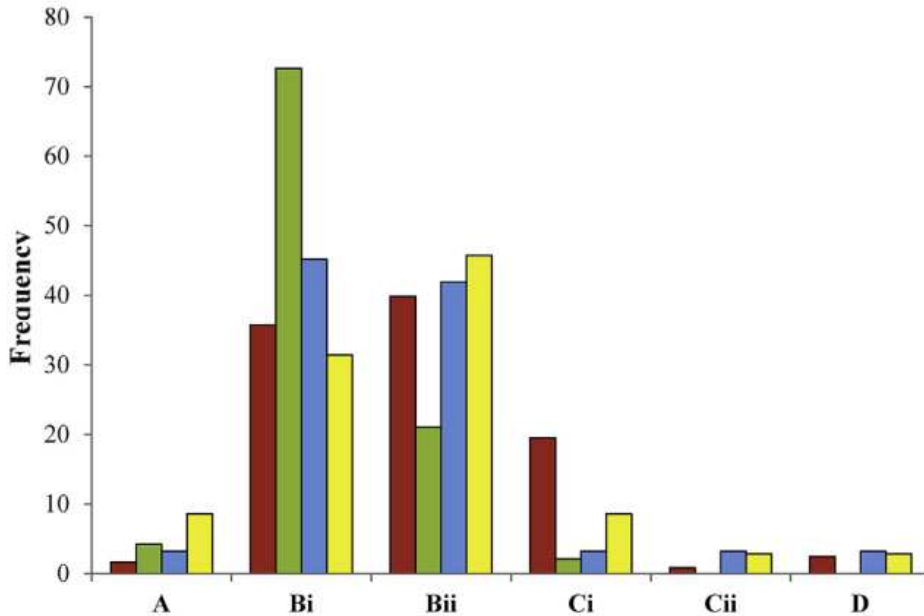


**Figure 2.5.** Frequency of the garnets according to their typology for Julian (red), Brkini (green), Istrian (blue), and Kvarner Islands (yellow) basins (Lenaz et al., 2018). For the garnet classification see in the text.

The first group corresponds to type B garnets, with high Alm + Sp and low-Py, that are derived from amphibolite-facies metasediments (Mange & Morton, 2007). Within them it is possible to further discriminate into Bi ( $X_{Gr} < 10\%$ ) and Bii ( $X_{Gr} > 10\%$ ) suggesting a possible supply from granitoids and metasediments, both types are present in the studied sediments (Lenaz et al., 2018). High-grade metabasic rocks are the main supplier of Type C garnets, high-containing pyrope. Within this group, it is possible a further division in Ci ( $X_{Py} < 40\%$ ) and Cii ( $X_{Py} > 40\%$ ) that can determine to relative contribution of mafic and ultramafic metamorphic sources. Other groups are

type A (high-grade granulite-facies) and type D from very low grade metabasic rocks.

In the Julian and Istrian basins, supplies are from amphibolite-facies rocks and mafic and ultramafic metamorphic rocks, while in the Brkini basin the latter are almost missing. Moreover, in the Julian and Istrian basins, supplies from skarns, very low-grade metabasites, or from ultra-high temperature metamorphosed calc-silicate granulites are present. Among these different groups, LA-ICP-MS analyses showed that trace element content can be very different in almandine-rich garnets from the different sources. In particular, the source that supplied the Julian Basin is significantly different from that of the Istrian Basin. From the Cretaceous to the Palaeocene the main supplies of Bi-type garnets derived from an area where feldspar-free garnet-bearing rocks were exposed. Successively, Bi-type garnets were supplied from an area where feldspar-garnet-bearing rocks were exposed. The presence of garnets from feldspar-free rocks in the Brkini and Istrian basins can be ascribed to both recycling of material from the Julian Basin as well as direct input from the same areas that supplied the Julian Basin (Lenaz et al., 2018). It is important to point out that, according to garnet chemistry, it was possible to assign to sample BK41 an age similar to that of the Flysch of Grivò/Cormons while BK35 and BKNV are younger.

A work on rutile and zircon added new knowledge about the dynamics of all the area (Velicogna, 2020). The data suggest that the rutile have been

crystallized mainly in amphibolite-eclogite facies and only a minority in greenschist and granulite facies. All the basins share sources with high Nb content suggesting a metapelitic-felsic nature, while JB, IB and partially BK, seem to share metamafic source rocks (Velicogna, 2020). These lithologies can be easily found all together in an ophiolitic suite. Furthermore, only few rutile with high Ta content have been recognized in BK and JB, possibly suggesting a pegmatitic origin. Even though, the main groups of temperature are similar for the three basins, the different ratio of the highest peaks suggest that the source rocks are similar but located in different areas (Velicogna, 2020).

Generally, the zircon geochemistry suggests a mainly magmatic origin for the studied crystals, but hydrothermal and metamorphic signatures are also present. Their crystallization ages span from the Late Cretaceous ( $81 \pm 4$  Ma) to the Archean ( $3127 \pm 27$  Ma), without the presence of Cenozoic crystals (Velicogna, 2020). Following the Belousova et al. (2002) classification, most of the crystals show granitoid origin, while doleritic, basaltic, carbonatitic, and syenitic-monzonitic are subordinates (Figure 2.6).

Furthermore, most of the crystals show continental affinity overlapping the post-collision granitoids area, and plot in the magmatic arc array suggesting that the source could have been involved in an active and/or past subduction setting (Grimes et al., 2015).

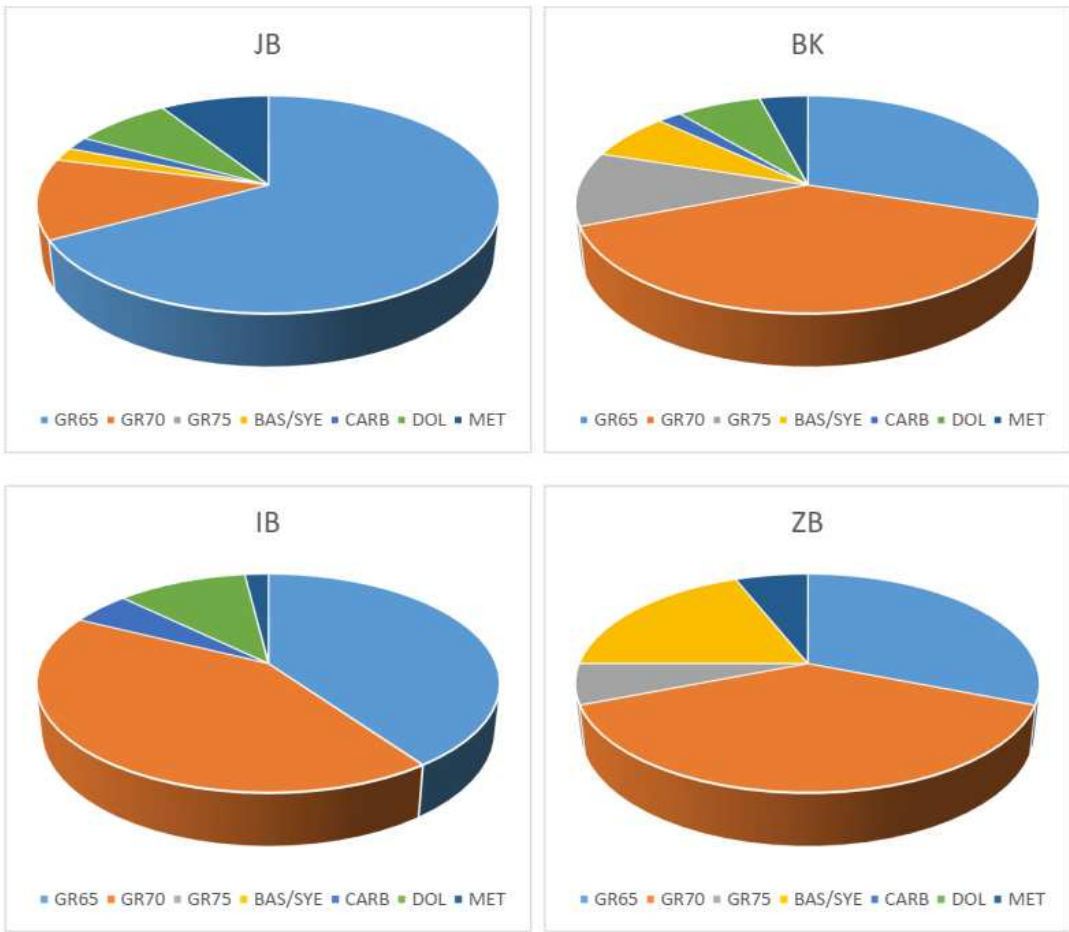


**Figure 2.6.** Pie chart representing the zircon host-rock affinity percentage for every basin. Crystals have been divided in metamorphic (MET); crystallized in granitoids with silica content <65%, between 70-75%, and >75% (GR65, GR70, GR75, respectively); basaltic (BAS); carbonatic (CARB); doleritic (DOL); and syenitic-monzonitic (SYE) according to Belousova et al. (2002). ZB indicates Zara Basin, which is not matter of study in this work (Velicogna et al., 2020)

Garlatti (2022-23) recently studied the tourmalines from JB and BK. From a quantitative point of view, the analyses showed that the number of tourmalines increases dramatically from the JB (1-14 crystals) to the BK (30-100 crystals) even if the percentages of heavy minerals in the two basins are similar (0.2-1.3 in JB; 0.4-1.1 in BK). The analyses of the different types of tourmalines found in the samples from the two basins demonstrated different rock sources. Tourmalines from JB are correlated almost exclusively with different Al-bearing metapelites. For the crystals coming from BK, the source rocks are metapelites (as for JB), but tourmalines from

metacarbonates, metapyroxenites, granitoids, and hydrothermally altered granites are present too (Garlatti, 2022-23). These results suggest both a quantitative and qualitative change in the source supply between JB and BK.

A work on igneous clasts in Bovec (JB) conglomerates found that they have a strong arc-type signature with chemical affinities with tholeiites from Internal Dinarides as well as Jurassic magmatism of the Dinaric-Carpathian region. Protoliths of these clasts are probably belonging to the Vardar arc system (De Min et al., 2007).

As far as concern the geochemistry of the basins, De Min et al. (2014) confirmed that the first arenaceous strata of the JB are strongly chemically influenced by the disaggregation of metamorphic and non-metamorphic rock types related to the ancient Vardar Sea closure, where Island Arc (IAB) and Back-arc Basin (BABB) basalts related rock types were generated. At about 56 Ma, the sample JB16 (coeval of here analysed JB17) testifies the strong involvement of continental upper crustal lithotypes (Figure 2.7), possibly the Driva-Ivanjica microcontinent (according to the reconstruction by Lenaz et al. 2003) as a consequence of the rapid arising of the Dinarides (Lawrence et al., 1995).

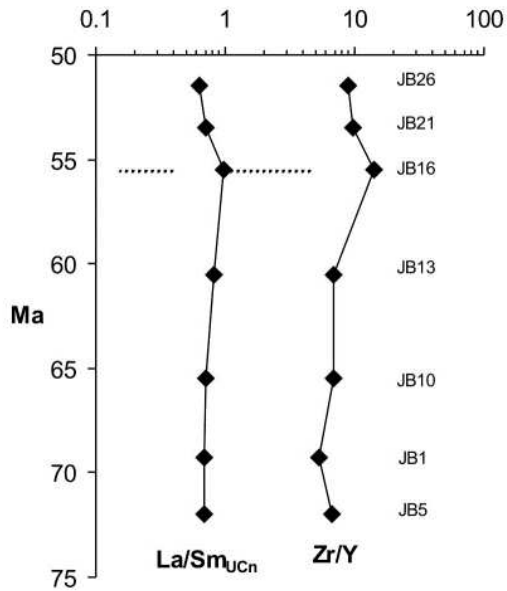


**Figure 2.7.** Stratigraphic age vs.  $\text{La}/\text{Sm}$  and  $\text{Zr}/\text{Y}$  ratios for JB (De Min et al., 2014).

After this first stage, a new moment of upwelling involved the Julian sediments which contributed, with recycled materials, to the Brkini Basin sediments. Moreover, other protolith rock types, representing the main source of the Istrian Basin, begin to be significant (Lenaz et al., 2001).

Finally, a preliminary work on OH-defects on detrital quartz of JB has already been done (Bernardi et al., 2022). Grains from samples JB1, JB17, JB23, and JB26 were analysed with FTIR in order to calculate and speciate their OH-defects and use them as a provenance tool (Figure 2.8). JB1 is the oldest sample of the analysed set, and shows moderate variability in defects, with an abundance of Al-related ones. A slightly more igneous source was suggested. Samples JB23 and JB26 (which are close both geographically and stratigraphically) display similar behaviour with a great number of grains bearing Al defects but corresponding to low OH content. An almost solely

metamorphic origin can be suggested for these samples. JB17 shows a different patterns than the others, with greater defects variability and higher OH content. Then, a main igneous source can be suggested (Bernardi et al., 2022).

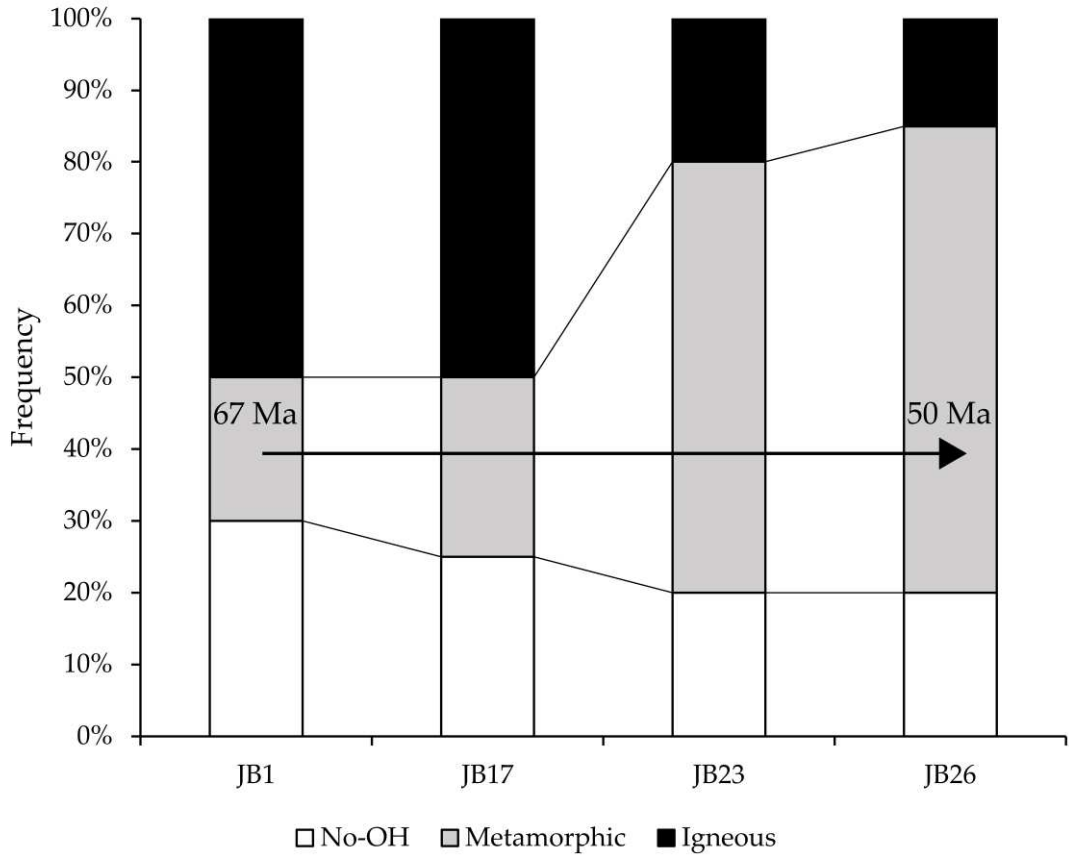


**Figure 2.8.** Frequencies of quartz from igneous and non-igneous source for JB samples. As igneous quartz was considered all grains with OH >5 ppm according to Stalder & Konzett (2012) and Stalder (2014) (Bernardi et al., 2022).

## CHAPTER 3. MATERIALS AND METHODS

### 3.1 Samples

Nine rock samples were selected for this study: five from Julian Basin (JB), two from Brkini Basin (BK), and two from Kvarner Islands Basin (KVI). Julian Basin is represented by samples JB1 (Bovec), JB5 (Obranche), JB10 (Podgora), JB17 (Monteaperta), JB26 (Monte Candia). JB5 and JB26 represent the bottom and the top of the stratigraphic column and therefore the oldest and the youngest in age. JB5 and JB1 are dated to be from Maastrichtian, JB10 from Danian, JB17 from Thanetian, and JB26 is dated from Ypresian (Figure 3.1).

Brkini Basin is represented by samples BK41 (Janezevo Brdo) and BKNV (Nova Vas), meanwhile Kvarner Islands Basin is represented by samples DOB (Dobrinj, from Krk Island) and RAB1 (from Rab Island).

Previous studies (Bertolla, 1996-97; Cigna, 1996-97) classified these rocks as lithic greywackes. For JB, the size fraction spans from 0.11 mm to 0.55 mm, being classified within very fine and coarse sand. Texturally the sediments are immature or sub mature, with low sphericity and angular granules. Siliceous lithic fragments to various lithic fragments ratio is between 0.7 and 1.4 (Bertolla, 1996-97). For BK, the size spans from 0.34 mm to 0.80 mm, classified within medium and coarse sand (Cigna, 1996-97). Sediments are immature and sub mature, with low sphericity and angular granules. Siliceous lithic fragments to various lithic fragments ratio is

between 0.25 and 2.05 (Cigna, 1996-97). Rab's sandstones are medium- to coarse-grained calcarenitic sub-greywackes (Mamužić & Milan, 1973). Their internal organization is usually quite complex, as several thinner cross-bedded packages can be distinguished (Marjanac & Marjanac, 2007).

The main mineral constituents are quartz and calcite; plagioclase, clay minerals and dolomite are minor components; K-feldspar (microcline) and phyllosilicates (muscovite, chlorite, and biotite) are very rare (Lenaz et al., 2000). In thin sections, clasts of dolostones, limestones, radiolarites, cherts, diabase, sandstones, quartzites, gneisses and low-grade schists have been recognized (Venturini & Tunis, 1992). Makes exception BKNV that is from the molasse segment and differs from the others for the presence of dolomite instead of calcite.

Heavy minerals are represented by spinel, garnet, tourmaline, zircon, pyrite, amphibole, pyroxene, and staurolite (Lenaz et al., 2000). Cr-spinels, garnets, zircons, rutile, pyroxenes, and tourmaline have been studied in detail by Lenaz et al. (2000; 2018), Lenaz & Princivalle (2002; 2005), Velicogna (2020), and Garlatti (2022-23); while De Min et al. (2007; 2014) studied the volcanic clasts present in the Bovec conglomerate and the geochemistry of the sandstones.

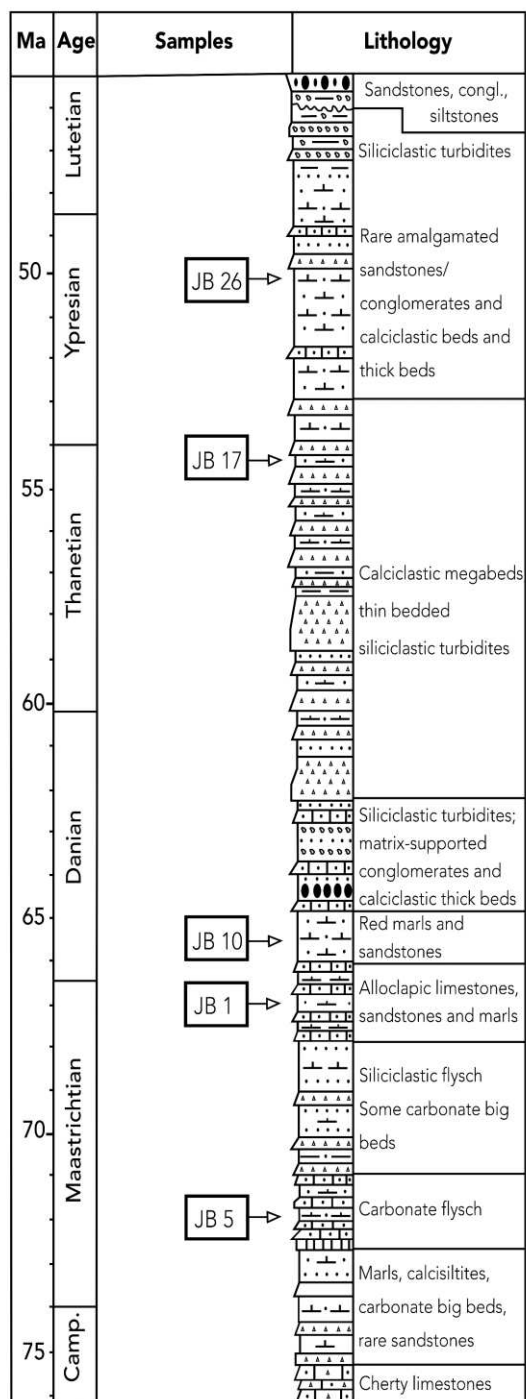


**Figure 3.1.** Stratigraphic column of the Julian Basin (redrawn after Lenaz et al., 2000).

### 3.2 Fourier Transform Infrared Spectroscopy

Infrared radiation (IR) can be used to investigate matter. An IR photon hitting a molecule can be absorbed changing the vibrational state of the molecule itself. This absorption occurs when the photon's wavelength ( $\lambda$ ) matches with the resonance  $\lambda$  of the molecule, which is characteristic for every compound.

Everything explained above, works with monochromatic IR radiation. It means it is necessary to continuously change the  $\lambda$  in order to match the resonance  $\lambda$  of the different chemical substances. This entails long time scanning and the use of a monochromator (typically a prism or a refractive grating). With FTIR spectroscopy it is possible to use a wide spectral range at the same time using the Michelson interferometer (Figure 3.2) coupled with the Fast-Fourier-Transform (FFT) algorithm.

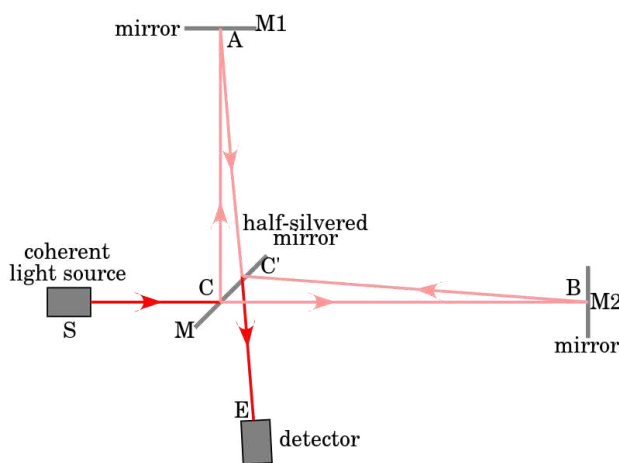


**Figure 3.2.** Scheme of a Michelson interferometer.

The major advantages of FTIR are that information in the entire  $\lambda$  range is collected simultaneously with less time for analyses and better signal-to-noise ratio (Fellgett's advantage), a better use of light power

(Jacquinot's advantage), and a more accurate  $\lambda$  calibration (Connes' advantage) (Griffiths & de Haseth, 1986).

Hydrogen is always attached to other atoms in a crystal structure, usually with oxygen forming OH bonds (Libowitzky & Beran, 2004). The geometry of these bonds can be characterised by IR spectroscopy (Beran & Libowitzky, 1999). Eventually, the amount of hydrous species can be determined by IR spectroscopy using general calibration curves following the Beer-Lambert law which correlate the absorbance ( $A$ ), with the concentration of an absorber ( $c$ ), the molar absorption coefficient ( $\varepsilon$ ), and the sample thickness ( $t$ ) according to:

$$A = \varepsilon c t \quad (1)$$

In contrast to many other minerals, quartz does not form solid solutions and it is considered a pure mineral. Nonetheless, trace of chemical impurities can be incorporated as crystal lattice defects. One of the most common is the  $\text{Si}^{4+}$  substitution with a trivalent cation like  $\text{Al}^{3+}$  or  $\text{B}^{3+}$  (with  $\text{H}^+$  as charge compensation), or by  $4\text{H}^+$  (Stalder & Neuser, 2013), in addition, monovalent alkaline cation like  $\text{Li}^+$  can be incorporated in channel sites, associated with anionic species ( $\text{OH}^-$ ) forming interstitial  $\text{LiOH}$  (Jollands et al., 2020). These substitutions lead to formation of O-H bond between charge balancing protons ( $\text{H}^+$ ) and silica oxygen atoms and are therefore called OH-defects.

Polarized IR-spectroscopy measurements allow to distinguish between molecular water ( $\text{H}_2\text{O}$ ), causing a broad band between 3000 and  $3700 \text{ cm}^{-1}$ ,

and water from OH-defects, causing sharp absorption peaks at characteristic wavenumbers, usually between 3250 and 3600  $\text{cm}^{-1}$  (Kats, 1962). Al-related substitution appears in a triplet peak at wavenumbers 3310-3378-3430  $\text{cm}^{-1}$ , Li-related substitution appears with a single peak at a wavenumber of 3480  $\text{cm}^{-1}$ , 4H-related defect (or hydrogarnet) appears with peak centred on wavenumber 3585  $\text{cm}^{-1}$ , while B-related defect displays a peak at wavenumber 3595  $\text{cm}^{-1}$  (Figure 3.3).

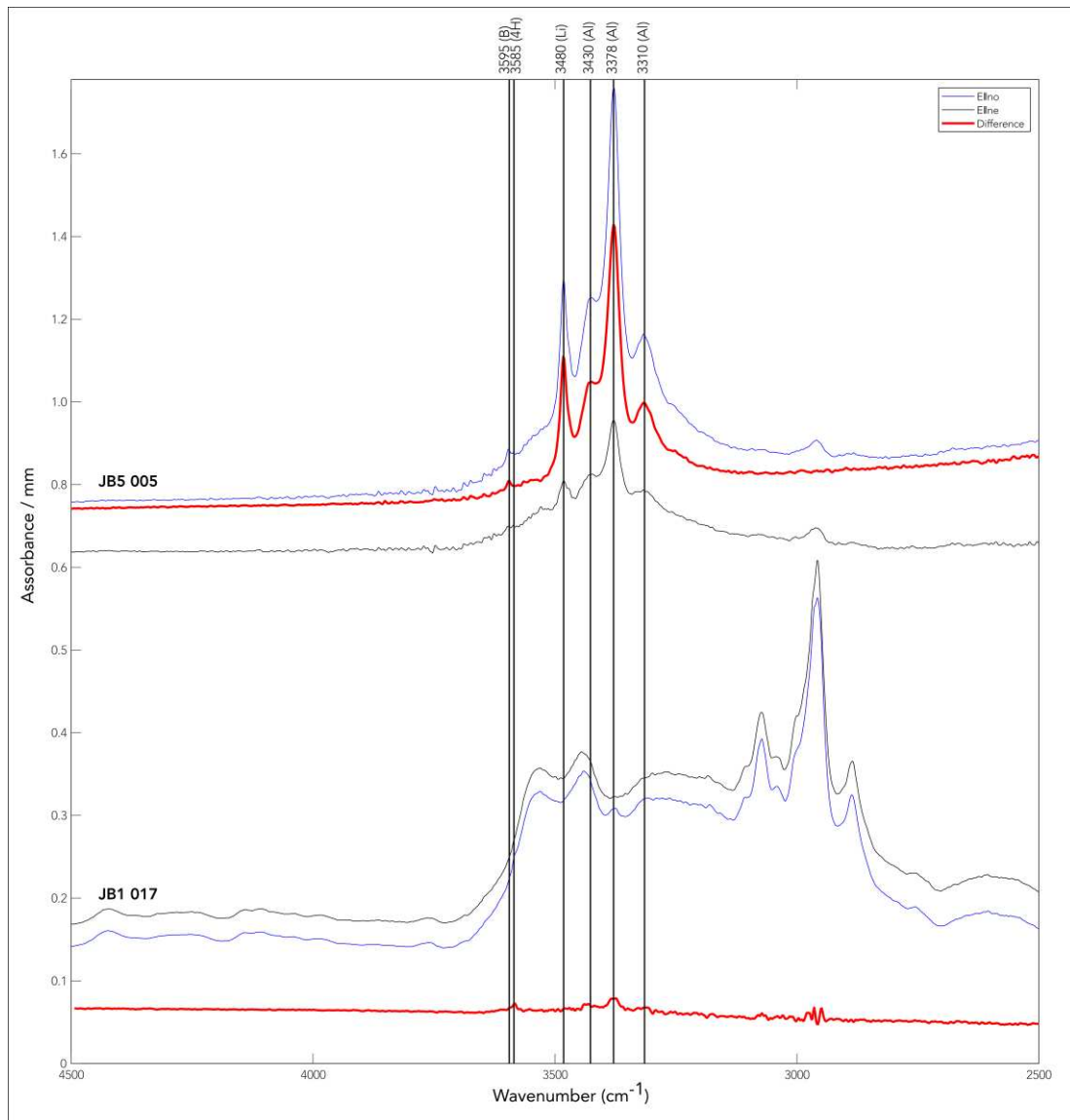


**Figure 3.3.** IR spectra of two representative grains, showing both  $E||n_o$  and  $E||n_e$  and the difference. The spectra are offset for clarity; peaks position marked with vertical lines. Absorption peaks between 2700  $\text{cm}^{-1}$  and 3200  $\text{cm}^{-1}$  are caused by the C-H stretching of the thermoplastic resin.

As long as the molecular water appears with an isotropic behaviour (identical absorption in all crystallographic directions), while most of OH-defect absorption bands are perfectly polarized perpendicular to the optical axis ( $E \parallel n_o$ ), it is possible to separate them. Therefore, the polarized measurements  $E \parallel n_o$  show OH-defect plus molecular water, while  $E \parallel n_e$  measurements show the molecular water only, for this reason the OH-defect contribution is easily derived by the subtraction  $E \parallel n_o - E \parallel n_e$  (Figure 3.3). For the B-related defect, the dipole is not perfectly oriented  $\parallel n_o$  but presents a component  $\parallel n_e$ , and to compensate this, Stalder & Neuser (2013) and Stalder (2021) suggest calculating the intensity as:  $A = \left( \frac{2n_o + n_e}{2} \right)$ .

### ***3.2.1. Previous studies***

Different works have tried to find a correlation between OH-defects and provenance of the quartz grains and some characteristics have been observed. Since the OH-defects method has been developed, it has been fundamental to understand correlation between OH-defects and petrological conditions. One of the first studies that sets the first knowledge about this kind of investigation is Müller & Koch-Müller (2009). In this study, the authors analysed 14 quartz samples from different geological settings (hydrothermal, igneous, metamorphic) in Norway. Quartz grains were analysed both via LA-ICP-MS in order to characterize the trace element content of quartz, and via FTIR to determine and specify OH-defect concentrations. The quartz that has been identified as igneous, compared to hydrothermal and metamorphic, show that it preferentially incorporates OH

as hydrogarnet defects in lieu of Li defects. These conclusions have been confirmed later by Stalder & Konzett (2012) who experimentally investigated OH incorporation in quartz from the system quartz-water, quartz-albite-water, and granite-water at pressure between 5 and 25 kbar, and temperature between 800 °C and 1000 °C. The two most important absorption features can be assigned to hydrogarnet (at 3585 cm<sup>-1</sup>) and Al-related (at 3310-3378-3430 cm<sup>-1</sup>) defects. The Al-related defects are related to mineral/melt partitioning and show a negatively pressure dependence. In contrast to the Al-defect, formation of hydrogarnet substitution appears to be positively correlated to pressure and water activity. Again, these correlations have been confirmed by other studies, based on detrital quartz from four localities in North-West Germany by Stalder & Neuser (2013) and on 433 detrital quartz from different worldwide large sedimentary reservoirs, by Stalder (2014). Reference materials used by Stalder & Neuser (2013) show an average low water content for metamorphic rocks (1.5-1.6 ppm in quartzite samples) compared to igneous rocks (from 5 to 16 ppm in samples of granites and rhyolites). Based on this, Stalder (2014) suggests a separation between water-poor (0-5 ppm) and water-rich (>5 ppm) as a threshold to determine if quartz is from non-igneous or igneous rocks, respectively.

During metamorphic processes the total water content decreases, and there is a species-dependent partitioning. By studying more than 500 quartz grains from Sweden, Austria, Germany, and South Africa, Stalder et al.

(2017) evaluated how the speciation of OH-defects can be used as a monitor of igneous, sedimentary, and metamorphic processes. According to the previous studies, quartz from igneous rocks show average content over 5 ppm while samples from metamorphic rocks are normally below this limit. In addition to this, some hydrothermal quartz grains have been thermally treated to simulate metamorphic processes. Cold-seal pressure vessel (CSPV) experiment between 1 and 3 kbar and between 650 °C and 750 °C have been performed. After these treatments, FTIR spectra have been performed on grains, showing a sensible decrease of Li-related and B-related peaks with no significant alteration of the Al-related peak. The experimental treatment demonstrates that Al-defects are more stable during metamorphic processes than B-related and Li-related defects, in fact Al is dominant in quartzites and metagranites. The correlation between overall content and igneous or non-igneous source and the OH-defect partition is proved also by Stalder et al. (2019) and Potrafke et al. (2020). Eventually, a work on fluvial and marine sediments from Japan by Jaeger et al. (2019) demonstrate that very diverse, and very high content (up to 211 ppm) are likely an effect of extensive sediment reworking and mixing.

### 3.3 Cathodoluminescence

Cathodoluminescence is one of the several types of possible luminescence, which is created during irradiation of a solid surface with an electron beam. It is possible to describe the process as follows: the hitting electron stimulates the system into an excited state, the system relaxes to a non-excited state by light emission (Marfunin, 1995) (Figure 3.4). The energy of the emitted photon (and therefore its colour) is dependent on the crystallo-chemical factors such as the types and structures of anions, molecules, and lattice as well as of specific luminescence centres (Götze & Kempe, 2009).

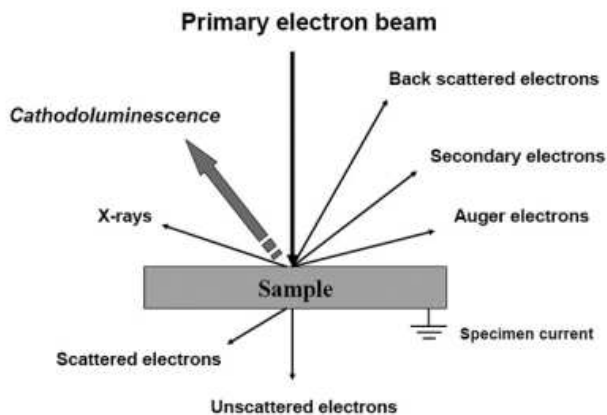


**Figure 3.4.** Schematic illustration of interaction of an electron beam and solid matter (Götze & Kempe, 2009).

Many different analytical instruments can be used as electron beam for excitation, meanwhile detectors can be confined into two different categories. The first is a group of CL detectors working with high spatial resolution coupled with scanning electron microscopes (SEM) or electron microprobes (EMP) providing panchromatic grey-scaled images. The second is CL detectors working with light microscopes presenting “true colour”

luminescence images. The electron guns of these latter CL microscopes may operate as “cold-cathode” when the discharge takes place in an ionized gas, or as “hot-cathode”, when the electrons are emitted from a heated metal filament.

### ***3.3.1. Previous studies***

As the emitted light is dependent on the crystallo-chemical features of the investigated matter, it is possible to use it to determine important information making CL one of the most widespread techniques in geoscience. During the last years a great amount of investigations was conducted on geomaterials to visualise growth textures and other internal structures that are not detectable with other analytical techniques. The information given by CL studies allow to reconstruct mineral formation and alteration processes, real minerals structures, and trace elements and lattice incorporation (Götze & Kempe, 2009; Götze, 2012).

CL is also one of the most used and most effective methods for determining provenance of detrital quartz (Zinkernagel, 1978; Matter & Ramsayer, 1985; Milliken, 1994; Boggs & Krinsley, 2006; Hooker & Laubach, 2007; Sales de Oliveira et al., 2017).

The causes of luminescence in quartz are not yet completely understood, but include Al substitution for Si, intracrystalline variation in trace element concentrations, and point or linear defects in the crystal lattice (Perny et al., 1992; Watt et al., 1997; Ramsayer & Mullis, 2000; Bernet & Bassett, 2005).

The defects causing CL can be related to either lattice defects (vacancies, broken bonds, etc.) or to the structural incorporation of certain trace elements (e.g.,  $\text{Mn}^{2+}$ ,  $\text{REE}^{2+/3+}$ ,  $\text{Cr}^{3+}$ ). Therefore, different phases can be contrasted as well as defects, zoning, and/or internal structures can be revealed using CL microscopy (Götze, 2012). More than 20 different types of those defects have been detected in quartz (Kostov & Bershov, 1987; Weil, 1984; 1993), which cause a range of luminescence emission bands in the ultraviolet, visible, and infrared region (Table 3.1). The occurrence of specific luminescence emission in quartz can often be related to specific conditions of formation (Ramseyer et al., 1988; Ramseyer & Mullis, 1990; Götze, 2009).

Hot-cathode cathodoluminescence provides CL colour images and has been frequently used as a tool to interpret provenance of quartz, applying the following classification scheme: (i) medium to bright blue: felsic plutonic and high-grade metamorphic quartz; (ii) red: groundmass quartz in volcanic rocks; (iii) brown: quartz from regionally low to medium grade metamorphosed rocks; (iv) non- or weakly luminescent: authigenic quartz; (v) short-lived green or blue: hydrothermal and pegmatitic quartz; (vi) blue with different spectrum to plutonic: volcanic quartz (Götze & Zimmerle, 2000; Boggs & Krinsley, 2006; Augustsson & Reker, 2012; Sawatzky & Pe-Piper, 2013; Sales de Oliveira et al., 2017).

**Table 3.1** Luminescence emission bands in quartz and related defects (Götze, 2012 and therein references).

Emission	Suggested Activator
175 nm (7.3 eV)	Intrinsic emission of pure SiO <sub>2</sub>
290 nm (4.28 eV)	Oxygen vacancy
330–340 nm (3.75–3.6 eV)	Oxygen vacancy [AlO <sub>4</sub> /Li <sup>+</sup> ] centre [TiO <sub>4</sub> /Li <sup>+</sup> ]
380–390 nm (3.2–3.1 eV)	[AlO <sub>4</sub> /M <sup>+</sup> ] centre; M <sup>+</sup> = Li <sup>+</sup> , Na <sup>+</sup> , H <sup>+</sup> [H <sub>3</sub> O <sub>4</sub> ] <sup>0</sup> hole centre
450 nm (2.8 eV)	E <sub>1'</sub> centre with self-trapped exciton
500 nm (2.45 eV)	Extrinsic emission Interstitial impurity cations (Li <sup>+</sup> , Na <sup>+</sup> , H <sup>+</sup> )
580 nm (2.1 eV)	E' centre (oxygen vacancy)
620–650 nm (1.97–1.91 eV)	NBOHC with several precursors
705 nm (1.7 eV)	Substitutional Fe <sup>3+</sup>
1280 nm (0.97 eV)	Interstitial molecular O

### **3.4 Laser Ablation-Inductively Coupled Plasma-Mass Spectrometry**

A mass spectrometer is an instrument designed to separate charged atoms and molecules on the basis of their masses following their motions into a magnetic field. There are different configurations for mass spectrometers, but the general operating scheme is set on the ionization of the analyte and its introduction in a magnetic mass analyser, with an inert carrier gas (commonly Ar). The magnetic field deflects the ions into circular paths whose radii are proportional to the ions' masses; the heavier are deflected less than the lighter ones.

As said, there are many different instrument's configurations depending on different way to introduce the analyte and its ionization. The design of a LA-ICP-MS is based on a high energy laser (commonly an ArF excimer laser) that atomise the sample and create atomic and small polyatomic ions. The so obtained analyte is then ionized with a plasma torch. The plasma is generated by an electromagnetic coil on the flowing gas, the magnetic field induce a circular current that is sufficient to ionise the gas and create the plasma. From this point the ionised analyte flows into the magnetic mass analyser as described above, for the ions' mass determination (Figure 3.5).

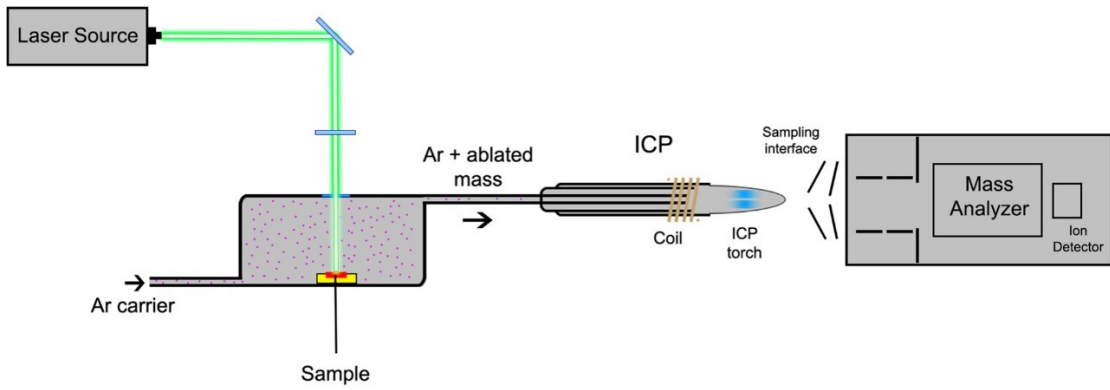


**Figure 3.5.** Schematic illustration of a LA-ICP-MS (Barbosa & Sussulini, 2020).

Compared to other mass spectrometers' architectures, LA-ICP has yielded a relatively simple and inexpensive instrument capable of direct analysis of elemental and isotopic ratios in solid samples with an extremely low limit of detection (Gray, 1985; Arrowsmith, 1987; Moenke-Blackenburg et al., 1990; Jackson et al., 1992). Laser ablation, moreover, has the potential to permit high resolution sampling, that other forms of atomisation are not able to consent.

The high sensitivity of this analytical technique allows to investigate chemical composition of minerals from major constituents to traces. Trace elements are largely used to characterise and determine mineral evolution, crystallisation, and alteration processes.

Quartz may contain trace elements such as H, Li, Be, B, Na, Al, P, K, Ca, Ti, Mn, Fe, Ge, etc. as a result of the growth conditions and evolution of geological environments. Titanium and aluminum are the most important trace elements because their content can be used to differentiate between different quartz types. Hydrothermal and pegmatitic quartz are characterized by lower temperatures and Ti concentrations. Rhyolitic quartz

is characterized by the lowest Al abundance, the highest temperatures, and lower Al/Ti ratios. Aluminum, Li, and H are most important in hydrothermal and metamorphic quartz, while magmatic quartz is generally enriched with Ti (Shah et al., 2022). In addition to these, Ti content can be used as a geothermometer for crystallization temperature (TitaniQ) (Wark & Watson, 2004; 2006).

### ***3.4.1. Previous studies***

Trace elements in quartz can be used also to discriminate within different granites. The contents of Al, Ge and Rb generally increase in the course of magmatic fractionation, while the contents of Ti decrease. The Ge/Ti value can be taken as a valuable indicator of fractionation of granitic melt from which quartz crystallized (Breiter et al., 2020).

Trace element composition of hydrothermal quartz reflects the P-T-X (pressure-temperature-concentration) conditions of the mineralizing fluids and can be a potential tracer of the fluid evolution. The continuous evolution of trace elements concentration reflects the cooling and/or compositional variations of the hydrothermal fluids. The Al/Ti, Sb/Ti, Ge/Ti, and (Sb+Ge)/Ti ratios are used to allow for discrimination of quartz from different vein generations of porphyry Cu-(Au-Mo) deposits (Rottier & Casanova, 2020).

Many other studies have been recently done to determine the concentrations of trace elements in quartz and better constrain magmatic, metamorphic,

and hydrothermal processes (e.g., Monnier et al., 2018; Müller et al., 2018; Wertich et al., 2018; Breiter et al., 2019; Hong et al., 2019; Wang et al., 2019; Feng et al., 2020; Li et al., 2020; Monnier et al., 2020; Sun et al., 2020; Wang et al., 2022; Zhang et al., 2022). These studies emphasize that the trace elements chemistry of quartz crystals can represent the signature of a specific type of mineralisation, making it useful as a powerful tool for mining prospection (Monnier et al., 2020) and provenance studies.

### 3.5 Methodology

Rocks were crushed in a mortar, then heavy minerals were concentrated by sieving, magnetic separation, and heavy liquids (1,1,2,2 Tetrabromooethane) for other studies (Lenaz et al., 2000, 2018; Lenaz & Princivalle, 2002, 2005; Velicogna, 2020; Garlatti, 2022-23). The residual part (mainly quartz, calcite, and feldspar) was treated with hydrochloric acid HCl 10% for dissolving calcite, rinsed with distilled water for removing acid traces, and dried in oven at a temperature of 90 °C.

For each of the nine samples, twenty oriented quartz wafers were firstly prepared for IR spectroscopy, according to the protocol described by Stalder & Konzett (2012), adding up to a total of 180 crystals.

Individual quartz crystals with dimension >250 µm were handpicked and oriented parallel to the c-axis in thermoplastic resin on a glass slide. Crystal alignment was checked with an optical microscope, confirmed by birefringence values of  $\Delta n = 0.009$  in orthoscopic and by “flash figures” in

conoscopic illumination. Oriented crystals were manually ground and polished on both sides and maintained in the resin.

For the water quantification, a crucial parameter is the crystal thickness. It has been determined by a mechanical Mitutoyo® micrometre gauge with an accuracy of  $\pm 2 \mu\text{m}$ . Crystal thicknesses in the investigated sample set range from 27 to 370  $\mu\text{m}$ .

IR spectra were recorded at Department of Geosciences of Swedish Museum of Natural History in Stockholm at room temperature, using a Bruker Vertex® 70 spectrometer equipped with a halogen-lamp source and a CaF<sub>2</sub> beam-splitter coupled to a Hyperion® 2000 microscope with a ZnSe wire-grid polarizer and a nitrogen-cooled InSb detector. From 200 to 400 scans were conducted on background and sample, with a resolution of 4  $\text{cm}^{-1}$  in the wavenumber range of 2000-7000  $\text{cm}^{-1}$ . On each crystal were run two measurements each ( $E \parallel n_o$  and  $E \parallel n_e$ ) by turning the polarizer for 90° after the first measurement. The two polarized IR spectra were subtracted in according to Stalder (2012), normalized to thickness and baseline-corrected by a linear baseline within the wavenumber range of 3600-3250  $\text{cm}^{-1}$ .

Defect water contents were calculated for the different substitutions (if present) by integration in the peaks' regions using Voigt area fitting procedure in PeakFit® 4.12 environment (Figure 3.6), applying then the integrated extinction coefficient from mineral-specific (Thomas et al., 2009) calibration.

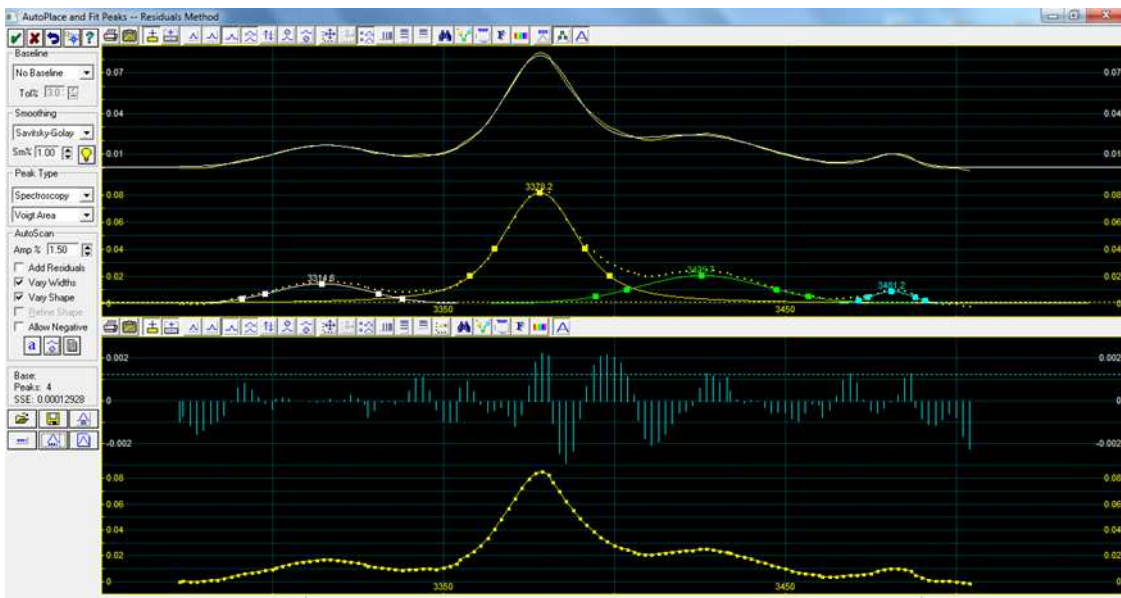


**Figure 3.6.** Example of peaks' integration using the PeakFit® 4.12 environment.

Results are expressed as ppm weight H<sub>2</sub>O notation. OH values were estimated to have a precision of  $\pm 10\%$ , considering errors caused by background correction, thickness measurement, and crystal orientation problems (Stalder et al., 2017). In addition, there is also a systematic error based on accuracy of the extinction coefficient, which was estimated to be  $\pm 15\text{--}20\%$  (Libowitzky & Rossman, 1997; Thomas et al., 2009). The detection limit for water concentration is strongly dependant on the spectral quality and sample thickness and estimated to vary from 0.1 ppm to 0.5 ppm for the studied samples.

On the same grains CL and LA-ICP-MS analyses were performed. For both methodologies the crystals were set on two 1-inch round epoxy mounts, one with grains from samples from JB1, JB5, JB10, JB17, and JB26 and the other one with all the remaining grains from samples BK41, BKNV, DOB, and RAB1.

Every single-crystal-bearer glass plate was immersed in acetone to dissolve the thermoplastic resin. The crystals thus freed were handpicked and positioned on a double-sided tape previously fixed on a specific support. Unfortunately, during this process, 20 grains were lost: JB1\_03, JB1\_12, JB1\_13, JB5\_02, JB5\_16, JB10\_12, JB10\_15, JB17\_05, JB26\_04, BK41\_14, BK41\_20, BKNV\_05, DOB\_14, DOB\_15, RAB1\_01, RAB1\_03, RAB1\_11, RB1\_17, RAB1\_19, and RAB1\_20, bringing the total to 160 grains.

At the end of the crystals' deposition, a one-inch-cylindrical PTFE (polytetrafluoroethylene) mould was placed for the two-component epoxy casting. The mixture was prepared by blending Struers EpoFix® resin with the hardener with a weight ratio of 25:3, it was gently stirred for about four minutes to trigger the reaction with caution paid to avoid the creation of air bubbles, and then casted in the before mentioned mould. The hardening time is about 12 hours at room temperature and pressure, a vacuum chamber can be used to be surer to get rid of any air bubble could occur during the blending and casting process.

When the mounts were perfectly hardened, they were separated from mould and tape, cleaned with water in ultrasonic bath, and prepared for grinding and polishing. The grinding was performed with silicon carbide abrasive paper sheets with decreasing grit sizes, from 800 to 2000, and distilled water as lubricant. Final polishing was executed with Buehler Metaserv® 2000 polisher with two different polishing cloths and respective polycrystalline diamond suspensions (3 µm and 1 µm).

Cathodoluminescence was recorded at Department of Geosciences of University of Padua using a CITL Cold Cathode Luminescence 8200 mk3 operating at 20 kV and 200-250  $\mu$ A. CL images were acquired at 10x magnification with Nikon Labophot-2 POL<sup>®</sup> microscope coupled with Canon EOS600D<sup>®</sup> camera.

Following the same mounting procedure, another set of 200 grains (20 per sample with more 20 grains from sample JB23), from the 63-250  $\mu$ m size class was analysed with LA-ICP-MS only, in order to have more statistically relevant results for trace elements and verify if there is the same behaviour within two different granulometries.

Trace element concentrations in quartz were determined using the ETH prototype of the GeoLas laser ablation system equipped with a Compex Pro 102F<sup>®</sup> (Coherent) Excimer 193 nm (ArF) laser source and coupled to a Perkin Elmer<sup>®</sup> Nexion2000 fast-scanning quadrupole ICP-MS, housed at the Institute of Geochemistry and Petrology, ETH Zürich. The on-sample energy density of the laser beam was set to 20 J·cm<sup>-2</sup> and the repetition rate was 10 Hz. Quartz crystals were ablated with a spot size of 40  $\mu$ m. The ablation was performed in an in-house cell designed for 1-inch mounts, using ca. 1.0 l·min<sup>-1</sup> He as carrier gas flow and ca. 1.0 l·min<sup>-1</sup> Ar make-up gas admixed downstream of the ablation chamber. The analysed set of elements are <sup>7</sup>Li, <sup>9</sup>Be, <sup>11</sup>B, <sup>23</sup>Na, <sup>25</sup>Mg, <sup>27</sup>Al, <sup>31</sup>P, <sup>35</sup>Cl, <sup>39</sup>K, <sup>45</sup>Sc, <sup>49</sup>Ti, <sup>71</sup>Ga, <sup>72</sup>Ge, <sup>85</sup>Rb, <sup>88</sup>Sr, and <sup>133</sup>Cs. All concentrations were quantified against the NIST SRM 610 glass wafer as the primary reference material (Jochum et al., 2011). The

raw data were reduced using the MathWorks MATLAB®-based SILLS program (Guillong et al., 2008) by using Si as internal standard for quartz (stoichiometric value). Errors and limit of detection were automatically calculated for each element and each grain during the data reduction process (Tables A.7, A.8, A.9, A.10, A.11, A.12, A.16, A.17, A.18, A.19, A.20, A.21 in Appendices). A natural quartz crystal characterised by Audéstat et al. (2015) was employed as a secondary reference material for quartz analyses. The average 2 SD reproducibility of concentrations in the secondary quartz reference material for all analytical sessions was on average 5% relative (2 SD).

All data elaboration (i.e., spectra subtraction, baseline correction, water content calculation, data reduction, and data plotting) was performed using suitable numerical analysis computer software such as MathWorks MATLAB® and Microsoft Excel®. Graphic restitutions and maps drawing were done using computer vector graphics editor Inkscape®.

## CHAPTER 4. RESULTS

### 4.1 OH-defects

Nine samples were selected for this study (five from the Julian Basin, two from the Brkini Basin, and two from the Kvarner Islands Basin). For each sample, 20 grains were analysed adding to 180 grains in total, from which, 129 (~72%) show recognizable peaks. Within the set, the frequency of recognizable peaks per sample spans from 19/20 (95%) for JB26 to 5/20 (25%) for RAB1 (Figure 4.1)

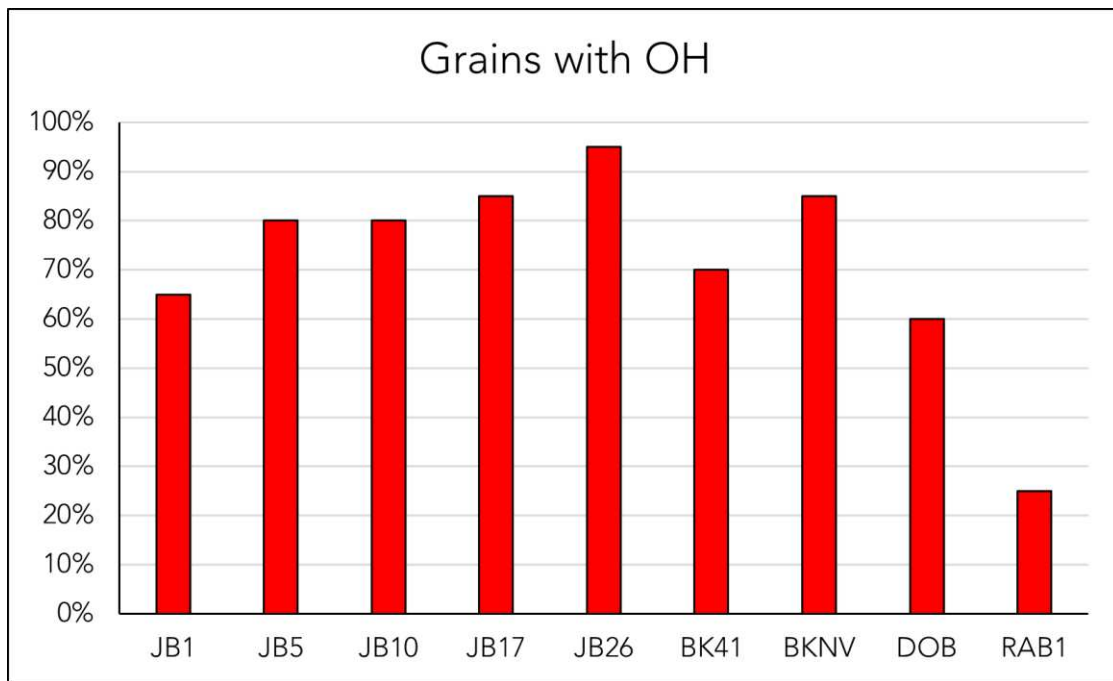


**Figure 4.1.** Grains with recognizable OH peaks per sample (in percentage).

In this work, not only the mere presence of the OH-defects but also their nature is considered. The investigation of the collected spectra shows a substantial predominance of single substitutions involving OH, only samples JB10, JB26, and BKNV show more than 50% of multiple substitutions (Figure 4.2).

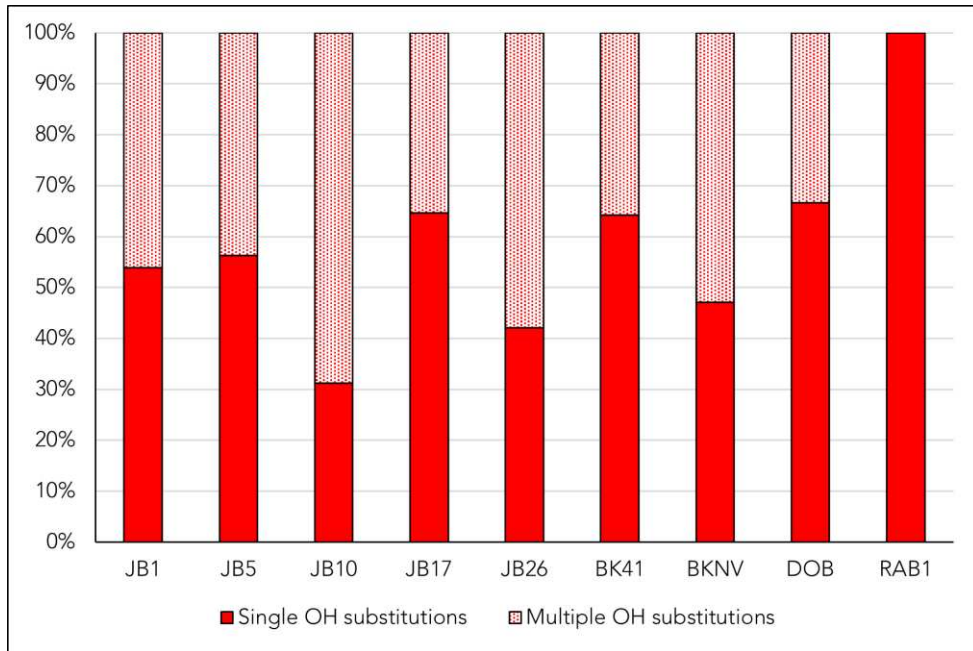


**Figure 4.2.** Ratio of grains showing only single OH-defects, and multiple OH-defects (in percentage).

Regarding the kind of the substitutions, the Al-related is highly dominant, both as single and with other substitution, followed by Li, and with B and 4H ones less abundant (Figure 4.3).

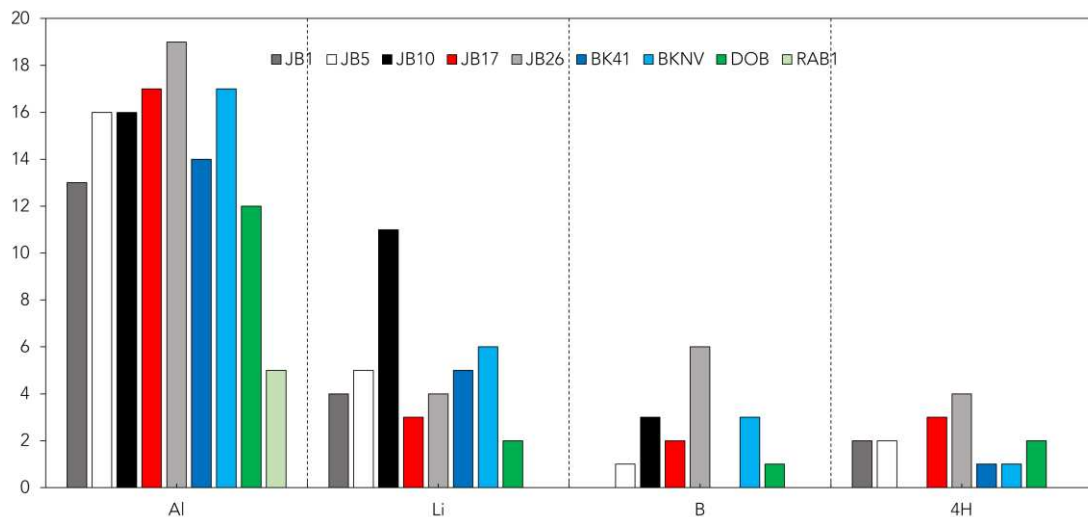


**Figure 4.3.** Distribution of the different OH-defects within the analysed samples.

The water content determination is based on different calibrations. Following the Beer-Lambert law (1), it is known that the concentration of an absorber ( $c$ ) – the unknown parameter of this work – is dependent on

absorbance (A), sample thickness (t), and the molar absorption coefficient ( $\varepsilon$ ) as seen in Chapter 3:

$$A = \varepsilon c t \quad (1)$$

While absorbance and thickness are directly obtained from the instruments, the molar absorption coefficient is given from different ways. Since IR spectroscopy is not self-calibrating, several general wavelength-dependent calibrations have been established (Paterson, 1982; Libowitzky & Rossman, 1997). These calibrations rely on hydrous minerals containing several percent water by weight and show a negative correlation between  $\varepsilon$  and the mean wavenumber of the corresponding OH pattern. It has been observed that these calibrations cannot be fully applied on NAMs (Rossman, 2006) that contain OH in ppm-level amount and mainly as OH-defects. To provide data for NAMs, single mineral specific calibrations are needed, and some has already been performed and proposed, e.g. for olivine (Bell et al., 2003; Koch-Müller et al., 2006), pyroxenes (Bell et al., 1995), garnets (Maldener et al., 2003), and for quartz polymorphs (Thomas et al., 2009).

In this work, defect water contents were calculated for the different substitutions using the integrated extinction coefficient from the mineral-specific calibration (Thomas et al., 2009).

The Al-related substitution appears in a triplet peak at wavenumbers 3310-3378-3430 cm<sup>-1</sup>, the Li-related substitution appears with a single peak at a wavenumber of 3480 cm<sup>-1</sup>, the 4H-related defect appears with peak

centred on wavenumber  $3585\text{ cm}^{-1}$ , and the B-related defect displays a peak at wavenumber  $3595\text{ cm}^{-1}$  (Figure 4.4).

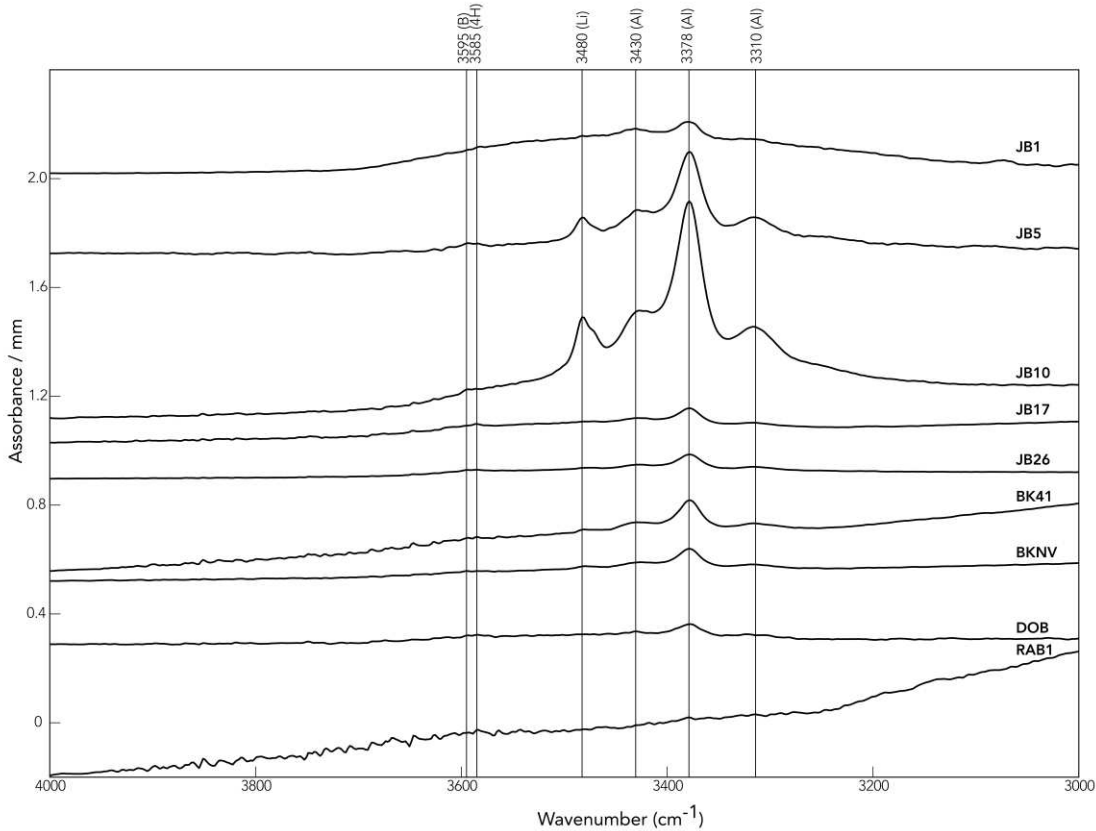


**Figure 4.4.** Average IR spectra of all samples. The spectra are offset for clarity; peaks position marked with vertical lines.

Sample JB5 is the lowest in the stratigraphic column so it is the oldest in age (70 Ma). The grains from this sample show a relevant variability regarding the defects with an abundance of single Al-related defect. The OH content is relevant for Al-defect, that spans from 1.2 to 295 ppm. The other defects' contents are Li: 0.31-37 ppm, 4H: 0.29-0.51 ppm, and B is 2.1 ppm. Sample JB1 (67 Ma) shows generally less variability than JB5, with less OH content. Grains display preferentially single Al-defect, there are not B-related defects. Al-defect content spans from 0.38 ppm to 23 ppm, Li is between 0.15-0.27 ppm, and 4H is 2.6-3.0 ppm. Sample JB10 (65 Ma) shows

a pattern more similar to JB5 than to JB1, with great variability both in defects type, their content, and overall OH content. Al-defect spans from 1.4 to 536 ppm (highest value of all the set), Li is between 0.34-40 ppm, B is from 0.54-2.8 ppm, there are not 4H-related defects. JB17 (56 Ma) shows little less variability and generally lower values. Al-defect is between 0.46-9.0 ppm, Li goes from 0.15 to 0.38 ppm, B is between 0.36-0.80 ppm, 4H is from 0.18 to 1.0 ppm. Sample JB26 is the highest in the JB's stratigraphic column (50 Ma) and appears similar to JB17, with moderate variability of defects and relative contents. Al-defect goes from 0.67 to 16 ppm, Li is between 0.08-0.76 ppm, B spans between 0.16-0.54 ppm, 4H settles between 0.12-0.66 ppm.

Brkini samples show similar behaviours, close to JB26 one. Al-defect spans between 3.8-32 ppm for BK41 and 0.36-27 ppm for BKNV, Li is between 0.18-1.0 ppm for BK41 and 0.31-1.1 ppm for BKNV, B is present only in BKNV and settles between 0.45-1.6 ppm, 4H is 1.2 ppm for BK41 and 0.46 ppm for BKNV.

Finally, Kvarner Islands samples are showing the least variability and the lowest defects content of all the set, crystals from RAB1 show Al-related defects only. Al-defect is between 0.63-14 ppm for DOB and between 1.0-7.4 ppm for RAB1, Li is set in the range 0.49-1.2 ppm, B is 0.22 ppm, 4H goes from 0.85 to 0.92 ppm.

Total OH goes from 1.2 to 304 ppm for JB5, between 0.38-26 ppm for JB1, between 1.4-571 ppm (highest overall value of all the dataset) for JB10, from

0.46 to 10 ppm for JB17, is between 0.67-16 ppm for JB26, between 3.8-33 ppm for BK41, 0.36-29 ppm for BKNV, spans from 0.63 to 15 ppm for DOB, and between 1.0-7.4 ppm for RAB1.

#### 4.2 Cathodoluminescence

CL analyses were performed on the same grains, unfortunately during the preparation for this (and further) analyses, 20 grains were lost, bringing the total to 160 grains, as mentioned before in Chapter 3.

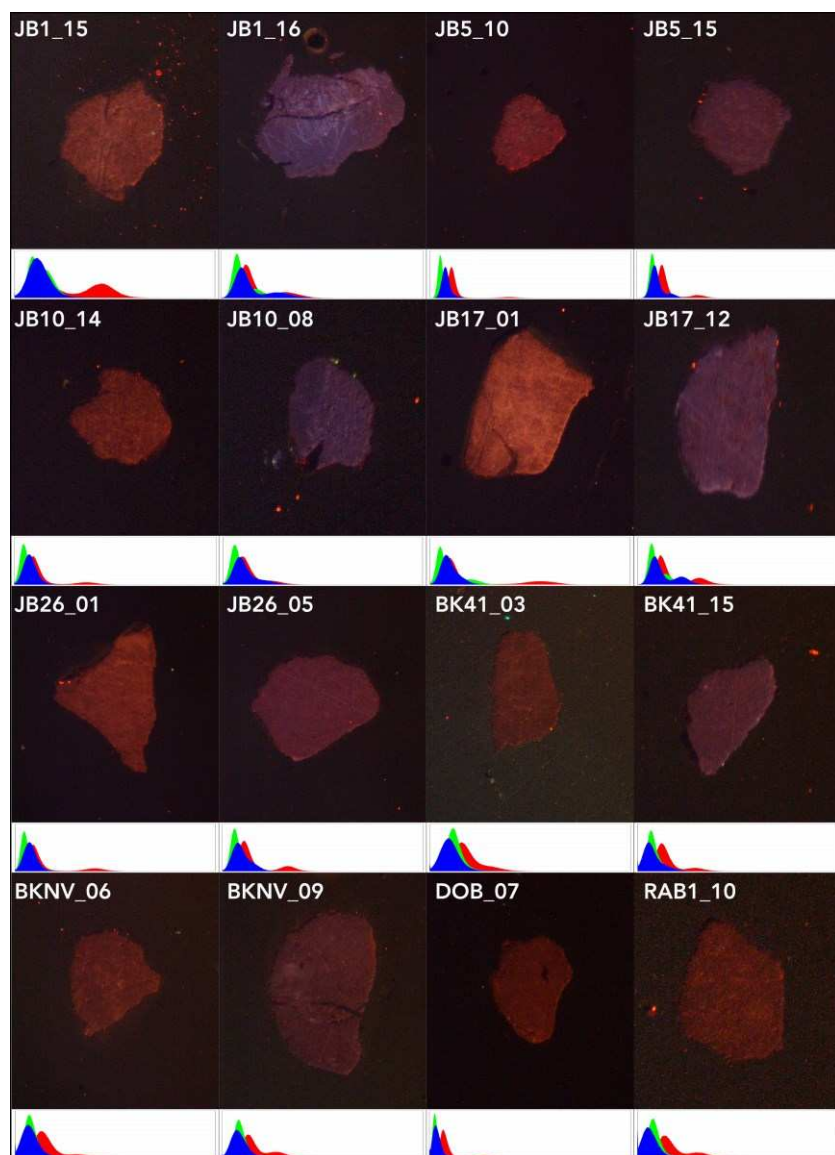


**Figure 4.5.** Cathodoluminescence images of representative grains for each sample, and their relative histograms.

CL images acquired within the samples show no relevant colour variation. All the grains display colour from red to purplish blue, with exception of KVI (Kvarner Islands) samples, showing only reddish ones (Figure 4.5).

#### 4.3 Trace elements

After cathodoluminescence, on the same 160 mounted grains, trace elements analyses were performed using LA-ICP-MS. In addition, another set of 200 grains (20 per sample, with more 20 grains from sample JB23), from 63-250 µm size class was analysed with LA-ICP-MS. The effective amount of analysed quartz is 157/160 for the >250 µm size class (due to laser-induced crystal explosions), and 148/200 for the 63-250 µm size class (due to laser-induced explosions, and crystal mismatch during the picking phase).

The analysed set of elements is  $^7\text{Li}$ ,  $^9\text{Be}$ ,  $^{11}\text{B}$ ,  $^{23}\text{Na}$ ,  $^{25}\text{Mg}$ ,  $^{27}\text{Al}$ ,  $^{31}\text{P}$ ,  $^{35}\text{Cl}$ ,  $^{39}\text{K}$ ,  $^{45}\text{Sc}$ ,  $^{49}\text{Ti}$ ,  $^{71}\text{Ga}$ ,  $^{72}\text{Ge}$ ,  $^{85}\text{Rb}$ ,  $^{88}\text{Sr}$ , and  $^{133}\text{Cs}$ .

By reason of uneven abundance and very variable limit of detection, only some elements were considered for the results (i.e.,  $^7\text{Li}$ ,  $^{11}\text{B}$ ,  $^{23}\text{Na}$ ,  $^{25}\text{Mg}$ ,  $^{27}\text{Al}$ ,  $^{31}\text{P}$ ,  $^{39}\text{K}$ ,  $^{49}\text{Ti}$ , and  $^{72}\text{Ge}$ ).

The element with the highest concentration per single grain is, as for the OH-defects, Al, with Na, K, P, Li following. Nonetheless, P shows higher average concentration than Al, but lower standard deviation (Table 4.1).

**Table 4.1.** Element minimum and maximum concentrations, average, standard deviation, and relative abundance for >250 µm grain fraction.

Element	Min [µg/g]	Max [µg/g]	Average	St. Dev	Abundance
Li	0.53 (RAB1-18)	244 (JB10_11)	17	38	49%
B	0.84 (BKNV_20)	15 (JB1_17)	2.7	2.1	48%
Na	0.42 (JB26_19)	499 (DOB_06)	38	70	97%
Mg	0.13 (DOB_05)	74 (JB5_04)	5.5	11	60%
Al	5.9 (DOB_12)	2850 (JB10_11)	195	423	100%
P	61 (DOB_08)	269 (BKNV_10)	209	42	100%
K	4.2 (DOB_03)	285 (DOB_06)	35	42	62%
Ti	1.0 (BK41_09)	129 (DOB_02)	25	26	84%
Ge	1.3 (DOB_12)	6.8 (JB10_19)	2.4	1.2	35%

The same was made for the second set of quartz coming from the 63-250 µm size fraction. Also in this set the highest concentrations per single grain are shown by Al (but with lower values than the coarser fraction), followed by Ti, K, Mg, and Na. Also in this set, P shows higher average concentration than Al, with lower standard deviation (Table 4.2).

**Table 4.2.** Element minimum and maximum concentrations, average, standard deviation, and relative abundance for 63-250  $\mu\text{m}$  grain fraction.

Element	Min [ $\mu\text{g/g}$ ] (Sample)	Max [ $\mu\text{g/g}$ ] (Sample)	Average	St. Dev	Abundance
Li	0.23 (RAB1-03)	28 (RAB1_01)	3.5	5.1	68%
B	1.3 (BKNV_04)	26 (JB10_03)	3.3	3.7	31%
Na	0.51 (DOB_16)	520 (JB5_19)	31	55	99%
Mg	0.46 (DOB_04)	533 (JB1_20)	15	60	67%
Al	7.0 (DOB_16)	1467 (RAB1_01)	152	210	100%
P	93 (JB1_14)	415 (JB17_11)	221	57	100%
K	5.4 (JB17_19)	561 (BKNV_09)	35	61	69%
Ti	1.9 (RAB1_05)	1007 (RAB1_16)	38	93	82%
Ge	1.6 (RAB1_03)	3.6 (JB26_08)	2.7	0.5	16%

## CHAPTER 5. DISCUSSIONS

### 5.1. OH-defects

Different behaviours and patterns can be distinguished within the basins' samples regarding the defects' variability, their respective contents, and the total OH content. Samples JB1, JB17, and JB26 were also analysed by Bernardi et al. (2022) (with the addition of sample JB23, not studied here) and some confrontations can be made (Figures 5.1 and 5.2). Unfortunately, those samples were lost during preparation for chemical analyses via LA-ICP-MS so that we decided to reanalyse them during this project. That study showed that the grains from JB1 had a dominating abundance of single Al-related defects (2.4-30 ppm) and only a few of the other types: Li: 2.6 ppm, 4H: 2.6 ppm, and B: 0.6 ppm, suggesting that both metamorphic and non-metamorphic sources are present (Bernardi et al., 2022).

The spectra of the grains from JB17 show different patterns to those of the others, both in terms of defect variability and the corresponding water contents, in fact, almost half of the grains show defects with multiple substitutions (Al + Li, Al + B, Al + 4H, and Al + Li + B), with very high values of water content, especially for the Al-related defect (1.6-214 ppm). The Li-related defect shows high variability and the highest content within the basin (1.8–15 ppm), and the same is also the case for B (0.1-0.6 ppm), which also shows the highest values, while the 4H defect is in the range 0.2-1.0 ppm. This indicates a mainly volcanic source, with possibly

late-stage volcanic (hydrothermal Li defect) source material and the presence of high-pressure rocks in the source area (presence of 4H defects).

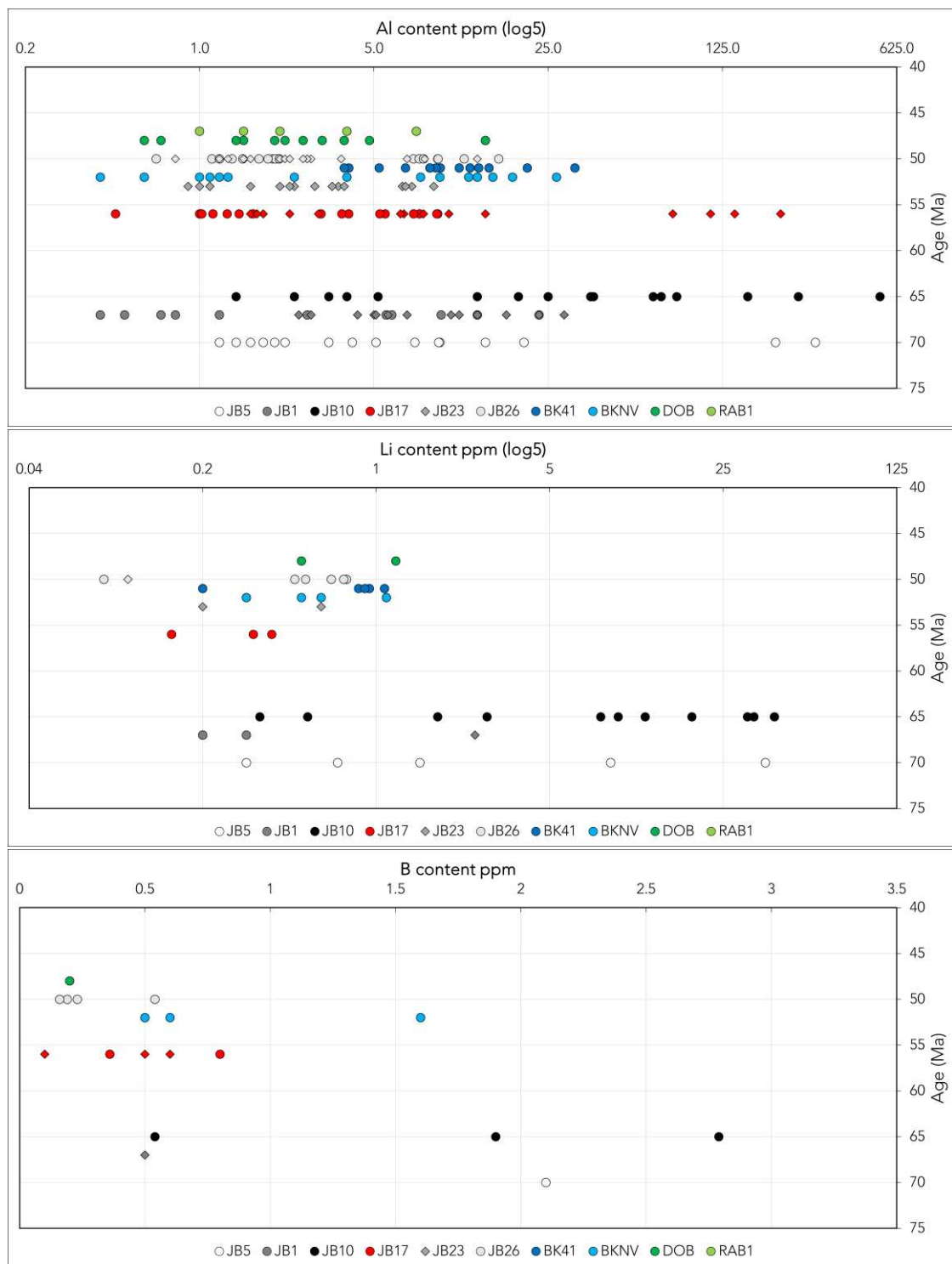
Samples JB23 and JB26 display very similar behaviors, with a great number of grains bearing Al defects but corresponding to relatively low water contents, for JB23 (0.8-8.8 ppm), and for JB26 (0.8-13 ppm). Li-related substitutions are in the range of 0.2-0.6 ppm in grains from JB23, and 0.2 ppm in the only grain in JB26. Boron substitutions are not present. An almost solely metamorphic origin can be suggested for these samples, according to the above-mentioned correlations.

As seen in the “Results” chapter, samples JB5 and JB10 show the greatest variability, the highest overall defects content (especially for Al- and Li-related ones), and the highest total OH content. These great variability and defects content can suggest a mainly volcanic source with possible late-stage volcanism due to the high presence of Li-related defect (Figure 5.1). The new quartz crystals from sample JB1 display an average variability of defects with lower contents than JB5 and JB10 meanwhile showing the greatest amount of 4H substitution within all the data set suggesting a high-pressure source (Figure 5.1). These observations suggest that both metamorphic and non-metamorphic sources are present, confirming what was suggested by Bernardi et al. (2022). Sample JB17 showed the greatest variability in the previous study, meanwhile in this work it plots closer to its average (Figure 5.1). The rock source of this sample was identified with a complex volcanic-metamorphic supply (Bernardi et al., 2022). This could be partially confirmed due to the presence

of all the kind of defects. In the present study, JB26 shows some more 4H-bearing grains (suggesting high-pressure source) and B-bearing grains (absent in the previous study) (Figure 5.1). For these reasons it is possible to confirm the identification that was made previously for JB23 and JB26, representing the final stage of JB sedimentation, with a mainly metamorphic source (including high-pressure rocks as proved by the 4H defect presence).

Samples from BK show very similar patterns, with low variability and relevant defects content (especially for Al- and Li-related defect). B is almost absent (only one grain per sample). The source rock for these samples could be interpreted as volcanic and metamorphic (total defects lower than 5 ppm), including high pressure rocks (4H-defect presence) (Figure 5.1). BK41 crystals presents a volcanic component relatively higher than that of BKNV and similar to that of JB10.

The lack of measurable OH-defects and the low amount of OH-defects when measurable suggest a main metamorphic supply for the crystals of both KVI samples. Sample RAB1 shows only five grains with recognizable OH-defects, and all of them are Al-related ones. Sample DOB shows similarities to late stage of JB (see JB23 and JB26), with also the same 4H content (Figure 5.1).



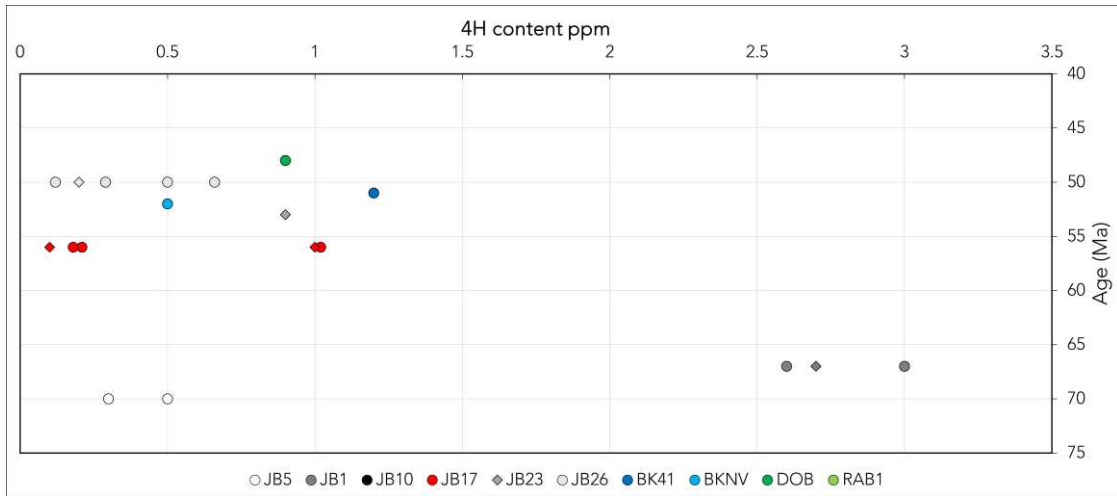


**Figure 5.1.** Al-, Li-, B-, and 4H-related defects concentrations within the samples. Circles show data from this work, diamonds display data from Bernardi et al. (2022). Al and Li content are plotted in logarithmic scale while B and 4H are in linear scale.

Regarding the total OH content it is possible to see that samples JB5, JB17 (especially the previous study's data), and JB10 show the highest overall values confirming the suggested volcanic source. The other samples, meanwhile, show a relevant decrease in total OH content, with JB23, JB26, DOB, and RAB1 showing average values below the 5 ppm threshold confirming the considerable metamorphic supply for these samples (Figures 5.2 and 5.3).

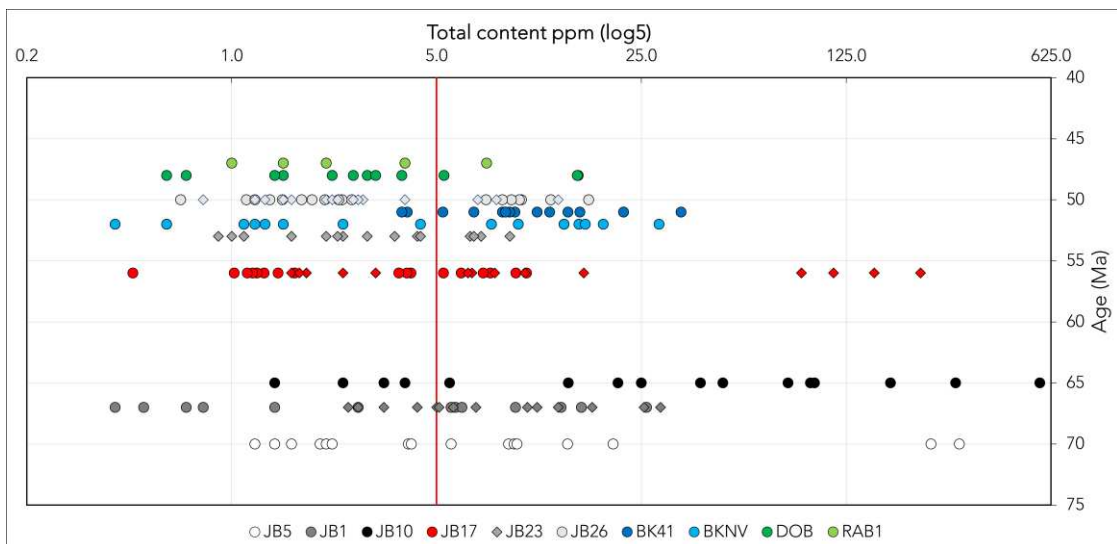


**Figure 5.2.** Total OH-defects concentration (in logarithmic scale) within the samples. 5 ppm marked with red line. Circles show data from this work, diamonds display data from Bernardi et al. (2022).

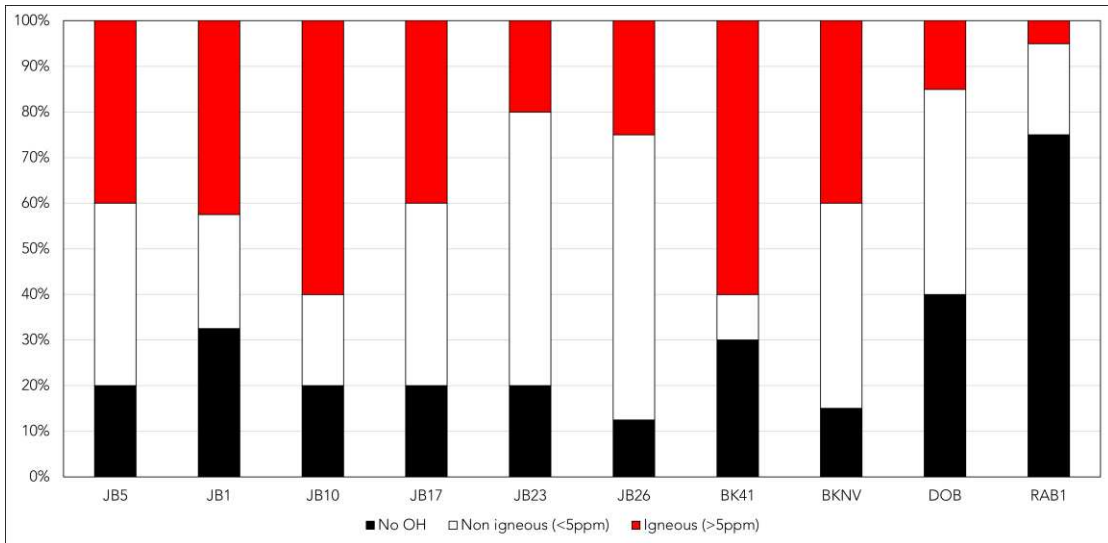


**Figure 5.3.** Distribution of grains considering the 5 ppm threshold. For JB1, JB17, and JB26 data are merged with data from Bernardi et al. (2022)

Samples JB5, JB1, and JB17 show a constant ~40% of igneous quartz, that reach 60% in sample JB10. A clear change can be identified in samples JB23 and JB26 with a neat predominance of non-igneous quartz. In BK it is possible to verify a difference between the two samples, with BK41 showing more igneous quartz than BKNV. Interestingly there is a continuous increase in metamorphic supply from BKNV to DOB and RAB1 (Figure 5.3).

## 5.2. Cathodoluminescence

Even if the CL images display no relevant colour variability, it is possible to try to separate grains with red CL images with grains with purple/blue CL images. The distribution of the CL colours can suggest a sort of trend within the analysed sample set. JB samples show a progressive increase in red CL images from JB5 to JB26. A similar trend can be distinguished in the BK samples with more red CL images in BKNV grains. Samples from Kvarner Islands Basin show only red CL images (Figure 5.4).

According to the classification scheme proposed by Sales de Oliveira et al. (2017) and reference therein, red CL images could be identified as groundmass quartz in volcanic rocks, meanwhile purplish blue ones could be assigned to felsic plutonic, and high-grade metamorphic quartz. It is highly questionable that this classification could be used in this work as suggests the opposite trend than the OH-defects proposed one.

It is important to state that this colour separation and distribution has been made without univocal values, but only following the personal capacity and sensibility of colour identification. For these reasons, the author is not confident to use CL images for quartz provenance reconstruction.

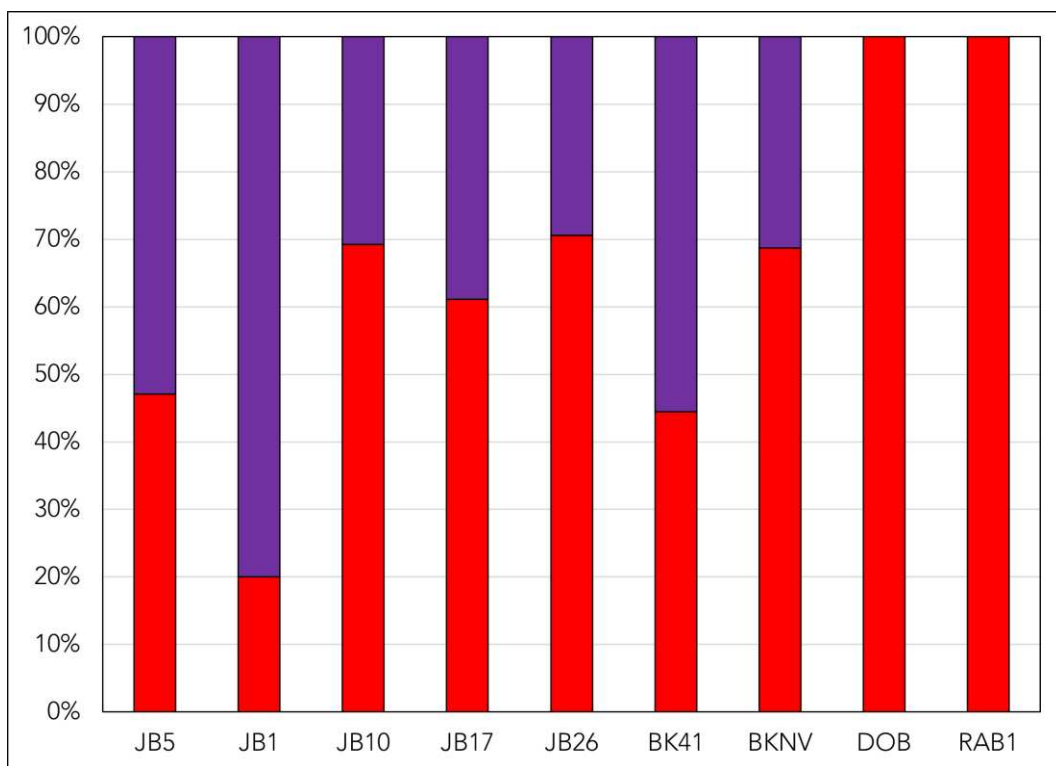


**Figure 5.4.** Proposed distribution of CL image colours.

### **5.3. Trace elements**

Even if quartz is one of the purest minerals on Earth, impurities in the form of trace elements can be incorporated into the crystal structure. There is a limited number of ions which can substitute for  $\text{Si}^{4+}$  in the crystal lattice because of its small size and its high valence. The structural incorporation in a regular  $\text{Si}^{4+}$  lattice position was proved by Weil (1984; 1993) for  $\text{Al}^{3+}$ ,  $\text{Ga}^{3+}$ ,  $\text{Fe}^{3+}$ ,  $\text{Ge}^{4+}$ ,  $\text{Ti}^{4+}$  and  $\text{P}^{5+}$ . Among them, Al is the most frequent trace element in quartz (up to 1000 ppm), which is due to its common occurrence in the Earth's crust and the similar ionic radii of  $\text{Si}^{4+}$  and  $\text{Al}^{3+}$ .

$\text{Ti}^{4+}$  and  $\text{Fe}^{3+}$ , are usually incorporated at the marginal parts of the crystals due to their relatively large ionic radius (Götze and Plötze, 1997), or can generate exsolution phenomena such as the formation of rutile inclusions at lower temperatures (Götze et al., 2004). In particular, the concentrations of Ti in metamorphic and igneous quartz can be relatively high (ranging from 1 to over 100 ppm). Furthermore, the activity of Ti in many systems is fixed by the presence of a nearly pure  $\text{TiO}_2$  phase (typically rutile). Consequently, the chemical potential of Ti, and hence the extent of Ti substitution for Si in quartz, should vary systematically with temperature.

The idea of using the titanium content of quartz as a thermometer was initially developed by Ostapenko et al. (1987). Wark and Watson (2006) were able to calibrate the TitaniQ thermometer. According to their results, the measurement of Ti content by EPMA can be used to obtain crystallization temperatures above 600 °C, while SIMS analyses allow to go

down to at least 400 °C due to the different sensitivity of the instrumentations. Resulting temperature estimates can be considered very precise, usually better than ±5 °C (Wark and Watson, 2006). Moreover, these temperatures seem to be independent of pressure. Some authors have used it to better understand magma chamber processes (Girard & Stix, 2010; Ehrlich et al., 2012). The TitaniQ geothermometer operates under the principle that, at higher temperatures, quartz incorporates increasing concentrations of Ti (Wark & Watson, 2006; Thomas et al., 2010; Huang & Audétat, 2012; Wehrle & McDonald, 2019).

Other cations such as H<sup>+</sup>, Li<sup>+</sup>, Na<sup>+</sup>, K<sup>+</sup>, Cu<sup>+</sup> or Ag<sup>+</sup> can be incorporated in interstitial positions, sometimes acting as charge-compensating ions. Among them, Li seems to be more frequently incorporated into the quartz structure (Götze et al., 2004). Germanium, Rb, B and Be concentrations in quartz increase with the fractionation degree of the melt (Larsen et al., 2000; Jacamon and Larsen, 2009; Müller et al., 2015, 2018). Elements such as Al, Ge, Li, REE, and the element ratios of Ge/Fe or Th/U appear to be reliable indicators of specific geological settings. For instance, the 10\*Ge-Ti-Al/50 triangle by Schrön et al. (1988) shows some general trends for different quartz types. Quartz crystallized at early stages is characterized by low Ge/Fe ratios, while this ratio is high in quartz from later generations (Schrön et al., 1982).

Hydrothermal quartz has higher Al, Li, Na, and K concentrations, while there is greater Ti enrichment in magmatic quartz (Larsen et al., 2004;

Müller & Koch-Müller, 2009; Götte et al., 2011; Rusk, 2012; Breiter et al., 2017).

Given that, the trace element composition can be used to distinguish between ore deposits and between magmatic and hydrothermal quartz, e.g., Al and Ti concentrations vary between epithermal deposits, orogenic Au deposits, and porphyry-type deposits (I-type granites) (Rusk, 2012; Müller et al., 2018). Considering this, Zhang et al. (2022) proposed an Al vs. Ti diagram discriminating (even if with large overlapping) epithermal, Carlin-type Au, skarn, pegmatite related, porphyry-type and carbonatite-related quartz adapting the previous diagram by Rusk (2012). Shah et al. (2022) found a correlation between Al and Ti in the case of magmatic quartz, while confusing behaviours of these two elements in the case of hydrothermal quartz were observed. This indicated that hydrothermal quartz grows in a relatively complex situation compared to magmatic quartz and the amounts of trace elements may vary between different ore deposits. Several researchers have previously used this relationship (based on Al and Ti concentrations) to differentiate between porphyry-type deposits, epithermal deposits, and orogenic Au deposits (Rusk et al., 2011; Rusk, 2012; Zhang et al., 2019). According to them, Ti ranges from 1–200 ppm in porphyry deposits, and Al ranges from 50–500 ppm (Landtwing & Pettke, 2005; Müller et al., 2010). Contrarily, epithermal ore deposits contain less than 3 ppm Ti and 20–4000 ppm Al. Additionally, orogenic gold deposits have 1–10 ppm Ti and 100–1000 ppm Al (Rusk, 2012; Zhang et al., 2019).

The Ge/Al ratios of magmatic quartz and hydrothermal quartz are less than 0.008 and greater than 0.008, respectively. Magmatic quartz has the highest Ti and lowest Ge contents, while hydrothermal quartz has the opposite scenario (Müller et al., 2018).

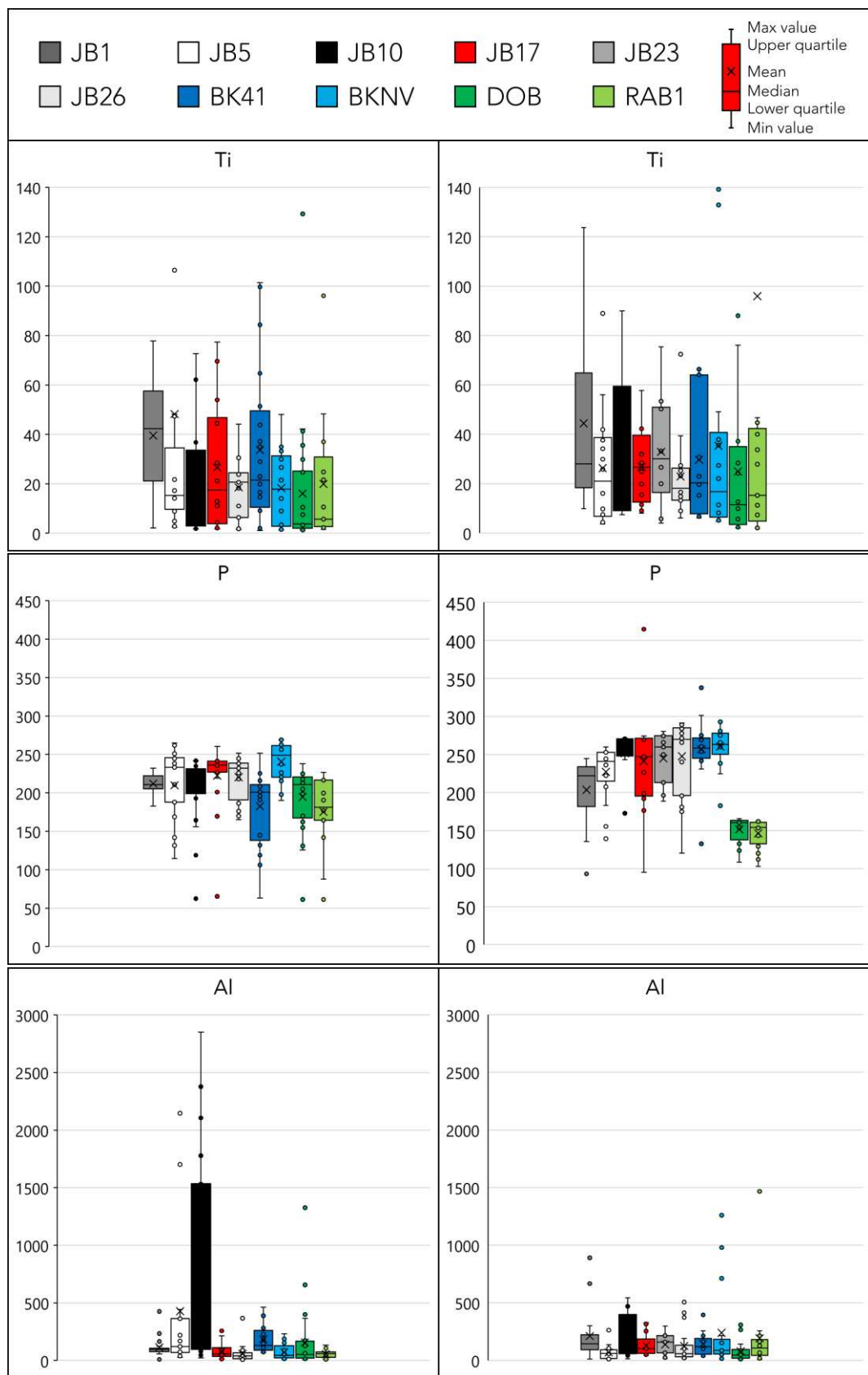
According to Müller et al. (2018), the Al-Ti, Al-Li, and Al/Ti-Ge/Ti binary plots effectively distinguish between the major groups of different pegmatites [the so-called Nb-Y-F – pegmatites (NYF), the Li-Cs-Ta pegmatites (LCT) and the pegmatites derived from residual melts of granitic magmatism (RMG)]. A threshold of roughly  $100 \mu\text{g}\cdot\text{g}^{-1}$  Al in quartz can be used to distinguish between the three major pegmatite categories. Most quartz from NYF pegmatites contains  $<100 \mu\text{g}\cdot\text{g}^{-1}$  Al, whereas quartz from LCT and RMG pegmatites contains  $>100 \mu\text{g}\cdot\text{g}^{-1}$  Al. The reason for this difference might be the Al saturation of the pegmatites because quartz growing in highly Al-saturated melts incorporates more Al. Plots of the incompatible elements Ge, B, Rb and Ga show weak positive correlations with Al reflecting the fractionation degree of the pegmatite melt but no discrimination between different pegmatite types.

Boron reaches higher concentrations in all types of quartz affiliated with S-type granites (strongly peraluminous plutons) than in their A-type analogues (from slightly peraluminous to sub-aluminous plutons), with medians of 2.7 and 1.15 ppm in granites, 1.15 and 0.49 ppm in greisens, 1.72 and 0.42 ppm in quartz veins, respectively, and 3.48 ppm in quartz-tourmaline rocks (Breiter et al., 2020). Similarly, also phosphorus is present in higher concentrations in quartz from peraluminous S-type

environment and does not decrease from magmatic quartz in granites through greisen quartz to hydrothermal veins (Breiter et al., 2020).

In the box and whiskers plot relative to the quartz crystals larger than 250 µm, it is possible to note a general enrichment trend from sample JB1 to sample JB10 for Al, Li, and Na (Figure 5.5). In the 63-250 µm fraction, this is visible for P and, to a lesser extent, for Na. The fate of B is quite peculiar because in the larger fraction it is possible to recognize three different groups comprising samples JB1, JB5 and JB10 (3-6 ppm), samples JB17 and JB26 (2-4 ppm) and samples from BK and KVI (<2 ppm).

The relatively high content of Ti (up to 60 ppm for the majority of the grains in both the fractions and with average of 25 and 38 ppm for the >250 µm, and for the 63-250 µm respectively) suggests a porphyry-type source rock according to Landtwing & Pettke (2005) and Müller et al. (2010). The sensible increase in Al content for sample JB10, coupled with its high Li content (in the coarse fraction) could indicate a relevant hydrothermal origin (Rusk, 2012; Zhang et al., 2019), even if the Ti content remains at almost the same level than the other samples leading to a possible mixed source.



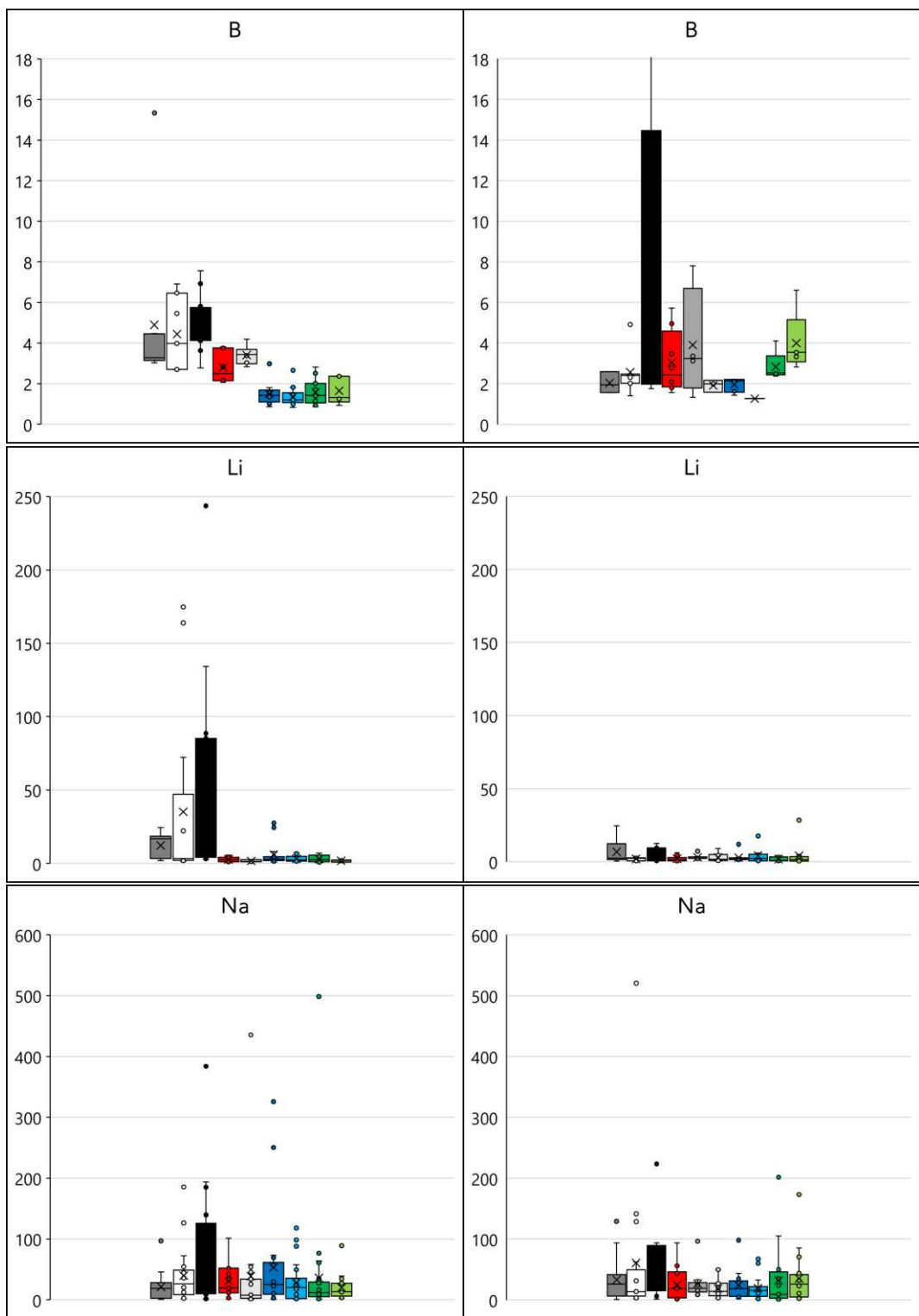


**Figure 5.5.** Concentrations of selected elements within the samples. On the left data from fraction >250 µm, on the right data from fraction 63-250 µm.

The B concentrations appear to separate JB from BK and KVI in the fraction >250 µm, and KVI from all the other basins in the fraction 63-250 µm (Figure 5.5). Meanwhile, the P content divide KVI from the other basins in the 63-250 µm fraction only (Figure 5.5).

As seen before, the relation between Al and Ti is widely used as a tool to discriminate quartz source rock. Figure 5.6 shows the classification based on the diagram proposed by Rusk (2012). Many researchers lately modified it, to add different fields, i.e. porphyry-related deposits (Landtwing & Pettke, 2005; Allan & Yardley, 2007; Maydagán et al., 2015; Mao et al., 2017; Rottier & Casanova, 2020), skarn deposits (Zhang et al., 2019), pegmatite-related deposits (Peterková & Dolejš, 2019; Müller et al., 2021), epithermal deposits (Rusk et al., 2011; Tanner et al., 2013), Carlin-type Au deposits (Li et al., 2020; Yan et al., 2020), and carbonatite-related REE deposits (Zhang et al., 2022).

It is clear that the grains from the >250 µm fraction are mainly plotted in the porphyry-related field, with relevant amount of grains spreading in the neighbouring pegmatite-related, carbonatite-related, and skarn deposits fields (Figure 5.6 top). It is also possible to notice that samples from JB are preferentially overlapping the porphyry-, pegmatite- and skarn related fields, meanwhile the carbonatite-related deposits field is almost entirely covered by samples from BK and especially from KVI. The grains from the 63-250 µm display less spreading within the different fields, with a neat predominance in the porphyry-related deposits field (Figure 5.6 bottom).

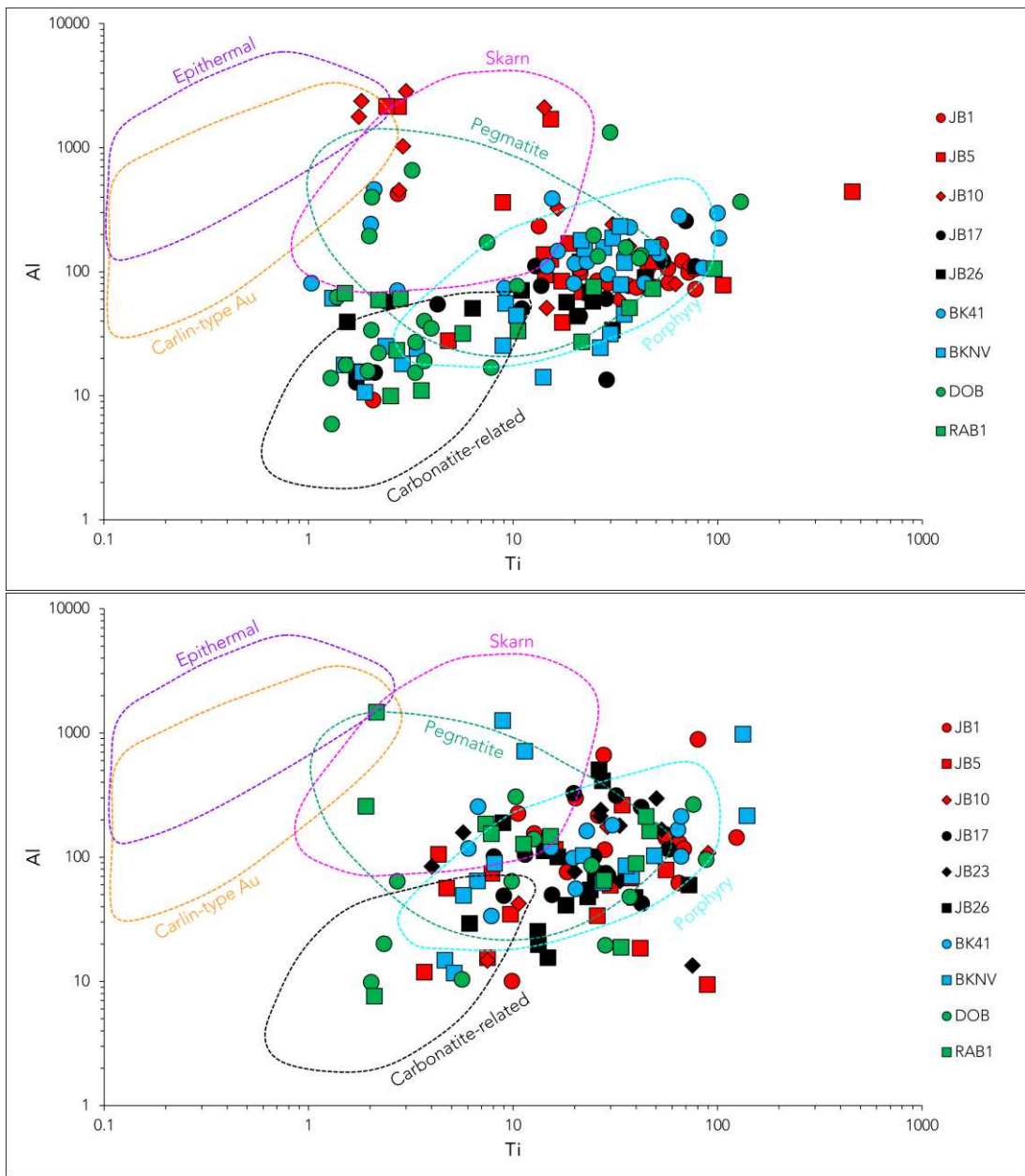
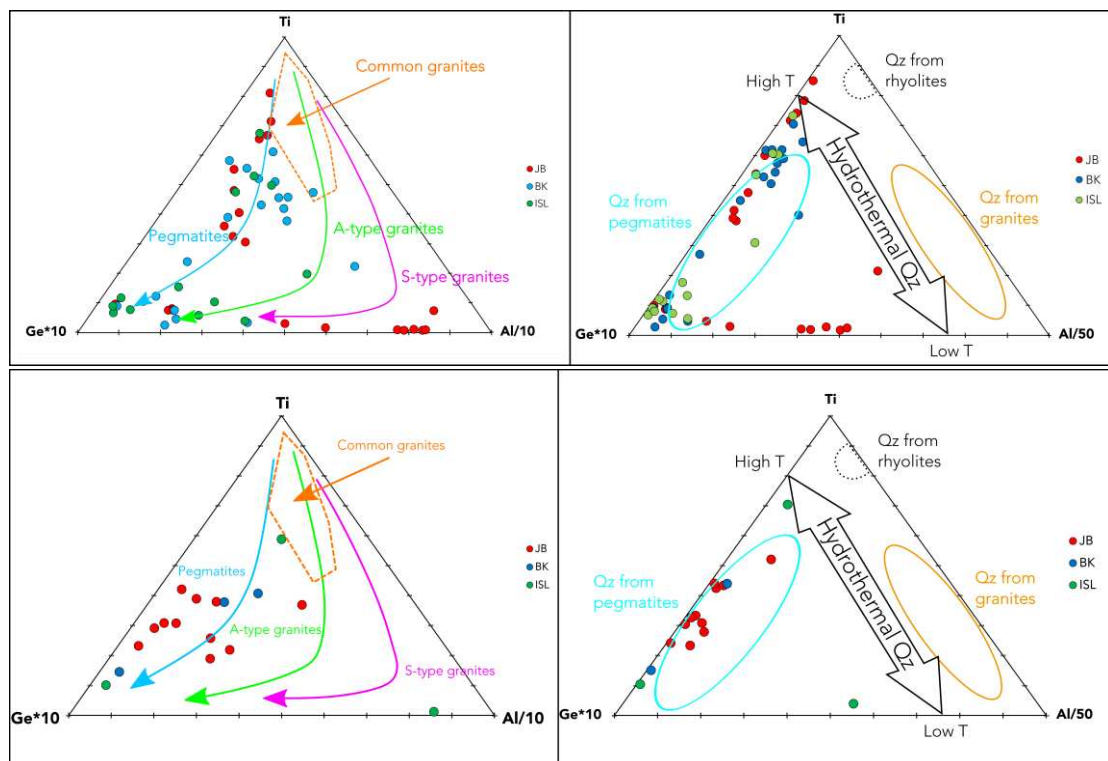


**Figure 5.6.** Discrimination diagram of Al-Ti for quartz (for the different fields, see references in the text). Top: data from  $>250\text{ }\mu\text{m}$  fraction; bottom: data from  $63\text{-}250\text{ }\mu\text{m}$  fraction (redrawn from Zhang et al., 2022).

The Ti-Al/10-10\*Ge and the Ti-Al/50-10\*Ge ternary diagrams proposed by Schrön et al. (1988) and modified by Götze (2009) represent as yet not only one of the best basis for the discrimination of pegmatitic vs. granitic quartz, but also help to distinguish between the common and rare-metal, and between the S- and A-type granites (Figure 5.7). Al, Li, and Ti median

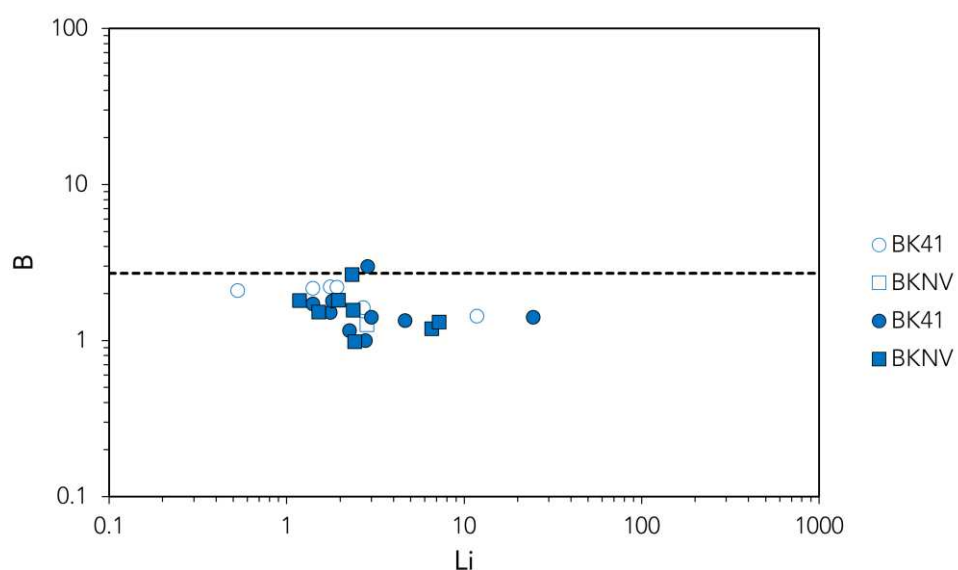
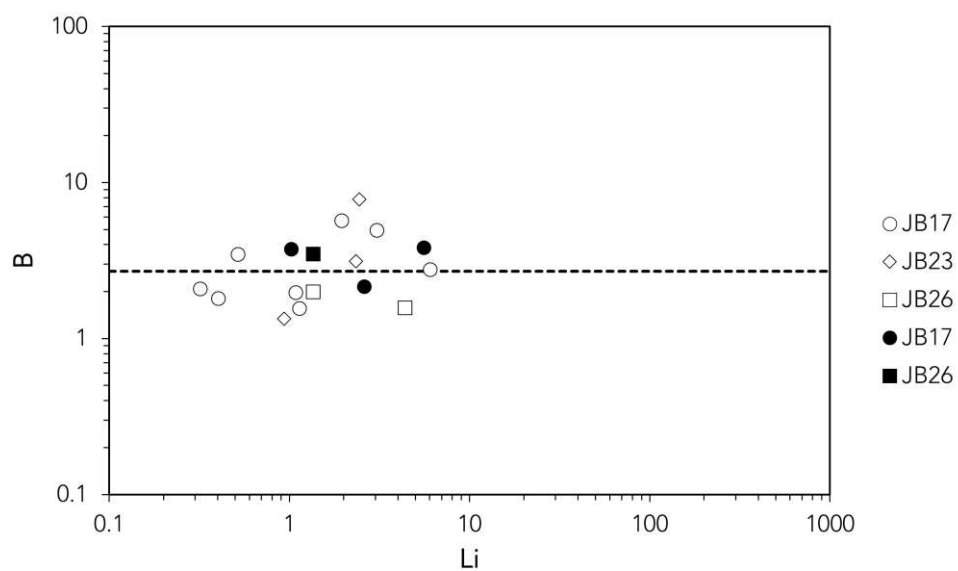
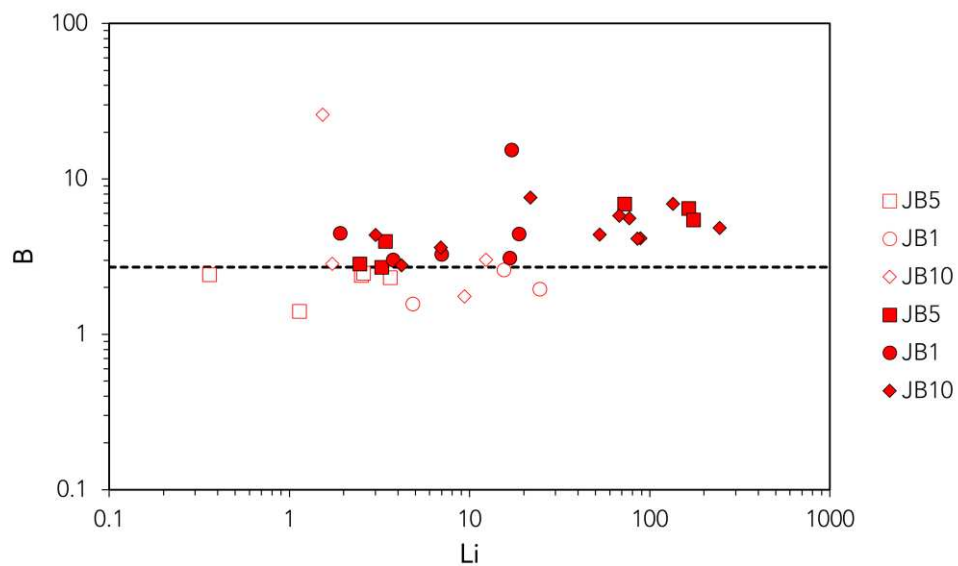
values are 447, 39.6, and 17.4 ppm, respectively for S-type granites, and 160, 15, and 6.6 ppm, respectively for A-type granites (Breiter et al., 2020).

It is possible to notice that the 63-250  $\mu\text{m}$  fraction shows less variability for the rock source of the quartz, as almost all the grains are placed within the pegmatites field with only few coming from A-type granites (Figure 5.7 bottom). Grains from >250  $\mu\text{m}$  fraction show a more diverse source, with more grains outside the pegmatite field, with some even identified as coming from S-type granite (Figure 5.7 top).



**Figure 5.7.** Triangular diagrams for quartz discrimination according to Schrön et al. (1988) and Götze (2009). Top: data from >250  $\mu\text{m}$  fraction; bottom: data from 63-250  $\mu\text{m}$  fraction.

Considering that most of the quartz crystals fall in the same field we tried to identify differences that could suggest that within the same lithological source (i.e. porphyry) the quartz crystals derived from different outcrops. For such purpose we used the B concentration that, according to the box and whiskers diagrams (Figure 5.5), seems to be promising. According to Breiter et al. (2020), the value of about 2.7 ppm (below which the 80% of A-type granites can be generally found) discriminates two different population for samples JB1, JB5, JB10, and Kvarner Islands ones. In JB1, JB5, and JB10, the coarser fraction appears enriched in B with respect to the smaller. In the KVI samples an opposite behavior can be noticed, with the finer fraction enriched in B (Figure 5.8) with respect to the coarser one. Within samples JB17, JB23 and JB26, it is not possible to recognize a clear trend with B values comprised between about 1 and 10 ppm, while in BK all the quartz crystals show B values below 3 ppm. This suggests a change in the supply of quartz within the different basins and even within the same basin during time, with possible exchange between fillings from S-type and A-type granite. In some cases, an S-type granite possibly was a close source for quartz (large quartz crystals), in other cases the S-type granite was a distant source (small quartz crystals).



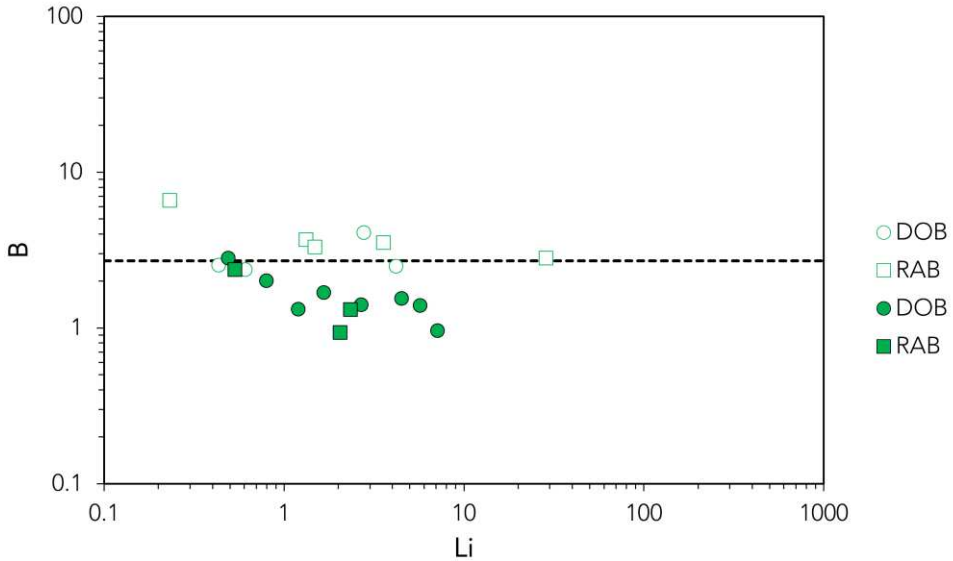


**Figure 5.8.** Relation between contents of B and Li, full markers represent data from  $>250 \mu\text{m}$ , empty markers represent data from 63-250  $\mu\text{m}$  fraction. A division line was drawn at 2.7 ppm of B concentration according to Breiter et al. (2020).

In addition to this, the P concentration seems to operate as a divider for samples from BK and KVI according to their size fraction. Grains from  $>250 \mu\text{m}$  show higher P concentrations meanwhile grains from 63-250  $\mu\text{m}$  display lower P concentrations (Figure 5.9).

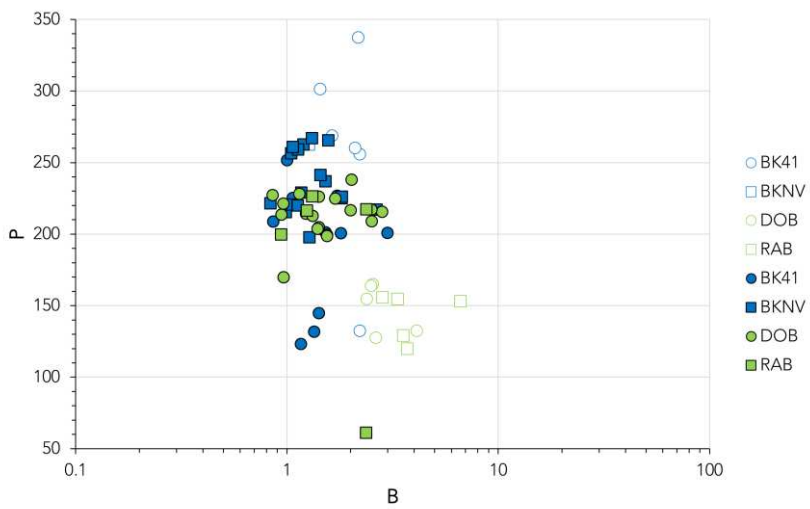


**Figure 5.9.** Relation between contents of P and B for BK and KVI samples, full markers represent data from  $>250 \mu\text{m}$ , empty markers represent data from 63-250  $\mu\text{m}$  fraction.

This behavior is going partially in contrast to what seen for B, as higher values of P (possibly related to S-type granites) are detected in the coarser

fraction of the BK and KVI samples. Enrichment in P could be also related to hydrothermal environment.

The contents of Li in quartz do not generally correlate with its bulk rock concentrations but show a relatively good positive correlation with Al. Lithium enters quartz lattice according to coupled substitution  $\text{Si}^{4+} \rightarrow \text{Al}^{3+} + \text{Li}^+$ , competing with water ( $\text{Si}^{4+} \rightarrow \text{Al}^{3+} + \text{H}^+$  substitution, Walsby et al., 2003; Müller et al., 2018; Potrafke et al., 2020). Thus, the maximum content of Li in quartz is theoretically limited by Al content in quartz with a molar ratio Li:Al = 1:1 (ca. 1:4 by weight). And really, some water- and fluxes-poor common granites (and some pegmatites as well) contain quartz grains with Li/Al values close to 1:4. Of course, grains with Li/Al values of  $\ll 1:4$  prevail, showing an important contribution of the  $\text{Si}^{4+} \rightarrow \text{Al}^{3+} + \text{H}^+$  substitution. Going to more evolved granite facies, the Li/Al values in quartz decrease in some plutons, indicating an increasing activity of magmatic water, e.g., at Panasqueira, Cínovec, and Orlovka (Breiter et al., 2019). In contrast, at Beauvoir and Nejdek-Podlesí, the Li/Al values become more stable or even increase. This diversity emphasizes the problematic nature of any interpretation. Besides water content, timing of mica crystallization and the resulting actual availability of Li in melt are also important factors for Li uptake into quartz (Breiter et al., 2020).

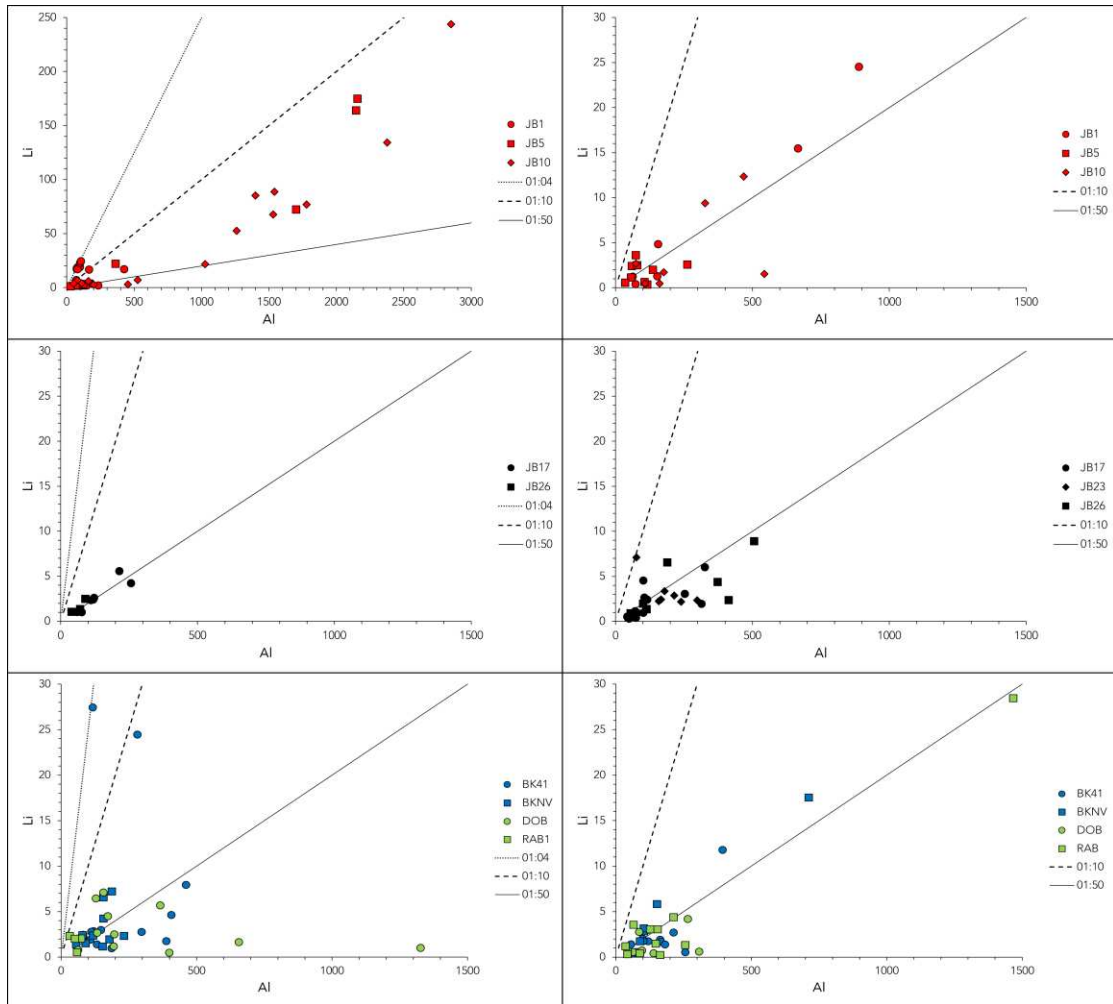


**Figure 5.10.** Li/Al ratio within the sample set. On the left data from  $>250\text{ }\mu\text{m}$ , on the right data from  $63\text{--}250\text{ }\mu\text{m}$  fraction.

Within the analysed set, the Li/Al ratio show values all below 1:10, and even lower than 1:50, for the  $63\text{--}250\text{ }\mu\text{m}$ , meanwhile grains  $>250\text{ }\mu\text{m}$  show generally higher values with some grains close to the above mentioned 1:4 ratio (Figure 5.10). According to Breiter et al. (2019, 2020) this could suggest a provenance from more evolved granite facies for the finer fraction.

As seen above, Ti content, when present, can be taken into account for TitaniQ temperature calculation for both the size fractions (Figure 5.11).

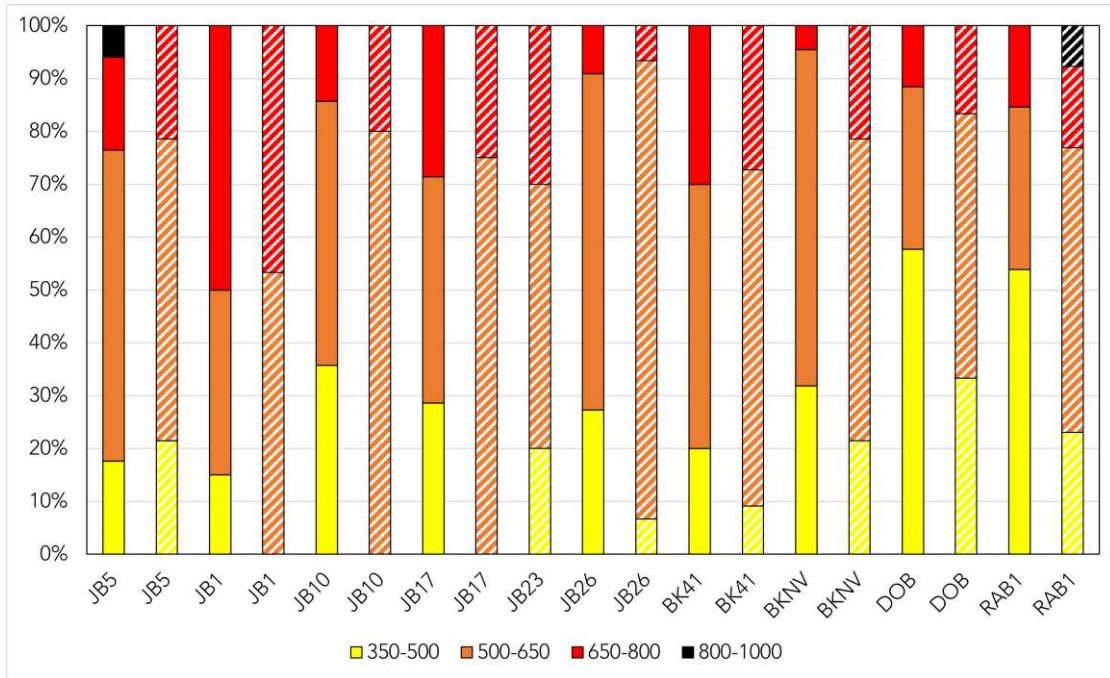


**Figure 5.11.** Crystallization temperature calculated using TitaniQ method for both fractions. Full bars show data from  $>250 \mu\text{m}$  fraction; striped bars show data from  $63-250 \mu\text{m}$  fraction.

For the  $>250 \mu\text{m}$  fraction, samples JB1 is dominated by temperatures above  $500^\circ\text{C}$ , with an increase of lower ones ( $<500^\circ\text{C}$ ) for samples JB5, JB10, and JB26. For JB5 and JB10 this could confirm the late stage volcanism source suggested by the Li-related defects presence. Sample JB17 shows a partial increase of grains with  $T_c > 650^\circ\text{C}$  suggesting a high temperature input confirming the volcanic source. Sample BK41 shows more grains with temperatures above than  $650^\circ\text{C}$  than BKNV, while samples DOB and RAB1 display a neat predominance of temperatures below  $650^\circ\text{C}$  with more than half of the grains even below  $500^\circ\text{C}$  (Figure 5.11).

Regarding grains from the  $63-250 \mu\text{m}$  fraction, JB samples show almost entirely grains with  $T_c > 500^\circ\text{C}$ , with some minor input  $<500^\circ\text{C}$  for samples

JB5, JB23, and JB26. Grains from BK and KVI show similar behaviour to their corresponding in the coarser fraction, with a localized input of grains with  $T_c > 800$  °C in sample RAB1 (Figure 5.11).

For all the before mentioned discussions, it is possible to state that the trace elements distribution is noticeably constrained by the size fraction. A possible explanation of this circumstance could be investigated focusing on the transport and sedimentation processes that differently involve the diverse grain size fractions.

The results of this study are in line of what stated by the previous ones based on different minerals (see chapter 2). Studies on the spinels testify a change in JB supply for sample JB17 (Lenaz et al., 2000) with an increase in magmatic over restitic peridotitic input. This change could have also interested areas of the crust where the obducted material has been placed and consequently the quartz supply. A return to peridotitic-style supply for BK and Istrian Basin is also proven by spinels (Lenaz et al., 2001; 2003), and rutile (Velicogna, 2020). The majority of 4H-defects (HP rocks) has been found in samples post JB17. Interestingly, Lenaz & Princivalle (2002) found HP-LT minerals such as of barroisite, glaucophane, and omphacites in young JB samples, suggesting the erosion of a possibly limited HP-LT rock outcrop. Notably, amphibolite-facies garnet (Lenaz et al., 2018), and amphibolite-eclogite facies rutile (Velicogna, 2020) are present in the same samples. The increase in metamorphic source supply for BK is proven also by the type and the abundancy of tourmalines (Garlatti, 2022-23). For BK

and KVI a more granitoids and subalkaline-facies source rocks are established by detrital pyroxenes from Krk Island (Lenaz et al., 2008), garnets (Lenaz et al., 2018), rutile, and zircon (Velicogna, 2020). The tourmalines from BK confirm a source from hydrothermally altered granites (Garlatti, 2022-23).

It remained to clarify the possible source of the quartz that have been identified as rhyolitic-type. It is interesting to note that in the Sava Zone (Internal Dinarides, between Bosnia-Herzegovina and Croatia) outcrops a bimodal igneous succession (comprising isotropic gabbros, doleritic dikes, basaltic pillow lavas, and rhyolites), that U-Pb ages on zircons from dolerites and rhyolites dated at  $81.39 \pm 0.11$  and  $81.6 \pm 0.12$  Ma, respectively (Ustaszewski et al., 2009). The intrusion of this bimodal magmatism led to formation of metamorphic soles in greenschist facies outcropping in the surrounding of the magmatic intrusion (Spahić & Gaudenyi, 2022). All of these rocks, although small in volume (covering areas of max 30 km<sup>2</sup>) show potential to be of great regional importance bearing new information about the evolution in the Late Cretaceous in the area of Sava Zone, a suture zone between Tisia Mega-Unit (European plate) and Adria microplate, which spatially and temporally marks the closure of the Neotethys Ocean (Schneider & Balen, 2020) and should be taken in account as possible source for the rhyolitic materials.

## CHAPTER 6. CONCLUSIONS

The main goal of the project was to try to verify changes in the provenance areas of the sediments filling the Julian, Brkini, and Kvarner Islands Basins by using OH-defects, cathodoluminescence and trace elements on quartz crystals.

The different analyses of the samples provide results to define, at least, tentatively, their origin. Basing on them the conclusions may be summarized as follow:

- Julian Basin's quartz shows differences in the supply source within the succession: the oldest ones (JB5 and JB1) show an almost 1:1 ratio between igneous and non-igneous origin; samples JB10 and JB17 show a change with a predominantly igneous source. The youngest samples (JB23 and JB26) have a neat predominance of a non-igneous source (about 75%; Bernardi et al., 2022).
- The Brkini samples also show a difference in the source with the older BK41 having a more abundant igneous source than the younger BKNV (60% and 40%, respectively).
- Samples from the Kvarner Islands Basin indicate a predominantly non-igneous source (DOB) while in RAB1 the non-igneous source seems to be clearly prevalent, even if only few clear spectra were obtained.
- Unfortunately, the cathodoluminescence results are not solid and clear enough to prove and give some sort of information about the origin of the

sediments. All the analysed quartz grains show almost the same CL effects.

- Trace element data such as Al, B, Li, and Na show some increasing trends from JB5 to JB17, while all the other samples show a similar behaviour with contents comparable to those of JB1.
- Discrimination diagram based on Ti and Al relation, constrains the source for the quartz grains mainly in the porphyry-type source rock and shows a more complex source for the coarse fraction.
- The Ti-Al/10-10\*Ge and Ti-Al/50-10\*Ge ternary diagrams (Schrön et al, 1988; Götze, 2009) suggest a pegmatitic and A-type granitic source for the finer fraction, while the coarser one appears with a more complex supply with a relevant amount of S-type granite sources.
- Boron differentiates all the Julian Basin samples ( $B > 2.7$  ppm) from those of Brkini and Kvarner Islands samples ( $B < 2.7$  ppm) within the  $> 250 \mu\text{m}$  size fraction. The behaviour is the opposite within the  $63-250 \mu\text{m}$  size fraction with JB B  $< 2.7$  ppm and KVI B  $> 2.7$  ppm.
- Phosphorus differentiates BK from KVI according to their size. The coarser fraction  $> 250 \mu\text{m}$  shows higher P concentration.
- Li/Al ratio values indicate a more evolved granite source for the finer fraction with values all below 1:10 and even lower than 1:50.
- Crystallization temperatures (TitaniQ) show a dominance of grains with  $T_c > 500^\circ\text{C}$  for JB1 and JB17, with lower ones for JB5 and JB10. BK41 shows more grains with  $T_c > 650^\circ\text{C}$  than BKNV, while DOB and RAB1

show a neat predominance of grains with  $T_c < 650$  °C. The finer fraction shows a general moderate increase in the  $T_c$ , with the exception of JB5.

- The proposed rock sources for the sediments are in line with the previous studies based on the heavy minerals. Porphyry-related quartz could be supplied by the Late Cretaceous rhyolite of the Sava zone.

It seems clear that, albeit with some distinctions, OH-defects, cathodoluminescence, and trace elements analyses on detrital quartz are quite a suitable tool for provenance studies, however, despite the large amounts of trace element analyses of quartz crystals published in the last years, many times researchers focused only on some trace elements so that the represented data can be considered such as a leopard spot. This fact and the consistent overlapping of fields in the common Al vs Ti causes several issues in the interpretations of possible sources. There is a need for more complete sets of analyses and for multidimensional approach able to massively improve the confidence on distinguishing quartz origin from different geological environments with a higher efficiency.

## APPENDICES

**Table A.1.** OH-defects content for samples from JB calculated with Thomas et al. (2009) calibration.

Sample	Thickness [µm]	Thickness [cm]	Area	M H <sub>2</sub> O	Density	epsilon	OH-defect [ppm]	Defect	TOTAL defects [ppm]
JB1_001	266	0.0266		18	2.65	89000			
JB1_002	246	0.0246	0.08190043	18	2.65	89000	0.51	Al	0.51
JB1_003	281	0.0281		18	2.65	89000			
JB1_004	238	0.0238	0.10155998	18	2.65	89000	0.65	Al	0.65
JB1_005	250	0.0250	0.91781007	18	2.65	89000	5.60	Al	5.75
	250	0.0250	0.02380568	18	2.65	89000	0.15	Li	
JB1_006	112	0.0112		18	2.65	89000			
JB1_007	184	0.0184	1.53060536	18	2.65	89000	12.70	Al	12.97
	184	0.0184	0.03269737	18	2.65	89000	0.27	Li	
JB1_008	136	0.0136		18	2.65	89000			
JB1_009	272	0.0272	0.47155469	18	2.65	89000	2.65	Al	2.65
JB1_010	273	0.0273	1.65602195	18	2.65	89000	9.26	Al	9.26
JB1_011	272	0.0272	0.14917413	18	2.65	89000	0.84	Al	0.84
JB1_012	191	0.0191	0.69779580	18	2.65	89000	5.58	Al	5.58
JB1_013	370	0.0370	0.09126773	18	2.65	89000	0.38	Al	0.38
JB1_014	186	0.0186		18	2.65	89000			
JB1_015	182	0.0182	1.51136566	18	2.65	89000	12.68	Al	15.25
	182	0.0182	0.30749815	18	2.65	89000	2.58	4H	
JB1_016	192	0.0192	0.1519535	18	2.65	89000	1.21	Al	1.45
	192	0.0192	0.02998947	18	2.65	89000	0.24	Li	
JB1_017	205	0.0205	3.14418114	18	2.65	89000	23.41	Al	26.41
	205	0.0205	0.40308181	18	2.65	89000	3.00	4H	

Sample	Thickness [µm]	Thickness [cm]	Area	M H <sub>2</sub> O	Density	epsilon	OH-defect [ppm]	Defect	TOTAL defects [ppm]
JB1_018	187	0.0187		18	2.65	89000			
JB1_019	122	0.0122		18	2.65	89000			
JB1_020	241	0.0241	0.93621544	18	2.65	89000	5.93	Al	6.14
	241	0.0241	0.03361013	18	2.65	89000	0.21	Li	
JB5_001	150	0.0150		18	2.65	89000			
JB5_002	27	0.0027	0.03520261	18	2.65	89000	1.99	Al	1.99
JB5_003	87	0.0087		18	2.65	89000			
JB5_004	93	0.0093	17.97936593	18	2.65	89000	295.09	Al	303.92
	93	0.0093	0.53767125	18	2.65	89000	8.82	Li	
JB5_005	117	0.0117	15.61098642	18	2.65	89000	203.66	Al	243.16
	117	0.0117	2.86574	18	2.65	89000	37.39	Li	
	117	0.0117	0.16152104	18	2.65	89000	2.11	B	
JB5_006	101	0.0101	0.07690346	18	2.65	89000	1.16	Al	1.16
JB5_007	47	0.0047		18	2.65	89000			
JB5_008	89	0.0089	0.19186787	18	2.65	89000	3.29	Al	3.95
	89	0.0089	0.03843454	18	2.65	89000	0.66	Li	
JB5_009	75	0.0075	0.36058911	18	2.65	89000	7.34	Al	8.80
	75	0.0075	0.07184249	18	2.65	89000	1.46	Li	
JB5_010	152	0.0152	1.38111637	18	2.65	89000	13.87	Al	13.87
JB5_011	125	0.0125	0.41345959	18	2.65	89000	5.05	Al	5.55
	125	0.0125	0.04145211	18	2.65	89000	0.51	4H	
JB5_012	105	0.0105		18	2.65	89000			
JB5_013	79	0.0079	0.08398579	18	2.65	89000	1.62	Al	1.62
JB5_014	70	0.0070	0.08022337	18	2.65	89000	1.75	Al	2.04
	70	0.0070	0.01323268	18	2.65	89000	0.29	4H	
JB5_015	75	0.0075	0.44972526	18	2.65	89000	9.15	Al	9.15

Sample	Thickness [µm]	Thickness [cm]	Area	M H <sub>2</sub> O	Density	epsilon	OH-defect [ppm]	Defect	TOTAL defects [ppm]
JB5_016	53	0.0053	0.14136651	18	2.65	89000	4.07	Al	4.07
JB5_017	83	0.0083	0.12017484	18	2.65	89000	2.21	Al	2.21
JB5_018	138	0.0138	0.82532279	18	2.65	89000	9.13	Al	9.44
	138	0.0138	0.02839668	18	2.65	89000	0.31	Li	
JB5_019	109	0.0109	0.10265322	18	2.65	89000	1.44	Al	1.44
JB5_020	126	0.0126	1.63572586	18	2.65	89000	19.82	Al	19.82
JB10_001	161	0.0161	0.14698435	18	2.65	89000	1.39	Al	1.39
JB10_002	88	0.0088	0.19104334	18	2.65	89000	3.31	Al	3.31
JB10_003	168	0.0168	0.57058870	18	2.65	89000	5.18	Al	5.52
	168	0.0168	0.03744356	18	2.65	89000	0.34	Li	
JB10_004	102	0.0102	5.51153797	18	2.65	89000	82.48	Al	94.62
	102	0.0102	0.81116829	18	2.65	89000	12.14	Li	
JB10_005	113	0.0113		18	2.65	89000			
JB10_006	121	0.0121	1.97550610	18	2.65	89000	24.92	Al	24.92
JB10_007	110	0.0110	38.64645978	18	2.65	89000	536.27	Al	571.47
	110	0.0110	2.39950642	18	2.65	89000	33.30	Li	
	110	0.0110	0.13704040	18	2.65	89000	1.90	B	
JB10_008	114	0.0114	0.99380091	18	2.65	89000	13.31	Al	14.38
	114	0.0114	0.03983058	18	2.65	89000	0.53	Li	
	114	0.0114	0.04039850	18	2.65	89000	0.54	B	
JB10_009	48	0.0048		18	2.65	89000			
JB10_010	87	0.0087	2.14504274	18	2.65	89000	37.63	Al	47.07
	87	0.0087	0.53804075	18	2.65	89000	9.44	Li	
JB10_011	120	0.0120	19.82318964	18	2.65	89000	252.15	Al	295.21
	120	0.0120	3.16539600	18	2.65	89000	40.26	Li	
	120	0.0120	0.21965096	18	2.65	89000	2.79	B	

Sample	Thickness [µm]	Thickness [cm]	Area	M H <sub>2</sub> O	Density	epsilon	OH-defect [ppm]	Defect	TOTAL defects [ppm]
JB10_012	46	0.0046	2.13972961	18	2.65	89000	71.00	Al	79.03
	46	0.0046	0.24187582	18	2.65	89000	8.03	Li	
JB10_013	106	0.0106	4.58200448	18	2.65	89000	65.98	Al	97.30
	106	0.0106	2.17528141	18	2.65	89000	31.32	Li	
JB10_014	82	0.0082		18	2.65	89000			
JB10_015	80	0.0080		18	2.65	89000			
JB10_016	92	0.0092	1.13200984	18	2.65	89000	18.78	Al	20.56
	92	0.0092	0.10692165	18	2.65	89000	1.77	Li	
JB10_017	173	0.0173	0.44526219	18	2.65	89000	3.93	Al	3.93
JB10_018	81	0.0081	8.38681320	18	2.65	89000	158.04	Al	176.77
	81	0.0081	0.99356665	18	2.65	89000	18.72	Li	
JB10_019	102	0.0102	2.48400759	18	2.65	89000	37.17	Al	39.97
	102	0.0102	0.18678842	18	2.65	89000	2.80	Li	
JB10_020	73	0.0073	0.11658669	18	2.65	89000	2.44	Al	2.44
JB17_001	114	0.0114	0.22964591	18	2.65	89000	3.07	Al	4.09
	114	0.0114	0.07600703	18	2.65	89000	1.02	4H	
JB17_002	136	0.0136	0.11470966	18	2.65	89000	1.29	Al	1.29
JB17_003	132	0.0132	0.34225502	18	2.65	89000	3.96	Al	3.96
JB17_004	123	0.0123	0.4473417	18	2.65	89000	5.55	Al	6.05
	123	0.0123	0.01178767	18	2.65	89000	0.15	Li	
	123	0.0123	0.0286853	18	2.65	89000	0.36	B	
JB17_005	84	0.0084	0.29065006	18	2.65	89000	5.28	Al	5.28
JB17_006	57	0.0057	0.33698821	18	2.65	89000	9.02	Al	10.15
	57	0.0057	0.01209396	18	2.65	89000	0.32	Li	
	57	0.0057	0.02996305	18	2.65	89000	0.80	B	
JB17_007	146	0.0146		18	2.65	89000			

Sample	Thickness [µm]	Thickness [cm]	Area	M H <sub>2</sub> O	Density	epsilon	OH-defect [ppm]	Defect	TOTAL defects [ppm]
JB17_008	170	0.017	0.1123196	18	2.65	89000	1.01	Al	1.21
	170	0.017	0.02297272	18	2.65	89000	0.21	4H	
JB17_009	140	0.014	0.09133665	18	2.65	89000	1.00	Al	1.18
	140	0.014	0.01659462	18	2.65	89000	0.18	4H	
JB17_010	121	0.0121		18	2.65	89000			
JB17_011	120	0.0120	0.70313317	18	2.65	89000	8.94	Al	9.32
	120	0.0120	0.02979184	18	2.65	89000	0.38	Li	
JB17_012	107	0.0107	0.53390303	18	2.65	89000	7.62	Al	7.62
JB17_013	135	0.0135	0.63836827	18	2.65	89000	7.22	Al	7.22
JB17_014	130	0.0130	0.08694852	18	2.65	89000	1.02	Al	1.02
JB17_015	137	0.0137	0.04159202	18	2.65	89000	0.46	Al	0.46
JB17_016	87	0.0087		18	2.65	89000			
JB17_017	86	0.0086	0.08131817	18	2.65	89000	1.44	Al	1.44
JB17_018	100	0.0100	0.24348132	18	2.65	89000	3.72	Al	3.72
JB17_019	119	0.0119	0.12818783	18	2.65	89000	1.64	Al	1.64
JB17_020	47	0.0047	0.03486403	18	2.65	89000	1.13	Al	1.13
JB26_001	157	0.0157	0.21271211	18	2.65	89000	2.07	Al	2.56
	157	0.0157	0.05108498	18	2.65	89000	0.50	4H	
JB26_002	140	0.0140	0.82733261	18	2.65	89000	9.02	Al	9.73
	140	0.0140	0.04740869	18	2.65	89000	0.52	Li	
	140	0.0140	0.01752419	18	2.65	89000	0.19	B	
JB26_003	215	0.0215	0.27583825	18	2.65	89000	1.96	Al	2.08
	215	0.0215	0.01644019	18	2.65	89000	0.12	4H	
JB26_004	145	0.0145	0.12815863	18	2.65	89000	1.35	Al	1.35
JB26_005	144	0.0144	1.49307934	18	2.65	89000	15.83	Al	16.49
	144	0.0144	0.06239993	18	2.65	89000	0.66	Li	

Sample	Thickness [µm]	Thickness [cm]	Area	M H <sub>2</sub> O	Density	epsilon	OH-defect [ppm]	Defect	TOTAL defects [ppm]
JB26_006	224	0.0224	0.29464356	18	2.65	89000	2.01	Al	2.38
	224	0.0224	0.01209334	18	2.65	89000	0.08	Li	
	224	0.0224	0.04255064	18	2.65	89000	0.29	4H	
JB26_007	220	0.0220	0.16110224	18	2.65	89000	1.12	Al	1.12
JB26_008	126	0.0126	0.05493511	18	2.65	89000	0.67	Al	0.67
JB26_009	178	0.0178	0.24339029	18	2.65	89000	2.09	Al	2.32
	178	0.0178	0.02665042	18	2.65	89000	0.23	B	
JB26_010	141	0.0141	1.06239144	18	2.65	89000	11.50	Al	12.26
	141	0.0141	0.07051474	18	2.65	89000	0.76	Li	
JB26_011	130	0.0130	0.14701621	18	2.65	89000	1.73	Al	1.73
JB26_012	223	0.0223	1.05382811	18	2.65	89000	7.21	Al	7.38
	223	0.0223	0.02378869	18	2.65	89000	0.16	B	
JB26_013	243	0.0243	1.44052376	18	2.65	89000	9.05	Al	9.59
	243	0.0243	0.08624138	18	2.65	89000	0.54	B	
JB26_014	162	0.0162	0.15847657	18	2.65	89000	1.49	Al	1.49
JB26_015	162	0.0162	0.12776741	18	2.65	89000	1.20	Al	1.20
JB26_016	207	0.0207		18	2.65	89000			
JB26_017	200	0.0200	0.99538612	18	2.65	89000	7.60	Al	9.00
	200	0.0200	0.09752921	18	2.65	89000	0.74	Li	
	200	0.0200	0.08649352	18	2.65	89000	0.66	4H	
JB26_018	186	0.0186	0.96422013	18	2.65	89000	7.91	Al	8.38
	186	0.0186	0.05734501	18	2.65	89000	0.47	Li	
JB26_019	236	0.0236	0.18589938	18	2.65	89000	1.20	Al	1.20
JB26_020	152	0.0152	0.18722923	18	2.65	89000	1.88	Al	1.88

**Table A.2.** OH-defects content for samples from BK calculated with Thomas et al. (2009) calibration.

Sample	Thickness [μm]	Thickness [cm]	Area	M H <sub>2</sub> O	Density	epsilon	OH-defect [ppm]	Defect	TOTAL defects [ppm]
BK41_001	120	0.0120	0.72605594	18	2.65	89000	9.24	Al	9.24
BK41_002	47	0.0047		18	2.65	89000			
BK41_003	115	0.0115		18	2.65	89000			
BK41_004	151	0.0151	0.82851531	18	2.65	89000	8.38	Al	8.38
BK41_005	150	0.0150	0.38974761	18	2.65	89000	3.97	Al	3.97
BK41_006	93	0.0093	0.54077571	18	2.65	89000	8.88	Al	8.88
BK41_007	180	0.0180	1.70709270	18	2.65	89000	14.48	Al	15.42
	180	0.0180	0.11079515	18	2.65	89000	0.94	Li	
BK41_008	160	0.0160	1.27312638	18	2.65	89000	12.15	Al	12.15
BK41_009	106	0.0106	0.36430055	18	2.65	89000	5.25	Al	5.25
BK41_010	89	0.0089	0.76794928	18	2.65	89000	13.17	Al	14.02
	89	0.0089	0.04931267	18	2.65	89000	0.85	Li	
BK41_011	47	0.0047		18	2.65	89000			
BK41_012	109	0.0109	0.47870610	18	2.65	89000	6.70	Al	6.70
BK41_013	82	0.0082	1.10829791	18	2.65	89000	20.63	Al	21.71
	82	0.0082	0.05786277	18	2.65	89000	1.08	Li	
BK41_014	42	0.0042		18	2.65	89000			
BK41_015	102	0.0102	0.56100036	18	2.65	89000	8.40	Al	8.58
	102	0.0102	0.01211126	18	2.65	89000	0.18	Li	
BK41_016	74	0.0074	1.53043825	18	2.65	89000	31.57	Al	33.60
	74	0.0074	0.04099931	18	2.65	89000	0.85	Li	
	74	0.0074	0.05770258	18	2.65	89000	1.19	4H	
BK41_017	37	0.0037		18	2.65	89000			
BK41_018	121	0.0121	0.89290669	18	2.65	89000	11.26	Al	11.26
BK41_019	132	0.0132	0.33233020	18	2.65	89000	3.84	Al	3.84

Sample	Thickness [µm]	Thickness [cm]	Area	M H <sub>2</sub> O	Density	epsilon	OH-defect [ppm]	Defect	TOTAL defects [ppm]
BK41_020	57	0.0057		18	2.65	89000			
BKNV_001	195	0.0195	0.07237374	18	2.65	89000	0.57	Al	0.57
BKNV_002	243	0.0243	1.47100073	18	2.65	89000	9.24	Al	9.55
	243	0.0243	0.04885764	18	2.65	89000	0.31	Li	
BKNV_003	265	0.0265	3.15157473	18	2.65	89000	18.15	Al	18.68
	265	0.0265	0.09083235	18	2.65	89000	0.52	Li	
BKNV_004	243	0.0243	2.42767745	18	2.65	89000	15.25	Al	15.58
	243	0.0243	0.05308358	18	2.65	89000	0.33	Li	
BKNV_005	127	0.0127		18	2.65	89000			
BKNV_006	238	0.0238	0.19881616	18	2.65	89000	1.28	Al	1.28
BKNV_007	208	0.0208	0.33043143	18	2.65	89000	2.42	Al	2.42
BKNV_008	218	0.0218	0.56105157	18	2.65	89000	3.93	Al	4.37
	218	0.0218	0.06365450	18	2.65	89000	0.45	B	
BKNV_009	231	0.0231	1.17045509	18	2.65	89000	7.73	Al	7.73
BKNV_010	156	0.0156	0.06097233	18	2.65	89000	0.60	Al	0.60
BKNV_011	245	0.0245	4.37476208	18	2.65	89000	27.26	Al	28.89
	245	0.0245	0.17140638	18	2.65	89000	1.07	Li	
	245	0.0245	0.09026102	18	2.65	89000	0.56	B	
BKNV_012	182	0.0182	0.04274233	18	2.65	89000	0.36	Al	0.36
BKNV_013	74	0.0074		18	2.65	89000			
BKNV_014	158	0.0158	0.11587733	18	2.65	89000	1.12	Al	1.12
BKNV_015	147	0.0147	1.45458754	18	2.65	89000	15.10	Al	16.21
	147	0.0147	0.10627317	18	2.65	89000	1.10	Li	
BKNV_016	111	0.0111	0.92725744	18	2.65	89000	12.75	Al	13.35
	111	0.0111	0.04362572	18	2.65	89000	0.60	Li	

Sample	Thickness [µm]	Thickness [cm]	Area	M H <sub>2</sub> O	Density	epsilon	OH-defect [ppm]	Defect	TOTAL defects [ppm]
BKNV_017	191	0.0191	1.53558716	18	2.65	89000	12.27	AI	13.92
	191	0.0191	0.20580429	18	2.65	89000	1.64	B	
BKNV_018	133	0.0133	0.10378465	18	2.65	89000	1.19	AI	1.19
BKNV_019	221	0.0221	0.14515864	18	2.65	89000	1.00	AI	1.46
	221	0.0221	0.06678041	18	2.65	89000	0.46	4H	
BKNV_020	106	0.0106		18	2.65	89000			

**Table A.3.** OH-defects content for samples from KVI calculated with Thomas et al. (2009) calibration.

Sample	Thickness [µm]	Thickness [cm]	Area	M H <sub>2</sub> O	Density	epsilon	OH-defect [ppm]	Defect	TOTAL defects [ppm]
DOB_001	105	0.0105	0.15418695	18	2.65	89000	2.24	AI	2.24
DOB_002	78	0.0078	0.72879389	18	2.65	89000	14.26	AI	15.44
	78	0.0078	0.06033638	18	2.65	89000	1.18	Li	
DOB_003	83	0.0083		18	2.65	89000			
DOB_004	109	0.0109		18	2.65	89000			
DOB_005	103	0.0103		18	2.65	89000			
DOB_006	59	0.0059	0.05813307	18	2.65	89000	1.50	AI	1.50
DOB_007	120	0.012	0.05514953	18	2.65	89000	0.70	AI	0.70
DOB_008	64	0.0064	0.20036622	18	2.65	89000	4.78	AI	5.27
	64	0.0064	0.02039917	18	2.65	89000	0.49	Li	
DOB_009	161	0.0161	0.40204791	18	2.65	89000	3.81	AI	3.81
DOB_010	88	0.0088		18	2.65	89000			
DOB_011	86	0.0086	0.14591375	18	2.65	89000	2.59	AI	2.59
DOB_012	112	0.0112	0.14974712	18	2.65	89000	2.04	AI	2.96
	112	0.0112	0.06764174	18	2.65	89000	0.92	4H	
DOB_013	97	0.0097		18	2.65	89000			
DOB_014	106	0.0106	0.04391467	18	2.65	89000	0.63	AI	0.63

Sample	Thickness [µm]	Thickness [cm]	Area	M H <sub>2</sub> O	Density	epsilon	OH-defect [ppm]	Defect	TOTAL defects [ppm]
DOB_015	76	0.0076		18	2.65	89000			
DOB_016	86	0.0086	0.77030831	18	2.65	89000	13.67	Al	14.74
	86	0.0086	0.04806260	18	2.65	89000	0.85	4H	
	86	0.0086	0.01219443	18	2.65	89000	0.22	B	
DOB_017	73	0.0073	0.06757163	18	2.65	89000	1.41	Al	1.41
DOB_018	138	0.0138	0.27634426	18	2.65	89000	3.06	Al	3.06
DOB_019	65	0.0065		18	2.65	89000			
DOB_020	89	0.0089		18	2.65	89000			
BK41_001	120	0.0120	0.72605594	18	2.65	89000	9.24	Al	9.24
BK41_002	47	0.0047		18	2.65	89000			
BK41_003	115	0.0115		18	2.65	89000			

**Table A.4.** LA-ICP-MS trace element contents for samples from JB, fraction >250 µm.

Sample	<sup>7</sup> Li	<sup>11</sup> B	<sup>23</sup> Na	<sup>25</sup> Mg	<sup>27</sup> Al	<sup>31</sup> P	<sup>35</sup> Cl	<sup>39</sup> K	<sup>45</sup> Sc	<sup>49</sup> Ti	<sup>71</sup> Ga	<sup>72</sup> Ge	<sup>133</sup> Cs	<sup>88</sup> Sr	<sup>9</sup> Be	<sup>85</sup> Rb
	µg/g	µg/g	µg/g	µg/g	µg/g	µg/g	µg/g	µg/g	µg/g	µg/g	µg/g	µg/g	µg/g	µg/g	µg/g	µg/g
JB1_01	18.80	4.44	0.80	0.87	81.31	182.82		16.33	0.52	57.64						
JB1_02	17.16			0.71	75.26	196.61		17.37	0.49	44.48		1.59				
JB1_04	16.72	3.10	27.97		165.20	189.15		28.23	0.62	52.56				1.00		
JB1_05	18.98				98.26	204.33		20.87	0.70	21.27		2.13				
JB1_06		4.04	21.24		84.31	204.52		44.27	0.59	25.80				0.50		
JB1_07	3.15		2.68		77.00	208.76		15.52	0.52	36.66						
JB1_08	17.81				74.78	206.91		19.45	0.57	40.03						
JB1_09	3.86		9.22	0.69	96.60	215.79		30.74	0.54	44.58				0.13		
JB1_10	2.06		0.70	0.77	106.56	217.43		21.74		57.05		1.77				
JB1_11	17.10			0.83	81.13	211.38		19.84		29.05						
JB1_14		3.17	18.99		9.26	208.83			0.48	2.06		1.84		0.21		
JB1_15		3.17	45.70	1.25	57.21	224.42		24.09	0.55	2.44		2.23		0.81		
JB1_16	7.00	3.28	6.20		72.23	227.26		16.19	0.67	77.81				0.12		
JB1_17	17.11	15.34	30.81		425.79	229.10		30.38		2.74				0.60		
JB1_18	1.91	4.47	97.01	3.21	233.74	220.57	216.82	67.08	0.60	13.36				2.02		

Sample	<sup>7</sup> Li	<sup>11</sup> B	<sup>23</sup> Na	<sup>25</sup> Mg	<sup>27</sup> Al	<sup>31</sup> P	<sup>35</sup> Cl	<sup>39</sup> K	<sup>45</sup> Sc	<sup>49</sup> Ti	<sup>71</sup> Ga	<sup>72</sup> Ge	<sup>133</sup> Cs	<sup>88</sup> Sr	<sup>9</sup> Be	<sup>85</sup> Rb
	µg/g	µg/g	µg/g	µg/g	µg/g	µg/g	µg/g	µg/g	µg/g	µg/g	µg/g	µg/g	µg/g	µg/g	µg/g	µg/g
JB1_19	23.69		0.86	1.64	101.99	221.76	216.12	16.53	0.56	74.47						
JB1_20	3.76	3.02	11.36		107.34	209.85		33.74		45.61			0.04	0.55		0.12
JB5_01			35.86	3.12	77.95	250.98		16.82	0.95	106.49		1.71	0.04	1.72		0.10
JB5_03			1.71		39.03	190.58		31.10		17.39						
JB5_04	72.21	6.92	126.32	73.84	1701.15	131.50		95.32		15.24		2.12	0.10	11.23		0.48
JB5_05	174.82	5.46	13.90		2156.66	238.19			0.57	2.41		6.27		0.35		
JB5_06	1.80		12.43		83.84	210.80		15.80	0.58	17.25		2.23	0.03	0.36		0.10
JB5_08	3.91		2.50		68.93	168.76	2108.11	15.50	0.53	21.69						
JB5_09	22.16		54.42	0.95	362.98	189.33	1219.67	35.89	0.59	8.89				2.66		
JB5_10	1.94		16.05	9.67	125.50	261.70		27.12	0.59	15.25		2.20		0.29		
JB5_11			8.43		39.56	264.98								0.11		
JB5_12			44.33	5.13	218.66	251.29		95.13	0.74			2.67		0.63		0.50
JB5_13	3.75		48.66	5.24	169.14	187.77	752.80	30.46		18.68				1.81		0.15
JB5_14	3.24	2.70	26.13		94.34	233.09		18.71	1.02	14.37		2.05		0.20		
JB5_15	2.46	2.84	38.39	2.12	75.06	233.89				47.38			0.07	2.86		
JB5_17	2.37		20.16		137.76	245.77		35.78		14.15				0.35		

Sample	<sup>7</sup> Li	<sup>11</sup> B	<sup>23</sup> Na	<sup>25</sup> Mg	<sup>27</sup> Al	<sup>31</sup> P	<sup>35</sup> Cl	<sup>39</sup> K	<sup>45</sup> Sc	<sup>49</sup> Ti	<sup>71</sup> Ga	<sup>72</sup> Ge	<sup>133</sup> Cs	<sup>88</sup> Sr	<sup>9</sup> Be	<sup>85</sup> Rb
	µg/g	µg/g	µg/g	µg/g	µg/g	µg/g	µg/g	µg/g	µg/g	µg/g	µg/g	µg/g	µg/g	µg/g	µg/g	µg/g
JB5_18		2.69	4.97		44.45	244.75		15.22	0.68	10.45				0.07		
JB5_19	1.20		3.28		27.75	189.09	494.80	15.54	0.58	4.83						
JB5_20	3.40	3.98	38.00		121.43	238.84		22.43	0.78	48.18				0.41		0.22
JB10_01			9.15		45.87	228.20		19.69	0.62	10.39				0.23		
JB10_02	2.69		27.64	0.90	200.65	215.26		39.66			2.81		1.01			
JB10_03	6.91	3.62	10.34		79.73	230.40		20.42	0.54	62.12				0.18		
JB10_04	70.65	4.26	123.96	6.72	1399.96	225.33		47.78	0.75		4.96		3.59		0.11	
JB10_05			12.46	0.83	60.00	232.56		18.67	0.51	32.55		2.04		0.55		
JB10_06	3.01	4.36	110.37		453.43	225.61		29.96		2.77	4.52		0.21			
JB10_07	134.26	6.92	45.35		2376.28	206.87	270.19	52.46		1.82	4.70		1.32			
JB10_08	4.20	2.77	1.45		111.87	215.67	250.18	12.12	0.72	72.72		1.77				
JB10_09		5.22	383.81	24.00	241.48	215.02		205.23		30.68			0.64	2.31		0.64
JB10_10	76.94	5.58	189.90	44.69	1778.71	192.90	476.41	118.82	0.78	1.76		4.71		8.46		0.37
JB10_11	243.73	4.83	106.24	4.53	2849.74	217.53		106.05	0.50	2.99		5.28		2.04		0.31
JB10_13	67.74	5.80	111.98	1.96	1531.54	234.84		46.82						18.51		
JB10_14			2.16		22.84	62.41	1148.62	20.23	1.10							

Sample	<sup>7</sup> Li	<sup>11</sup> B	<sup>23</sup> Na	<sup>25</sup> Mg	<sup>27</sup> Al	<sup>31</sup> P	<sup>35</sup> Cl	<sup>39</sup> K	<sup>45</sup> Sc	<sup>49</sup> Ti	<sup>71</sup> Ga	<sup>72</sup> Ge	<sup>133</sup> Cs	<sup>88</sup> Sr	<sup>9</sup> Be	<sup>85</sup> Rb
	μg/g	μg/g	μg/g	μg/g	μg/g	μg/g	μg/g	μg/g	μg/g	μg/g	μg/g	μg/g	μg/g	μg/g	μg/g	μg/g
JB10_16	6.12		6.42		160.67	155.92	582.47	20.04	0.67	36.74				0.08		
JB10_17	3.96		1.47		51.07	241.58		17.09	0.56	14.59						
JB10_18	85.20	4.12	33.91	10.87	1399.61	164.36		23.86	0.58			3.92		1.54		
JB10_19	21.75	7.57	185.04	1.27	1027.15	241.76		113.57	0.75	2.89		6.83		1.19		
JB17_01	5.57	3.82	56.95	1.17	213.83	219.02		37.07	0.66			1.93		1.49		
JB17_02	2.42		41.89	1.23	118.57	241.16		22.19	0.76					0.77	0.10	
JB17_03		2.07	57.11	15.71	50.40	239.02	212.18	17.60	0.84	11.02				0.21		
JB17_04	1.02	3.75	44.22		60.72	242.89		26.93	0.50	28.46				0.40		
JB17_06			16.92	2.21	88.40	200.96	542.91	20.11	0.77	44.45						
JB17_07			101.32		48.21	260.56		24.01						2.16		
JB17_08		2.17	57.99	4.03	34.01	242.71		17.92	0.66					0.57		
JB17_09	4.22		16.50	3.69	257.19	238.84		28.08		69.60				0.30		
JB17_10			3.11		13.44	230.44			0.73	28.65				0.14		
JB17_11	2.60	2.16	13.19	1.16	122.13	243.02		24.53	0.95	53.93			0.11	1.46	0.11	
JB17_12	2.35		25.71	1.17	110.39	239.22		27.27	0.69	77.42			0.05	0.26	0.12	
JB17_13			5.77		43.87	236.99		13.56	0.67	21.11						

Sample	<sup>7</sup> Li	<sup>11</sup> B	<sup>23</sup> Na	<sup>25</sup> Mg	<sup>27</sup> Al	<sup>31</sup> P	<sup>35</sup> Cl	<sup>39</sup> K	<sup>45</sup> Sc	<sup>49</sup> Ti	<sup>71</sup> Ga	<sup>72</sup> Ge	<sup>133</sup> Cs	<sup>88</sup> Sr	<sup>9</sup> Be	<sup>85</sup> Rb
	μg/g	μg/g	μg/g	μg/g	μg/g	μg/g	μg/g	μg/g	μg/g	μg/g	μg/g	μg/g	μg/g	μg/g	μg/g	μg/g
JB17_14			51.95	0.69	35.24	236.31	229.26	20.84	0.82		2.00		1.52			
JB17_15			1.43		15.38	235.43				2.11						
JB17_16	1.00		19.40		77.05	169.56	410.12	12.77	0.85	13.69			0.49			
JB17_17			9.32	0.85	12.82	226.92	242.49	11.68	0.49	1.71			0.19			
JB17_18			11.56		54.61	229.18	246.81	19.07		4.27			0.27			
JB17_19		2.83	33.96		57.35	230.61		20.00	0.69	2.39		2.36		0.52		
JB17_20			18.03	5.36	111.01	65.32	577.21	30.32	0.62	12.83			0.49			
JB26_01		3.52	28.76		15.68	239.40		11.42		1.72			0.42			
JB26_02	1.35	3.49	7.59		70.79	234.84		19.99	0.55	10.98			0.34			
JB26_03			53.91		23.76	238.15		23.55					0.63			
JB26_05	2.48		1.12		89.88	238.83			0.47	44.14						
JB26_06			34.18		12.13	237.05		13.28					0.73			
JB26_07			8.23		9.05	244.53		15.40								
JB26_08			57.87	0.91	25.00	228.97		17.11	0.52				0.29	0.39		
JB26_09			2.47		33.87	228.51		21.65	0.63	30.51						
JB26_10			4.73	1.22	120.59	251.51		57.76		21.24			0.14		0.14	

Sample	<sup>7</sup> Li	<sup>11</sup> B	<sup>23</sup> Na	<sup>25</sup> Mg	<sup>27</sup> Al	<sup>31</sup> P	<sup>35</sup> Cl	<sup>39</sup> K	<sup>45</sup> Sc	<sup>49</sup> Ti	<sup>71</sup> Ga	<sup>72</sup> Ge	<sup>133</sup> Cs	<sup>88</sup> Sr	<sup>9</sup> Be	<sup>85</sup> Rb
	µg/g	µg/g	µg/g	µg/g	µg/g	µg/g	µg/g	µg/g	µg/g	µg/g	µg/g	µg/g	µg/g	µg/g	µg/g	µg/g
JB26_11		3.38	435.44	8.50	366.06	236.11	585.41	122.74	0.61			0.39	12.82		0.34	
JB26_12			6.45		56.70	218.16				18.28			0.31			
JB26_13		4.19	6.54		50.84	241.66		18.68		6.33			0.04			
JB26_14		2.83	4.35		43.88	232.20		16.94	0.79	20.61						
JB26_15			25.79	1.44	17.25	225.87		13.22	0.41				0.21			
JB26_16			45.50	2.27	67.97	164.89			0.77	23.77		1.89		1.12		
JB26_17			1.98	0.80	8.58	169.88			0.71			2.46				
JB26_18	1.06		2.31		39.39	176.12			0.75	1.55		1.50		0.07		
JB26_19			0.42		7.31	186.49		10.24	0.67							
JB26_20		3.03	13.60	1.89	57.67	191.02		37.27	0.51	24.46			0.21		0.12	

**Table A.5.** LA-ICP-MS trace element contents for samples from BK, fraction >250 µm.

Sample	<sup>7</sup> Li	<sup>11</sup> B	<sup>23</sup> Na	<sup>25</sup> Mg	<sup>27</sup> Al	<sup>31</sup> P	<sup>35</sup> Cl	<sup>39</sup> K	<sup>45</sup> Sc	<sup>49</sup> Ti	<sup>71</sup> Ga	<sup>72</sup> Ge	<sup>133</sup> Cs	<sup>88</sup> Sr	<sup>9</sup> Be	<sup>85</sup> Rb
	µg/g	µg/g	µg/g	µg/g	µg/g	µg/g	µg/g	µg/g	µg/g	µg/g	µg/g	µg/g	µg/g	µg/g	µg/g	µg/g
BK41_01	1.76	1.52	63.19	5.98	388.10	201.30		63.02	1.01	15.51		1.52		1.49	0.15	0.17
BK41_03		1.55	250.27	3.87	70.53	199.54	212.82		0.85	2.72		2.62	0.09	4.93		
BK41_04			10.69	1.61	139.37	202.88		40.68	0.77	51.37		1.86		0.11		0.21

Sample	<sup>7</sup> Li	<sup>11</sup> B	<sup>23</sup> Na	<sup>25</sup> Mg	<sup>27</sup> Al	<sup>31</sup> P	<sup>35</sup> Cl	<sup>39</sup> K	<sup>45</sup> Sc	<sup>49</sup> Ti	<sup>71</sup> Ga	<sup>72</sup> Ge	<sup>133</sup> Cs	<sup>88</sup> Sr	<sup>9</sup> Be	<sup>85</sup> Rb
	µg/g	µg/g	µg/g	µg/g	µg/g	µg/g	µg/g	µg/g	µg/g	µg/g	µg/g	µg/g	µg/g	µg/g	µg/g	µg/g
BK41_05	27.44		0.64	0.52	116.69	190.91	139.60		0.79	20.04						
BK41_06	2.25	1.16	3.15		80.58	123.31	744.66		0.85	19.83						
BK41_07	1.81	1.80	69.08	0.58	95.02	200.55			0.77	28.97			0.05	0.20		
BK41_08	2.46				81.36	208.09			0.87	43.80	0.07					
BK41_09		0.86	4.70	2.75	80.90	208.77		14.51	0.88	1.03		3.19			0.12	
BK41_10	24.46	1.41	33.53	0.93	281.50	144.76	496.07	13.95	0.66	64.72		3.40	0.32	0.10	0.35	0.45
BK41_11			16.75	8.93	73.96	106.20	296.41	9.51	1.03	9.06				0.50		
BK41_12	2.20	1.57	28.95	4.17	139.69	215.28	164.10	9.01	0.80	25.72				0.27		
BK41_13	1.88		21.12	9.91	241.99	204.51	214.95	10.09	0.85	100.55				0.43		
BK41_15	1.92		10.46	3.96	107.71	215.82	159.97	10.38	0.84	84.35			0.03	0.15		0.27
BK41_16	4.63	1.34	73.36	1.88	407.36	131.87	387.56	21.92	0.69			1.94		1.51		
BK41_17			325.84	20.93	228.84	62.94	895.27	101.82	0.95	37.16			5.46			2.80
BK41_18	2.85	2.98	7.94	0.46	120.39	200.90	261.07		0.77	22.92		1.80				
BK41_19	2.78	1.00	8.42	0.33	111.43	251.71	152.85		0.75	14.62				0.15		
BKNV_01			1.66		10.67	257.19	155.59		0.82	1.89		1.81				
BKNV_02	1.42		1.79		55.66	257.21			0.88	9.20		2.37				

Sample	<sup>7</sup> Li	<sup>11</sup> B	<sup>23</sup> Na	<sup>25</sup> Mg	<sup>27</sup> Al	<sup>31</sup> P	<sup>35</sup> Cl	<sup>39</sup> K	<sup>45</sup> Sc	<sup>49</sup> Ti	<sup>71</sup> Ga	<sup>72</sup> Ge	<sup>133</sup> Cs	<sup>88</sup> Sr	<sup>9</sup> Be	<sup>85</sup> Rb
	μg/g	μg/g	μg/g	μg/g	μg/g	μg/g	μg/g	μg/g	μg/g	μg/g	μg/g	μg/g	μg/g	μg/g	μg/g	μg/g
BKNV_03	6.56	1.20	1.71		156.35	262.64	186.90		0.73	48.01						
BKNV_04	2.36	1.57	35.13	0.94	118.77	265.47			0.85	34.99		2.04	0.06	0.35		
BKNV_06	1.51	1.28	41.38	2.01	75.75	246.77		5.78	0.81	1.31		1.82		0.72		
BKNV_07			34.43		25.11	261.33	181.42		0.76	2.38		1.46		0.27		
BKNV_08		1.13	4.34		25.42	259.13			0.88	8.93				0.08		
BKNV_09			17.24		45.26	260.17	178.44		0.91	34.92		2.06				
BKNV_10			3.94		13.94	269.40			0.91					0.19		
BKNV_11	7.21	1.31	1.52		186.96	267.12	179.37		0.90	30.62		1.75			0.24	
BKNV_12			3.79	0.63	14.09	266.58			0.73	14.05				0.13		
BKNV_13		1.28	93.26	4.09	45.73	193.88	281.08	12.09	0.86			2.51	0.06	1.88		
BKNV_14		1.25	40.70	0.62	27.96	251.08	196.30		0.96	28.27			0.04	0.13		
BKNV_15	2.33	2.65	36.93	2.35	232.45	217.15	142.33	30.60	0.78	33.21		1.35	0.04	0.46	0.18	
BKNV_16	2.42	0.99	0.99	0.71	78.83	215.42	152.52		0.97	33.61		1.89				
BKNV_17	1.56	1.82	75.14	1.49	166.19	225.65	196.94	27.62	0.88	21.91		1.64	0.13	0.78	0.45	
BKNV_18		1.12	7.62		24.10	219.90			0.88	3.39				0.18		
BKNV_19		1.17	25.50		18.12	229.10	149.58		0.96	2.87				0.26		

Sample	<sup>7</sup> Li	<sup>11</sup> B	<sup>23</sup> Na	<sup>25</sup> Mg	<sup>27</sup> Al	<sup>31</sup> P	<sup>35</sup> Cl	<sup>39</sup> K	<sup>45</sup> Sc	<sup>49</sup> Ti	<sup>71</sup> Ga	<sup>72</sup> Ge	<sup>133</sup> Cs	<sup>88</sup> Sr	<sup>9</sup> Be	<sup>85</sup> Rb
	µg/g	µg/g	µg/g	µg/g	µg/g	µg/g	µg/g	µg/g	µg/g	µg/g	µg/g	µg/g	µg/g	µg/g	µg/g	µg/g
BKNV_20		0.84	2.18	1.57	16.59	210.74	317.48		0.90	1.66						

**Table A.6.** LA-ICP-MS trace element contents for samples from KVI, fraction >250 µm.

Sample	<sup>7</sup> Li	<sup>11</sup> B	<sup>23</sup> Na	<sup>25</sup> Mg	<sup>27</sup> Al	<sup>31</sup> P	<sup>35</sup> Cl	<sup>39</sup> K	<sup>45</sup> Sc	<sup>49</sup> Ti	<sup>71</sup> Ga	<sup>72</sup> Ge	<sup>133</sup> Cs	<sup>88</sup> Sr	<sup>9</sup> Be	<sup>85</sup> Rb
	µg/g	µg/g	µg/g	µg/g	µg/g	µg/g	µg/g	µg/g	µg/g	µg/g	µg/g	µg/g	µg/g	µg/g	µg/g	µg/g
DOB_01	4.49	1.55	12.22	1.83	172.87	198.70	244.12	39.84	0.83	7.47		1.31	0.04			0.14
DOB_02	5.67	1.40	60.78	5.18	365.69	203.74	191.93	36.12	0.97	129.29			0.07	1.16		0.27
DOB_03		1.23	52.04	2.32	25.39	219.79	188.26	4.19	0.75			1.63		47.17		
DOB_04			6.50	0.74	40.00	199.23	178.72		0.73	3.68		1.63		0.54		
DOB_05		0.90	12.27	0.13	16.15	220.49	126.76		0.79	5.56				0.08		
DOB_06	1.02		498.45	53.59	1326.99	154.78		284.88	0.82	29.80				1.03		1.06
DOB_07		1.42	1.63		15.88	226.12			0.72	1.95		2.60				
DOB_08	2.51		29.03	22.71	196.23	61.24	486.23	45.19	0.56	24.69				0.65		
DOB_09		0.96	2.88		24.62	212.18			0.84	2.77		1.65		0.31	0.07	
DOB_10		1.14	6.82	0.80	27.05	223.02			0.86	3.83				0.75		
DOB_11			35.31	22.63	135.26	163.34	479.76		0.89	42.21				0.77		
DOB_12		2.50	0.99	3.02	5.90	217.19			0.85	1.30		1.26		0.66		

Sample	<sup>7</sup> Li	<sup>11</sup> B	<sup>23</sup> Na	<sup>25</sup> Mg	<sup>27</sup> Al	<sup>31</sup> P	<sup>35</sup> Cl	<sup>39</sup> K	<sup>45</sup> Sc	<sup>49</sup> Ti	<sup>71</sup> Ga	<sup>72</sup> Ge	<sup>133</sup> Cs	<sup>88</sup> Sr	<sup>9</sup> Be	<sup>85</sup> Rb
	µg/g	µg/g	µg/g	µg/g	µg/g	µg/g	µg/g	µg/g	µg/g	µg/g	µg/g	µg/g	µg/g	µg/g	µg/g	µg/g
DOB_13	1.66	1.69	63.85	32.73	656.37	224.81		210.36	1.04	3.21		0.05	1.86		1.01	
DOB_16	1.20	1.32	28.96	3.23	194.27	212.72		17.74	0.84	1.98		2.91		2.93		
DOB_17	6.77	0.96	5.38	2.12	142.36	150.41	291.45	18.17	0.77	38.43		2.02		0.18		
DOB_18		2.26	26.86	4.01	75.68	212.84	166.78		0.81	17.62		1.98		1.06		
DOB_19			6.63	0.99	23.89	145.91	330.03		0.81	1.66				0.28		
DOB_20			1.75		17.66	162.19	288.80		0.87	1.52		1.66				
RAB1_02			38.98	2.94	27.18	202.07	221.86		0.82	21.61				7.30		
RAB1_04	2.33	1.32	4.02		31.87	226.49			0.83	5.67				0.13		
RAB1_05	2.04	0.94	12.71	1.29	73.28	199.67			0.97	48.21		1.60				
RAB1_06		1.24	16.55	0.49	33.32	216.50	197.11		0.69	10.56				0.41		
RAB1_07			16.30	0.57	63.69	180.79	310.72	5.94	0.89	2.16				0.70		
RAB1_08	2.02		3.32	3.26	51.25	181.20		25.83	0.87	36.98						
RAB1_09			89.00	3.43	60.88	164.32	489.29		0.72					3.38		
RAB1_10			2.54		9.94	164.65	373.47		0.84	2.52		1.79				
RAB1_12			6.26	1.71	75.49	176.82	360.33	15.11	0.77	24.74		1.44		0.18		
RAB1_13			13.51	0.79	23.22	87.76	349.71		0.86	2.70				0.62		

Sample	<sup>7</sup> Li	<sup>11</sup> B	<sup>23</sup> Na	<sup>25</sup> Mg	<sup>27</sup> Al	<sup>31</sup> P	<sup>35</sup> Cl	<sup>39</sup> K	<sup>45</sup> Sc	<sup>49</sup> Ti	<sup>71</sup> Ga	<sup>72</sup> Ge	<sup>133</sup> Cs	<sup>88</sup> Sr	<sup>9</sup> Be	<sup>85</sup> Rb
	µg/g	µg/g	µg/g	µg/g	µg/g	µg/g	µg/g	µg/g	µg/g	µg/g	µg/g	µg/g	µg/g	µg/g	µg/g	µg/g
RAB1_14			8.06		11.03	190.42	208.60		0.75	3.56			0.17			
RAB1_15		2.36	34.44	21.12	132.75	61.30	746.06	15.66	0.76				0.94			
RAB1_16			27.00	1.67	105.82	177.24	354.64	27.37	0.78	96.09			0.86		0.16	
RAB1_18	0.53	2.37	13.17	0.50	59.14	217.31	142.97		0.79	2.20	0.10	1.31	0.05	0.38		

**Table A.7.** LA-ICP-MS trace element limits of detection for samples from JB, fraction >250 µm.

Sample	<sup>7</sup> Li	<sup>11</sup> B	<sup>23</sup> Na	<sup>25</sup> Mg	<sup>27</sup> Al	<sup>31</sup> P	<sup>35</sup> Cl	<sup>39</sup> K	<sup>45</sup> Sc	<sup>49</sup> Ti	<sup>71</sup> Ga	<sup>72</sup> Ge	<sup>133</sup> Cs	<sup>88</sup> Sr	<sup>9</sup> Be	<sup>85</sup> Rb
	µg/g	µg/g	µg/g	µg/g	µg/g	µg/g	µg/g	µg/g	µg/g	µg/g	µg/g	µg/g	µg/g	µg/g	µg/g	µg/g
JB1_01	0.67	2.62	0.37	0.68	0.88	7.19	174.37	8.58	0.37	1.43	0.22	1.34	0.03	0.06	0.32	0.07
JB1_02	0.66	2.71	0.38	0.63	0.88	7.00	173.38	8.40	0.36	1.46	0.19	1.27	0.03	0.07	0.36	0.08
JB1_04	0.68	2.63	0.35	0.60	0.91	7.27	178.14	8.49	0.36	1.36	0.17	1.40	0.03	0.07	0.24	0.07
JB1_05	0.72	2.75	0.40	0.62	0.97	7.69	191.45	8.99	0.38	1.26	0.22	1.33	0.03	0.06	0.24	0.09
JB1_06	1.58	6.27	0.92	1.63	2.15	16.61	417.32	19.06	0.86	4.11	0.64	3.53	0.09	0.16	1.09	0.23
JB1_07	0.80	3.12	0.43	0.43	1.07	8.70	219.74	9.92	0.45	1.53	0.30	1.69	0.04	0.06	0.41	0.11
JB1_08	0.81	3.05	0.47	0.74	1.07	8.80	222.01	9.96	0.42	1.72	0.26	1.60	0.04	0.07	0.50	0.12
JB1_09	0.85	3.09	0.44	0.62	1.10	9.03	233.38	10.37	0.45	1.79	0.37	1.75	0.04	0.07	0.58	0.11
JB1_10	0.75	2.73	0.43	0.70	0.99	8.01	208.33	9.13	0.41	1.50	0.18	1.50	0.03	0.07	0.33	0.09
JB1_11	0.75	2.74	0.42	0.46	1.00	8.08	209.76	9.12	0.40	1.77	0.30	1.58	0.03	0.07	0.45	0.08
JB1_14	0.82	2.95	0.46	0.93	1.10	9.01	234.27	10.02	0.46	1.87	0.34	1.67	0.04	0.08	0.37	0.08
JB1_15	0.71	2.54	0.41	0.67	0.94	7.87	199.34	8.69	0.38	1.28	0.26	1.41	0.03	0.07	0.36	0.07
JB1_16	0.74	2.58	0.43	0.61	1.01	8.09	205.95	9.02	0.39	1.56	0.22	1.53	0.03	0.05	0.38	0.07
JB1_17	0.96	3.17	0.58	0.67	1.32	10.53	263.32	11.64	0.53	1.96	0.25	2.00	0.04	0.10	0.56	0.14
JB1_18	0.78	2.71	0.43	0.73	1.04	8.38	214.89	9.48	0.42	1.60	0.25	1.67	0.04	0.07	0.27	0.10

Sample	<sup>7</sup> Li	<sup>11</sup> B	<sup>23</sup> Na	<sup>25</sup> Mg	<sup>27</sup> Al	<sup>31</sup> P	<sup>35</sup> Cl	<sup>39</sup> K	<sup>45</sup> Sc	<sup>49</sup> Ti	<sup>71</sup> Ga	<sup>72</sup> Ge	<sup>133</sup> Cs	<sup>88</sup> Sr	<sup>9</sup> Be	<sup>85</sup> Rb
	µg/g	µg/g	µg/g	µg/g	µg/g	µg/g	µg/g	µg/g	µg/g	µg/g	µg/g	µg/g	µg/g	µg/g	µg/g	µg/g
JB1_19	0.75	2.66	0.41	0.63	1.04	8.17	208.33	9.24	0.42	1.68	0.22	1.65	0.03	0.08	0.35	0.08
JB1_20	1.10	3.91	0.63	0.95	1.46	11.93	298.79	13.27	0.60	2.38	0.36	2.29	0.04	0.10	0.79	0.15
JB5_01	0.83	2.33	0.52	0.91	1.20	9.51	262.82	11.71	0.51	1.70	0.33	1.79	0.04	0.09	0.50	0.10
JB5_03	0.83	2.16	0.47	0.55	1.15	9.35	278.46	11.61	0.48	1.75	0.29	1.87	0.04	0.07	0.44	0.10
JB5_04	1.00	2.85	0.63	1.14	1.44	11.38	381.46	14.03	0.60	2.37	0.36	2.24	0.05	0.10	0.42	0.13
JB5_05	0.95	2.58	0.58	1.20	1.38	10.69	412.53	13.28	0.55	2.14	0.40	2.04	0.05	0.12	0.32	0.13
JB5_06	0.91	2.58	0.56	1.02	1.34	10.46	468.23	13.16	0.56	2.11	0.40	2.05	0.04	0.11	0.52	0.12
JB5_07	1.05	2.94	0.65	0.72	1.52	11.78	599.80	15.20	0.61	2.06	0.40	2.30	0.05	0.11	0.58	0.13
JB5_08	0.95	2.59	0.60	0.79	1.38	10.77	655.13	13.85	0.59	2.08	0.36	2.05	0.05	0.09	0.50	0.15
JB5_09	0.85	2.35	0.51	0.64	1.25	9.81	698.22	12.82	0.53	1.79	0.36	1.74	0.04	0.08	0.13	0.11
JB5_10	0.85	2.37	0.52	0.81	1.23	9.63	898.05	12.63	0.50	1.85	0.35	1.87	0.04	0.09	0.54	0.12
JB5_11	0.86	2.32	0.54	0.76	1.26	9.81	1148.59	12.99	0.53	2.07	0.30	1.75	0.04	0.08	0.43	0.11
JB5_12	2.12	6.18	1.37	2.89	3.21	23.59	3700.34	30.84	1.27	5.99	0.90	4.89	0.12	0.28	1.86	0.44
JB5_13	0.82	2.40	0.50	0.55	1.23	9.50	25044.16	12.85	0.50	1.92	0.27	1.73	0.03	0.08	0.40	0.08
JB5_14	0.82	2.25	0.52	0.54	1.17	9.38	3680.33	12.93	0.49	1.51	0.19	1.64	0.04	0.07	0.48	0.09
JB5_15	0.91	2.43	0.57	0.97	1.33	10.40	1511.53	14.47	0.56	1.81	0.32	1.93	0.04	0.11	0.30	0.11

Sample	<sup>7</sup> Li	<sup>11</sup> B	<sup>23</sup> Na	<sup>25</sup> Mg	<sup>27</sup> Al	<sup>31</sup> P	<sup>35</sup> Cl	<sup>39</sup> K	<sup>45</sup> Sc	<sup>49</sup> Ti	<sup>71</sup> Ga	<sup>72</sup> Ge	<sup>133</sup> Cs	<sup>88</sup> Sr	<sup>9</sup> Be	<sup>85</sup> Rb
	µg/g	µg/g	µg/g	µg/g	µg/g	µg/g	µg/g	µg/g	µg/g	µg/g	µg/g	µg/g	µg/g	µg/g	µg/g	µg/g
JB5_17	1.05	2.88	0.68	0.92	1.57	11.85	1307.05	16.57	0.65	2.09	0.37	2.21	0.05	0.13	0.62	0.18
JB5_18	1.06	2.80	0.67	0.96	1.59	12.19	1076.17	17.07	0.66	2.05	0.39	2.32	0.05	0.10	0.69	0.15
JB5_19	0.85	2.50	0.53	0.58	1.26	9.96	681.70	14.17	0.52	1.65	0.27	1.65	0.03	0.08	0.28	0.08
JB5_20	0.81	2.21	0.50	0.57	1.29	9.47	288.78	14.07	0.51	1.53	0.34	1.68	0.04	0.10	0.39	0.10
JB10_01	0.78	2.73	0.43	0.83	1.04	8.37	211.87	9.48	0.41	1.43	0.25	1.59	0.03	0.06	0.27	0.09
JB10_02	0.81	2.91	0.46	0.53	1.12	8.81	221.42	9.87	0.44	1.82	0.30	1.63	0.04	0.06	0.52	0.12
JB10_03	0.83	2.59	0.48	0.64	1.11	8.94	223.97	10.12	0.44	1.62	0.31	1.66	0.04	0.08	0.29	0.10
JB10_04	1.03	3.47	0.60	1.00	1.39	11.19	273.65	12.38	0.57	2.20	0.33	2.05	0.04	0.11	0.44	0.14
JB10_05	0.78	2.56	0.44	0.56	1.01	8.27	205.44	9.39	0.41	1.61	0.19	1.49	0.04	0.08	0.28	0.10
JB10_06	1.12	3.91	0.66	1.04	1.52	11.91	291.98	13.33	0.62	2.48	0.43	2.46	0.05	0.12	0.82	0.15
JB10_07	0.76	2.48	0.45	0.54	1.01	8.23	198.82	9.18	0.41	1.71	0.26	1.58	0.04	0.06	0.27	0.09
JB10_08	0.74	2.55	0.43	0.63	0.98	7.98	193.47	8.95	0.39	1.02	0.27	1.53	0.03	0.06	0.27	0.08
JB10_09	1.31	4.57	0.75	1.33	1.74	13.55	331.49	15.12	0.72	3.82	0.45	2.98	0.08	0.19	0.76	0.24
JB10_10	0.80	2.71	0.44	0.52	1.08	8.56	206.67	9.57	0.42	1.61	0.27	1.58	0.04	0.07	0.31	0.08
JB10_11	0.80	2.68	0.46	0.35	1.06	8.70	206.07	9.56	0.42	1.76	0.22	1.61	0.03	0.07	0.43	0.11
JB10_13	1.14	3.91	0.70	1.12	1.52	12.38	291.84	13.59	0.63	2.38	0.33	2.53	0.05	0.13	0.67	0.17

Sample	<sup>7</sup> Li	<sup>11</sup> B	<sup>23</sup> Na	<sup>25</sup> Mg	<sup>27</sup> Al	<sup>31</sup> P	<sup>35</sup> Cl	<sup>39</sup> K	<sup>45</sup> Sc	<sup>49</sup> Ti	<sup>71</sup> Ga	<sup>72</sup> Ge	<sup>133</sup> Cs	<sup>88</sup> Sr	<sup>9</sup> Be	<sup>85</sup> Rb
	µg/g	µg/g	µg/g	µg/g	µg/g	µg/g	µg/g	µg/g	µg/g	µg/g	µg/g	µg/g	µg/g	µg/g	µg/g	µg/g
JB10_14	1.26	4.28	0.79	1.42	1.70	13.70	321.28	14.82	0.64	3.15	0.59	2.79	0.06	0.16	0.59	0.17
JB10_16	0.90	2.97	0.51	0.71	1.22	9.90	234.76	10.91	0.47	1.92	0.30	2.02	0.05	0.08	0.48	0.08
JB10_17	0.75	2.57	0.45	0.65	1.00	8.27	194.91	9.04	0.39	1.58	0.31	1.72	0.03	0.08	0.26	0.09
JB10_18	1.08	3.48	0.69	1.41	1.47	11.87	276.76	12.69	0.55	2.96	0.50	2.26	0.06	0.12	0.73	0.16
JB10_19	0.88	2.78	0.51	0.56	1.18	9.75	232.42	10.61	0.46	1.97	0.28	2.07	0.04	0.09	0.55	0.11
JB10_20	1.49	5.19	0.96	1.77	2.04	16.03	378.31	17.10	0.80	3.82	0.69	3.28	0.08	0.14	1.29	0.26
JB17_01	1.03	2.82	0.61	1.04	1.39	11.58	264.45	13.24	0.56	2.35	0.29	2.27	0.05	0.10	0.60	0.11
JB17_02	0.96	2.78	0.56	1.02	1.29	10.87	246.72	12.41	0.53	2.26	0.36	2.16	0.05	0.11	0.50	0.14
JB17_03	0.76	2.18	0.46	0.56	1.03	8.63	198.03	10.03	0.44	1.59	0.28	1.76	0.04	0.06	0.47	0.09
JB17_04	0.79	2.29	0.50	0.88	1.08	9.13	205.62	10.48	0.45	1.86	0.25	1.87	0.04	0.10	0.53	0.10
JB17_06	0.74	2.16	0.45	0.69	1.00	8.12	188.42	9.64	0.42	1.60	0.27	1.74	0.03	0.08	0.41	0.09
JB17_07	0.71	1.96	0.44	0.69	0.97	7.99	181.28	9.32	0.38	1.55	0.27	1.59	0.03	0.07	0.43	0.07
JB17_08	0.80	2.19	0.47	0.67	1.10	9.03	205.69	10.60	0.45	1.73	0.22	1.83	0.03	0.08	0.12	0.13
JB17_09	0.81	2.26	0.47	0.64	1.12	9.07	208.28	10.84	0.44	1.62	0.31	1.94	0.04	0.08	0.47	0.09
JB17_10	0.75	2.07	0.47	0.55	1.03	8.40	190.85	9.93	0.41	1.41	0.29	1.78	0.04	0.07	0.34	0.10
JB17_11	0.91	2.50	0.56	1.25	1.27	10.34	229.97	12.02	0.50	2.06	0.40	2.12	0.04	0.07	0.58	0.12

Sample	<sup>7</sup> Li	<sup>11</sup> B	<sup>23</sup> Na	<sup>25</sup> Mg	<sup>27</sup> Al	<sup>31</sup> P	<sup>35</sup> Cl	<sup>39</sup> K	<sup>45</sup> Sc	<sup>49</sup> Ti	<sup>71</sup> Ga	<sup>72</sup> Ge	<sup>133</sup> Cs	<sup>88</sup> Sr	<sup>9</sup> Be	<sup>85</sup> Rb
	µg/g	µg/g	µg/g	µg/g	µg/g	µg/g	µg/g	µg/g	µg/g	µg/g	µg/g	µg/g	µg/g	µg/g	µg/g	µg/g
JB17_12	0.95	2.52	0.54	1.10	1.31	10.76	242.99	12.71	0.57	2.30	0.31	2.09	0.05	0.09	0.42	0.10
JB17_13	0.75	1.92	0.46	0.67	1.01	8.30	190.19	10.00	0.42	1.77	0.27	1.74	0.04	0.08	0.12	0.09
JB17_14	1.12	3.12	0.71	1.21	1.55	12.54	283.94	14.89	0.63	2.64	0.38	2.46	0.06	0.11	0.75	0.15
JB17_15	1.22	3.77	0.82	1.40	1.70	13.69	305.84	16.02	0.73	3.46	0.62	3.06	0.08	0.17	0.98	0.17
JB17_16	0.79	2.22	0.50	0.62	1.08	8.73	198.38	10.53	0.45	1.76	0.24	1.77	0.04	0.09	0.39	0.09
JB17_17	0.74	1.96	0.44	0.72	1.06	8.57	189.89	10.18	0.44	1.64	0.28	1.69	0.04	0.08	0.46	0.11
JB17_18	0.81	2.33	0.50	0.69	1.12	9.00	205.78	11.02	0.47	1.78	0.25	1.76	0.03	0.08	0.31	0.09
JB17_19	0.80	2.19	0.48	0.74	1.14	9.18	204.67	11.03	0.46	1.74	0.26	1.73	0.04	0.07	0.32	0.11
JB17_20	0.79	2.27	0.48	0.71	1.11	9.02	200.06	10.94	0.46	1.54	0.22	1.83	0.04	0.09	0.44	0.11
JB26_01	0.76	2.41	0.45	0.67	1.03	8.24	222.83	9.72	0.40	1.67	0.26	1.75	0.03	0.09	0.38	0.09
JB26_02	0.95	2.79	0.60	0.89	1.23	10.60	279.05	12.22	0.49	2.07	0.25	2.09	0.04	0.11	0.17	0.10
JB26_03	0.86	2.43	0.51	0.80	1.18	9.40	253.01	11.12	0.47	1.95	0.31	1.93	0.03	0.09	0.44	0.11
JB26_05	1.00	3.18	0.66	1.43	1.43	10.92	285.77	12.65	0.57	2.44	0.41	2.44	0.05	0.13	1.01	0.17
JB26_06	0.81	2.33	0.50	0.97	1.09	8.89	235.97	10.54	0.43	1.73	0.31	1.94	0.04	0.08	0.40	0.12
JB26_07	1.09	3.29	0.61	0.92	1.52	12.03	317.09	14.19	0.59	2.50	0.36	2.58	0.04	0.12	0.60	0.11
JB26_08	0.77	2.36	0.51	0.68	1.02	8.66	224.82	10.12	0.42	1.38	0.29	1.78	0.04	0.10	0.32	0.07

Sample	<sup>7</sup> Li	<sup>11</sup> B	<sup>23</sup> Na	<sup>25</sup> Mg	<sup>27</sup> Al	<sup>31</sup> P	<sup>35</sup> Cl	<sup>39</sup> K	<sup>45</sup> Sc	<sup>49</sup> Ti	<sup>71</sup> Ga	<sup>72</sup> Ge	<sup>133</sup> Cs	<sup>88</sup> Sr	<sup>9</sup> Be	<sup>85</sup> Rb
	µg/g	µg/g	µg/g	µg/g	µg/g	µg/g	µg/g	µg/g	µg/g	µg/g	µg/g	µg/g	µg/g	µg/g	µg/g	µg/g
JB26_09	0.96	2.98	0.62	0.78	1.28	10.77	276.95	12.47	0.52	2.10	0.32	2.18	0.06	0.12	0.24	0.14
JB26_10	0.80	2.39	0.51	0.77	1.09	8.82	227.15	10.28	0.43	1.89	0.29	1.85	0.04	0.09	0.39	0.11
JB26_11	0.83	2.50	0.52	0.85	1.10	9.21	235.47	10.73	0.47	1.70	0.28	1.87	0.04	0.10	0.43	0.13
JB26_12	0.85	2.56	0.53	0.76	1.14	9.34	240.74	10.92	0.45	1.79	0.36	1.90	0.04	0.10	0.45	0.09
JB26_13	0.87	2.54	0.50	0.62	1.21	9.58	243.56	11.16	0.46	1.77	0.30	1.95	0.04	0.08	0.44	0.10
JB26_14	0.81	2.21	0.49	0.60	1.13	9.10	230.58	10.60	0.44	1.83	0.28	2.01	0.04	0.07	0.34	0.10
JB26_15	0.82	1.99	0.49	0.59	1.10	9.22	229.03	10.62	0.45	1.64	0.24	1.78	0.05	0.06	0.13	0.13
JB26_16	0.55	3.81	0.30	0.42	0.74	6.16	154.08	8.78	0.27	1.34	0.16	1.22	0.02	0.04	0.28	0.07
JB26_17	0.79	3.72	0.42	0.56	1.04	8.21	197.20	10.78	0.40	1.78	0.21	1.53	0.03	0.06	0.38	0.08
JB26_18	0.67	3.01	0.36	0.57	0.87	7.01	170.71	8.98	0.33	1.42	0.20	1.29	0.02	0.07	0.48	0.08
JB26_19	0.68	2.91	0.36	0.34	0.88	6.99	171.71	8.80	0.34	1.47	0.24	1.43	0.02	0.05	0.28	0.07
JB26_20	0.68	2.77	0.36	0.45	0.91	7.12	175.24	8.78	0.36	1.37	0.27	1.39	0.03	0.06	0.28	0.05

**Table A.8.** LA-ICP-MS trace element limits of detection for samples from BK, fraction >250 µm.

Sample	<sup>7</sup> Li	<sup>11</sup> B	<sup>23</sup> Na	<sup>25</sup> Mg	<sup>27</sup> Al	<sup>31</sup> P	<sup>35</sup> Cl	<sup>39</sup> K	<sup>45</sup> Sc	<sup>49</sup> Ti	<sup>71</sup> Ga	<sup>72</sup> Ge	<sup>133</sup> Cs	<sup>88</sup> Sr	<sup>9</sup> Be	<sup>85</sup> Rb
	µg/g	µg/g	µg/g	µg/g	µg/g	µg/g	µg/g	µg/g	µg/g	µg/g	µg/g	µg/g	µg/g	µg/g	µg/g	µg/g
BK41_01	0.48	1.06	0.42	0.23	0.56	6.55	125.95	4.44	0.18	0.99	0.11	1.22	0.03	0.06	0.12	0.09
BK41_03	0.55	1.32	0.42	0.59	0.74	7.65	148.85	4.84	0.28	1.31	0.20	1.44	0.04	0.06	0.09	0.12
BK41_04	0.61	1.39	0.48	0.29	0.77	8.31	162.52	5.42	0.28	1.42	0.17	1.60	0.05	0.08	0.29	0.14
BK41_05	0.48	1.08	0.38	0.43	0.58	6.59	127.58	4.32	0.22	0.98	0.07	1.29	0.04	0.08	0.17	0.09
BK41_06	0.50	1.05	0.36	0.49	0.59	6.53	127.05	4.33	0.21	1.17	0.08	1.29	0.03	0.07	0.20	0.08
BK41_07	0.54	1.11	0.43	0.46	0.66	7.20	139.16	4.85	0.23	1.06	0.15	1.44	0.04	0.09	0.23	0.11
BK41_08	0.47	0.92	0.36	0.42	0.52	6.16	119.59	4.24	0.19	0.87	0.07	1.20	0.03	0.06	0.15	0.07
BK41_09	0.45	0.86	0.33	0.38	0.50	5.92	113.07	4.04	0.18	0.91	0.10	1.16	0.03	0.06	0.15	0.09
BK41_10	0.52	1.00	0.40	0.35	0.61	6.73	129.51	4.61	0.21	1.08	0.13	1.36	0.04	0.08	0.21	0.10
BK41_11	0.79	1.52	0.59	0.65	0.91	9.71	185.44	6.71	0.31	1.87	0.23	2.17	0.06	0.12	0.43	0.19
BK41_12	0.49	0.93	0.37	0.49	0.54	6.43	121.63	4.44	0.20	1.01	0.09	1.29	0.03	0.07	0.13	0.11
BK41_13	0.61	1.14	0.47	0.76	0.69	7.73	145.12	5.44	0.23	1.34	0.17	1.58	0.04	0.08	0.21	0.13
BK41_15	0.54	0.97	0.40	0.46	0.57	6.85	127.25	4.83	0.20	1.15	0.16	1.32	0.03	0.06	0.19	0.11
BK41_16	0.72	1.34	0.54	0.71	0.79	8.97	166.40	6.29	0.28	1.69	0.21	1.87	0.05	0.12	0.42	0.17
BK41_17	1.72	3.28	1.29	2.28	2.02	20.85	381.12	14.26	0.68	5.37	0.68	4.69	0.13	0.33	1.43	0.45

Sample	<sup>7</sup> Li	<sup>11</sup> B	<sup>23</sup> Na	<sup>25</sup> Mg	<sup>27</sup> Al	<sup>31</sup> P	<sup>35</sup> Cl	<sup>39</sup> K	<sup>45</sup> Sc	<sup>49</sup> Ti	<sup>71</sup> Ga	<sup>72</sup> Ge	<sup>133</sup> Cs	<sup>88</sup> Sr	<sup>9</sup> Be	<sup>85</sup> Rb
	µg/g	µg/g	µg/g	µg/g	µg/g	µg/g	µg/g	µg/g	µg/g	µg/g	µg/g	µg/g	µg/g	µg/g	µg/g	µg/g
BK41_18	0.49	0.88	0.39	0.33	0.53	6.21	120.52	4.40	0.18	1.11	0.13	1.26	0.03	0.07	0.12	0.10
BK41_19	0.51	0.95	0.39	0.32	0.55	6.48	127.02	4.56	0.19	1.10	0.13	1.33	0.03	0.07	0.17	0.10
BKNV_01	0.56	0.98	0.42	0.50	0.60	7.11	144.52	5.09	0.20	1.11	0.11	1.48	0.04	0.08	0.04	0.11
BKNV_02	0.69	1.26	0.52	0.41	0.73	8.69	178.10	6.13	0.24	1.40	0.10	1.61	0.05	0.11	0.17	0.15
BKNV_03	0.51	0.96	0.42	0.46	0.55	6.50	135.48	4.64	0.20	1.09	0.11	1.42	0.04	0.08	0.17	0.11
BKNV_04	0.64	1.20	0.51	0.55	0.66	8.10	171.36	5.76	0.23	1.35	0.14	1.69	0.04	0.10	0.23	0.14
BKNV_06	0.56	1.03	0.43	0.40	0.61	6.97	152.18	5.00	0.21	1.22	0.13	1.39	0.03	0.08	0.19	0.11
BKNV_07	0.57	1.02	0.44	0.32	0.63	7.10	159.90	5.19	0.22	1.20	0.08	1.45	0.03	0.08	0.13	0.12
BKNV_08	0.60	1.11	0.43	0.39	0.62	7.60	168.19	5.36	0.21	1.25	0.15	1.56	0.04	0.07	0.20	0.12
BKNV_09	0.58	1.05	0.45	0.44	0.63	7.24	168.10	5.21	0.22	1.22	0.13	1.46	0.03	0.09	0.21	0.12
BKNV_10	0.66	1.24	0.51	0.59	0.71	8.38	194.56	5.91	0.24	1.47	0.11	1.78	0.05	0.11	0.23	0.13
BKNV_11	0.55	1.02	0.43	0.44	0.60	6.99	166.29	5.00	0.20	1.05	0.15	1.37	0.04	0.08	0.16	0.12
BKNV_12	0.62	1.17	0.48	0.48	0.68	7.82	188.16	5.52	0.24	1.44	0.17	1.61	0.04	0.09	0.19	0.14
BKNV_13	0.67	1.30	0.54	0.66	0.76	8.23	202.63	5.81	0.26	1.59	0.19	1.74	0.05	0.11	0.34	0.14
BKNV_14	0.49	0.89	0.38	0.25	0.54	6.33	159.34	4.46	0.17	0.99	0.11	1.29	0.03	0.07	0.13	0.11
BKNV_15	0.42	0.79	0.34	0.32	0.45	5.35	134.60	3.74	0.15	0.90	0.06	1.10	0.02	0.06	0.12	0.08

Sample	<sup>7</sup> Li	<sup>11</sup> B	<sup>23</sup> Na	<sup>25</sup> Mg	<sup>27</sup> Al	<sup>31</sup> P	<sup>35</sup> Cl	<sup>39</sup> K	<sup>45</sup> Sc	<sup>49</sup> Ti	<sup>71</sup> Ga	<sup>72</sup> Ge	<sup>133</sup> Cs	<sup>88</sup> Sr	<sup>9</sup> Be	<sup>85</sup> Rb
	µg/g	µg/g	µg/g	µg/g	µg/g	µg/g	µg/g	µg/g	µg/g	µg/g	µg/g	µg/g	µg/g	µg/g	µg/g	µg/g
BKNV_16	0.44	0.83	0.34	0.24	0.48	5.58	141.31	3.95	0.15	0.85	0.10	1.11	0.03	0.06	0.10	0.10
BKNV_17	0.45	0.87	0.37	0.39	0.49	5.88	145.48	4.08	0.17	0.89	0.09	1.19	0.03	0.07	0.15	0.09
BKNV_18	0.45	0.89	0.36	0.33	0.48	5.82	142.49	4.09	0.17	1.03	0.10	1.20	0.03	0.06	0.11	0.09
BKNV_19	0.41	0.78	0.34	0.28	0.45	5.30	127.89	3.72	0.15	0.88	0.07	1.14	0.03	0.08	0.11	0.09
BKNV_20	0.45	0.85	0.35	0.37	0.48	5.77	138.12	4.09	0.17	0.95	0.10	1.17	0.03	0.07	0.14	0.11

**Table A.9.** LA-ICP-MS trace element limits of detection for samples from KVI, fraction >250 µm.

Sample	<sup>7</sup> Li	<sup>11</sup> B	<sup>23</sup> Na	<sup>25</sup> Mg	<sup>27</sup> Al	<sup>31</sup> P	<sup>35</sup> Cl	<sup>39</sup> K	<sup>45</sup> Sc	<sup>49</sup> Ti	<sup>71</sup> Ga	<sup>72</sup> Ge	<sup>133</sup> Cs	<sup>88</sup> Sr	<sup>9</sup> Be	<sup>85</sup> Rb
	µg/g	µg/g	µg/g	µg/g	µg/g	µg/g	µg/g	µg/g	µg/g	µg/g	µg/g	µg/g	µg/g	µg/g	µg/g	µg/g
DOB_01	0.63	1.13	0.50	0.60	0.69	7.98	152.24	5.82	0.23	1.56	0.18	1.63	0.05	0.10	0.34	0.15
DOB_02	0.48	0.87	0.38	0.33	0.51	6.16	118.56	4.48	0.17	1.10	0.08	1.31	0.04	0.09	0.18	0.12
DOB_03	0.53	0.96	0.43	0.53	0.56	6.67	129.36	4.84	0.20	1.28	0.12	1.38	0.04	0.08	0.24	0.13
DOB_04	0.43	0.77	0.36	0.36	0.45	5.55	107.72	4.03	0.16	0.90	0.11	1.11	0.03	0.06	0.14	0.10
DOB_05	0.46	0.82	0.37	0.24	0.47	5.81	115.05	4.27	0.17	1.03	0.12	1.23	0.03	0.07	0.05	0.10
DOB_06	0.84	1.63	0.70	1.30	0.95	10.54	207.49	7.64	0.29	2.25	0.31	2.25	0.07	0.16	0.57	0.23
DOB_07	0.54	0.91	0.43	0.52	0.53	6.70	134.34	4.97	0.19	1.36	0.14	1.40	0.04	0.09	0.10	0.12
DOB_08	1.14	2.32	0.97	1.61	1.38	14.05	278.13	10.14	0.45	3.41	0.51	3.31	0.11	0.23	1.13	0.29

Sample	<sup>7</sup> Li	<sup>11</sup> B	<sup>23</sup> Na	<sup>25</sup> Mg	<sup>27</sup> Al	<sup>31</sup> P	<sup>35</sup> Cl	<sup>39</sup> K	<sup>45</sup> Sc	<sup>49</sup> Ti	<sup>71</sup> Ga	<sup>72</sup> Ge	<sup>133</sup> Cs	<sup>88</sup> Sr	<sup>9</sup> Be	<sup>85</sup> Rb
	µg/g	µg/g	µg/g	µg/g	µg/g	µg/g	µg/g	µg/g	µg/g	µg/g	µg/g	µg/g	µg/g	µg/g	µg/g	µg/g
DOB_09	0.47	0.89	0.38	0.30	0.50	6.01	121.13	4.44	0.16	0.94	0.12	1.23	0.03	0.08	0.09	0.10
DOB_10	0.52	1.01	0.41	0.34	0.55	6.51	133.19	4.83	0.18	1.28	0.14	1.41	0.04	0.08	0.24	0.12
DOB_11	0.59	1.08	0.52	0.58	0.64	7.32	153.92	5.47	0.21	1.42	0.18	1.57	0.04	0.11	0.27	0.13
DOB_12	0.45	0.80	0.37	0.29	0.47	5.61	123.62	4.21	0.15	0.91	0.11	1.19	0.03	0.07	0.15	0.11
DOB_13	0.55	0.96	0.43	0.62	0.57	6.67	148.29	4.99	0.19	1.29	0.16	1.45	0.03	0.10	0.27	0.12
DOB_16	0.70	1.27	0.60	0.66	0.77	8.54	190.42	6.46	0.27	1.67	0.24	1.92	0.06	0.13	0.39	0.17
DOB_17	0.52	0.94	0.43	0.48	0.57	6.48	145.87	4.84	0.19	1.23	0.13	1.41	0.04	0.09	0.30	0.13
DOB_18	0.46	0.78	0.38	0.27	0.47	5.74	131.85	4.33	0.16	0.91	0.11	1.22	0.03	0.07	0.15	0.10
DOB_19	0.50	0.92	0.40	0.38	0.54	6.17	143.01	4.62	0.18	1.13	0.13	1.37	0.04	0.08	0.16	0.12
DOB_20	0.47	0.85	0.41	0.37	0.50	5.82	137.07	4.41	0.17	1.00	0.14	1.23	0.03	0.08	0.18	0.11
RAB1_02	0.46	0.89	0.38	0.28	0.49	5.82	138.38	4.14	0.17	0.91	0.12	1.26	0.03	0.07	0.17	0.10
RAB1_04	0.50	0.87	0.40	0.46	0.54	6.33	147.98	4.48	0.19	1.17	0.15	1.30	0.02	0.08	0.15	0.11
RAB1_05	0.48	0.92	0.39	0.54	0.51	6.19	143.26	4.35	0.17	1.01	0.08	1.27	0.03	0.08	0.19	0.12
RAB1_06	0.52	1.04	0.42	0.36	0.56	6.55	151.86	4.63	0.20	1.09	0.15	1.46	0.04	0.09	0.25	0.11
RAB1_07	0.53	0.99	0.42	0.47	0.58	6.78	153.89	4.76	0.19	1.17	0.14	1.40	0.04	0.08	0.20	0.11
RAB1_08	0.68	1.23	0.57	0.75	0.74	8.52	191.85	6.01	0.26	1.70	0.18	1.81	0.05	0.13	0.36	0.16

Sample	<sup>7</sup> Li	<sup>11</sup> B	<sup>23</sup> Na	<sup>25</sup> Mg	<sup>27</sup> Al	<sup>31</sup> P	<sup>35</sup> Cl	<sup>39</sup> K	<sup>45</sup> Sc	<sup>49</sup> Ti	<sup>71</sup> Ga	<sup>72</sup> Ge	<sup>133</sup> Cs	<sup>88</sup> Sr	<sup>9</sup> Be	<sup>85</sup> Rb
	µg/g	µg/g	µg/g	µg/g	µg/g	µg/g	µg/g	µg/g	µg/g	µg/g	µg/g	µg/g	µg/g	µg/g	µg/g	µg/g
RAB1_09	0.59	1.10	0.47	0.53	0.64	7.57	166.91	5.33	0.23	1.33	0.14	1.61	0.04	0.09	0.23	0.13
RAB1_10	0.54	1.03	0.43	0.54	0.60	7.10	153.90	4.92	0.20	1.32	0.16	1.42	0.03	0.09	0.23	0.12
RAB1_12	0.52	0.95	0.43	0.54	0.56	6.68	146.01	4.69	0.19	1.17	0.08	1.32	0.03	0.09	0.21	0.11
RAB1_13	0.54	0.93	0.45	0.50	0.60	6.73	125.95	5.02	0.18	1.23	0.16	1.43	0.04	0.08	0.26	0.12
RAB1_14	0.49	0.89	0.38	0.53	0.53	6.27	118.09	4.63	0.18	1.07	0.14	1.33	0.04	0.08	0.22	0.12
RAB1_15	1.12	2.27	0.97	1.69	1.33	13.81	258.74	9.96	0.44	3.28	0.41	3.06	0.10	0.23	0.92	0.35
RAB1_16	0.50	0.91	0.42	0.37	0.51	6.36	120.77	4.71	0.18	1.08	0.14	1.35	0.03	0.09	0.18	0.12
RAB1_18	0.48	0.88	0.38	0.31	0.50	6.23	116.57	4.54	0.17	1.13	0.08	1.28	0.02	0.08	0.17	0.10

**Table A.10.** LA-ICP-MS trace element errors for samples from JB, fraction >250 µm.

Sample	<sup>7</sup> Li	<sup>11</sup> B	<sup>23</sup> Na	<sup>25</sup> Mg	<sup>27</sup> Al	<sup>31</sup> P	<sup>35</sup> Cl	<sup>39</sup> K	<sup>45</sup> Sc	<sup>49</sup> Ti	<sup>71</sup> Ga	<sup>72</sup> Ge	<sup>133</sup> Cs	<sup>88</sup> Sr	<sup>9</sup> Be	<sup>85</sup> Rb
	µg/g	µg/g	µg/g	µg/g	µg/g	µg/g	µg/g	µg/g	µg/g	µg/g	µg/g	µg/g	µg/g	µg/g	µg/g	µg/g
JB1_01	18.80	4.44	0.80	0.87	81.31	182.82		16.33	0.52	57.64						
JB1_02	17.16			0.71	75.26	196.61		17.37	0.49	44.48		1.59				
JB1_04	16.72	3.10	27.97		165.20	189.15		28.23	0.62	52.56				1.00		
JB1_05	18.98				98.26	204.33		20.87	0.70	21.27		2.13				
JB1_06		4.04	23.30		95.02	206.37		54.86	0.59	23.43				0.73		
JB1_07	3.15		2.68		77.00	208.76		15.52	0.52	36.66						
JB1_08	17.81				74.78	206.91		19.45	0.57	40.03						
JB1_09	3.86		9.22	0.69	96.60	215.79		30.74	0.54	44.58				0.13		
JB1_10	2.06		0.70	0.77	106.56	217.43		21.74		57.05		1.77				
JB1_11	17.10			0.83	81.13	211.38		19.84		29.05						
JB1_14		3.17	18.99		9.26	208.83			0.48	2.06		1.84		0.21		
JB1_15		3.17	45.70	1.25	57.21	224.42		24.09	0.55	2.44		2.23		0.81		
JB1_16	7.00	3.28	6.20		72.23	227.26		16.19	0.67	77.81				0.12		
JB1_17	17.11	15.34	30.81		425.79	229.10		30.38		2.74				0.60		
JB1_18	1.91	4.47	97.01	3.21	233.74	220.57	216.82	67.08	0.60	13.36				2.02		

Sample	<sup>7</sup> Li	<sup>11</sup> B	<sup>23</sup> Na	<sup>25</sup> Mg	<sup>27</sup> Al	<sup>31</sup> P	<sup>35</sup> Cl	<sup>39</sup> K	<sup>45</sup> Sc	<sup>49</sup> Ti	<sup>71</sup> Ga	<sup>72</sup> Ge	<sup>133</sup> Cs	<sup>88</sup> Sr	<sup>9</sup> Be	<sup>85</sup> Rb
	µg/g	µg/g	µg/g	µg/g	µg/g	µg/g	µg/g	µg/g	µg/g	µg/g	µg/g	µg/g	µg/g	µg/g	µg/g	µg/g
JB1_19	23.69		0.86	1.64	101.99	221.76	216.12	16.53	0.56	74.47						
JB1_20	3.32	3.02	16.46		114.83	220.94		47.39		56.35			0.09	0.55		0.22
JB5_01	0.17		0.33		0.75	10.90	100.02	5.18	0.23	0.70						
JB5_03		0.63	0.31		0.98	6.71		5.32	0.24	0.79				0.03		
JB5_04	0.20	0.83	1.72	1.49	2.28	6.76		6.40		2.05			0.03	0.59		
JB5_05	0.30	0.67	1.43		3.27	6.85		6.22	0.25	1.61		0.92		0.06		
JB5_06	0.28		3.58	1.15	11.70	12.14	181.61	7.77		1.33				0.22		0.07
JB5_07			1.08	0.85	15.69	7.53		10.87	0.28			0.97		0.10		0.10
JB5_08			0.51		1.21	8.37								0.05		
JB5_09	0.20		0.48	0.99	3.18	8.33		6.58	0.23	1.13		0.81		0.05		
JB5_10	0.75		2.68	0.39	12.98	11.07	320.73	6.54	0.22	0.99				0.26		
JB5_11	0.19		0.41		1.38	13.40	449.10	6.06	0.24	1.45						
JB5_12			56.11	33.69	40.50	15.86		37.27		160.31				0.69		
JB5_13	0.17		0.50		1.40	10.69		6.28	0.22	1.09		0.84	0.01	0.06		0.04
JB5_14	2.84	0.71	0.66		29.61	6.22			0.21	0.61		0.86		0.06		
JB5_15	2.61	0.78	3.53	8.97	35.21	11.82		10.46		1.95		0.86	0.02	0.44		0.08

Sample	<sup>7</sup> Li	<sup>11</sup> B	<sup>23</sup> Na	<sup>25</sup> Mg	<sup>27</sup> Al	<sup>31</sup> P	<sup>35</sup> Cl	<sup>39</sup> K	<sup>45</sup> Sc	<sup>49</sup> Ti	<sup>71</sup> Ga	<sup>72</sup> Ge	<sup>133</sup> Cs	<sup>88</sup> Sr	<sup>9</sup> Be	<sup>85</sup> Rb
	µg/g	µg/g	µg/g	µg/g	µg/g	µg/g	µg/g	µg/g	µg/g	µg/g	µg/g	µg/g	µg/g	µg/g	µg/g	µg/g
JB5_17	4.18	0.91	1.75	0.76	50.74	14.30		8.01	0.29	1.10		1.15		0.18		
JB5_18			0.35		1.57	14.83		8.50		1.41						
JB5_19			1.11	0.53	2.73	6.67		7.82	0.24	3.02		0.73	0.02	0.14		0.04
JB5_20	0.64	0.73	0.32	0.31	2.77	5.44			0.23	1.87		0.74				
JB10_01			9.15		45.87	228.20		19.69	0.62	10.39				0.23		
JB10_02	2.69		27.64	0.90	200.65	215.26		39.66				2.81		1.01		
JB10_03	6.91	3.62	10.34		79.73	230.40		20.42	0.54	62.12				0.18		
JB10_04	70.65	4.26	123.96	6.72	1399.96	225.33		47.78	0.75			4.96		3.59		0.11
JB10_05			12.46	0.83	60.00	232.56		18.67	0.51	32.55		2.04		0.55		
JB10_06	5.03	4.36	98.72	11.50	490.14	215.26		29.66		2.77		6.02		1.04		
JB10_07	134.26	6.92	45.35		2376.28	206.87	270.19	52.46		1.82		4.70		1.32		
JB10_08	4.20	2.77	1.45		111.87	215.67	250.18	12.12	0.72	72.72		1.77				
JB10_09		5.22	383.81	24.00	241.48	215.02		205.23		30.68			0.64	2.31		0.64
JB10_10	76.94	5.58	189.90	44.69	1778.71	192.90	476.41	118.82	0.78	1.76		4.71		8.46		0.37
JB10_11	243.73	4.83	106.24	4.53	2849.74	217.53		106.05	0.50	2.99		5.28		2.04		0.31
JB10_13	67.74	5.80	111.98	1.96	1531.54	234.84		46.82					0.06	18.51		

Sample	<sup>7</sup> Li	<sup>11</sup> B	<sup>23</sup> Na	<sup>25</sup> Mg	<sup>27</sup> Al	<sup>31</sup> P	<sup>35</sup> Cl	<sup>39</sup> K	<sup>45</sup> Sc	<sup>49</sup> Ti	<sup>71</sup> Ga	<sup>72</sup> Ge	<sup>133</sup> Cs	<sup>88</sup> Sr	<sup>9</sup> Be	<sup>85</sup> Rb
	µg/g	µg/g	µg/g	µg/g	µg/g	µg/g	µg/g	µg/g	µg/g	µg/g	µg/g	µg/g	µg/g	µg/g	µg/g	µg/g
JB10_14			2.16		22.84	62.41	1148.62	20.23	1.10							
JB10_16	6.12		6.42		160.67	155.92	582.47	20.04	0.67	36.74			0.08			
JB10_17	3.96		1.47		51.07	241.58		17.09	0.56	14.59						
JB10_18	85.20	4.12	33.91	10.87	1399.61	164.36		23.86	0.58		3.92		1.54			
JB10_19	21.75	7.57	185.04	1.27	1027.15	241.76		113.57	0.75	2.89	6.83		1.19			
JB10_20			112.67	6.29	1215.26	179.15		322.01	0.79	15.35			1.43		0.43	
JB17_01		0.77	1.34		1.95	7.45		5.61	0.24	0.78		1.05		0.10		
JB17_02			0.63		2.47	8.04	77.46	5.80		0.82			0.07			
JB17_03			0.40	0.36	0.60	7.61	68.21	4.97	0.20	0.54			0.04			
JB17_04	0.15		0.68		1.42	11.85	79.46	5.06	0.22	1.22			0.08			
JB17_06			0.25		0.65	6.07				0.60						
JB17_07			2.48	0.32	0.86	5.25	57.62	4.32	0.18		0.72		0.12			
JB17_08			0.43		1.15	5.94		4.87	0.22	1.11						
JB17_09	0.17		1.72	0.48	2.42	5.99		5.04	0.20	2.15			0.02	0.05		0.04
JB17_10	0.17	0.57	0.59	0.34	1.91	6.98		4.82	0.19	1.69			0.02	0.24		0.05
JB17_11			0.34		0.70	6.92			0.27	1.69			0.04			

Sample	<sup>7</sup> Li	<sup>11</sup> B	<sup>23</sup> Na	<sup>25</sup> Mg	<sup>27</sup> Al	<sup>31</sup> P	<sup>35</sup> Cl	<sup>39</sup> K	<sup>45</sup> Sc	<sup>49</sup> Ti	<sup>71</sup> Ga	<sup>72</sup> Ge	<sup>133</sup> Cs	<sup>88</sup> Sr	<sup>9</sup> Be	<sup>85</sup> Rb
	µg/g	µg/g	µg/g	µg/g	µg/g	µg/g	µg/g	µg/g	µg/g	µg/g	µg/g	µg/g	µg/g	µg/g	µg/g	µg/g
JB17_12	0.33		1.24	0.76	12.69	6.98		5.91		2.47				0.08		
JB17_13		0.59	2.72	0.54	1.24	5.61		4.35	0.19					0.07		
JB17_14			4.60		1.61	7.65		7.68						0.19		
JB17_15			1.35	0.89	3.26	12.12	256.98	5.93	0.23	3.11						
JB17_16	0.17	0.73	2.58		1.34	5.80		4.70	0.21	1.73				0.07		
JB17_17		0.59	1.76	0.99	1.17	5.76	57.04	4.72	0.19	0.84				0.05		
JB17_18	0.17		0.75	0.46	2.57	6.39		4.93	0.20				0.02	0.07	0.04	
JB17_19	0.31	0.69	1.76	0.43	6.81	5.81		5.06	0.19				0.74		0.11	
JB17_20	0.64	0.80	0.46		2.99	6.10	60.31		0.21	1.98			0.85		0.16	
JB26_01			1.09	0.49	0.58	6.20		4.71	0.17					0.05		
JB26_02		0.81	0.49		1.77	7.70		5.38	0.21	1.41						
JB26_03		0.72	0.54		1.55	7.18		4.77		0.86			0.02			
JB26_05			0.41		1.52	6.98				1.25				0.07		
JB26_06		0.71	5.97		8.59	6.64	75.50	5.20	0.18				0.03	0.26	0.07	
JB26_07			0.41	0.50	5.18	8.10		7.54		1.46				0.06		
JB26_08			0.32		1.23	6.07		4.11	0.20	1.38						

Sample	<sup>7</sup> Li	<sup>11</sup> B	<sup>23</sup> Na	<sup>25</sup> Mg	<sup>27</sup> Al	<sup>31</sup> P	<sup>35</sup> Cl	<sup>39</sup> K	<sup>45</sup> Sc	<sup>49</sup> Ti	<sup>71</sup> Ga	<sup>72</sup> Ge	<sup>133</sup> Cs	<sup>88</sup> Sr	<sup>9</sup> Be	<sup>85</sup> Rb
	μg/g	μg/g	μg/g	μg/g	μg/g	μg/g	μg/g	μg/g	μg/g	μg/g	μg/g	μg/g	μg/g	μg/g	μg/g	μg/g
JB26_09			1.74	0.43	0.73	6.73		5.71	0.21					0.08	0.15	
JB26_10			0.63		0.45	6.38		4.46								
JB26_11			2.46		0.56	6.40		4.85						0.09		
JB26_12	0.19		0.25		2.06	6.86			0.22	1.95						
JB26_13			2.10		0.68	6.18		5.19						0.07		
JB26_14	0.17	0.67	0.46		1.84	6.20		4.95	0.19	0.99				0.06		
JB26_15		0.63	0.74		0.55	6.15		5.14		0.54				0.06		
JB26_16			45.50	2.27	67.97	164.89			0.77	23.77		1.89		1.12		
JB26_17			1.98	0.80	8.58	169.88			0.71			2.46				
JB26_18	1.06		2.31		39.39	176.12			0.75	1.55		1.50		0.07		
JB26_19			0.42		7.31	186.49		10.24	0.67							
JB26_20		3.03	13.60	1.89	57.67	191.02		37.27	0.51	24.46				0.21		0.12

**Table A.11.** LA-ICP-MS trace element errors for samples from BK, fraction >250 µm.

Sample	<sup>7</sup> Li	<sup>11</sup> B	<sup>23</sup> Na	<sup>25</sup> Mg	<sup>27</sup> Al	<sup>31</sup> P	<sup>35</sup> Cl	<sup>39</sup> K	<sup>45</sup> Sc	<sup>49</sup> Ti	<sup>71</sup> Ga	<sup>72</sup> Ge	<sup>133</sup> Cs	<sup>88</sup> Sr	<sup>9</sup> Be	<sup>85</sup> Rb
	µg/g	µg/g	µg/g	µg/g	µg/g	µg/g	µg/g	µg/g	µg/g	µg/g	µg/g	µg/g	µg/g	µg/g	µg/g	µg/g
BK41_01	0.11	0.33	0.94	0.78	4.60	4.64		3.03	0.09	0.75		0.60		0.07	0.05	0.05
BK41_03		0.37	3.62	0.59	3.00	6.46	48.03		0.14	0.50		0.60	0.02	0.16		
BK41_04			0.56	0.31	3.08	5.31		3.18	0.12	1.53		0.68		0.04		0.07
BK41_05	0.45		0.19	0.22	1.47	7.25	44.13		0.10	0.88						
BK41_06	0.12	0.29	0.25		1.92	10.81	99.37		0.11	1.00						
BK41_07	0.15	0.40	3.82	0.24	2.62	5.43			0.11	1.34			0.02	0.05		
BK41_08	0.17				1.42	5.04			0.09	1.11	0.04					
KB41_09		0.25	1.06	0.91	9.82	4.80	35.60	5.34	0.09	0.35		0.56	0.02	0.13		0.06
BK41_10	1.01	0.27	3.45	0.25	5.42	11.57	81.99	2.69	0.08	2.35		0.67	0.04	0.04	0.09	0.07
BK41_11			1.50	2.61	12.29	8.09	83.30	3.33	0.19	0.97				0.13		
BK41_12	0.13	0.27	1.32	0.87	3.73	5.76	42.81	2.93	0.10	0.98				0.05		
BK41_13	0.13		0.83	1.09	5.68	8.14	52.38	2.61	0.12	2.57				0.06		
BK41_15	0.20		1.05	2.04	4.99	6.68	41.36	3.48	0.10	1.94			0.01	0.04		0.07
BK41_16	0.24	0.32	1.34	0.52	9.46	9.41	67.21	4.48	0.15	0.80		0.68		0.12		
BK41_17			11.47	12.47	11.15	9.97	173.72	6.04	0.34	5.90			0.43			0.33

Sample	<sup>7</sup> Li	<sup>11</sup> B	<sup>23</sup> Na	<sup>25</sup> Mg	<sup>27</sup> Al	<sup>31</sup> P	<sup>35</sup> Cl	<sup>39</sup> K	<sup>45</sup> Sc	<sup>49</sup> Ti	<sup>71</sup> Ga	<sup>72</sup> Ge	<sup>133</sup> Cs	<sup>88</sup> Sr	<sup>9</sup> Be	<sup>85</sup> Rb
	µg/g	µg/g	µg/g	µg/g	µg/g	µg/g	µg/g	µg/g	µg/g	µg/g	µg/g	µg/g	µg/g	µg/g	µg/g	µg/g
BK41_18	0.12	0.30	0.61	0.25	2.14	9.50	48.76		0.10	0.89		0.57				
BK41_19	0.12	0.30	0.29	0.16	1.22	4.72	43.47		0.10	0.79			0.04			
BKNV_01			0.22		0.51	6.53	46.93		0.09	0.39		0.60				
BKNV_02	0.14		0.26		1.08	6.94			0.12	0.74		0.70				
BKNV_03	0.19	0.27	0.27		2.71	5.28	38.31		0.10	1.33						
BKNV_04	0.15	0.38	3.21	0.33	3.79	6.75			0.13	1.18		0.78	0.02	0.07		
BKNV_06	0.23	0.30	2.02	0.37	2.27	6.33		2.58	0.11	0.42		0.62		0.08		
BKNV_07			3.70		0.89	6.53	46.70		0.11	0.44		0.66		0.05		
BKNV_08		0.32	0.39		1.16	6.86			0.11	0.61				0.03		
BKNV_09	0.39		0.90		4.88	6.18	52.90		0.11	1.16		0.65		0.04		
BKNV_10			0.39		0.53	7.40			0.12					0.06		
BKNV_11	0.26	0.29	0.24		5.87	5.93	50.45		0.11	1.22		0.63			0.07	
BKNV_12			0.35	0.27	0.56	5.66			0.13	1.09				0.05		
BKNV_13		0.36	3.14	2.80	3.12	13.13	82.45	2.98	0.13			0.77	0.03	0.14		
BKNV_14		0.25	2.02	0.16	1.26	5.17	53.84		0.09	1.02			0.02	0.04		
BKNV_15	0.14	0.25	1.07	0.26	3.20	4.77	41.16	1.88	0.08	1.04		0.48	0.01	0.04	0.04	

Sample	<sup>7</sup> Li	<sup>11</sup> B	<sup>23</sup> Na	<sup>25</sup> Mg	<sup>27</sup> Al	<sup>31</sup> P	<sup>35</sup> Cl	<sup>39</sup> K	<sup>45</sup> Sc	<sup>49</sup> Ti	<sup>71</sup> Ga	<sup>72</sup> Ge	<sup>133</sup> Cs	<sup>88</sup> Sr	<sup>9</sup> Be	<sup>85</sup> Rb
	μg/g	μg/g	μg/g	μg/g	μg/g	μg/g	μg/g	μg/g	μg/g	μg/g	μg/g	μg/g	μg/g	μg/g	μg/g	μg/g
BKNV_16	0.13	0.24	0.17	0.17	1.81	5.92	43.56		0.09	0.90		0.53				
BKNV_17	0.11	0.27	3.22	0.28	5.59	4.95	43.69	3.28	0.09	0.89		0.53	0.02	0.05	#DIV/0!	0.05
BKNV_18		0.25	0.48	1.22	1.85	4.98		3.63	0.09	0.71		0.48		0.04		0.05
BKNV_19		0.21	0.69		0.37	4.58	41.18		0.08	0.37				0.04		
BKNV_20		0.23	0.28	0.53	0.95	7.20	61.42		0.09	0.35						

**Table A.12.** LA-ICP-MS trace element errors for samples from KVI, fraction >250 μm.

Sample	<sup>7</sup> Li	<sup>11</sup> B	<sup>23</sup> Na	<sup>25</sup> Mg	<sup>27</sup> Al	<sup>31</sup> P	<sup>35</sup> Cl	<sup>39</sup> K	<sup>45</sup> Sc	<sup>49</sup> Ti	<sup>71</sup> Ga	<sup>72</sup> Ge	<sup>133</sup> Cs	<sup>88</sup> Sr	<sup>9</sup> Be	<sup>85</sup> Rb
	μg/g	μg/g	μg/g	μg/g	μg/g	μg/g	μg/g	μg/g	μg/g	μg/g	μg/g	μg/g	μg/g	μg/g	μg/g	μg/g
DOB_01	0.19	0.28	0.92	0.44	3.70	6.57	42.92	4.36	0.12	1.19		0.59	0.02			0.05
DOB_02	0.15	0.27	1.45	0.57	4.14	7.10	50.90	2.49	0.10	2.29			0.02	0.08		0.07
DOB_03		0.26	2.41	0.36	0.59	5.61	37.93	1.96	0.10			0.49		6.08		
DOB_04			0.32	0.21	1.30	6.77	42.24		0.08	0.44		0.48		0.05		
DOB_05		0.26	0.84	0.06	0.54	3.99	34.68		0.09	0.92				0.04		
DOB_06	0.20		95.15	3.56	183.08	11.71		40.96	0.13	2.44				0.21		0.18
DOB_07		0.27	0.23		0.42	4.35			0.12	0.48		0.61				
DOB_08	0.28		2.02	3.64	14.28	7.69	56.17	6.18	0.16	2.81				0.13		

Sample	<sup>7</sup> Li	<sup>11</sup> B	<sup>23</sup> Na	<sup>25</sup> Mg	<sup>27</sup> Al	<sup>31</sup> P	<sup>35</sup> Cl	<sup>39</sup> K	<sup>45</sup> Sc	<sup>49</sup> Ti	<sup>71</sup> Ga	<sup>72</sup> Ge	<sup>133</sup> Cs	<sup>88</sup> Sr	<sup>9</sup> Be	<sup>85</sup> Rb
	μg/g	μg/g	μg/g	μg/g	μg/g	μg/g	μg/g	μg/g	μg/g	μg/g	μg/g	μg/g	μg/g	μg/g	μg/g	μg/g
DOB_09		0.24	0.25		0.67	4.59			0.09	0.39		0.51		0.07	0.02	
DOB_10		0.27	0.37	0.24	0.71	4.49			0.10	0.55				0.06		
DOB_11			1.18	2.16	3.62	12.25	88.19		0.10	2.29				0.09		
DOB_12c		0.28	0.19	0.51	0.32	4.08			0.09	0.36		0.56		0.07		
DOB_13	0.22	0.37	1.72	4.96	65.22	4.55		29.77	0.12	0.48			0.02	0.14		0.19
DOB_16	0.21	0.36	1.14	0.72	2.94	5.51		4.06	0.15	0.63		0.82		0.23		
DOB_17	0.25	0.27	0.63	0.48	6.03	8.94	66.15	2.83	0.11	1.55		0.58		0.06		
DOB_18		0.27	0.75	0.54	1.95	5.65	43.07		0.08	0.77		0.55		0.08		
DOB_19			0.53	0.43	1.21	7.46	71.13		0.11	0.41				0.05		
DOB_20			0.28		0.39	9.05	54.71		0.09	0.36		0.62				
RAB1_02	0.46	0.89	0.38	0.28	0.49	5.82	138.38	4.14	0.17	0.91	0.12	1.26	0.03	0.07	0.17	0.10
RAB1_04	0.50	0.87	0.40	0.46	0.54	6.33	147.98	4.48	0.19	1.17	0.15	1.30	0.02	0.08	0.15	0.11
RAB1_05	0.48	0.92	0.39	0.54	0.51	6.19	143.26	4.35	0.17	1.01	0.08	1.27	0.03	0.08	0.19	0.12
RAB1_06	0.52	1.04	0.42	0.36	0.56	6.55	151.86	4.63	0.20	1.09	0.15	1.46	0.04	0.09	0.25	0.11
RAB1_07	0.53	0.99	0.42	0.47	0.58	6.78	153.89	4.76	0.19	1.17	0.14	1.40	0.04	0.08	0.20	0.11
RAB1_08	0.68	1.23	0.57	0.75	0.74	8.52	191.85	6.01	0.26	1.70	0.18	1.81	0.05	0.13	0.36	0.16

Sample	<sup>7</sup> Li	<sup>11</sup> B	<sup>23</sup> Na	<sup>25</sup> Mg	<sup>27</sup> Al	<sup>31</sup> P	<sup>35</sup> Cl	<sup>39</sup> K	<sup>45</sup> Sc	<sup>49</sup> Ti	<sup>71</sup> Ga	<sup>72</sup> Ge	<sup>133</sup> Cs	<sup>88</sup> Sr	<sup>9</sup> Be	<sup>85</sup> Rb
	μg/g	μg/g	μg/g	μg/g	μg/g	μg/g	μg/g	μg/g	μg/g	μg/g	μg/g	μg/g	μg/g	μg/g	μg/g	μg/g
RAB1_09	0.59	1.10	0.47	0.53	0.64	7.57	166.91	5.33	0.23	1.33	0.14	1.61	0.04	0.09	0.23	0.13
RAB1_10	0.54	1.03	0.43	0.54	0.60	7.10	153.90	4.92	0.20	1.32	0.16	1.42	0.03	0.09	0.23	0.12
RAB1_12	0.52	0.95	0.43	0.54	0.56	6.68	146.01	4.69	0.19	1.17	0.08	1.32	0.03	0.09	0.21	0.11
RAB1_13	0.54	0.93	0.45	0.50	0.60	6.73	125.95	5.02	0.18	1.23	0.16	1.43	0.04	0.08	0.26	0.12
RAB1_14	0.49	0.89	0.38	0.53	0.53	6.27	118.09	4.63	0.18	1.07	0.14	1.33	0.04	0.08	0.22	0.12
RAB1_15	1.12	2.27	0.97	1.69	1.33	13.81	258.74	9.96	0.44	3.28	0.41	3.06	0.10	0.23	0.92	0.35
RAB1_16	0.50	0.91	0.42	0.37	0.51	6.36	120.77	4.71	0.18	1.08	0.14	1.35	0.03	0.09	0.18	0.12
RAB1_18	0.48	0.88	0.38	0.31	0.50	6.23	116.57	4.54	0.17	1.13	0.08	1.28	0.02	0.08	0.17	0.10

**Table A.13.** LA-ICP-MS trace element contents for samples from JB, fraction 63-250 µm.

Sample	<sup>7</sup> Li	<sup>11</sup> B	<sup>23</sup> Na	<sup>25</sup> Mg	<sup>27</sup> Al	<sup>31</sup> P	<sup>35</sup> Cl	<sup>39</sup> K	<sup>45</sup> Sc	<sup>49</sup> Ti	<sup>71</sup> Ga	<sup>72</sup> Ge	<sup>133</sup> Cs	<sup>88</sup> Sr	<sup>9</sup> Be	<sup>85</sup> Rb
	µg/g	µg/g	µg/g	µg/g	µg/g	µg/g	µg/g	µg/g	µg/g	µg/g	µg/g	µg/g	µg/g	µg/g	µg/g	µg/g
JB1_1	3.25		31.74	5.01	216.05	204.16	173.12	29.49	0.61	26.03				0.80		
JB1_2	1.41		41.17	1.04	225.38	222.00		53.42	0.87	10.56				1.40		
JB1_3	1.93		7.24		75.86	186.18		6.93	1.01	18.35		2.24		0.07		
JB1_4	2.38		23.03	1.43	143.41	224.53		12.47	0.62	55.71				0.40		
JB1_6	2.59		28.74	1.89	129.96	177.22		13.24	0.78	64.84				0.85		
JB1_8	14.50		23.30	2.44	299.43	239.23		31.43	0.81	20.21				0.68		0.17
JB1_9	5.62		0.80	2.35	116.69	141.85			0.83	68.25						
JB1_10	1.15		40.12	3.76	107.86	241.45		16.65	0.82					1.07		
JB1_11	24.23		5.19	2.87	143.79	244.46			0.75	123.76				0.14		
JB1_12	2.08		50.25	1.03	114.88	204.80		9.02	0.72	28.05				0.61		
JB1_13	4.83	1.57	14.97		155.43	228.38		5.98	0.79	12.69		2.96		0.69	0.74	
JB1_14	1.24		1.56		62.11	93.11			0.74	64.65						
JB1_15			1.58		10.09	234.51			0.71	9.88						
JB1_16	15.46	2.60	129.12	17.51	666.18	220.58		100.18	0.95	27.70				4.41		0.34
JB1_17	0.40		25.96		72.84	228.91		12.11	0.89					0.51		

Sample	<sup>7</sup> Li	<sup>11</sup> B	<sup>23</sup> Na	<sup>25</sup> Mg	<sup>27</sup> Al	<sup>31</sup> P	<sup>35</sup> Cl	<sup>39</sup> K	<sup>45</sup> Sc	<sup>49</sup> Ti	<sup>71</sup> Ga	<sup>72</sup> Ge	<sup>133</sup> Cs	<sup>88</sup> Sr	<sup>9</sup> Be	<sup>85</sup> Rb
	μg/g	μg/g	μg/g	μg/g	μg/g	μg/g	μg/g	μg/g	μg/g	μg/g	μg/g	μg/g	μg/g	μg/g	μg/g	μg/g
JB1_18	1.27		42.41	4.98	152.43	232.88		40.75	0.50	55.35				1.37		
JB1_20	24.52		93.95	533.32	889.43	135.52	878.52	82.79	0.96	80.22	0.48		0.04	3.39		0.23
JB5_1			13.44	0.52	18.58	222.63		5.85	0.79	41.88				0.28		
JB5_2		2.02	3.28	0.68	11.89	155.45			0.83	3.68						
JB5_3	1.14	1.41	37.07	0.82	56.33	222.15		7.73	0.82	4.73				0.92		
JB5_4		4.91	9.33		68.01	240.53		23.48	0.45	37.57				0.24		
JB5_5	3.62	2.31	6.94	2.51	74.04	139.42			0.79	7.87						
JB5_6			4.39		9.44	247.23			0.73	88.95						
JB5_7			8.36		15.56	240.76			0.71	7.49		2.32		0.16		
JB5_10	2.50		9.38		76.60	207.54		5.91	0.63					0.29		
JB5_11	0.36	2.42	128.75	5.02	115.60	252.82		62.72	0.80	16.07			0.74	0.80		0.26
JB5_12	1.99		35.17	1.70	136.48	259.66		26.51	0.62					1.02		
JB5_13	2.42		5.63	0.82	59.52	182.98		20.44	0.83	29.89						
JB5_14	0.64		62.34	2.56	105.48	244.30		13.51	0.82	4.31				1.15		
JB5_16	0.57		1.63		34.79	252.82		5.82	0.90	9.71						
JB5_17	2.51	2.40	141.29		79.15	256.50	268.24	12.66	0.97	56.01			0.22	0.21		

Sample	<sup>7</sup> Li	<sup>11</sup> B	<sup>23</sup> Na	<sup>25</sup> Mg	<sup>27</sup> Al	<sup>31</sup> P	<sup>35</sup> Cl	<sup>39</sup> K	<sup>45</sup> Sc	<sup>49</sup> Ti	<sup>71</sup> Ga	<sup>72</sup> Ge	<sup>133</sup> Cs	<sup>88</sup> Sr	<sup>9</sup> Be	<sup>85</sup> Rb
	µg/g	µg/g	µg/g	µg/g	µg/g	µg/g	µg/g	µg/g	µg/g	µg/g	µg/g	µg/g	µg/g	µg/g	µg/g	µg/g
JB5_18	2.58	2.48	16.75	1.21	261.99	247.53		77.56	0.71	34.13			0.62		0.83	
JB5_19			520.44	4.84	11.19	235.99	534.82	25.62	0.89			0.38	24.22		0.25	
JB5_20			31.42		33.91	253.89			0.59	25.81		3.21				
JB10_1	12.35	3.02	75.60	0.74	468.36	257.37		41.17	0.68		3.29		3.05		0.13	
JB10_2		2.20	6.27		42.37	271.61			0.57	10.63			0.19			
JB10_3	1.53	25.91	223.53	3.48	543.40	172.61		141.47	0.98		0.27		10.27		0.64	
JB10_4	2.70				74.46	270.56			0.70	26.93						
JB10_5	1.73	2.84	60.98	3.01	175.93	243.13		10.14	0.73	28.93			1.85			
JB10_8	9.39	1.75	93.64		326.88	261.13		16.77	0.46				3.78			
JB10_12	0.48		48.28	2.30	160.62	253.15		20.08	0.50				1.04			
JB10_16			1.12		14.70	270.80			0.65	7.48						
JB10_17	0.47		42.03	0.49	108.06	265.26		24.12	0.71	89.94			0.07	2.95		0.16
JB17_3	1.94	5.72	48.69	9.65	314.32	247.22		40.31	0.56	31.90		2.31	0.36	1.08		0.18
JB17_4	1.14	1.56	4.16	0.52	71.32	198.54			0.66	29.09						
JB17_5	1.08	1.98	56.13	9.47	71.60	176.32		6.67	0.72		2.33		1.67			
JB17_6	0.53		93.93	3.02	49.01	226.43		11.00	0.69	9.02			0.09	0.87		

Sample	<sup>7</sup> Li	<sup>11</sup> B	<sup>23</sup> Na	<sup>25</sup> Mg	<sup>27</sup> Al	<sup>31</sup> P	<sup>35</sup> Cl	<sup>39</sup> K	<sup>45</sup> Sc	<sup>49</sup> Ti	<sup>71</sup> Ga	<sup>72</sup> Ge	<sup>133</sup> Cs	<sup>88</sup> Sr	<sup>9</sup> Be	<sup>85</sup> Rb
	μg/g	μg/g	μg/g	μg/g	μg/g	μg/g	μg/g	μg/g	μg/g	μg/g	μg/g	μg/g	μg/g	μg/g	μg/g	μg/g
JB17_7	0.32	2.09	3.99		49.64	229.05		5.75	0.79	15.48		2.99				
JB17_8	0.52	3.47	1.16	28.44	42.34	271.05				42.56						
JB17_9	3.06	4.96	20.87	0.97	252.83	191.82		53.79	0.74	42.22				0.48		0.38
JB17_11	4.54		2.60		100.85	414.67			0.83	24.91						
JB17_12	6.03	2.77	43.79	5.05	326.58	95.20	260.04	53.31		19.81				1.44		0.15
JB17_17	0.40	1.80	20.29	1.06	74.27	274.49		14.48	0.75	28.42				0.30		
JB17_18	0.96		18.61		100.96	269.29		11.10	0.70	8.06		2.43		1.57		
JB17_19	2.41		1.27	1.52	115.52	271.39	279.23	5.35	0.58	57.71				0.02		
JB17_20	2.65		3.93		104.79	270.29		6.77	0.61	11.44				0.19		0.13
JB23_1	2.19		18.81	3.69	239.27	265.77	397.47	45.51		26.85				2.10		0.22
JB23_3	7.11		8.79	1.08	76.26	274.42		8.95	0.63	19.98				0.12		
JB23_6	2.44	7.81	18.77	0.99	166.04	249.88		8.47	0.82	53.38				0.31		0.22
JB23_7			7.93	6.22	64.52	276.57		22.41	0.54	33.39				0.40		
JB23_8			15.78		24.59	213.01			0.58					0.20		
JB23_9	2.87		28.59	3.56	213.82	188.71		17.66	0.77	26.63				0.88		
JB23_11	2.34	3.13	25.06	18.58	297.72	280.16		48.48	0.67	50.20				1.72		0.26

Sample	<sup>7</sup> Li	<sup>11</sup> B	<sup>23</sup> Na	<sup>25</sup> Mg	<sup>27</sup> Al	<sup>31</sup> P	<sup>35</sup> Cl	<sup>39</sup> K	<sup>45</sup> Sc	<sup>49</sup> Ti	<sup>71</sup> Ga	<sup>72</sup> Ge	<sup>133</sup> Cs	<sup>88</sup> Sr	<sup>9</sup> Be	<sup>85</sup> Rb
	μg/g	μg/g	μg/g	μg/g	μg/g	μg/g	μg/g	μg/g	μg/g	μg/g	μg/g	μg/g	μg/g	μg/g	μg/g	μg/g
JB23_13		3.36	96.45	2.27	13.47	196.19	346.00	10.57	0.64	75.36				1.55		
JB23_17	2.25		33.07	6.29	157.37	213.01		12.65	0.68	5.70				1.65		
JB23_18	3.37		26.56	1.26	179.17	259.70		13.04	1.03	33.17				0.77		
JB23_19	0.94	1.34	13.13	1.00	84.22	274.54		12.27	0.83	4.00				0.23		
JB26_1			19.74	1.04	29.29	268.27		6.94	0.58	6.12				0.46		
JB26_2	1.37		11.95	0.52	112.43	265.81		10.86	0.98	14.20		2.96		1.14		
JB26_3			7.27	2.54	59.60	283.85				72.40				0.36		
JB26_4	6.54		16.45	1.04	189.08	277.69			0.52	8.92				0.51		
JB26_5			13.48	0.48	30.49	271.35		19.71	0.83							
JB26_7			2.84		19.74	288.67			0.96	13.28				0.10		
JB26_8			10.26	1.37	41.08	283.73		14.38	0.57	18.10		3.65		0.15		
JB26_10	1.96		15.16	1.15	100.38	288.99		11.74	0.73	16.55				0.36		
JB26_11	8.90		32.17	15.29	506.10	174.86		61.94	0.71	26.29				1.42		
JB26_12	2.37		28.79	30.25	413.03	120.46		113.53	0.62	27.33			0.04	1.09		0.43
JB26_13	0.49		26.09	13.45	47.55	196.05		6.68	0.52	39.40	0.16			0.46		
JB26_14	4.37	1.58	49.74	2.70	372.44	240.21		47.95	0.84			3.30		5.31		0.16

Sample	<sup>7</sup> Li	<sup>11</sup> B	<sup>23</sup> Na	<sup>25</sup> Mg	<sup>27</sup> Al	<sup>31</sup> P	<sup>35</sup> Cl	<sup>39</sup> K	<sup>45</sup> Sc	<sup>49</sup> Ti	<sup>71</sup> Ga	<sup>72</sup> Ge	<sup>133</sup> Cs	<sup>88</sup> Sr	<sup>9</sup> Be	<sup>85</sup> Rb
	µg/g	µg/g	µg/g	µg/g	µg/g	µg/g	µg/g	µg/g	µg/g	µg/g	µg/g	µg/g	µg/g	µg/g	µg/g	µg/g
JB26_15			12.99		15.52	289.71			0.56	14.81				0.31		
JB26_16		2.17	50.00	3.64	47.97	180.87		16.96	0.80	23.19			0.06	1.50		
JB26_17	0.65		6.07		68.63	271.33			0.68	25.23		3.28		0.11		
JB26_18			4.40	6.90	25.26	291.31		8.37	0.42	13.19		2.96				
JB26_19	1.36	2.00	27.07	0.62	113.23	266.43		11.98	0.66					0.84		
JB26_20	0.90		3.40		54.56	195.55			0.66	23.88				0.06		

**Table A.14.** LA-ICP-MS trace element contents for samples from BK, fraction 63-250 µm.

Sample	<sup>7</sup> Li	<sup>11</sup> B	<sup>23</sup> Na	<sup>25</sup> Mg	<sup>27</sup> Al	<sup>31</sup> P	<sup>35</sup> Cl	<sup>39</sup> K	<sup>45</sup> Sc	<sup>49</sup> Ti	<sup>71</sup> Ga	<sup>72</sup> Ge	<sup>133</sup> Cs	<sup>88</sup> Sr	<sup>9</sup> Be	<sup>85</sup> Rb
	µg/g	µg/g	µg/g	µg/g	µg/g	µg/g	µg/g	µg/g	µg/g	µg/g	µg/g	µg/g	µg/g	µg/g	µg/g	µg/g
BK41_1	1.75	2.21	30.02		119.51	255.96	244.57	9.57	0.42	15.29				0.31		
BK41_2	2.03		8.24		98.29	253.98			0.77	19.58				0.16		
BK41_3	1.41		8.82		55.77	275.17			0.51	20.28				0.16		
BK41_5	2.99		1.98		117.45	241.72			0.49	6.05				0.06		
BK41_6			5.91		33.57	261.29			0.55	7.82				0.25		
BK41_7	0.53	2.10	98.32	11.06	255.97	260.47		62.95	0.65	6.74				2.45		0.25
BK41_8	1.76		6.05		101.75	256.19			0.65	66.32						

Sample	<sup>7</sup> Li	<sup>11</sup> B	<sup>23</sup> Na	<sup>25</sup> Mg	<sup>27</sup> Al	<sup>31</sup> P	<sup>35</sup> Cl	<sup>39</sup> K	<sup>45</sup> Sc	<sup>49</sup> Ti	<sup>71</sup> Ga	<sup>72</sup> Ge	<sup>133</sup> Cs	<sup>88</sup> Sr	<sup>9</sup> Be	<sup>85</sup> Rb
	µg/g	µg/g	µg/g	µg/g	µg/g	µg/g	µg/g	µg/g	µg/g	µg/g	µg/g	µg/g	µg/g	µg/g	µg/g	µg/g
BK41_9	1.91	2.20	27.97	0.89	163.07	132.51		18.96	0.59	22.92			0.38		0.11	
BK41_13			30.14	0.65	47.06	230.85		6.54	0.54				0.19			
BK41_14	1.67		34.85	1.99	166.19	270.37		34.73	0.58	64.08			0.54		0.20	
BK41_16			5.27		39.73	245.99	291.84		0.54				0.18			
BK41_17	1.40	2.17	30.22		181.21	337.62		26.09		30.62		2.64	0.05	0.63	0.42	
BK41_18	11.79	1.43	43.60	10.00	394.33	301.51		25.24			0.36		0.48			
BK41_20	2.69	1.63	4.90	26.50	213.26	268.96		81.34	0.69	66.36			0.18		0.82	
BKNV_1			19.06	1.36	215.71	293.51		78.62	0.58	139.20			0.51			
BKNV_2			4.96	11.45	14.78	275.05			0.54	4.64		2.58		0.10		
BKNV_3			16.38		64.39	280.84		8.26	0.71	6.69			0.26			
BKNV_4	2.83	1.27	5.93	0.95	103.14	262.69		5.99	0.76	22.06		2.60		0.18		
BKNV_5			1.94		11.69	266.25				5.16						
BKNV_6	5.82		17.18		151.86	293.20		18.13	0.96				0.56			
BKNV_9			24.83	55.34	1259.14	263.19		560.71	0.63	8.90			0.11	0.59		3.02
BKNV_10			67.09	1.56	49.21	224.53		12.29		5.73			2.52			
BKNV_11	0.50		15.68		62.34	259.74			0.59	27.36			0.10			

Sample	<sup>7</sup> Li	<sup>11</sup> B	<sup>23</sup> Na	<sup>25</sup> Mg	<sup>27</sup> Al	<sup>31</sup> P	<sup>35</sup> Cl	<sup>39</sup> K	<sup>45</sup> Sc	<sup>49</sup> Ti	<sup>71</sup> Ga	<sup>72</sup> Ge	<sup>133</sup> Cs	<sup>88</sup> Sr	<sup>9</sup> Be	<sup>85</sup> Rb
	µg/g	µg/g	µg/g	µg/g	µg/g	µg/g	µg/g	µg/g	µg/g	µg/g	µg/g	µg/g	µg/g	µg/g	µg/g	µg/g
BKNV_13			1.68	1.13	15.20	238.42			0.44					0.11		
BKNV_14	3.16		5.10	1.11	102.81	260.85			0.55	49.06				0.10		
BKNV_15			16.57	6.55	86.01	266.43		39.44						0.20		0.34
BKNV_16	1.74		10.97		89.25	261.70		13.23	0.78	8.11				0.28		
BKNV_17	17.53		60.12	133.20	712.10	240.36		36.78	0.59	11.39				2.35		0.14
BKNV_18	0.40		10.51	1.57	70.51	265.98			0.64	37.89				0.10		
BKNV_19	0.57		15.81		85.08	292.88			0.80	35.62				0.24		0.11
BKNV_20			32.93	256.61	979.29	182.61	2684.44	153.31		132.95						1.34

**Table A.15.** LA-ICP-MS trace element contents for samples from KVI, fraction 63-250 µm.

Sample	<sup>7</sup> Li	<sup>11</sup> B	<sup>23</sup> Na	<sup>25</sup> Mg	<sup>27</sup> Al	<sup>31</sup> P	<sup>35</sup> Cl	<sup>39</sup> K	<sup>45</sup> Sc	<sup>49</sup> Ti	<sup>71</sup> Ga	<sup>72</sup> Ge	<sup>133</sup> Cs	<sup>88</sup> Sr	<sup>9</sup> Be	<sup>85</sup> Rb
	µg/g	µg/g	µg/g	µg/g	µg/g	µg/g	µg/g	µg/g	µg/g	µg/g	µg/g	µg/g	µg/g	µg/g	µg/g	µg/g
DOB_2			3.80	2.02	19.52	108.46	232.95	9.76	1.02	28.32						
DOB_4	2.77	4.11	50.28	0.46	86.18	132.58		26.20	0.81	24.19			0.23	0.11	0.20	0.37
DOB_5	0.74		3.42	41.05	95.81	161.76	181.06	72.80	0.86	88.02				0.10		0.18
DOB_7	0.61	2.38	9.57	5.43	307.52	154.84	228.86	142.54	1.06	10.29				0.15		0.29
DOB_8			0.76		9.83	158.01			0.64	2.02						

Sample	<sup>7</sup> Li	<sup>11</sup> B	<sup>23</sup> Na	<sup>25</sup> Mg	<sup>27</sup> Al	<sup>31</sup> P	<sup>35</sup> Cl	<sup>39</sup> K	<sup>45</sup> Sc	<sup>49</sup> Ti	<sup>71</sup> Ga	<sup>72</sup> Ge	<sup>133</sup> Cs	<sup>88</sup> Sr	<sup>9</sup> Be	<sup>85</sup> Rb
	µg/g	µg/g	µg/g	µg/g	µg/g	µg/g	µg/g	µg/g	µg/g	µg/g	µg/g	µg/g	µg/g	µg/g	µg/g	µg/g
DOB_9			5.58		47.83	161.33			0.76	37.17			0.13		0.08	
DOB_10	0.43	2.54	105.09	0.56	139.82	165.15		38.76	0.99	12.67		0.04	2.09		0.09	
DOB_11	0.57		23.65	14.94	63.90	160.79		5.84	0.75	9.85	0.05		0.04	0.14		
DOB_12			34.83	6.89	64.20	153.77		21.70	0.63	2.72				4.21		
DOB_13			2.60	0.55	20.06	162.75			0.69	2.34	0.05					
DOB_14		2.63	201.62	6.89	35.24	127.83		11.86	0.57			1.83	0.09	4.66		
DOB_15	4.18	2.49	50.08	3.91	265.30	164.07		9.93	0.68	76.07		0.03	3.13			
DOB_16			0.51		6.98	160.36			0.82							
DOB_17			9.37	1.14	42.24	163.72		6.50	0.78			1.84		0.42		
DOB_18			1.46		10.42	165.57			1.08	5.63				0.09		
DOB_19			9.13	2.29	40.08	123.67			0.64			2.48		0.43		
RAB1_1			1.75		18.85	156.33	416.38			33.71				0.10		
RAB1_2			36.11	20.85	185.08	157.70		47.97	0.97	7.36				1.16	0.32	
RAB1_3	0.23	6.61	173.21	1.18	163.07	153.32		106.80	0.69	46.66		1.63	0.09	2.35	0.73	
RAB1_5	1.32	3.70	70.80	44.43	256.60	120.09		57.27	0.70	1.91		0.05	1.64		0.28	
RAB1_6			2.25		7.59	112.03			0.69	2.09		1.78				

Sample	<sup>7</sup> Li	<sup>11</sup> B	<sup>23</sup> Na	<sup>25</sup> Mg	<sup>27</sup> Al	<sup>31</sup> P	<sup>35</sup> Cl	<sup>39</sup> K	<sup>45</sup> Sc	<sup>49</sup> Ti	<sup>71</sup> Ga	<sup>72</sup> Ge	<sup>133</sup> Cs	<sup>88</sup> Sr	<sup>9</sup> Be	<sup>85</sup> Rb
	µg/g	µg/g	µg/g	µg/g	µg/g	µg/g	µg/g	µg/g	µg/g	µg/g	µg/g	µg/g	µg/g	µg/g	µg/g	µg/g
RAB1_7	1.48	3.33	28.62	8.46	147.46	154.71		33.56	1.02	15.26			0.40		0.10	
RAB1_8	3.06		32.01	2.44	126.96	153.33		24.76	0.84	11.26			0.78			
RAB1_9	0.49		5.11		43.64	103.05			0.74				0.45			
RAB1_10	0.42		22.93		88.65	161.89			0.78	39.99			0.16	0.39		0.06
RAB1_11	4.40		36.76	2.90	213.00	153.29		16.61	0.75	44.71			0.08	1.47		
RAB1_12	28.45	2.82	85.16	1.22	1466.81	155.85		52.24	0.62	2.14		2.34	0.07	10.73	0.17	0.30
RAB1_13	3.56	3.54	10.62	0.80	65.17	129.27		5.53	0.83	27.89			0.30			
RAB1_14	1.19		7.01		36.14	143.31			0.89				0.35			
RAB1_16			4.60	2.28	49.79	161.80		11.50	0.89	1006.52			0.11			
RAB1_18	0.32		4.76		43.14	161.81		8.74	0.63				0.26			
RAB1_19	3.04		43.56	2.08	154.00	162.84		10.75	0.45	7.82	0.12		1.74			

**Table A.16.** LA-ICP-MS trace element limits of detection for samples from JB, fraction 63-250 µm.

Sample	<sup>7</sup> Li	<sup>11</sup> B	<sup>23</sup> Na	<sup>25</sup> Mg	<sup>27</sup> Al	<sup>31</sup> P	<sup>35</sup> Cl	<sup>39</sup> K	<sup>45</sup> Sc	<sup>49</sup> Ti	<sup>71</sup> Ga	<sup>72</sup> Ge	<sup>133</sup> Cs	<sup>88</sup> Sr	<sup>9</sup> Be	<sup>85</sup> Rb
	µg/g	µg/g	µg/g	µg/g	µg/g	µg/g	µg/g	µg/g	µg/g	µg/g	µg/g	µg/g	µg/g	µg/g	µg/g	µg/g
JB1_1	0.24	1.41	0.37	0.10	0.67	12.87	122.69	5.59	0.40	2.59	0.20	2.37	0.04	0.09	0.18	0.12
JB1_2	0.22	1.26	0.35	0.58	0.64	11.71	116.01	5.23	0.34	2.63	0.24	2.14	0.02	0.07	0.09	0.09
JB1_3	0.24	1.40	0.36	0.49	0.67	12.74	132.59	5.54	0.30	3.23	0.27	2.07	0.03	0.05	0.24	0.10
JB1_4	0.25	1.42	0.38	0.61	0.68	13.51	135.46	5.91	0.34	3.52	0.31	2.37	0.03	0.08	0.20	0.10
JB1_6	0.25	1.52	0.40	0.67	0.74	13.46	142.31	5.86	0.39	3.97	0.21	2.26	0.04	0.11	0.31	0.11
JB1_8	0.26	1.44	0.40	0.53	0.75	14.04	155.62	6.10	0.34	3.01	0.22	2.59	0.03	0.09	0.29	0.10
JB1_9	0.25	1.49	0.38	0.54	0.72	13.05	147.94	5.64	0.31	3.49	0.21	2.11	0.03	0.05	0.30	0.12
JB1_10	0.26	1.54	0.40	0.69	0.83	14.51	164.15	6.23	0.39	3.64	0.26	2.27	0.04	0.09	0.22	0.13
JB1_11	0.26	1.44	0.39	0.67	0.73	13.76	160.48	5.90	0.33	3.53	0.17	2.34	0.04	0.11	0.37	0.13
JB1_12	0.26	1.57	0.37	0.40	0.72	14.04	164.86	5.90	0.36	2.84	0.28	2.66	0.03	0.09	0.29	0.11
JB1_13	0.24	1.40	0.34	0.42	0.69	12.86	154.17	5.50	0.36	3.05	0.16	2.18	0.03	0.08	0.19	0.09
JB1_14	0.30	1.70	0.45	0.93	0.91	15.77	192.01	6.55	0.39	3.88	0.31	2.77	0.05	0.14	0.33	0.16
JB1_15	0.26	1.52	0.40	0.32	0.76	14.23	177.95	5.98	0.42	3.51	0.06	2.46	0.03	0.08	0.36	0.13
JB1_16	0.29	1.58	0.44	0.65	0.83	15.09	195.63	6.42	0.38	3.73	0.28	2.66	0.04	0.10	0.17	0.15
JB1_17	0.35	1.98	0.55	0.91	1.01	18.70	243.66	7.80	0.49	5.27	0.40	3.32	0.05	0.09	0.42	0.16

Sample	<sup>7</sup> Li	<sup>11</sup> B	<sup>23</sup> Na	<sup>25</sup> Mg	<sup>27</sup> Al	<sup>31</sup> P	<sup>35</sup> Cl	<sup>39</sup> K	<sup>45</sup> Sc	<sup>49</sup> Ti	<sup>71</sup> Ga	<sup>72</sup> Ge	<sup>133</sup> Cs	<sup>88</sup> Sr	<sup>9</sup> Be	<sup>85</sup> Rb
	µg/g	µg/g	µg/g	µg/g	µg/g	µg/g	µg/g	µg/g	µg/g	µg/g	µg/g	µg/g	µg/g	µg/g	µg/g	µg/g
JB1_18	0.25	1.39	0.39	0.56	0.75	13.51	179.55	5.57	0.37	2.82	0.27	2.36	0.03	0.08	0.08	0.12
JB1_20	0.34	1.68	0.49	0.64	0.95	17.44	248.89	7.36	0.53	3.41	0.35	3.08	0.04	0.09	0.37	0.19
JB5_1	0.24	1.32	0.38	0.34	0.69	12.83	188.73	4.99	0.28	2.84	0.21	2.32	0.03	0.09	0.22	0.13
JB5_2	0.26	1.45	0.40	0.42	0.79	14.34	212.80	5.76	0.30	3.21	0.23	2.43	0.03	0.08	0.22	0.13
JB5_3	0.25	1.25	0.36	0.73	0.71	13.41	197.97	5.29	0.33	2.96	0.24	2.12	0.04	0.07	0.29	0.07
JB5_4	0.26	1.39	0.38	0.47	0.75	14.23	209.78	5.58	0.38	3.36	0.17	2.66	0.04	0.06	0.30	0.13
JB5_5	0.27	1.45	0.38	0.66	0.80	14.24	212.68	5.69	0.35	3.84	0.26	2.30	0.02	0.11	0.33	0.14
JB5_6	0.31	1.55	0.47	0.72	0.87	16.27	244.14	6.37	0.38	3.49	0.30	2.77	0.03	0.10	0.32	0.17
JB5_7	0.24	1.24	0.35	0.39	0.72	12.87	196.16	5.14	0.35	3.53	0.25	2.13	0.02	0.05	0.35	0.11
JB5_10	0.28	1.54	0.38	0.80	0.85	14.67	228.19	5.58	0.35	4.54	0.26	2.62	0.04	0.06	0.32	0.16
JB5_11	0.30	1.47	0.42	0.60	0.88	16.00	246.51	5.92	0.43	3.71	0.33	2.77	0.03	0.10	0.49	0.13
JB5_12	0.37	2.04	0.60	1.01	1.10	19.45	305.15	7.35	0.54	4.27	0.30	3.56	0.05	0.11	0.20	0.13
JB5_13	0.30	1.69	0.47	0.69	0.90	15.86	246.78	5.91	0.44	4.81	0.35	2.97	0.04	0.11	0.40	0.16
JB5_14	0.27	1.38	0.39	0.71	0.82	14.44	226.84	5.51	0.29	3.40	0.19	2.51	0.03	0.07	0.30	0.16
JB5_16	0.25	1.38	0.38	0.49	0.76	13.81	219.93	5.22	0.33	3.22	0.18	2.42	0.04	0.09	0.29	0.15
JB5_17	0.26	1.25	0.40	0.68	0.74	13.53	215.81	5.20	0.27	3.78	0.29	2.32	0.04	0.07	0.28	0.12

Sample	<sup>7</sup> Li	<sup>11</sup> B	<sup>23</sup> Na	<sup>25</sup> Mg	<sup>27</sup> Al	<sup>31</sup> P	<sup>35</sup> Cl	<sup>39</sup> K	<sup>45</sup> Sc	<sup>49</sup> Ti	<sup>71</sup> Ga	<sup>72</sup> Ge	<sup>133</sup> Cs	<sup>88</sup> Sr	<sup>9</sup> Be	<sup>85</sup> Rb
	µg/g	µg/g	µg/g	µg/g	µg/g	µg/g	µg/g	µg/g	µg/g	µg/g	µg/g	µg/g	µg/g	µg/g	µg/g	µg/g
JB5_18	0.36	1.95	0.57	0.85	1.11	18.64	295.80	7.07	0.37	5.92	0.31	3.23	0.05	0.12	0.25	0.18
JB5_19	0.30	1.58	0.41	0.63	0.94	16.22	261.07	6.30	0.41	3.55	0.31	2.77	0.04	0.11	0.33	0.13
JB5_20	0.26	1.26	0.37	0.58	0.80	13.64	219.44	5.32	0.34	2.85	0.22	2.10	0.03	0.10	0.28	0.13
JB10_1	0.25	1.30	0.40	0.60	0.77	13.52	210.83	5.18	0.35	3.02	0.30	2.31	0.03	0.08	0.09	0.10
JB10_2	0.37	1.94	0.59	0.81	1.09	19.78	304.48	7.42	0.45	5.20	0.40	3.37	0.05	0.10	0.43	0.16
JB10_3	0.26	1.36	0.41	0.70	0.81	13.42	205.26	5.20	0.35	3.98	0.27	2.46	0.04	0.10	0.29	0.12
JB10_4	0.28	1.65	0.48	0.61	0.87	15.23	232.86	5.96	0.42	3.76	0.26	2.69	0.03	0.08	0.33	0.13
JB10_5	0.27	1.28	0.44	0.63	0.82	14.54	217.25	5.54	0.28	3.35	0.28	2.63	0.03	0.09	0.09	0.12
JB10_8	0.29	1.50	0.41	0.53	0.87	15.57	228.13	5.99	0.39	3.43	0.25	2.72	0.04	0.05	0.31	0.12
JB10_12	0.38	1.92	0.59	0.85	1.08	19.87	283.34	7.65	0.48	4.71	0.37	3.40	0.06	0.13	0.53	0.22
JB10_16	0.26	1.23	0.37	0.60	0.69	13.74	191.25	5.21	0.34	3.19	0.27	2.34	0.04	0.08	0.23	0.11
JB10_17	0.25	1.35	0.37	0.41	0.73	13.38	182.22	5.18	0.26	3.17	0.07	2.27	0.03	0.07	0.28	0.11
JB17_3	0.27	1.22	0.40	0.58	0.80	14.28	196.45	5.30	0.36	3.73	0.22	2.30	0.04	0.08	0.22	0.14
JB17_4	0.25	1.27	0.39	0.51	0.76	13.82	191.33	5.19	0.33	2.49	0.21	2.30	0.03	0.09	0.26	0.12
JB17_5	0.24	1.17	0.36	0.31	0.70	12.94	180.36	4.89	0.24	2.84	0.21	2.18	0.03	0.05	0.26	0.12
JB17_6	0.38	1.91	0.62	0.63	1.11	20.92	298.32	7.81	0.48	4.32	0.28	3.74	0.05	0.13	0.59	0.17

Sample	<sup>7</sup> Li	<sup>11</sup> B	<sup>23</sup> Na	<sup>25</sup> Mg	<sup>27</sup> Al	<sup>31</sup> P	<sup>35</sup> Cl	<sup>39</sup> K	<sup>45</sup> Sc	<sup>49</sup> Ti	<sup>71</sup> Ga	<sup>72</sup> Ge	<sup>133</sup> Cs	<sup>88</sup> Sr	<sup>9</sup> Be	<sup>85</sup> Rb
	µg/g	µg/g	µg/g	µg/g	µg/g	µg/g	µg/g	µg/g	µg/g	µg/g	µg/g	µg/g	µg/g	µg/g	µg/g	µg/g
JB17_7	0.27	1.42	0.42	0.56	0.83	14.87	212.68	5.55	0.28	3.46	0.18	2.27	0.04	0.08	0.23	0.14
JB17_8	0.40	1.85	0.58	1.15	1.13	21.21	305.28	7.79	0.61	5.07	0.45	3.51	0.05	0.11	0.43	0.18
JB17_9	0.33	1.71	0.50	0.54	0.97	17.68	256.77	6.52	0.38	4.93	0.36	3.14	0.05	0.11	0.52	0.15
JB17_11	0.55	2.79	0.85	1.22	1.62	30.12	445.91	11.03	0.64	6.52	0.52	5.09	0.08	0.12	0.65	0.22
JB17_12	0.27	1.37	0.44	0.50	0.78	15.02	226.62	5.59	0.40	2.87	0.23	2.33	0.04	0.09	0.29	0.14
JB17_17	0.30	1.41	0.46	0.74	0.92	16.33	268.23	6.16	0.43	3.90	0.37	2.88	0.04	0.10	0.42	0.14
JB17_18	0.25	1.21	0.41	0.39	0.86	14.04	228.22	5.23	0.37	2.11	0.17	2.28	0.03	0.07	0.22	0.11
JB17_19	0.27	1.36	0.41	0.62	0.76	14.44	241.12	5.27	0.34	3.18	0.28	2.31	0.02	0.09	0.34	0.11
JB17_20	0.27	1.31	0.41	0.43	0.76	14.10	240.18	5.27	0.40	3.31	0.28	2.40	0.04	0.08	0.34	0.11
JB23_1	0.44	2.00	0.65	0.79	1.28	22.15	363.78	7.57	0.61	7.05	0.34	3.68	0.05	0.10	0.47	0.16
JB23_3	0.29	1.41	0.45	0.55	0.86	15.05	260.26	5.50	0.36	2.73	0.30	3.00	0.03	0.09	0.11	0.17
JB23_6	0.28	1.37	0.45	0.68	0.88	15.22	264.63	5.66	0.37	3.37	0.25	3.00	0.03	0.08	0.32	0.10
JB23_7	0.31	1.44	0.46	0.60	0.92	15.98	281.79	6.07	0.50	4.29	0.32	2.77	0.03	0.08	0.45	0.17
JB23_8	0.36	1.92	0.56	0.72	1.01	18.27	314.95	6.86	0.45	4.89	0.51	3.39	0.04	0.11	0.53	0.20
JB23_9	0.33	1.68	0.47	0.83	0.94	16.56	295.17	6.43	0.39	4.88	0.34	3.01	0.04	0.09	0.13	0.12
JB23_11	0.37	1.81	0.62	0.78	1.16	19.75	344.86	7.49	0.50	4.85	0.41	3.52	0.05	0.12	0.18	0.18

Sample	<sup>7</sup> Li	<sup>11</sup> B	<sup>23</sup> Na	<sup>25</sup> Mg	<sup>27</sup> Al	<sup>31</sup> P	<sup>35</sup> Cl	<sup>39</sup> K	<sup>45</sup> Sc	<sup>49</sup> Ti	<sup>71</sup> Ga	<sup>72</sup> Ge	<sup>133</sup> Cs	<sup>88</sup> Sr	<sup>9</sup> Be	<sup>85</sup> Rb
	µg/g	µg/g	µg/g	µg/g	µg/g	µg/g	µg/g	µg/g	µg/g	µg/g	µg/g	µg/g	µg/g	µg/g	µg/g	µg/g
JB23_13	0.38	1.71	0.57	0.83	1.04	19.17	344.32	7.44	0.40	4.65	0.39	3.49	0.05	0.09	0.36	0.22
JB23_17	0.30	1.49	0.48	0.49	0.87	15.47	275.95	6.03	0.36	3.17	0.30	2.56	0.05	0.06	0.26	0.11
JB23_18	0.28	1.38	0.46	0.49	0.82	14.98	268.45	5.72	0.30	3.59	0.34	2.93	0.04	0.09	0.34	0.14
JB23_19	0.31	1.32	0.45	0.74	0.91	15.87	288.07	6.02	0.35	2.97	0.32	2.88	0.03	0.08	0.29	0.12
JB26_1	0.33	1.56	0.49	0.77	1.00	16.90	300.65	6.48	0.37	4.55	0.32	3.05	0.05	0.05	0.17	0.19
JB26_2	0.33	1.68	0.52	0.44	1.03	17.09	305.19	6.66	0.33	4.56	0.35	2.80	0.03	0.11	0.13	0.12
JB26_3	0.58	2.78	0.93	1.43	2.00	30.33	535.77	11.63	0.83	7.88	0.60	5.73	0.08	0.18	1.00	0.31
JB26_4	0.30	1.48	0.47	0.67	0.97	15.94	280.59	6.17	0.45	4.26	0.07	2.75	0.04	0.09	0.45	0.14
JB26_5	0.30	1.46	0.49	0.46	0.99	15.25	268.71	5.86	0.39	4.86	0.34	2.72	0.04	0.09	0.45	0.14
JB26_7	0.28	1.40	0.44	0.53	0.89	14.72	261.85	5.79	0.36	3.41	0.31	2.47	0.04	0.07	0.26	0.16
JB26_8	0.31	1.52	0.50	0.16	1.00	16.77	293.41	6.41	0.40	4.13	0.34	2.86	0.05	0.10	0.31	0.14
JB26_10	0.49	2.30	0.80	1.00	1.51	26.23	454.54	9.90	0.71	6.94	0.46	4.15	0.05	0.15	0.59	0.26
JB26_11	0.35	1.76	0.58	0.75	1.15	18.41	319.00	7.01	0.48	5.38	0.17	3.10	0.05	0.12	0.66	0.17
JB26_12	0.36	1.84	0.54	0.82	1.20	19.54	334.98	7.32	0.53	5.09	0.39	3.26	0.04	0.08	0.50	0.18
JB26_13	0.29	1.40	0.47	0.13	0.96	16.22	277.54	6.04	0.45	3.84	0.07	2.74	0.04	0.08	0.28	0.13
JB26_14	0.28	1.32	0.43	0.47	0.94	14.87	255.88	5.48	0.31	3.55	0.25	2.53	0.04	0.09	0.37	0.11

Sample	<sup>7</sup> Li	<sup>11</sup> B	<sup>23</sup> Na	<sup>25</sup> Mg	<sup>27</sup> Al	<sup>31</sup> P	<sup>35</sup> Cl	<sup>39</sup> K	<sup>45</sup> Sc	<sup>49</sup> Ti	<sup>71</sup> Ga	<sup>72</sup> Ge	<sup>133</sup> Cs	<sup>88</sup> Sr	<sup>9</sup> Be	<sup>85</sup> Rb
	µg/g	µg/g	µg/g	µg/g	µg/g	µg/g	µg/g	µg/g	µg/g	µg/g	µg/g	µg/g	µg/g	µg/g	µg/g	µg/g
JB26_15	0.28	1.41	0.46	0.63	0.94	15.47	262.43	5.68	0.33	4.35	0.37	2.50	0.04	0.08	0.27	0.15
JB26_16	0.28	1.35	0.39	0.49	0.92	14.74	250.90	5.48	0.36	3.08	0.08	2.61	0.04	0.10	0.14	0.15
JB26_17	0.28	1.32	0.43	0.63	0.90	15.36	260.52	5.68	0.32	3.28	0.26	2.42	0.04	0.08	0.33	0.15
JB26_18	0.28	1.42	0.47	0.62	0.93	15.55	263.41	5.77	0.37	3.77	0.26	2.28	0.04	0.09	0.42	0.13
JB26_19	0.27	1.30	0.45	0.45	0.90	15.05	254.76	5.45	0.35	3.58	0.28	2.58	0.04	0.10	0.36	0.18
JB26_20	0.28	1.28	0.43	0.79	0.88	15.37	252.74	5.52	0.30	4.03	0.21	2.68	0.04	0.04	0.38	0.14

**Table A.17.** LA-ICP-MS trace element limits of detection for samples from BK, fraction 63-250 µm.

Sample	<sup>7</sup> Li	<sup>11</sup> B	<sup>23</sup> Na	<sup>25</sup> Mg	<sup>27</sup> Al	<sup>31</sup> P	<sup>35</sup> Cl	<sup>39</sup> K	<sup>45</sup> Sc	<sup>49</sup> Ti	<sup>71</sup> Ga	<sup>72</sup> Ge	<sup>133</sup> Cs	<sup>88</sup> Sr	<sup>9</sup> Be	<sup>85</sup> Rb
	µg/g	µg/g	µg/g	µg/g	µg/g	µg/g	µg/g	µg/g	µg/g	µg/g	µg/g	µg/g	µg/g	µg/g	µg/g	µg/g
BK41_1	0.26	1.19	0.40	0.45	0.77	13.75	209.63	4.71	0.34	3.15	0.28	2.66	0.03	0.09	0.36	0.12
BK41_2	0.31	1.48	0.45	0.76	1.01	16.47	252.93	5.90	0.39	3.14	0.32	3.06	0.04	0.09	0.52	0.11
BK41_3	0.26	1.25	0.40	0.58	0.86	14.39	223.23	5.15	0.29	3.33	0.07	2.53	0.04	0.10	0.47	0.14
BK41_5	0.30	1.46	0.48	0.76	0.92	15.18	235.48	5.67	0.39	3.99	0.27	2.57	0.04	0.05	0.53	0.16
BK41_6	0.28	1.42	0.41	0.62	0.84	14.04	221.18	5.18	0.34	3.19	0.30	2.42	0.04	0.08	0.33	0.16
BK41_7	0.30	1.35	0.45	0.74	0.96	15.52	244.88	5.77	0.36	2.93	0.28	2.93	0.04	0.12	0.35	0.08
BK41_8	0.32	1.57	0.47	0.76	1.02	15.74	248.01	5.89	0.31	5.06	0.13	2.75	0.05	0.08	0.50	0.18

Sample	<sup>7</sup> Li	<sup>11</sup> B	<sup>23</sup> Na	<sup>25</sup> Mg	<sup>27</sup> Al	<sup>31</sup> P	<sup>35</sup> Cl	<sup>39</sup> K	<sup>45</sup> Sc	<sup>49</sup> Ti	<sup>71</sup> Ga	<sup>72</sup> Ge	<sup>133</sup> Cs	<sup>88</sup> Sr	<sup>9</sup> Be	<sup>85</sup> Rb
	µg/g	µg/g	µg/g	µg/g	µg/g	µg/g	µg/g	µg/g	µg/g	µg/g	µg/g	µg/g	µg/g	µg/g	µg/g	µg/g
BK41_9	0.29	1.36	0.47	0.61	0.89	15.26	242.60	5.65	0.35	4.07	0.37	2.81	0.05	0.10	0.29	0.11
BK41_13	0.31	1.55	0.50	0.47	0.95	16.59	259.51	6.20	0.49	4.31	0.54	2.97	0.05	0.07	0.41	0.15
BK41_14	0.31	1.43	0.50	0.45	0.92	15.81	251.13	6.00	0.46	4.68	0.35	2.78	0.04	0.07	0.45	0.13
BK41_16	0.27	1.23	0.40	0.52	0.81	13.66	216.40	5.14	0.32	3.67	0.19	2.31	0.03	0.09	0.35	0.11
BK41_17	0.28	1.28	0.46	0.69	0.85	14.22	228.89	5.43	0.39	4.21	0.11	2.64	0.04	0.07	0.41	0.14
BK41_18	0.27	1.27	0.43	0.60	0.80	13.64	219.97	5.22	0.35	3.06	0.08	2.67	0.04	0.10	0.27	0.12
BK41_20	0.30	1.47	0.50	0.84	0.90	14.94	244.18	5.79	0.37	3.40	0.28	2.66	0.04	0.11	0.41	0.15
BKNV_1	0.26	1.22	0.38	0.53	0.80	12.96	212.93	5.02	0.32	3.51	0.35	2.76	0.04	0.10	0.26	0.15
BKNV_2	0.27	1.18	0.47	0.49	0.84	14.05	229.72	5.32	0.35	4.07	0.21	2.34	0.05	0.08	0.39	0.15
BKNV_3	0.34	1.54	0.59	0.72	0.96	16.77	270.25	6.23	0.46	4.63	0.26	2.98	0.04	0.05	0.14	0.14
BKNV_4	0.25	1.02	0.42	0.77	0.81	12.55	204.74	4.79	0.26	3.53	0.34	2.31	0.03	0.06	0.35	0.14
BKNV_5	0.35	1.78	0.60	0.77	1.18	18.32	295.88	7.17	0.52	4.16	0.41	3.10	0.04	0.11	0.52	0.17
BKNV_6	0.54	2.18	0.89	1.04	1.62	25.69	407.90	9.84	0.60	7.56	0.56	4.80	0.07	0.20	0.91	0.28
BKNV_9	0.44	1.83	0.67	1.16	1.43	23.45	311.25	8.55	0.60	6.24	0.47	4.53	0.07	0.16	0.24	0.22
BKNV_10	0.34	1.49	0.50	0.77	1.08	17.95	240.51	6.78	0.44	4.89	0.40	3.25	0.04	0.13	0.53	0.18
BKNV_11	0.26	1.22	0.42	0.67	0.81	13.91	192.74	5.39	0.33	2.76	0.32	2.74	0.05	0.10	0.48	0.13

Sample	<sup>7</sup> Li	<sup>11</sup> B	<sup>23</sup> Na	<sup>25</sup> Mg	<sup>27</sup> Al	<sup>31</sup> P	<sup>35</sup> Cl	<sup>39</sup> K	<sup>45</sup> Sc	<sup>49</sup> Ti	<sup>71</sup> Ga	<sup>72</sup> Ge	<sup>133</sup> Cs	<sup>88</sup> Sr	<sup>9</sup> Be	<sup>85</sup> Rb
	µg/g	µg/g	µg/g	µg/g	µg/g	µg/g	µg/g	µg/g	µg/g	µg/g	µg/g	µg/g	µg/g	µg/g	µg/g	µg/g
BKNV_13	0.27	1.26	0.42	0.65	0.84	14.18	191.62	5.41	0.34	3.08	0.20	2.68	0.03	0.07	0.34	0.11
BKNV_14	0.28	1.33	0.44	0.60	0.87	14.57	197.24	5.71	0.40	3.04	0.27	2.51	0.04	0.10	0.28	0.12
BKNV_15	0.40	1.80	0.63	0.77	1.32	20.33	274.17	7.97	0.51	5.82	0.40	3.69	0.05	0.11	0.48	0.18
BKNV_16	0.42	1.92	0.61	0.95	1.34	21.73	291.94	8.24	0.55	5.22	0.43	4.11	0.06	0.15	0.57	0.22
BKNV_17	0.29	1.43	0.47	0.77	0.98	15.62	207.54	5.95	0.37	2.74	0.37	2.95	0.04	0.09	0.42	0.13
BKNV_18	0.30	1.41	0.47	0.62	1.01	16.15	217.19	6.21	0.39	3.61	0.28	3.00	0.04	0.10	0.12	0.16
BKNV_19	0.32	1.51	0.52	0.77	1.07	16.32	222.05	6.40	0.38	4.21	0.33	3.00	0.05	0.06	0.30	0.10
BKNV_20	2.21	11.36	3.47	5.86	7.44	113.30	1516.46	43.82	2.74	31.63	3.07	20.09	0.28	0.84	1.88	0.99

**Table A.18.** LA-ICP-MS trace element limits of detection for samples from KVI, fraction 63-250 µm.

Sample	<sup>7</sup> Li	<sup>11</sup> B	<sup>23</sup> Na	<sup>25</sup> Mg	<sup>27</sup> Al	<sup>31</sup> P	<sup>35</sup> Cl	<sup>39</sup> K	<sup>45</sup> Sc	<sup>49</sup> Ti	<sup>71</sup> Ga	<sup>72</sup> Ge	<sup>133</sup> Cs	<sup>88</sup> Sr	<sup>9</sup> Be	<sup>85</sup> Rb
	µg/g	µg/g	µg/g	µg/g	µg/g	µg/g	µg/g	µg/g	µg/g	µg/g	µg/g	µg/g	µg/g	µg/g	µg/g	µg/g
DOB_2	0.20	2.15	0.31	0.37	0.60	7.96	157.45	4.26	0.30	1.70	0.18	1.62	0.03	0.03	0.22	0.09
DOB_4	0.17	1.91	0.27	0.39	0.52	7.21	147.18	3.74	0.29	1.55	0.13	1.42	0.03	0.04	0.13	0.05
DOB_5	0.20	2.18	0.30	0.42	0.61	8.30	174.32	4.39	0.33	1.69	0.16	1.67	0.03	0.06	0.07	0.07
DOB_7	0.19	2.04	0.32	0.29	0.61	7.88	169.80	4.04	0.28	1.61	0.14	1.67	0.03	0.05	0.22	0.04
DOB_8	0.24	2.58	0.41	0.41	0.68	9.42	208.45	5.03	0.39	1.93	0.22	1.87	0.03	0.06	0.27	0.08

Sample	<sup>7</sup> Li	<sup>11</sup> B	<sup>23</sup> Na	<sup>25</sup> Mg	<sup>27</sup> Al	<sup>31</sup> P	<sup>35</sup> Cl	<sup>39</sup> K	<sup>45</sup> Sc	<sup>49</sup> Ti	<sup>71</sup> Ga	<sup>72</sup> Ge	<sup>133</sup> Cs	<sup>88</sup> Sr	<sup>9</sup> Be	<sup>85</sup> Rb
	µg/g	µg/g	µg/g	µg/g	µg/g	µg/g	µg/g	µg/g	µg/g	µg/g	µg/g	µg/g	µg/g	µg/g	µg/g	µg/g
DOB_9	0.26	2.70	0.38	0.54	0.78	10.42	228.87	5.36	0.43	2.00	0.18	1.98	0.04	0.06	0.32	0.06
DOB_10	0.20	2.24	0.32	0.40	0.56	8.18	182.80	4.23	0.31	1.28	0.20	1.64	0.02	0.07	0.24	0.06
DOB_11	0.27	2.89	0.42	0.60	0.79	10.96	247.01	5.52	0.43	2.06	0.04	2.11	0.02	0.05	0.26	0.08
DOB_12	0.25	2.66	0.37	0.37	0.71	10.07	233.51	5.13	0.36	2.13	0.23	1.97	0.03	0.05	0.31	0.10
DOB_13	0.21	2.12	0.32	0.45	0.58	8.38	193.26	4.17	0.35	1.72	0.03	1.75	0.03	0.04	0.17	0.06
DOB_14	0.21	2.19	0.32	0.42	0.59	8.47	200.35	4.20	0.34	1.71	0.14	1.53	0.02	0.04	0.07	0.06
DOB_15	0.21	2.23	0.34	0.48	0.59	8.66	205.50	4.19	0.31	1.99	0.23	1.58	0.02	0.06	0.20	0.08
DOB_16	0.20	2.01	0.29	0.47	0.55	7.95	191.67	3.87	0.30	1.86	0.13	1.61	0.02	0.05	0.20	0.05
DOB_17	0.23	2.36	0.37	0.63	0.63	9.30	229.76	4.43	0.34	2.00	0.22	1.69	0.03	0.05	0.26	0.06
DOB_18	0.21	2.07	0.30	0.49	0.59	8.20	202.63	3.89	0.27	1.50	0.15	1.62	0.03	0.05	0.21	0.07
DOB_19	0.28	2.93	0.45	0.91	0.79	11.33	286.91	5.40	0.43	2.77	0.31	2.31	0.04	0.06	0.32	0.09
RAB1_1	0.37	3.81	0.64	1.14	1.08	15.41	385.33	7.08	0.53	3.08	0.27	3.02	0.05	0.09	0.64	0.15
RAB1_2	0.21	2.20	0.33	0.35	0.61	8.86	220.74	4.03	0.29	1.42	0.17	1.67	0.03	0.06	0.21	0.06
RAB1_3	0.20	2.01	0.29	0.49	0.58	8.32	211.17	3.82	0.29	1.77	0.16	1.57	0.02	0.05	0.16	0.08
RAB1_5	0.22	2.26	0.35	0.53	0.62	9.06	231.32	4.12	0.33	1.83	0.20	1.85	0.02	0.06	0.23	0.08
RAB1_6	0.21	2.12	0.35	0.36	0.60	8.85	224.77	4.04	0.30	1.47	0.14	1.53	0.03	0.06	0.28	0.09

Sample	<sup>7</sup> Li	<sup>11</sup> B	<sup>23</sup> Na	<sup>25</sup> Mg	<sup>27</sup> Al	<sup>31</sup> P	<sup>35</sup> Cl	<sup>39</sup> K	<sup>45</sup> Sc	<sup>49</sup> Ti	<sup>71</sup> Ga	<sup>72</sup> Ge	<sup>133</sup> Cs	<sup>88</sup> Sr	<sup>9</sup> Be	<sup>85</sup> Rb
	µg/g	µg/g	µg/g	µg/g	µg/g	µg/g	µg/g	µg/g	µg/g	µg/g	µg/g	µg/g	µg/g	µg/g	µg/g	µg/g
RAB1_7	0.26	2.39	0.39	0.30	0.66	10.22	258.34	4.74	0.30	2.40	0.26	2.08	0.03	0.08	0.39	0.07
RAB1_8	0.23	2.34	0.37	0.54	0.65	9.27	237.81	4.28	0.34	1.82	0.11	1.80	0.03	0.06	0.29	0.10
RAB1_9	0.37	3.56	0.58	0.96	0.98	14.38	367.56	6.65	0.49	2.53	0.33	2.98	0.04	0.09	0.43	0.08
RAB1_10	0.22	2.14	0.34	0.54	0.60	8.90	224.79	4.05	0.30	1.91	0.20	1.72	0.03	0.05	0.18	0.05
RAB1_11	0.22	2.06	0.33	0.40	0.56	8.50	217.18	3.93	0.29	1.97	0.04	1.77	0.02	0.05	0.22	0.07
RAB1_12	0.23	2.25	0.36	0.42	0.62	9.21	235.15	4.27	0.30	1.72	0.17	1.68	0.03	0.07	0.08	0.09
RAB1_13	0.21	2.02	0.34	0.47	0.58	8.51	218.30	3.94	0.28	1.71	0.10	1.69	0.03	0.05	0.32	0.06
RAB1_14	0.26	2.55	0.41	0.44	0.72	10.52	262.10	4.77	0.32	2.39	0.24	2.00	0.03	0.07	0.27	0.08
RAB1_16	0.40	3.97	0.66	0.82	1.12	16.38	411.95	7.52	0.58	3.46	0.33	3.31	0.05	0.08	0.67	0.16
RAB1_18	0.24	2.19	0.36	0.70	0.67	9.19	225.40	3.96	0.28	2.01	0.17	1.79	0.03	0.06	0.31	0.07
RAB1_19	0.26	2.44	0.37	0.53	0.73	10.07	248.53	4.43	0.33	1.80	0.05	2.15	0.03	0.08	0.36	0.11

**Table A.19.** LA-ICP-MS trace element errors for samples from JB, fraction 63-250  $\mu\text{m}$ .

Sample	$^7\text{Li}$	$^{11}\text{B}$	$^{23}\text{Na}$	$^{25}\text{Mg}$	$^{27}\text{Al}$	$^{31}\text{P}$	$^{35}\text{Cl}$	$^{39}\text{K}$	$^{45}\text{Sc}$	$^{49}\text{Ti}$	$^{71}\text{Ga}$	$^{72}\text{Ge}$	$^{133}\text{Cs}$	$^{88}\text{Sr}$	$^9\text{Be}$	$^{85}\text{Rb}$
	$\mu\text{g/g}$	$\mu\text{g/g}$	$\mu\text{g/g}$	$\mu\text{g/g}$	$\mu\text{g/g}$	$\mu\text{g/g}$	$\mu\text{g/g}$	$\mu\text{g/g}$	$\mu\text{g/g}$	$\mu\text{g/g}$	$\mu\text{g/g}$	$\mu\text{g/g}$	$\mu\text{g/g}$	$\mu\text{g/g}$	$\mu\text{g/g}$	$\mu\text{g/g}$
JB1_1	0.13		1.35	0.65	9.81	11.75	41.87	3.78	0.21	2.26				0.08		
JB1_2	0.09		1.09	0.36	6.33	7.81		3.36	0.20	1.46				0.10		
JB1_3	0.10		0.62		1.57	7.05		2.36	0.20	2.03		0.99		0.03		
JB1_4	0.09		1.33	0.38	3.62	8.20		3.04	0.19	3.09				0.06		
JB1_6	0.09		0.80	0.59	1.82	7.35		2.62	0.22	3.86				0.12		
JB1_8	0.68		1.11	0.55	12.92	9.07		3.49	0.17	1.84				0.08		0.06
JB1_9	0.18		0.28	0.43	2.90	6.78			0.18	3.76						
JB1_10	0.11		2.60	3.29	5.40	9.13		3.27	0.21					0.11		
JB1_11	0.50		0.43	0.51	2.64	8.91			0.17	4.60				0.06		
JB1_12	0.08		2.17	0.31	2.39	9.53		2.68	0.20	2.17				0.08		
JB1_13	0.10	0.40	0.42		1.55	7.21		2.43	0.20	1.57		0.96		0.08	0.12	
JB1_14	0.08		0.38		1.35	7.13			0.22	3.73						
JB1_15			0.25		0.47	9.81			0.25	1.59						
JB1_16	0.25	0.48	1.69	1.67	14.39	8.17		6.08	0.24	2.75				0.19		0.10
JB1_17	0.08		1.88		6.60	11.09		3.83	0.28					0.09		

Sample	<sup>7</sup> Li	<sup>11</sup> B	<sup>23</sup> Na	<sup>25</sup> Mg	<sup>27</sup> Al	<sup>31</sup> P	<sup>35</sup> Cl	<sup>39</sup> K	<sup>45</sup> Sc	<sup>49</sup> Ti	<sup>71</sup> Ga	<sup>72</sup> Ge	<sup>133</sup> Cs	<sup>88</sup> Sr	<sup>9</sup> Be	<sup>85</sup> Rb
	µg/g	µg/g	µg/g	µg/g	µg/g	µg/g	µg/g	µg/g	µg/g	µg/g	µg/g	µg/g	µg/g	µg/g	µg/g	µg/g
JB1_18	0.09		1.65	0.64	4.73	8.74		3.32	0.19	2.92			0.10			
JB1_20	2.44	0.53	9.89	44.24	63.84	16.44	81.44	11.55	0.30	10.12	0.21		0.02	0.37	0.11	
JB5_1			0.64	0.22	0.45	8.07		2.32	0.15	2.24			0.06			
JB5_2		0.46	0.62	0.31	0.67	7.40			0.19	1.17						
JB5_3	0.08	0.36	1.44	0.55	1.66	7.39		2.51	0.18	1.18			0.10			
JB5_4		0.51	1.30		1.58	9.40		2.75	0.20	2.51			0.05			
JB5_5	0.12	0.55	1.00	0.77	1.65	6.74			0.19	1.70						
JB5_6			0.34		0.54	9.61			0.20	15.75						
JB5_7			0.82		0.67	7.03			0.19	1.52		1.02		0.05		
JB5_10	0.27		0.91		6.77	8.47		2.62	0.20				0.06			
JB5_11	0.07	0.48	8.39	0.68	6.87	9.27		5.82	0.23	1.94			0.07	0.10	0.08	
JB5_12	0.16		1.33	0.62	6.31	12.50		4.07	0.25				0.12			
JB5_13	0.09		0.79	0.52	2.58	8.95		3.91	0.23	3.60						
JB5_14	0.06		1.73	0.52	2.41	8.78		2.90	0.20	1.21			0.10			
JB5_16	0.08		0.22		0.67	8.23		2.31	0.21	1.39						
JB5_17	0.12	0.43	13.52		2.54	8.55	78.01	2.43	0.18	3.51			0.03	0.06		

Sample	<sup>7</sup> Li	<sup>11</sup> B	<sup>23</sup> Na	<sup>25</sup> Mg	<sup>27</sup> Al	<sup>31</sup> P	<sup>35</sup> Cl	<sup>39</sup> K	<sup>45</sup> Sc	<sup>49</sup> Ti	<sup>71</sup> Ga	<sup>72</sup> Ge	<sup>133</sup> Cs	<sup>88</sup> Sr	<sup>9</sup> Be	<sup>85</sup> Rb
	μg/g	μg/g	μg/g	μg/g	μg/g	μg/g	μg/g	μg/g	μg/g	μg/g	μg/g	μg/g	μg/g	μg/g	μg/g	μg/g
JB5_18	0.15	0.61	0.93	0.49	4.74	10.49		5.08	0.19	4.00			0.11		0.17	
JB5_19			58.15	1.15	0.47	10.23	90.04	4.30	0.22			0.04	1.37		0.08	
JB5_20			1.58		0.98	8.33			0.19	2.11		0.97				
JB10_1	0.33	0.42	1.26	0.33	7.47	8.28		3.03	0.19		1.19		0.13		0.06	
JB10_2		0.60	0.47		1.97	12.78			0.21	2.36			0.06			
JB10_3	0.07	0.90	2.64	0.63	4.77	7.11		4.42	0.24		0.13		0.31		0.11	
JB10_4	0.10				1.54	10.08			0.22	2.46						
JB10_5	0.11	0.48	0.85	0.47	2.74	7.90		2.55	0.16	2.48			0.13			
JB10_8	0.20	0.43	1.87		3.08	9.45		2.82	0.18				0.17			
JB10_12	0.08		1.83	0.69	4.12	11.46		3.38	0.27				0.14			
JB10_16			0.22		0.49	8.37			0.19	1.44						
JB10_17	0.06		1.16	0.22	1.64	8.45		2.32	0.15	4.02		0.02	0.15		0.06	
JB17_3	0.07	0.58	1.72	0.95	5.31	8.08		3.52	0.20	2.69		1.02	0.04	0.09		
JB17_4	0.07	0.38	0.46	0.24	1.91	7.35			0.18	2.35						
JB17_5	0.09	0.39	2.57	1.38	2.07	6.55		2.05	0.16		1.04		0.19			
JB17_6	0.08		3.80	0.60	1.30	12.08		3.44	0.25	1.90		0.03	0.14			

Sample	<sup>7</sup> Li	<sup>11</sup> B	<sup>23</sup> Na	<sup>25</sup> Mg	<sup>27</sup> Al	<sup>31</sup> P	<sup>35</sup> Cl	<sup>39</sup> K	<sup>45</sup> Sc	<sup>49</sup> Ti	<sup>71</sup> Ga	<sup>72</sup> Ge	<sup>133</sup> Cs	<sup>88</sup> Sr	<sup>9</sup> Be	<sup>85</sup> Rb
	μg/g	μg/g	μg/g	μg/g	μg/g	μg/g	μg/g	μg/g	μg/g	μg/g	μg/g	μg/g	μg/g	μg/g	μg/g	μg/g
JB17_7	0.06	0.44	0.60		1.49	7.57		2.71	0.17	1.82		1.04				
JB17_8	0.10	0.69	0.29	10.66	2.65	13.20				3.74						
JB17_9	0.20	0.82	1.73	0.40	10.04	9.17		4.32	0.22	3.92				0.08		0.12
JB17_11	0.27		0.50		3.55	27.95			0.32	3.34						
JB17_12	0.22	0.57	1.76	0.70	10.05	7.37	76.05	4.34		2.05				0.11		0.07
JB17_17	0.07	0.40	1.29	0.48	4.62	9.79		3.06	0.23	2.24				0.07		
JB17_18	0.09		1.13		5.33	8.85		2.55	0.19	1.23		1.06		0.12		
JB17_19	0.10		0.24	0.38	2.79	9.56	70.36	2.50	0.18	3.01			0.01			
JB17_20	0.10		0.47		2.42	9.63		2.58	0.22	1.63			0.03			0.06
JB23_1	0.11		0.78	0.68	5.21	13.70	109.83	4.16		3.82				0.19		0.09
JB23_3	0.21		1.02	0.33	2.89	9.39		3.04	0.19	2.02				0.05		
JB23_6	0.12	0.58	1.44	0.38	10.48	8.76		2.83	0.20	3.13			0.05			0.06
JB23_7			0.63	1.29	2.84	10.92		3.46	0.27	3.10				0.07		
JB23_8			2.11		1.22	10.23			0.25					0.06		
JB23_9	0.25		1.79	0.64	11.47	8.70		2.96	0.22	2.69				0.11		
JB23_11	0.12	0.59	1.02	1.68	7.40	10.87		4.82	0.26	3.77				0.17		0.11

Sample	<sup>7</sup> Li	<sup>11</sup> B	<sup>23</sup> Na	<sup>25</sup> Mg	<sup>27</sup> Al	<sup>31</sup> P	<sup>35</sup> Cl	<sup>39</sup> K	<sup>45</sup> Sc	<sup>49</sup> Ti	<sup>71</sup> Ga	<sup>72</sup> Ge	<sup>133</sup> Cs	<sup>88</sup> Sr	<sup>9</sup> Be	<sup>85</sup> Rb
	µg/g	µg/g	µg/g	µg/g	µg/g	µg/g	µg/g	µg/g	µg/g	µg/g	µg/g	µg/g	µg/g	µg/g	µg/g	µg/g
JB23_13		0.64	12.24	0.57	0.52	9.53	123.53	3.48	0.20	5.33			0.23			
JB23_17	0.33		1.78	1.18	11.72	8.25		3.03	0.18	1.33			0.12			
JB23_18	0.20		0.97	0.36	5.00	9.45		2.57	0.22	2.82			0.08			
JB23_19	0.08	0.41	0.65	0.44	2.25	10.36		2.67	0.21	1.20			0.05			
JB26_1			0.85	0.45	0.98	11.18		3.08	0.20	1.66			0.07			
JB26_2	0.09		0.63	0.24	3.30	11.04		3.47	0.22	2.21		1.25		0.11		
JB26_3			1.19	0.79	3.01	19.14				6.15			0.14			
JB26_4	0.44		0.98	0.42	8.76	10.28			0.21	1.75			0.08			
JB26_5			1.90	0.24	1.81	9.00		3.44	0.24							
JB26_7			0.30		0.70	9.65			0.20	1.80			0.04			
JB26_8			0.71	0.30	2.04	9.70		3.19	0.22	2.25		1.37		0.06		
JB26_10	0.17		1.71	0.75	6.38	19.66		4.23	0.36	3.02			0.10			
JB26_11	0.25		1.22	2.16	22.75	8.93		7.81	0.21	3.34			0.16			
JB26_12	0.11		1.15	2.22	18.66	9.40		9.55	0.28	3.00			0.02	0.10	0.10	
JB26_13	0.07		0.81	8.54	1.56	8.99		2.67	0.23	3.10	0.06		0.07			
JB26_14	0.16	0.44	1.18	0.48	4.72	9.15		3.12	0.20			1.19		0.30	0.06	

Sample	<sup>7</sup> Li	<sup>11</sup> B	<sup>23</sup> Na	<sup>25</sup> Mg	<sup>27</sup> Al	<sup>31</sup> P	<sup>35</sup> Cl	<sup>39</sup> K	<sup>45</sup> Sc	<sup>49</sup> Ti	<sup>71</sup> Ga	<sup>72</sup> Ge	<sup>133</sup> Cs	<sup>88</sup> Sr	<sup>9</sup> Be	<sup>85</sup> Rb
	µg/g	µg/g	µg/g	µg/g	µg/g	µg/g	µg/g	µg/g	µg/g	µg/g	µg/g	µg/g	µg/g	µg/g	µg/g	µg/g
JB26_15			0.88		0.55	10.62			0.19	2.08			0.06			
JB26_16		0.43	1.44	0.67	1.86	7.47		2.61	0.20	2.22		0.02	0.13			
JB26_17	0.06		0.47		2.02	9.25			0.19	2.14		1.15		0.04		
JB26_18			0.78	5.91	1.82	10.01		2.91	0.18	1.91		1.05				
JB26_19	0.09	0.39	0.64	0.24	1.99	9.27		2.50	0.19				0.09			
JB26_20	0.07		0.42		1.59	7.82			0.19	2.65			0.03			

**Table A.20.** LA-ICP-MS trace element errors for samples from BK, fraction 63-250 µm.

Sample	<sup>7</sup> Li	<sup>11</sup> B	<sup>23</sup> Na	<sup>25</sup> Mg	<sup>27</sup> Al	<sup>31</sup> P	<sup>35</sup> Cl	<sup>39</sup> K	<sup>45</sup> Sc	<sup>49</sup> Ti	<sup>71</sup> Ga	<sup>72</sup> Ge	<sup>133</sup> Cs	<sup>88</sup> Sr	<sup>9</sup> Be	<sup>85</sup> Rb
	µg/g	µg/g	µg/g	µg/g	µg/g	µg/g	µg/g	µg/g	µg/g	µg/g	µg/g	µg/g	µg/g	µg/g	µg/g	µg/g
BK41_1	0.07	0.41	1.62		2.87	9.32	72.21	2.15	0.18	1.84			0.06			
BK41_2	0.10		0.59		1.66	10.86			0.22	2.43			0.05			
BK41_3	0.08		0.49		1.35	9.23			0.16	2.10			0.05			
BK41_5	0.11		0.28		2.29	9.05			0.20	1.55			0.04			
BK41_6			0.41		1.00	7.81			0.18	1.41			0.05			
BK41_7	0.07	0.42	3.24	1.50	11.66	9.98		5.19	0.21	1.57			0.20		0.06	
BK41_8	0.10		1.68		1.52	9.64			0.20	4.95						

Sample	<sup>7</sup> Li	<sup>11</sup> B	<sup>23</sup> Na	<sup>25</sup> Mg	<sup>27</sup> Al	<sup>31</sup> P	<sup>35</sup> Cl	<sup>39</sup> K	<sup>45</sup> Sc	<sup>49</sup> Ti	<sup>71</sup> Ga	<sup>72</sup> Ge	<sup>133</sup> Cs	<sup>88</sup> Sr	<sup>9</sup> Be	<sup>85</sup> Rb
	μg/g	μg/g	μg/g	μg/g	μg/g	μg/g	μg/g	μg/g	μg/g	μg/g	μg/g	μg/g	μg/g	μg/g	μg/g	μg/g
BK41_9	0.10	0.43	1.98	0.55	1.94	7.54		3.02	0.19	2.36			0.08		0.06	
BK41_13			1.08	0.28	2.85	13.33		3.04	0.24				0.06			
BK41_14	0.12		1.20	0.46	6.95	9.27		3.73	0.26	4.17			0.06		0.07	
BK41_16			0.37		1.44	13.41	68.41		0.17				0.05			
BK41_17	0.10	0.37	0.79		3.80	9.87		2.85		2.96		1.12	0.02	0.08	0.16	
BK41_18	0.34	0.62	1.41	6.60	9.27	10.83		2.74			0.11		0.10			
BK41_20	0.12	0.50	0.45	3.58	9.45	10.20		6.69	0.21	4.28			0.03		0.12	
BKNV_1			0.71	0.40	6.15	8.67		3.89	0.18	15.67			0.08			
BKNV_2			0.81	6.01	0.66	8.95			0.17	1.36		1.11		0.04		
BKNV_3			1.43		2.83	11.30		2.67	0.25	1.76			0.06			
BKNV_4	0.11	0.29	0.46	0.45	2.14	7.96		2.17	0.16	2.14		1.07		0.05		
BKNV_5			0.32		0.68	11.18				1.43						
BKNV_6	0.43		1.20		8.97	15.40		5.15	0.33				0.15			
BKNV_9			0.97	2.43	13.36	14.10		9.42	0.32	2.16			0.04	0.11	0.25	
BKNV_10			3.07	0.47	1.77	9.99		3.17		1.88			0.21			
BKNV_11	0.06		0.97		1.52	9.08			0.17	2.35			0.05			

Sample	<sup>7</sup> Li	<sup>11</sup> B	<sup>23</sup> Na	<sup>25</sup> Mg	<sup>27</sup> Al	<sup>31</sup> P	<sup>35</sup> Cl	<sup>39</sup> K	<sup>45</sup> Sc	<sup>49</sup> Ti	<sup>71</sup> Ga	<sup>72</sup> Ge	<sup>133</sup> Cs	<sup>88</sup> Sr	<sup>9</sup> Be	<sup>85</sup> Rb
	μg/g	μg/g	μg/g	μg/g	μg/g	μg/g	μg/g	μg/g	μg/g	μg/g	μg/g	μg/g	μg/g	μg/g	μg/g	μg/g
BKNV_13			0.28	0.65	0.79	8.53			0.17				0.04			
BKNV_14	0.11		0.40	0.36	2.15	9.54			0.21	3.16			0.05			
BKNV_15			0.92	1.22	7.83	13.64		5.81					0.07		0.11	
BKNV_16	0.24		0.72		5.10	12.91		3.70	0.29	2.14			0.08			
BKNV_17	0.27		1.57	10.23	11.62	8.74		3.28	0.20	1.43			0.12		0.07	
BKNV_18	0.07		0.52	0.42	1.97	11.99			0.21	2.99			0.05			
BKNV_19	0.09		1.32		4.21	11.12			0.23	2.99			0.05		0.06	
BKNV_20			3.40	15.91	22.89	49.32	438.29	21.19		21.45					0.59	

**Table A.21.** LA-ICP-MS trace element errors for samples from KVI, fraction 63-250 μm.

Sample	<sup>7</sup> Li	<sup>11</sup> B	<sup>23</sup> Na	<sup>25</sup> Mg	<sup>27</sup> Al	<sup>31</sup> P	<sup>35</sup> Cl	<sup>39</sup> K	<sup>45</sup> Sc	<sup>49</sup> Ti	<sup>71</sup> Ga	<sup>72</sup> Ge	<sup>133</sup> Cs	<sup>88</sup> Sr	<sup>9</sup> Be	<sup>85</sup> Rb
	μg/g	μg/g	μg/g	μg/g	μg/g	μg/g	μg/g	μg/g	μg/g	μg/g	μg/g	μg/g	μg/g	μg/g	μg/g	μg/g
DOB_2			0.77	0.65	2.37	6.47	48.24	2.27	0.18	11.20						
DOB_4	0.07	0.61	3.24	0.22	2.36	4.24		4.41	0.17	1.39			0.03	0.07	0.07	
DOB_5	0.06		0.31	2.82	5.31	5.68	57.46	5.67	0.17	3.45			0.03		0.04	
DOB_7	0.05	0.52	0.61	0.55	22.20	5.16	55.07	11.64	0.15	1.23	0.08		0.04		0.06	
DOB_8			0.24		0.41	5.88			0.23	0.69						

Sample	<sup>7</sup> Li	<sup>11</sup> B	<sup>23</sup> Na	<sup>25</sup> Mg	<sup>27</sup> Al	<sup>31</sup> P	<sup>35</sup> Cl	<sup>39</sup> K	<sup>45</sup> Sc	<sup>49</sup> Ti	<sup>71</sup> Ga	<sup>72</sup> Ge	<sup>133</sup> Cs	<sup>88</sup> Sr	<sup>9</sup> Be	<sup>85</sup> Rb
	μg/g	μg/g	μg/g	μg/g	μg/g	μg/g	μg/g	μg/g	μg/g	μg/g	μg/g	μg/g	μg/g	μg/g	μg/g	μg/g
DOB_9			0.40		2.40	7.09			0.22	2.56			0.04		0.03	
DOB_10	0.05	0.65	2.58	0.27	2.43	5.14		2.45	0.18	1.18			0.01	0.11		0.03
DOB_11	0.09		0.87	8.84	2.06	7.11		2.51	0.22	1.18	0.03		0.01	0.03		
DOB_12			1.93	2.83	3.76	5.56		2.80	0.17	0.90				0.26		
DOB_13			0.21	0.31	0.85	5.49			0.17	0.70	0.03					
DOB_14		0.63	8.38	0.59	1.12	4.73		2.01	0.18			0.66	0.02	0.21		
DOB_15	0.15	0.61	1.31	0.47	5.39	7.19		2.07	0.16	2.66			0.01	0.40		
DOB_16			0.14		0.30	6.69			0.17							
DOB_17			0.60	0.33	1.67	6.54		1.94	0.20			0.72		0.06		
DOB_18			0.19		0.39	4.86			0.18	0.90				0.03		
DOB_19			0.66	0.65	2.50	9.33			0.23			1.12		0.08		
RAB1_1			0.32		0.95	10.22	123.26			2.53				0.04		
RAB1_2			1.14	1.72	5.18	5.74		2.12	0.16	0.90				0.09		0.05
RAB1_3	0.05	0.68	5.05	0.31	5.59	5.28		5.70	0.15	2.25		0.77	0.02	0.12		0.08
RAB1_5	0.11	0.75	2.01	3.93	17.27	5.41		4.77	0.17	0.66			0.01	0.10		0.06
RAB1_6			0.30		0.32	5.35			0.16	0.58		0.79				

Sample	<sup>7</sup> Li	<sup>11</sup> B	<sup>23</sup> Na	<sup>25</sup> Mg	<sup>27</sup> Al	<sup>31</sup> P	<sup>35</sup> Cl	<sup>39</sup> K	<sup>45</sup> Sc	<sup>49</sup> Ti	<sup>71</sup> Ga	<sup>72</sup> Ge	<sup>133</sup> Cs	<sup>88</sup> Sr	<sup>9</sup> Be	<sup>85</sup> Rb
	μg/g	μg/g	μg/g	μg/g	μg/g	μg/g	μg/g	μg/g	μg/g	μg/g	μg/g	μg/g	μg/g	μg/g	μg/g	μg/g
RAB1_7	0.09	0.68	1.08	3.17	3.75	7.30		2.59	0.18	1.80			0.06		0.04	
RAB1_8	0.17		1.39	0.48	2.76	5.80		2.08	0.19	1.22			0.07			
RAB1_9	0.09		0.44		1.98	7.63			0.23				0.07			
RAB1_10	0.06		2.16		0.99	5.48			0.17	2.06			0.03	0.05	0.02	
RAB1_11	0.34		2.13	0.50	9.51	5.58		2.37	0.17	2.37			0.02	0.13		
RAB1_12	0.72	0.65	2.09	0.29	30.85	5.84		2.82	0.16	0.68		0.84	0.02	0.40	0.05	0.07
RAB1_13	0.09	0.65	0.71	0.30	2.03	4.77		1.93	0.17	1.75			0.05			
RAB1_14	0.11		0.53		2.14	6.07			0.18				0.06			
RAB1_16			0.55	0.73	4.44	10.68		3.34	0.30	100.98			0.05			
RAB1_18	0.05		0.37		0.98	5.88		1.91	0.15				0.05			
RAB1_19	0.18		1.95	0.58	4.83	6.75		2.00	0.20	1.21	0.05		0.11			

## REFERENCES

- Allan M. M., Yardley W. D. B., (2007) – Tracking meteoric infiltration into a magmatic-hydrothermal system: A cathodoluminescence, oxygen isotope and trace element study of quartz from Mt. Leyshon, Australia. *Chemical Geology* 240: 343–360
- Arrowsmith P., (1987) – Laser ablation of solids for elemental analysis by inductively coupled plasma mass spectrometry. *Analytical Chemistry* 59: 1437-1444
- Audétat A., Garbe-Schönberg D., Kronz A., Pettke T., Rusk B., Donovan J. J., Lowers H. A., (2015) – Characterisation of a natural quartz crystal as a reference material for microanalytical determination of Ti, Al, Li, Fe, Mn, Ga and Ge. *Geostandards and Geoanalytical Research* 39: 171–184
- Augustsson C., Reker A., (2012) – Cathodoluminescence spectra of quartz as provenance indicators revisited. *Journal of Sedimentary Research* 82: 559-570
- Babić L., Hernitz Kučenjak M., Čorić S., Zupanić J., (2007) – The Middle Eocene age of the supposed Late Oligocene sediments in the flysch of the Pazin basin (Istria, Outer Dinarides). *Natura Croatica* 16: 83-103
- Barbosa L. D., Sussolini A., (2019) – Recent advances in LA-ICP-MS for biomedical applications. *Biomedical Spectroscopy and Imaging* 8: 47-54
- Bell D. R., Thinger P. D., Rossman G. R., (1995) – Quantitative analysis of trace OH in garnet and pyroxene. *American Mineralogist* 80: 465-474
- Bell D. R., Rossman G. R., Maldener J., Endisch D., Rauch F., (2003) – Hydroxide in olivine: a quantitative determination of possible amount and calibration of the IR spectrum. *Journal of Geophysical Research* 108: 2105-2113
- Belousova E., Griffin W., O'Reilly S. Y., Fisher N., (2002) – Igneous zircon: trace element composition as an indicator of source rock type. *Contributions to Mineralogy and Petrology* 143: 602–622.
- Benac Č., Juračić M., Matičec D., Ružić I., Pikelj K., (2013) – Fluviokarst and classical karst: Examples from the Dinarics (Krk Island, Northern Adriatic, Croatia). *Geomorphology* 184: 64-73
- Beran A., Libowitzky E., (1999) – IR spectroscopy and hydrogen bonding in minerals. In Wright K., Catlow C. R. A.: *Microscopic properties and processes in minerals / NATO Science Series C* 543: 493-508
- Bernardi F., Skogby H., Lenaz D., (2022) – OH-defects in detrital quartz grains from the Julian Basin (NE Italy and Slovenia): a Fourier Transform Infrared study. *Geosciences* 12: 90

Bernet M., Bassett K., (2005) – Provenance analysis by single-quartz-grain SEM-CL/optical microscopy. *Journal of Sedimentary Research* 45: 873-882

Bertolla A., (1996-97) – Litologie arenacee della successione flyschoide del Bacino Giulio: significato della cromite e dei parametri petrochimici. *Thesis, Università degli Studi di Trieste, academic year 1996-1997*

Boggs S., Krinsley D. H., (2006) – Application of cathodoluminescence imaging to the study of sedimentary rocks. *Cambridge University Press*, p. 165

Breiter K., Ďurišová J., Dosbaba M., (2017) – Quartz chemistry - A step to understanding magmatic-hydrothermal processes in ore-bearing granites: Cínovec/Zinnwald Sn-W-Li deposit, Central Europe. *Ore Geology Reviews* 90: 25–35

Breiter K., Badanina E., Ďurišová J., Dosbaba M., Syritso L., (2019) – Chemistry of quartz - A new insight into the origin of the Orlovka Ta-Li deposit, Eastern Transbaikalia Russia. *Lithos* 348-349

Breiter K., Ďurišová J., Dosbaba M., (2020) – Chemical signature of quartz from S- and A-type rare-metal granites – A summary. *Ore Geology Reviews* 125: 103674

Channell J. E. T., Horvath F., (1976) – The African/Adriatic promontory as a paleogeographic premise for alpine orogeny and plate movements in the Carpatho-Balkan region. *Tectonophysics* 35: 71-101

Channell J. E. T., Kozur H. W., (1997) – How many oceans? Meliata, Vardar, and Pindos oceans in Mesozoic Alpine paleogeography. *Geology* 25: 183-186

Cigna E., (1996-97) – Litologie arenacee della successione del flysch di Clauzetto (Prealpi Carniche) e del flysch del Brkini (Slovenia Occidentale): significato della cromite e dei parametri petrochimici. *Thesis, Università degli Studi di Trieste, academic year 1996-1997*

Csontos L., Vörös A., (2004) – Mesozoic plate tectonic reconstruction of the Carpathian region. *Paleogeography, Paleoclimatology, Paleoecology* 210: 1-56

De Min A., Rosset A., Tunis G., Kocmann C., Tosone A., Lenaz D., (2007) – Igneous rock clasts from the Maastrichtian Bovec flysch (Slovenia): petrology and geodynamic aspects. *Geologica Carpathica* 58: 169-179

De Min A., Princivalle F., Lenaz D., (2014) – Geochemistry of the Late Mesozoic – Early Cenozoic turbidites from the NE part of Adria microplate. *Periodico di Mineralogia* 83: 141-158

Doglioni C., Flores G., (1997) – An introduction to the Italian Geology. *LAMISCO, Potenza*

Ehrlich K., Vers E., Kirs J., Soesoo A., (2012) – Using a titanium-in-quartz geothermometer for crystallization temperature estimation of the Palaeoproterozoic Suursaari quartz porphyry. *Estonia Journal of Earth Sciences* 61: 195

Feng Y., Zhang Y., Xie Y., Shao Y., Tan H., Li H., Lai C., (2020) – Ore-forming mechanism and physicochemical evolution of Gutaishan Au deposit, South China: perspective from quartz geochemistry and fluid inclusions. *Ore Geology Reviews* 119: 103382

Garlatti G., (2022-23) – Le tormaline detritiche del Bacino Giulio e del Bacino del Brkini: possibili provenienze. *Master thesis, Università degli Studi di Trieste, academic year 2022-2023*

Girard G., Stix J., (2010) – Rapid extraction of discrete magma batches from a large differentiating magma chamber: The Central Plateau Member rhyolites, Yellowstone Caldera, Wyoming. *Contributions to Mineralogy and Petrology* 160: 441–465

Gray A. L., (1985) – Solid sample introduction by laser ablation for inductively coupled plasma source mass spectrometry. *Analyst* 110: 551-556

Grimes C. B., Wooden J. L., Cheadle M. J., John B. E., (2015) – “Fingerprinting” tectono-magmatic provenance using trace elements in igneous zircon. *Contributions to Mineralogy and Petrology* 158: 757–783

Gregorič M., Caffau M., Lenaz D., De Min A., (1998) – Late Maastrichtian – Paleocene unaltered glassy microspherules at Padriciano (Trieste Karst, NE Italy): a preliminary report. *Razprave SAZU, Razred IV (Dissertation Academia Scientiarum et Artium Slovenica. Classis IV: Historia Naturalis)* 39: 211-233

Götze T., Pettke T., Ramseyer K., Koch-Müller M., Mullis J., (2011) – Cathodoluminescence properties and trace element signature of hydrothermal quartz: a fingerprint of growth dynamics. *American Mineralogist* 96: 802–813

Götze J., (2009) – Chemistry, textures and physical properties of quartz—Geological interpretation and technical application. *Mineralogical Magazine* 73: 645–671

Götze J., (2012) – Application of cathodoluminescence microscopy and spectroscopy in geosciences. *Microscopy and Microanalysis* 18: 1270-1284

Götze J., Kempe U., (2009) – Physical principles of cathodoluminescence and its application to geosciences. In Gucsik A. (Ed.): *Cathodoluminescence and its application in the Planetary Sciences*, pp. 1-22

Götze J., Plötze M., (1997) – Investigation of trace-element distribution in detrital quartz by Electron Paramagnetic Resonance (EPR). *European Journal of Mineralogy* 9: 529-538

Götze J., Zimmerle W., (2000) – Quartz and silica as guide to provenance in sediments and sedimentary rocks. *Contributions to Sedimentary Geology* 21: 1-91

Götze J., Plötze M., Graupner T., Hallbauer D. K., Bray C. J., (2004) – Trace elements incorporation into quartz: a combined study by ICP-MS, electron spin resonance, cathodoluminescence, capillary ion analysis, and gas chromatography. *Geochimica et Cosmochimica Acta* 68: 3741-3759

Griffiths I. P., de Haseth J., (1986) – Fourier Transform Infrared Spectrometry. *Wiley*, New York

Guillong M., Meier D. K., Allan M. M., Heinrich C. A., Yardley B. W. D., (2008) – SILLS: A Matlab-Based Program for the Reduction of Laser Ablation ICP–MS Data of Homogeneous Materials and Inclusions. *Mineralogical Association of Canada Short Course, Vancouver, B.C.* pp. 328–333

Hong W., Cooke D. R., Zhang L., Fox N., Thompson J., (2019) – Cathodoluminescence features, trace elements, and oxygen isotopes of quartz in unidirectional solidification textures from the Sn-mineralized Heemskirk Granite, western Tasmania. *American Mineralogist* 104: 100–117

Hooker J. N., Laubach S. E., (2007) – The geologic history of quartz grains, as revealed by color SEM-CL. *Gulf Coast Association of Geological Societies Transactions* 57: 375-386

Huang R., Audétat A., (2012) – The titanium-in-quartz (TitaniQ) thermobarometer: A critical examination and re-calibration. *Geochimica et Cosmochimica Acta* 84: 75–89

Jacamon F., Larsen R. B., (2009) – Trace element evolution of quartz in the charnockitic Kleivan granite, SW-Norway: the Ge/Ti ratio of quartz as an index of igneous differentiation. *Lithos* 107: 281-291

Jackson S. E., Longerich H. P., Dunning G. R., Fryer B. J., (1992) – The application of laser-ablation microprobe – inductively coupled plasma – mass spectrometry (LAM-ICP-MS) to in situ trace-element determinations in minerals. *The Canadian Mineralogist* 30: 1049-1064

Jaeger D., Stalder R., Masago H., Strasser M., (2019) – OH defects in quartz as a provenance tool: Application to fluvial and deep marine sediments from SW Japan. *Sedimentary Geology* 338: 66-80

Jochum K. P., Weis U., Stoll B., Kuzmin D., Yang Q., Raczek I., Jacob D. E., Stracke A., Birbaum K., Frick D. A., Günther D., Enzweiler J., (2011) – Determination of reference values for NIST SRM 610–617 glasses following ISO guidelines. *Geostandards and Geoanalytical Research* 35: 397–429

Jollands M. C., Blanchard M., Balan E., (2020) – Structure and theoretical infrared spectra of OH defects in quartz. *European Journal of Mineralogy* 32(3): 311-323

Jurkovsek B., Toman M., Ogorelec B., Sribar L., Drobne K., Poljak M., Sribar L., (1996) – Formacijska geoloska karta juznega dela Trzasko-Komenske Planote 1:50000 (Geological map of the southern part of the Trieste-Komen Plateau 1:50000). *Institu za geologijo, geotehniko in geofiziko* 143 pp., Ljubljana

Kamenetsky V., Crawford A. J., Meffre S., (2001) – Factors controlling chemistry of magmatic spinel: an empirical study of associated olivine, Cr-spinel and melt inclusions from primitive rocks. *Journal of Petrology* 42: 655-671

- Kats A., (1962) – Hydrogen in alpha quartz. *Philips Research Reports* 17: 133-279
- Koch-Müller M., Matsyuk S. S., Rhede D., Wirth R., Khisina N., (2006) – Hydroxyl in mantle olivine xenocrysts from the Udachnaya kimberlite pipe. *Physics and Chemistry of Minerals* 33: 276-287
- Kostov R. I., Bershov L. V., (1987) – Systematics of paramagnetic electron-hole centres in natural quartz (in Russ.). *Izvestiya Akademii nauk SSSR, Seria geologija* 7, 80–87
- Landtwing T., Pettke M., (2005) – Relationships between SEM-cathodoluminescence response and trace element composition of hydrothermal vein quartz. *American Mineralogist* 90: 122–131
- Larsen R. B., Polv   M., Juve G., (2000) – Granite pegmatite quartz from Evje-Iveland: trace element chemistry and implications for the formation of high-purity quartz. *NGU Bulletin* 436: 57
- Larsen R. B., Henderson I., Ihlen P. M., Jacamon F., (2004) – Distribution and petrogenetic behaviour of trace elements in granitic pegmatite quartz from South Norway. *Contributions to Mineralogy and Petrology* 147: 615–628
- Lawrence S. R., Tari-Kova  i   V., Gjuki   B., (1995) – Geological evolution model of the Dinarides. *Nafta* 46: 103-113
- Lenaz D., (2008) – Detrital pyroxenes in the Eocene flysch of the Istrian Basin (Slovenia, Croatia). *Geologica Acta Vol 6 N° 3*: 259-266
- Lenaz D., Princivalle F., (1996) – Crystal chemistry of detrital chromites in sandstones from Trieste (NE Italy). *Neues Jahrbuch f  r Mineralogie Abhandlungen* 429-434
- Lenaz D., Princivalle F., (2002) – Detrital high pressure – low temperature minerals in Lower Eocene deep-sea turbidites of the Julian Alps (NE Italy). *Periodico di Mineralogia* 71: 127-135
- Lenaz D., Princivalle F., (2005) – The crystal chemistry of detrital chromian spinel from the Southeastern Alps and Outer Dinarides: the discrimination of supplies from areas of similar tectonic setting? *The Canadian Mineralogist* 43: 1305-1314
- Lenaz D., Kamenetsky V. S., Crawford A. J., Princivalle F., (2000) – Melt inclusions in detrital spinel from SE Alps (Italy-Slovenia): a new approach to provenance studies of sedimentary basins. *Contributions to Mineralogy and Petrology* 139: 748-758
- Lenaz D., Alberti A., Tunis G., Princivalle F., (2001) – A heavy mineral association and its paleogeographic implications in the Eocene Brkini flysch basin (Slovenia). *Geologica Carpathica* 52: 239-245
- Lenaz D., Kamenetsky V. S., Princivalle F., (2003) – Cr-spinel supply in the Brkini, Istrian and Krk Island flysch basins (Slovenia, Italy, and Croatia). *Geological Magazine* 140: 335-342

Lenaz D., Mazzoli C., Velicogna M., Princivalle F., (2018) – Trace and Rare Earth Elements chemistry of detrital garnets in the SE Alps and Outer Dinarides flysch basins: An important tool to better define the source areas of sandstones. *Marine and Petroleum Geology* 98: 653-661

Li J., Hu R., Xiao J., Zuo Y., Yan J., Oyebamiji A., (2020) – Genesis of gold and antimony deposits in the Youjiang metallogenic province, SW China: evidence from in situ oxygen isotopic and trace element compositions of quartz. *Ore Geology Reviews* 116: 103257

Libowitzky E., Beran A., (2004) – IR characterisation of hydrous species in minerals. *EMU Notes in Mineralogy* 6: 227-279

Libowitzky E., Rossman G., (1997) – An IR absorption calibration for water in minerals. *American Mineralogist* 82: 1111-1115

Lukeneder A., (2011) – The Biancone and Rosso Ammonitico facies of the Northern Trento Plateau (Dolomites, Southern Alps, Italy). *Annales des naturhistorischen Museum in Wien Serie A*-113

Magaš D., (2000) – Contribution to the knowledge of the geographical characteristics of the Pag Island. *Geoadria* 5: 5- 48

Magdalenić Z., (1972) – Sedimentology of Central Istra Flysch deposits. *Acta Geologica Zagreb* 7: 71-100 (in Croatian)

Maldener J., Hösch A., Langer K., Rauch F., (2003) – Hydrogen in some natural garnets studied by nuclear reaction analysis and vibrational spectroscopy. *Physics and Chemistry of Minerals* 30: 337-344

Mamužić P., Milan A., (1973) – Osnovna geološka karta SFRJ 1:100,000, Tumač za list Rab L33–144. *Instituta za Geološka Istraživanja Zagreb, Savezni Geološki Zavod, Belgrade*, pp 5-39

Mange M. A., Morton A. C., (2007) – Geochemistry of heavy minerals. In Mange M. A., Wright D. T.: *Heavy Minerals in Use, vol 58. Developments in Sedimentology* pp. 345-391

Mao W., Rusk B., Yang F., Zhang M., (2017) – Physical and chemical evolution of the dabaoshan porphyry Mo deposit, South China: Insights from fluid inclusions, cathodoluminescence, and trace elements in quartz. *Economic Geology* 112: 889–918

Marfunin A. S., (1995) – Systematics of the methods of investigation of minerals: logic of development. In Marfunin A. S.: *Methods and instrumentations: results and recent developments, vol 2. Advanced Mineralogy* pp. 1-13

Marinčić S., Šparica M., Tunis G., Uchman A., (1996) – The Eocene flysch deposits of the Istrian peninsula in Croatia and Slovenia: regional, stratigraphic, sedimentological and ichnological analyses. *Annales – Annals for Istrian and Mediterranean Studies* 9: 139-156

Marjanac T., Marjanac L., (1991) – Shallow-marine clastic Paleogene on the Island of Rab (northern Adriatic). *Dolomieu Conference on Carbonate Platforms and Dolomitization*, Ortisei

Marjanac T., Marjanac L., (2007) – Sequence stratigraphy of Eocene incised valley clastics and associated sediments, Island of Rab, northern Adriatic Sea, Croatia. *Facies* 53: 493–508

Matter A., Ramsayer K., (1985) – Cathodoluminescence microscopy as a tool for provenance studies of sandstones. In Zuffa G. G. (Ed.): *Provenance of arenites: NATO, ASI Series C, vol 148* pp. 191–211

Maydagán L., Franchini M., Rusk B., Lentz D. R., Mcfarlane C., Impiccini A., Rios F. J., Rey R., (2015) – Porphyry to epithermal transition in the Altar Cu-(Au-Mo) Deposit, Argentina, studied by cathodoluminescence, LA-ICP-MS, and fluid inclusion analysis. *Economic Geology* 110: 889–923

Miklavič B., Rožič B., (2008) – The onset of Maastrichtian basinal sedimentation on Mt. Matajur, NW Slovenia. *Materials and Geoenvironment* 55: 199–214

Milliken K. L., (1994) – Cathodoluminescence textures and the origin of quartz silt in Oligocene mudrocks south Texas. *Journal of Sedimentary Research* 64: 567–571

Mindszenty A., D'Argenio B., Aiello G., (1995) – Lithospheric bulges recorded by regional unconformities. The case of Mesozoic-Tertiary Apulia. *Tectonophysics* 252: 137–161.

Moenke-Blackenburg L., Gäckle M., Günther D., Kammel J., (1990) – Process of laser ablation and vapour transport to ICP. *Royal Society of Chemistry* 85: 1–17

Monnier L., Lach P., Salvi S., Melleton J., Bailly L., Béziat D., Monnier Y., Gouy S., (2018) – Quartz trace-element composition by LA-ICP-MS as proxy for granite differentiation hydrothermal episodes, and related mineralization: the Beauvoir granite (Echassières district), France. *Lithos* 320: 355–377

Monnier L., Salvi S., Jourdan V., Sall S., Bailly L., Melleton J., Béziat D., (2020) – Contrasting fluid behavior during two styles of greisen alteration leading to distinct wolframite mineralizations: the Echassières district (Massif Central, France). *Ore Geology Reviews* 103648

Müller A., Koch-Müller M., (2009) – Hydrogen speciation and trace elements contents of igneous, hydrothermal and metamorphic quartz from Norway. *Mineralogical Magazine* 73: 569–583

Müller A., van den Kerkhof A. M., Behr H. J., Kronz A., Koch-Müller M., (2010) – The evolution of late-Hercynian granites and rhyolites documented by quartz—A review. *Earth and Environmental Science Transactions of The Royal Society of Edinburgh* 100: 185–204

Müller A., Ihlen P. M., Snook B., Larsen R. B., Flem B., Bingen B., Williamson B. J., (2015) – The chemistry of quartz in granitic pegmatites of southern Norway: petrogenetic and economic implications. *Economic Geology* 110: 1737-1757

Müller A., Herklotz G., Giegling H., (2018) – Chemistry of quartz related to the Zinnwald/Cínovec Sn-W-Li greisen-type deposit, Eastern Erzgebirge, Germany. *Journal of Geochemical Exploration* 190: 357-373

Müller A., Keyser W., Simmons W. B., Webber K., Wise M., Beurlen H., Garate-Olave I., Roda-Robles E., Galliski M. A., (2021) – Quartz chemistry of granitic pegmatites: Implications for classification, genesis and exploration. *Chemical Geology* 584: 120507

Ogata K., Pogačnik Ž., Pini G. A., Festa A., Camerlenghi A., Rebesco M., (2014) – The carbonate mass transport deposits of the Paleogene Friuli Basin (Italy/Slovenia): Internal anatomy and inferred genetic processes. *Marine Geology* 356: 88-110

Ogata K., Pogačnik Ž., Tunis G., Pini G. A., Festa A., Senger K., (2019) – A geophysical-geochemical approach to the study of the Paleogene Julian-Slovenian Basin “Megabeds” (Southern Alps-Northwestern Dinarides, Italy/Slovenia). *Geosciences* 9 article 155

Ogorelec B., Sribar L., Buser S., (1976) – On lithology and biostratigraphy of Volce Limestone. *Geologija* 19: 126-151

Orehek S., (1972) – The Eocene flysch of Pivška kotlina and Brkini. 7. Kongres Geolog. SFRJ, Predavanja 252-270 (in Slovenian)

Orehek S., (1991) – Palaeotransport of SW Slovenian Flysch. *Field Trip Guidebook IGCP Project 286 – Early Paleogene Benthos, 2<sup>nd</sup> Meeting Postojna*, 27-31

Ostapenko G. T., Gamarnik M. Y., Gorogotskaya L. I., Kuznetsov G. V., Tarashchan A. N., Timoshkova L. P., (1987) – Isomorphism of titanium substitution for silicon in quartz: Experimental data. *Mineral Zhurnal* 9: 30–40

Paterson M. S., (1982) – The determination of hydroxyl by infrared absorption in quartz, silicate glasses and similar material. *Bulletin de Minéralogie (Paris)* 105: 20-29

Pavlovec R., Knez M., Drobne K., Pavsic J., (1991) – Profiles: Košana, Sv. Trojica and Leskovec; the disintegration of the carbonate platform. *Field Trip Guidebook. IGCP Project 286 – Early Paleogene Benthos, 2<sup>nd</sup> Meeting Postojna*, 69-72

Peh Z., Kovačević Galović E. K., (2014) – Geochemistry of Istrian Lower Palaeogene bauxites – Is it relevant to the extent of subaerial exposure during Cretaceous time? *Ore Geology Reviews* 63: 296-306

Perny B., Eberhardt P., Ramsayer K., Mullis J., Pankrath R., (1992) – Microdistribution of Al, Li, and Na in alpha quartz: possible causes and correlation with short-lived cathodoluminescence. *American Mineralogist* 77: 534-544

Peterková T., Dolejš D., (2019) – Magmatic-hydrothermal transition of Mo-W-mineralized granite-pegmatite-greisen system recorded by trace elements in quartz: Krupka district, Eastern Krušné hory/Erzgebirge. *Chemical Geology* 523: 179–202

Potrafke A., Breiter K., Ludwig T., Neuser R. D., Stalder R., (2020) – Variations of OH defects and chemical impurities in natural quartz within igneous bodies. *Physics and Chemistry of Minerals* 47: 24

Ramseyer K., Mullis J., (1990) – Factors influencing short-lived blue cathodoluminescence of alpha-quartz. *American Mineralogist* 75: 791–800

Ramsayer K., Mullis J., (2000) – Geologic application of cathodoluminescence of silicates. In Pagel M., Barbin V., Blanc P., Ohnenstetter D. (Eds): *Cathodoluminescence in Geosciences* pp. 177-191

Ramseyer K., Baumann J., Matter A., Mullis J. (1988) – Cathodoluminescence colours of alpha-quartz. *Mineralogical Magazine* 52: 669–677

Robertson A. H. F., Karamata S., (1994) – The role of subduction-accretion processes in the tectonic evolution of the Mesozoic Tethys in Serbia. *Tectonophysics* 234: 73-94

Rossmann G. R., (2006) – Analytical methods for measuring water in nominally anhydrous minerals. In Keppler H., Smyth J. R.: Water in nominally anhydrous minerals. *Reviews in Mineralogy and Geochemistry*, Mineralogical Society of America 62: 1-28

Rottier B., Casanova V., (2020) – Trace element composition of quartz from porphyry systems: a tracer of the mineralizing fluid evolution. *Mineralium Deposita* 56: 843-862

Rusk B., (2012) – Cathodoluminescent textures and trace elements in hydrothermal quartz. In Götze J., Möckel R. (Eds.) *Quartz: Deposits, Mineralogy and Analytics*. Springer: Berlin/Heidelberg, Germany, pp. 307–329

Rusk B., Koenig A., Lowers H., (2011) – Visualizing trace element distribution in quartz using cathodoluminescence, electron microprobe, and laser ablation-inductively coupled plasma-mass spectrometry. *American Mineralogist* 96: 703–708

Sales de Oliveira C. E., Pe-Piper G., Piper D. J. W., Zhang Y., Corney R., (2017) – Integrated methodology for determining provenance of detrital quartz using optical petrographic microscopy and cathodoluminescence (CL) properties. *Marine and Petroleum Geology* 88: 41-53

Sawatzky C. C., Pe-Piper G., (2012) – Provenance identification of detrital quartz using hot-cathode cathodoluminescence: an atlas of source rocks. *Geological Survey of Canada, open file* 7894 p. 507

Schneider P., Balen D., (2020) – High-temperature acid magmatic rocks from the Late Cretaceous suture zone between European plate and Adria microplate (Croatia). *EGU General Assembly* 2020-10088

Schrön W., Baumann L., Rank K., (1982) – Zur Charakterisierung von Quarzgenerationen in den postmagmatogen Erzformationen des Erzgebirges. *Zeitschrift für Geologische Wissenschaften* 10: 1499-1521

Schrön W., Schmädicke E., Thomas R., Schmidt, W., (1988) – Geochemische Untersuchungen an Pegmatitquarzen. *Zeitschrift für Geologische Wissenschaften* 16: 229-244.

Shah S. A., Shao Y., Zhang Y., Zhao H., Zhao L., (2022) – Texture and trace element geochemistry of quartz: a review. *Minerals* 12: 1042

Spahić D., Gaudenyi T., (2022) – On the Sava Suture zone: post-Neotethyan oblique subduction and the origin of the Late Cretaceous mini-magma pools. *Cretaceous Research* 131: 105062

Stalder R., (2014) – OH-defects content in detrital quartz grains as an archive for crystallisation conditions. *Sedimentary Geology* 307: 1-6

Stalder R., Konzett J., (2012) – OH defects in quartz in the system quartz-albite-water and granite-water between 5 and 25 kbar. *Physics and Chemistry of Minerals* 39: 817-827

Stalder R., Neuser R. D., (2013) – OH-defects in detrital quartz grains: Potential for application as tool for provenance analysis ad overview over crustal average. *Sedimentary Geology* 294: 118-126

Stalder R., Potrafke A., Billström K., Skogby H., Meinhold G., Gögele C., Berberich T., (2017). – OH defects in quartz as monitor for igneous, metamorphic, and sedimentary processes. *American Mineralogist* 102: 1832-1842

Stalder R., von Eynatten H., Costamoling J., Potrafke. A., Dunkl I., Meinhold G., (2019) – OH in detrital quartz grains as tool for provenance analysis: Case studies on various setting from Cambrian to Recent. *Sedimentary Geology* 389: 121-126

Sun G., Zhou J. X., Luo K., Xiang Z. Z., Bao Z. A., Sun T., (2020) – New insights into the hydrothermal evolution of skarn deposits: a case study of the Dongzhongla Pb-Zn deposit in Tibet, SW China. *Journal of Asian Earth Sciences* 191: 104215

Tanner D., Henley R. W., Mavrogenes J. A., Holden P., (2013) – Combining in situ isotopic, trace element and textural analyses of quartz from four magmatic-hydrothermal ore deposits. *Contributions to Mineralogy and Petrology* 166: 1119–1142

Thomas S. M., Koch-Müller M., Reichart P., Rhede D., Thomas R., Wirth R., Matsyuk S., (2009). IR calibrations for water determination in olivine, r-GeO<sub>2</sub>, and SiO<sub>2</sub> polymorphs. *Physics and Chemistry of Minerals* 36: 489-509

Thomas J. B., Watson E. B., Spear F. S., Shemella P. T., Nayak S. K., Lanzirotti A., (2010) – TitaniQ under pressure: The effect of pressure and temperature on the solubility of Ti in quartz. *Contributions to Mineralogy and Petrology* 160: 743–759

Tunis G., Pirini Radizzani C., (1987) – Flyschoid deposits of Goriska Brda (Collio) between Soča (Isonzo) River and Idrija (Iudrio) River – facies and paleoenvironments. *Geologija* 30: 123-148

Tunis G., Uchmann A., (1996) – Trace fossils and facies changes in Cretaceous-Eocene flysch deposits of the Julian Prealps (Italy and Slovenia): Consequences of regional and world-wide changes. *Ichnos* 4: 169-190

Tunis G., Venturini S., (1984) – Stratigrafia e sedimentologia del flysch Maastrichtiano-Paleocenico del Friuli orientale. *Gortania* 6: 5-58

Tunis G., Venturini S., (1996) – L'Eocene delle Prealpi Carniche, dell'altipiano di Brkini e dell'Istria: precisazioni biostratigrafiche e paleoambientali. *Natura Nascosta* 13: 40-49

Ustaszewski K., Schmid S. M., Lugović B., Schister R., Schaltegger U., Bernoulli D., Hottinger L., Kounov A., Fügenschuh B., Schefer S., (2009) – Late Cretaceous intra-oceanic magmatism in the internal Dinarides (northern Bosnia and Herzegovina): Implications for the collision of the Adriatic and European plates. *Lithos* 108: 106-125

Velić I., Tišljar J., Matičec D., Vlahović I. (1995) – Opći prikaz geološke gradi Istre (A review of the geology of Istria). In Vlahović I., Velić I. (eds.): *First Croatian Geological Congress Excursion Guidebook*, Zagreb pp. 5-30

Velicogna M., (2020) – Zircon dating and trace element content of transparent heavy minerals in sandstones from the NE Alps and Outer Dinarides flysch basins. *Doctoral thesis, Università degli Studi di Trieste, XXXII Cycle 2016-2019*

Venturini S., Tunis G., (1992) – La composizione dei conglomerati cenozoici del Friuli: dati preliminari. *Studi Geologici Camerti Special Issue 1992/2, CROP 1-1A*, pp. 285-295

Walsby C. J., Lees N. S., Claridge R. F. S., Weil J. A., (2003) – The magnetic properties of oxygen-hole aluminium centres in crystalline SiO<sub>2</sub>. VI: A stable AlO<sub>4</sub>/Li centre. *Canadian Journal of Physics* 81: 583–598

Wang D., Liu J., Carranza E. J. M., Zhai D., Wang Y., Zhen S., Zhang F., (2019) – Formation and evolution of snowball quartz phenocrysts in the Dongping porphyritic granite, Hebei Province, China: Insights from fluid inclusions, cathodoluminescence, trace elements, and crystal size distribution study. *Lithos* 340: 239–254

Wang S-I, Peng H-j, Wang T-r, Zou H., Zhou Q., Yang D-j, Sun C., Tian X., (2022) – Trace element composition and cathodoluminescence of quartz in the Hongniu-Hongshan skarn deposit in Yunnan Province, Southwest China. *Frontiers in Earth Science* 10: 864118

Wark D. A., Watson E. B., (2004) – The TitaniQ: a Ti-in-quartz thermometer. *Geochimica et Cosmochimica Acta Supplementary* 68: A543

Wark D. A., Watson E. B., (2006) – TitaniQ: a titanium-in-quartz geothermometer. *Contributions to Mineralogy and Petrology* 152: 743-754

Watt G. R., Wright P., Galloway S., McLean C., (1997) – Cathodoluminescence and trace element zoning in quartz phenocrysts and xenocrysts. *Geochimica et Cosmochimica Acta* 61: 4337-4348

Wehrle E. A., McDonald A. M., (2019) – Cathodoluminescence and trace-element chemistry of quartz from Sudbury offset dikes: Observations, interpretations, and genetic implications. *The Canadian Mineralogist* 57: 947–963

Weil J. A., (1984) – A review of electron spin spectroscopy and its application to the study of paramagnetic defects in crystalline quartz. *Physics and Chemistry of Minerals* 10: 149–165.

Weil J. A. (1993) – A review of the EPR spectroscopy of the point defects in  $\alpha$ -quartz: The decade 1982–1992. In Helms C. R., Deal B. E. (Eds): *Physics and Chemistry of SiO<sub>2</sub> and the Si-SiO Interface* 2 pp. 131–144

Wertich V., Leichmann J., Dosbaba M., Götze J., (2018) – Multi-stage evolution of gold-bearing hydrothermal quartz veins at the Mokrsko gold deposit (Czech Republic) based on cathodoluminescence, spectroscopic, and trace elements analyses. *Minerals* 8: 335

Yan J., Mavrogenes J. A., Liu S., Coulson I. M., (2020) – Fluid properties and origins of the Lannigou Carlin-type gold deposit, SW China: Evidence from SHRIMP oxygen isotopes and LA-ICP-MS trace element compositions of hydrothermal quartz. *Journal of Geochemical Exploration* 215: 106546

Zhang Y., Cheng J., Tian J., Pan J., Sun S., Zhang L., Zhang S., Chu G., Zhao Y., Lai C., (2019) – Texture and trace element geochemistry of quartz in skarn system: Perspective from Jiguanzui Cu–Au skarn deposit, Eastern China. *Ore Geology Reviews* 109: 535–544

Zhang W., Chen W. T., Zhang X-C, Tang Y-W, (2022) – The trace element chemistry of quartz in carbonatite-related REE deposits: implications for REE exploration- *Ore Geology Reviews* 149

Zinkernagel U., (1978) – Cathodoluminescence of quartz and its application to sandstone petrology. *Contributions to Sedimentology* 8: 1-69

Živkovic S., Glumac B., (2007) – Paleoenvironmental reconstruction of the Middle Eocene Trieste-Pazin basin (Croatia) from benthic foraminiferal assemblages. *Micropaleontology* 53: 285-310

## **ACKNOWLEDGMENTS**

To my supervisor Davide, that made all this possible. For your immense patience, especially in these last days, and for your essential help throughout all these years.

To my co-supervisor Henrik, and all the Museum's staff, that hosted me warmly, again. For your teachings, your trust in me, and your willingness.

To my dearest friends, Alessandra, and Chiara and Alessio, that helped me to face the stress with their advice, with the aperitif-gossip sessions, and with the amusing game nights.

To my parents Adriana and Giorgio, that made me the man and the scientist I am. For teaching me the respect, the hard-work, and the curiosity. For allowing and encouraging me to follow my dreams.

To my brother Giacomo, my perfect, life-lasting right-hand man. For our capacity to range from silly jokes to (actual) rocket science within the same conversation (with some Simpsons quotes here and there).

Last, but absolutely not least, to my partner Giulia, my perfect half. For your vital support not only in this agitated last month, but since the very first moment you entered in my life. There are no words in the whole Universe to describe how much I am grateful to you and how much I love you.

*I don't like sand.*

*It's coarse, and rough, and irritating,  
and it gets everywhere.*